

ALTERNATIVE COATINGS FOR
REED SWITCHES

by

KEVIN JOSEPH LODGE, B.Sc.

669-015 LOD
190407 27 APR 1976

A Thesis submitted for the degree of
Doctor of Philosophy of the University
of Aston in Birmingham.

September, 1975.

SUMMARY.

A method of coating the contact areas of electrical reed switches was developed which reduced the amount of precious metals required, and allowed the development of alloy coatings not easily produced by electrodeposition.

The method consisted of printing the metals on to the reed blanks in the form of a paste, composed of small metal particles mixed with an organic vehicle. The pastes were then heated to 800°C - 1000°C in an inert atmosphere, to drive off the vehicle and sinter the remaining particles. The sintered coating had up to 80% solid density with an adhesion to the substrate approaching that obtained from electrodeposition.

The work was carried out with gold powders, which were produced from aqueous gold chloride solution by various reducing agents. The morphology of the gold powders was studied with the scanning electron microscope and a scheme of morphology changes outlined. This related the morphology changes to alterations in the rate of the reducing reaction. The best gold powders produced were spherical with a diameter of between 1 and 5 μm .

The sintering of the deposits was found to be inhibited by firing in either vacuum or nitrogen 10% hydrogen mixture, and this was considered to be due to the presence of vapour phase transport of gold at the start of the sintering process. Firing in nitrogen or argon produced dense deposits with a surface finish comparable to that of worn electroplated reeds. The electrical resistance was slightly higher than that of electrodeposited metals.

Alloys of gold with palladium, palladium and tin, palladium and nickel, iron and copper were examined. The morphology of sintered 1% alloys of nickel, iron and copper with gold were found to be discontinuous.

Key words: 'Powder Metallurgy' and 'Chemical Precipitation'

INDEX

		<u>Page No.</u>
1.	INTRODUCTION AND LITERATURE SURVEY.	1
1.1.	Reed Switches.	1
1.1.1.	Description and operation.	1
1.1.2.	Construction.	1
1.1.3.	Uses.	3
1.1.4.	Contact physics.	6
1.1.4.1.	Switching 'dry' currents.	6
1.1.4.2.	Switching currents.	7
1.1.5.	Contact materials.	8
1.1.5.1.	Usual contact materials.	8
1.1.5.2.	Special purpose materials.	10
1.1.5.3.	Composite contact coatings.	11
1.1.5.4.	Other contact coatings.	12
1.1.6.	Problems with reeds.	12
1.2.	Project Outline.	13
1.2.1.	Outline of problems.	13
1.2.2.	Alternative coating methods.	14
1.2.3.	Choice of method.	16
1.2.4.	Thick films.	16
1.2.5.	Thick film problems.	17
1.3.	Powder Production.	17
1.3.1.	Powder requirements.	17
1.3.2.	Production route.	18
1.3.3.	Theoretical considerations for chemical precipitation.	19

		<u>Page No.</u>
1.3.3.1.	The reduction reaction.	19
1.3.3.2.	The nucleation process.	20
1.3.3.3.	Growth reactions.	22
1.3.4.	Particle morphology.	23
1.3.5.	Particle size.	26
1.3.6.	Gold powders.	28
1.4.	Paste and Film Production.	31
1.4.1.	Mixing and firing.	31
1.4.2.	Surface finish.	33
1.4.3.	Sintering and firing the deposits.	33
1.4.4.	Sintering of gold and gold alloys.	35
2.	EXPERIMENTAL DETAILS OF POWDER PRECIPITATION.	37
2.1.	Materials Used.	37
2.2.	Experimental Method.	40
2.3.	Reduction Systems for Reducing Gold Salts.	40
2.3.1.	Gold salts.	40
2.3.2.	Reducing agents.	41
2.4.	Precipitation of Gold Alloys.	43
2.5.	Other Metal Powders.	44
3.	RESULTS OF POWDER PRECIPITATION.	45
3.1.	Experimental Errors.	45
3.2.	Gold Powders.	45
3.2.1.	Reduction by hydrogen.	45
3.2.2.	Reduction by nascent hydrogen.	45

3.2.3.	Reduction by hydrogen sulphide.	51
3.2.4.	Reduction by hydrogen peroxide.	51
3.2.5.	Reduction by sodium hydroxide.	51
3.2.6.	Reduction by acetone.	58
3.2.7.	Reduction by sulphur dioxide.	58
3.2.8.	Reduction by sodium sulphite.	58
3.2.9.	Reduction by ferrous chloride.	67
3.2.10.	Reduction by ferrous sulphate.	67
3.2.11.	Reduction by sodium nitrite.	67
3.2.12.	Reduction by formaldehyde.	76
3.2.13.	Reduction by trisodium citrate.	76
3.2.14.	Reduction by hydroxylamine hydrochloride.	76
3.2.15.	Reduction by hydrazine hydrochloride.	82
3.2.16.	Reduction by oxalic acid.	82
3.2.17.	Reduction by Faraday's solution.	82
3.2.18.	Reduction by zinc.	82
3.2.19.	Reduction by electrolysis.	87
3.3.	Nucleation and Growth.	87
3.4.	Alloy Gold Powders.	87
3.5.	Other Metal Powders.	92
3.6.	Production of Gold Powders for Pastes.	100
4.	DISCUSSION OF POWDER PRECIPITATION.	105
4.1.	Particle Size.	105
4.1.1.	Variations in mixing.	105
4.1.2.	Reduction and precipitation reaction.	106

4.1.3.	Measurement errors.	108
4.1.4.	The use of distribution curves.	112
4.2.	Morphology.	112
4.2.1.	Solubility of gold.	112
4.2.2.	Effect of reaction rates on morphology.	113
4.2.3.	Gold powders.	116
4.2.4.	Problems.	122
4.2.5.	Other metal powders.	123
4.2.6.	Alloy precipitation.	124
4.3.	Choice of Materials.	125
4.3.1.	Gold powder.	125
4.3.2.	Other metal powders.	126
5.	EXPERIMENTAL DETAILS OF PASTE PRODUCTION AND FIRING.	128
5.1.	Materials.	128
5.2.	Mixing.	128
5.3.	Substrate Preparation.	131
5.4.	Printing.	131
5.5.	Firing the Sample.	131
5.6.	Testing.	132
5.6.1.	Visual examination	132
5.6.2.	Surface finish.	132
5.6.3.	Electrical resistance.	134
5.6.4.	Spark resistance.	134

		<u>Page No.</u>
5.6.5.	Adhesion.	138
6.	RESULTS OF PASTE FIRING.	139
6.1.	Test Methods.	139
6.1.1.	Electrical resistance.	139
6.1.2.	Neck growth.	140
6.1.3.	Spark resistance.	140
6.2.	Mixing variables.	142
6.2.1.	Influence of mixing method.	142
6.2.2.	Influence of the vehicle.	142
6.3.	Printing.	146
6.3.1.	Influence of printing method.	146
6.3.2.	Influence of drying temperature.	146
6.4.	Firing.	149
6.4.1.	Influence of substrate preparation.	149
6.4.2.	Influence of firing atmosphere.	149
6.4.3.	Influence of firing time.	156
6.4.4.	Influence of firing temperature.	163
6.5.	Paste Composition.	163
6.5.1.	Influence of particle morphology.	163
6.5.2.	Influence of glass frit.	168
6.5.3.	Gold/palladium alloys.	168
6.5.4.	Gold/palladium/tin alloys.	172
6.5.5.	Gold/palladium/nickel alloys.	182
6.5.6.	Gold/nickel alloys.	182
6.5.7.	Gold/iron alloys.	187
6.5.8.	Gold/copper alloys.	187

6.6.	Deposit Properties.	192
6.6.1.	Adhesion.	192
6.6.2.	Density.	195
6.6.3.	Deposit/substrate interdiffusion.	195
6.6.4.	Electrical resistance.	195
6.6.5.	Spark resistance.	203
6.6.6.	Deposit thickness.	207
6.6.7.	Surface finish.	207
7.	DISCUSSION OF RESULTS OF PASTE FIRING.	214
7.1.	Relevance of Test Methods.	214
7.1.1.	Visual assessment.	214
7.1.2.	Electrical resistance.	214
7.1.3.	Spark resistance.	216
7.1.4.	Adhesion.	216
7.2.	Nature of Adhesion.	218
7.3.	Sintering Mechanism.	219
7.3.1.	Material transported by vapour phase.	219
7.3.2.	Surface diffusion.	221
7.3.3.	Volume diffusion.	222
7.3.4.	Viscous flow.	222
7.3.5.	Overall sintering reactions.	222
7.4.	Influence of Preparation of the Pastes and Substrates.	223
7.4.1.	Substrate preparation.	223
7.4.2.	Influence of the vehicle.	223
7.4.3.	Influence of printing/painting.	223

		<u>Page No.</u>
7.4.4.	Influence of particle morphology.	224
7.4.5.	Influence of precompressing the printed surface.	224
7.4.6.	Influence of deposit thickness.	225
7.5.	Pure Gold Pastes.	227
7.6.	Alloy Pastes.	227
7.6.1.	Possible range of alloys.	227
7.6.2.	Gold/palladium alloys.	229
7.6.3.	Gold/palladium/tin alloys.	229
7.6.4.	Gold/palladium/nickel alloys.	230
7.6.5.	Gold/nickel alloys.	230
7.6.6.	Gold/iron alloys.	231
7.6.7.	Gold/copper alloys.	231
7.6.8.	Selection of alloy pastes.	233
8.	GENERAL DISCUSSION.	234
9.	CONCLUSIONS.	237
10.	FUTURE WORK.	238
11.	ACKNOWLEDGEMENTS.	240
12.	REFERENCES.	241

LIST OF FIGURES.

	<u>PAGE</u>
1.1. a) Normal size reed switch. b) Schematic diagram of a reed relay.	2
1.2. Normal size and miniature reed switches (scale in cm).	5
1.3. Stages of growth by mononuclear layer growth mechanism.	23
1.4. Stages of growth by polynuclear layer growth mechanism.	23
1.5. Stages of growth by spiral dislocation growth mechanism.	24
2.1. Kevex X-ray spectrum of gold chloride from Hopkins and Williams.	38
2.2. Kevex X-ray spectrum of reclaimed gold.	39
2.3. Kevex X-ray spectrum of wrought fine gold.	39
3.1. Particle size distribution of four samples taken from the same powder.	46
3.2. Particle size distribution of a re-measurement of the same four samples of the same powder used in fig. 3.1.	47
3.3. Influence of mixing rates on the particle size distribution of gold powder reduced from gold chloride by sodium sulphite.	48
3.4. Kevex X-ray spectrum of gold reduced by gaseous hydrogen.	49
3.5. Scanning electron micrograph of gold reduced by gaseous hydrogen. x 10,000	49
3.6. Scanning electron micrograph of gold reduced by nascent hydrogen produced from lithium hydride. x 5,400	50
3.7. Scanning electron micrograph of gold reduced by hydrogen sulphide. x 2,100	52
3.8. Sulphur distribution in gold reduced by hydrogen sulphide. (Sulphur $K\alpha_1$ X-rays.) x 2,100	52
3.9. Kevex X-ray spectrum of gold reduced by hydrogen sulphide.	53
3.10. Scanning electron micrograph of gold reduced under acid conditions by hydrogen peroxide. x 2,250	54
3.11. Influence of temperature on the particle size distribution of gold reduced under acid conditions by hydrogen peroxide.	54
3.12. Scanning electron micrograph of gold reduced from a low gold concentration solution by hydrogen peroxide. x 1,600	55

	<u>PAGE</u>
3.13. Scanning electron micrograph of gold reduced under alkaline conditions by hydrogen peroxide. x 5,000	55
3.14. Scanning electron micrograph of gold reduced at room temperature by sodium hydroxide. x 9,000	56
3.15. Kevex X-ray spectrum of gold reduced at room temperature by sodium hydroxide.	56
3.16. Kevex X-ray spectrum of gold reduced at 100°C by sodium hydroxide.	57
3.17. Scanning electron micrograph of gold reduced at 100°C by sodium hydroxide. x 1,900	57
3.18. Scanning electron micrograph of gold reduced by acetone at room temperature. x 2,000	59
3.19. Scanning electron micrograph of gold reduced by acetone at 100°C. x 5,000	59
3.20. Particle size distribution of gold reduced by acetone at 100°C.	60
3.21. Scanning electron micrograph of gold reduced at room temperature by sulphur dioxide. x 4,400	61
3.22. Particle size distribution of gold reduced at room temperature by sulphur dioxide.	61
3.23. Scanning electron micrograph of gold reduced at boiling point by sulphur dioxide. x 5,600	62
3.24. Scanning electron micrograph of gold reduced at varying temperatures by sulphur dioxide. x 10,000	62
3.25. Scanning electron micrograph of gold reduced at pH 0 by sodium sulphite. x 6,500	63
3.26. Scanning electron micrograph of gold reduced at pH 0.7 by sodium sulphite. x 6,500	63
3.27. Scanning electron micrograph of gold reduced at pH 1.2 by sodium sulphite. x 5,600	64
3.28. Scanning electron micrograph of gold reduced at pH 1.7 by sodium sulphite. x 5,800	64
3.29. Influence of pH on the particle size distribution of gold reduced by sodium sulphite.	65
3.30. Scanning electron micrograph of gold reduced at pH 6 and 100°C by sodium sulphite. x 5,000	66
3.31. Scanning electron micrograph of gold reduced at pH 2 with a gold chloride : sodium sulphite ratio of 0.5 x 2,900	66

	<u>PAGE</u>
3.32. Effect of the ratio of gold chloride to sodium sulphite on the particle size distribution.	68
3.33. Scanning electron micrograph of gold reduced by ferrous chloride. x 1,550	69
3.34. Kevex X-ray spectra of a) spherical and b) plate-like gold particles reduced by ferrous chloride.	70
3.35. Particle size distribution of spheres of gold reduced by ferrous chloride.	71
3.36. Scanning electron micrograph of gold reduced under acid conditions by ferrous sulphate at room temperature. x 10,000	72
3.37. Kevex X-ray spectra of gold reduced by ferrous sulphate under a) neutral and b) alkaline conditions.	73
3.38. Kevex X-ray spectrum of gold reduced at 100°C by ferrous sulphate.	74
3.39. Scanning electron micrograph of gold reduced under acid conditions by sodium nitrite. x 1,700	75
3.40. Scanning electron micrograph of gold reduced under neutral conditions by sodium nitrite. x 1,800	75
3.41. Scanning electron micrograph of gold reduced from dilute gold chloride solution under acid conditions by sodium nitrite. x 4,500	77
3.42. Scanning electron micrograph of gold reduced at room temperature by formaldehyde. x 5,500	78
3.43. Scanning electron micrograph of gold reduced at 100°C by formaldehyde. x 5,500	78
3.44. Kevex X-ray spectrum of gold reduced under hot alkaline conditions by formaldehyde.	79
3.45. Scanning electron micrograph of gold reduced from a boiling solution of pH 6 by trisodium citrate. x 5,500	80
3.46. Kevex X-ray spectrum of gold reduced from boiling solution to pH 6 by trisodium citrate.	80
3.47. Scanning electron micrograph of gold reduced from neutral solution by hydroxylamine hydrochloride. x 22,000	81
3.48. Scanning electron micrograph of gold reduced from alkaline solution by hydroxylamine hydrochloride. x 21,000	81
3.49. Scanning electron micrograph of gold reduced under acid conditions by hydroxylamine hydrochloride. x 23,000	83

		<u>PAGE</u>
3.50.	Scanning electron micrograph of gold reduced by hydrazine hydrochloride via gold fulminate. x 5,500	83
3.51.	Scanning electron micrograph of gold reduced at boiling point by oxalic acid solution. x 690.	84
3.52.	Scanning electron micrograph of gold reduced by Faraday's solution. x 22,000	85
3.53.	KeveX X-ray spectrum of gold reduced by Faraday's solution.	85
3.54.	Scanning electron micrograph of gold reduced by zinc dust. x 2,600	86
3.55.	KeveX X-ray spectrum of gold reduced by zinc.	86
3.56.	Scanning electron micrograph of gold found on the cathode after electrolysis. x 2,200	88
3.57.	Scanning electron micrograph of gold found in the body of the electrolyte after electrolysis. x 2,300	88
3.58.	KeveX X-ray spectrum of gold found in the body of the electrolyte after electrolysis.	89
3.59.	Particle size distribution of nuclei and particles grown from acidified hydroxylamine hydrochloride.	90
3.60.	KeveX X-ray spectrum of gold/palladium reduced by hydrazine hydrochloride via gold/palladium fulminate.	91
3.61.	Scanning electron micrograph of gold reduced from a gold/palladium chloride mixture by sulphur dioxide. x 7,000.	91
3.62.	Particle size analysis of gold powder reduced from a gold/palladium chloride mixture by sulphur dioxide.	93
3.63.	Scanning electron micrograph of palladium reduced by nascent hydrogen. x 10,000	94
3.64.	Scanning electron micrograph of palladium/nickel powder reduced from mixed solution of chlorides by sodium thiosulphate. x 5,400	95
3.65.	KeveX X-ray spectrum of palladium/nickel reduced from mixed solution of chlorides by sodium thiosulphate.	95
3.66.	Scanning electron micrograph of nickel reduced by nascent hydrogen from sodium hydride. x 6,400	96
3.67.	Scanning electron micrograph of copper reduced by iron powder and ferrous sulphate. x 2,000	97
3.68.	KeveX X-ray spectrum of copper reduced by iron powder.	97

	<u>PAGE</u>
3.69. Kevex X-ray spectrum of palladium from Hopkins and Williams.	98
3.70. Scanning electron micrograph of palladium from Hopkins and Williams. x 11,500	98
3.71. Scanning electron micrograph of palladium/tin powder from plating on plastics waste. x 10,500	99
3.72. Kevex X-ray spectrum of palladium/tin powder from plating on plastics waste.	99
3.73. Scanning electron micrograph of nickel reduced by carbonyl process. x 5,400	101
3.74. Scanning electron micrograph of iron reduced by carbonyl process. x 5,400	101
3.75. Particle size distribution of nickel and iron powders.	102
3.76. Particle size distribution of five identical samples reduced by sodium sulphite under acid conditions at room temperature.	103
3.77. Particle size distribution of 'production' batches.	104
4.1. Particle size distribution of gold reduced by ferrous sulphate or by sodium sulphite, with a size mode of 0.5 μ m.	107
4.2. Probability curve for size distribution shown in fig. 3.1.	110
4.3. Probability curve for size distribution shown in fig. 3.76.	111
4.4. Scanning electron micrograph of gold reduced by acetone at room temperature. x 2,000	115
4.5. Relationship between morphology and reaction speed.	117
4.6. Scanning electron micrograph of sulphur content of gold reduced by hydrogen sulphide. x 2,100	119
5.1. Scanning electron micrograph of gold powder used in Engelhard pastes. x 6,500	129
5.2. Scanning electron micrograph of nickel/iron substrate surface finish. x 650	130
5.3. Scanning electron micrograph of reed blank surface finish. x 460	130
5.4. Thermal history of a typical paste, fired in nitrogen.	133
5.5. Electrical resistance testing rig.	135
5.6. Spark testing rig.	136

	<u>PAGE</u>
5.7. Circuit diagram of spark generator.	137
6.1. Kevex X-ray spectrum for substrate sample No. 4, showing high silicon content.	141
6.2. Scanning electron micrograph of spark damage on polished nickel/iron substrate. x 220	143
6.3. Scanning electron micrograph of spark damage on polished nickel/iron substrate. x 240	143
6.4. Scanning electron micrograph of spark damage on polished nickel/iron substrate. x 250	144
6.5. Scanning electron micrograph of paste mixed with a palette knife. x 230	145
6.6. Scanning electron micrograph of paste mixed with a three roll mill. x 280	145
6.7. Scanning electron micrograph of fired paste mixed with a water based vehicle. x 2,200	147
6.8. Scanning electron micrograph of paste dried at 250°C x 24	148
6.9. Scanning electron micrograph of paste dried at 150°C. x 23.	148
6.10. Kevex X-ray spectra of Engelhard gold printed on a) cleaned substrate b) uncleaned substrate.	150
6.11. Cross-section of paste fired in air, showing oxide layer beneath the gold deposit. x 1,000	151
6.12. Scanning electron micrograph of Engelhard gold, showing film on deposit surface. x 2,600	151
6.13. Kevex X-ray spectrum of Engelhard gold after firing.	153
6.14. Kevex X-ray spectrum of same Engelhard gold after cleaning.	153
6.15. Scanning electron micrograph of Engelhard gold after firing. x 2,800	154
6.16. Scanning electron micrograph of same Engelhard gold after cleaning. x 2,800	154
6.17. Scanning electron micrograph of gold paste fired under nitrogen/10% hydrogen, showing zero neck growth. x 2,100	155
6.18. Kevex X-ray spectrum of gold paste fired for 5 minutes at 800°C in nitrogen.	157
6.19. Kevex X-ray spectrum of gold paste fired for 10 minutes at 850°C in nitrogen.	157

	<u>PAGE</u>
6.20. Kevex X-ray spectrum of gold paste fired for 15 minutes at 850°C in nitrogen.	158
6.21. Kevex X-ray spectrum of gold paste fired for 20 minutes at 850°C in nitrogen.	158
6.22. Scanning electron micrograph of a cross-section of a gold paste fired for 25 hours in argon. x 1,200.	159
6.23. Distribution of gold in fig. 6.22. (Gold M α line). x 1,200.	159
6.24. Distribution of iron in fig. 6.22. (Iron K α line). x 1,200.	160
6.25. Distribution of nickel in fig. 6.22. (Nickel K α line). x 1,200.	160
6.26. Scanning electron micrograph of gold fired in argon at 900°C for 10 minutes. x 1,300	161
6.27. Scanning electron micrograph of gold fired in argon at 900°C for 60 minutes. x 1,280	161
6.28. Scanning electron micrograph of gold fired in argon at 900°C for 60 minutes. x 6,500	162
6.29. Variation of electrical resistance with firing temperature for pure gold.	164
6.30. Scanning electron micrograph of gold fired for 10 minutes at 800°C. x 2,600	165
6.31. Scanning electron micrograph of gold fired for 10 minutes at 950°C. x 2,100	165
6.32. Scanning electron micrograph of gold fired for 10 minutes at 1000°C. x 1,000	166
6.33. Kevex X-ray spectrum of gold fired for 10 minutes at 1000°C.	166
6.34. Scanning electron micrograph of gold powder in the form of flat plates after firing. x 1,200	167
6.35. Scanning electron micrograph of gold powder showing rough spheres before firing. x 4,700	169
6.36. Scanning electron micrograph of the same gold powder as in fig. 6.35, after firing at 900°C for 10 minutes. x 3,700	169
6.37. Scanning electron micrograph showing the surface finish of a fired gold paste containing no glass. x 30.	170
6.38. Scanning electron micrograph showing the surface finish of a fired gold paste containing glass frit. x 23.	170

	<u>PAGE</u>
6.39. Scanning electron micrograph of a gold/palladium paste after firing at 900°C for 10 minutes. x 150.	171
6.40. Distribution of palladium in figure 6.39. (Palladium L α line). x 150	171
6.41. Scanning electron micrograph of a gold/palladium paste after firing at 900°C for 10 minutes. x 3,700	173
6.42. Scanning electron micrograph of a gold/palladium paste after firing at 900°C for 60 minutes. x 2,100	173
6.43. Scanning electron micrograph of a gold/palladium paste after firing at 950°C for 10 minutes. x 2,100	174
6.44. Scanning electron micrograph of a gold/palladium paste after firing at 1000°C for 10 minutes. x 2,400	174
6.45. Scanning electron micrograph of a gold/palladium paste after firing at 1000°C for 10 minutes in a nitrogen 10% hydrogen atmosphere. x 5,400	175
6.46. Scanning electron micrograph of a gold/palladium/tin paste fired at 900°C for 10 minutes. x 375.	176
6.47. Distribution of gold in fig. 6.46. (Gold M α line). x 375.	176
6.48. Distribution of palladium in fig. 6.46. (Palladium L α line). x 375.	177
6.49. Scanning electron micrograph of gold/palladium/tin paste fired at 900°C for 10 minutes. x 3,750	178
6.50. Scanning electron micrograph of a gold/palladium/tin paste fired at 950°C for 10 minutes. x 2,100	179
6.51. Distribution of palladium in fig. 6.50. (Palladium L α line). x 2,100	179
6.52. Scanning electron micrograph of a gold/palladium/tin paste fired at 950°C for 10 minutes. x 21.	180
6.53. Scanning electron micrograph of gold/palladium/tin paste fired at 1000°C for 10 minutes. x 520.	181
6.54. Kevex X-ray spectrum of melted area of gold/palladium/tin paste fired at 1000°C for 10 minutes.	181
6.55. Scanning electron micrograph of palladium/nickel/ (sulphur) precipitate after crushing. x 2,100	183
6.56. Scanning electron micrograph of gold/palladium/nickel paste after firing at 950°C for 10 minutes. x 2,100	183
6.57. Scanning electron micrograph of gold/palladium/nickel paste after firing at 950°C for 10 minutes. x 21.	184

	<u>PAGE</u>
6.58. Scanning electron micrograph of a gold/nickel paste after firing at 950°C for 10 minutes, showing the surface finish. x 110	184
6.59. Scanning electron micrograph of a gold/20% nickel paste after firing at 900°C for 10 minutes. x 1,100	185
6.60. Distribution of nickel in fig. 6.56. (Nickel K α line). x 1,100	185
6.61. Nickel background radiation for gold/nickel alloys. (Nickel K α line).	188
6.62. Scanning electron micrograph of gold/1% nickel alloy fired at 900°C for 10 minutes. x 1,100	189
6.63. Distribution of nickel in fig. 6.62. (Nickel K α line). x 1,100	189
6.64. Scanning electron micrograph of a gold/1% iron alloy fired at 950°C for 10 minutes. x 1,100	190
6.65. Scanning electron micrograph of gold/1% iron alloy fired at 950°C for 10 minutes. x 5,500	190
6.66. Scanning electron micrograph of gold/10% iron alloy fired at 950°C for 10 minutes. x 1,100	191
6.67. Scanning electron micrograph of gold/1% copper alloy fired at 950°C for 10 minutes. x 1,000	192
6.68. Scanning electron micrograph of gold/5% copper alloy fired at 950°C for 10 minutes. x 1,000	192
6.69. Scanning electron micrograph of the substrate after adhesion testing using a soldered wire. x 28.	193
6.70. Scanning electron micrograph of the underside of the soldered area pulled off the substrate shown in fig. 6.69. x 32.	193
6.71. Scanning electron micrograph of the underside of a pure gold deposit peeled off a nickel/iron substrate. x 100	194
6.72. Scanning electron micrograph of the underside of a gold/palladium/nickel deposit peeled off a nickel/iron substrate. x 21.	196
6.73. Scanning electron micrograph of the holes in the gold/palladium/nickel deposit peeled off a nickel/iron substrate, showing the copper overplate at the base of the holes. x 110	196
6.74. Scanning electron micrograph of a cross-section of a pure gold deposit fired at 900°C for 10 minutes in argon. x 650.	197

	<u>PAGE</u>
6.75. Scanning electron micrograph of a cross-section of the gold shown in fig. 6.74. x 2,600	198
6.76. Distribution of gold in fig. 6.75. (Gold $M\alpha$ line). x 2,600	198
6.77. Distribution of iron in fig. 6.75. (Iron $K\alpha$ line). x 2,600	199.
6.78. Distribution of nickel in fig. 6.75. (Nickel $K\alpha$ line) x 2,600.	199
6.79. Scanning electron micrograph of a pure gold which has been fired at 850°C for 25 hours in argon. x 600.	200
6.80. Distribution of gold in fig. 6.79. (Gold $M\alpha$ line) x 600.	200
6.81. Distribution of iron in fig. 6.79. (Iron $K\alpha$ line) x 600.	201
6.82. Distribution of nickel in fig. 6.79. (Nickel $K\alpha$ line). x 600.	201
6.83. X-ray microprobe analysis trace for gold shown in fig. 6.79.	202
6.84. Scanning electron micrograph of a pure gold deposit showing damage caused by electrical resistance probe tip. x 22.	204
6.85. Kevex X-ray spectra of pure golds fired at 950°C for 10 minutes in nitrogen. The three pastes had different viscosities.	205
6.86. Scanning electron micrograph of the spark damage on an Aston painted deposit. x 1,150	206
6.87. Scanning electron micrograph of the spark damage on an Engelhard silk screen printed deposit. x 770	206
6.88. Engelhard printed gold deposit after compressing to a loading of 1.5 Kg/mm^2 . Dark areas have been compressed.	208
6.89. Scanning electron micrograph of a compressed area of fig. 6.88. x 750.	209
6.90. Scanning electron micrograph of an uncompressed area of fig. 6.88. x 750.	209
6.91. Scanning electron micrograph of the underside of a transfer painted onto art paper. x 1,800	211
6.92. Scanning electron micrograph of the lines seen on a gold/palladium/tin deposit fired at 1000°C for 10 minutes in argon. x 12,000	212

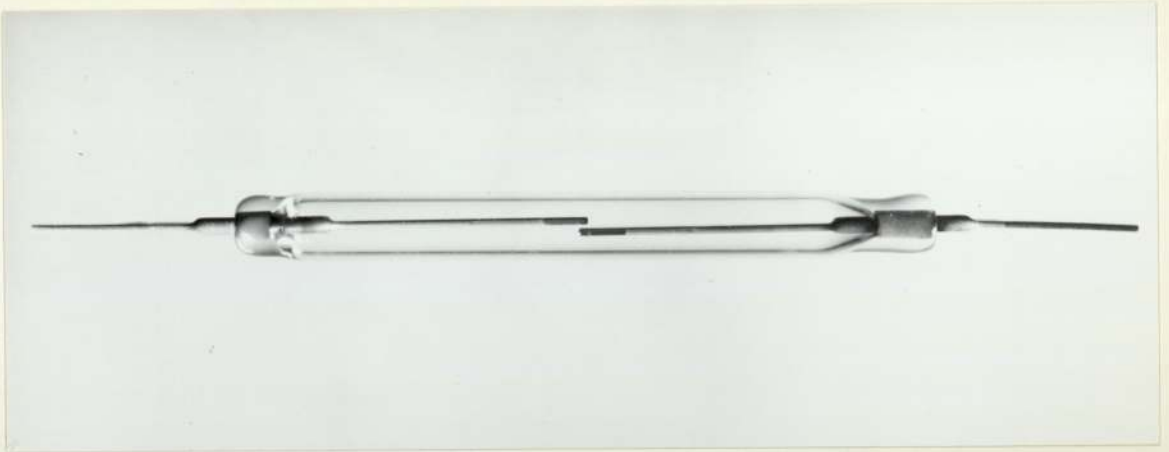
		<u>PAGE</u>
6.93.	Scanning electron micrograph of the lines seen on gold/palladium/tin deposit fired at 950°C for 10 minutes in nitrogen. x 10,500	212
6.94.	Scanning electron micrograph of the lines seen on a pure gold deposit fired at 950°C for 10 minutes in argon. x 11,000	213
7.1.	Scanning electron micrograph of a worn electroplated reed after switching more than 10 ⁶ cycles. x 1,400	217
7.2.	Scanning electron micrograph of pure gold deposit showing grain boundary grooves. x 5,500	226

1. INTRODUCTION AND LITERATURE SURVEY.

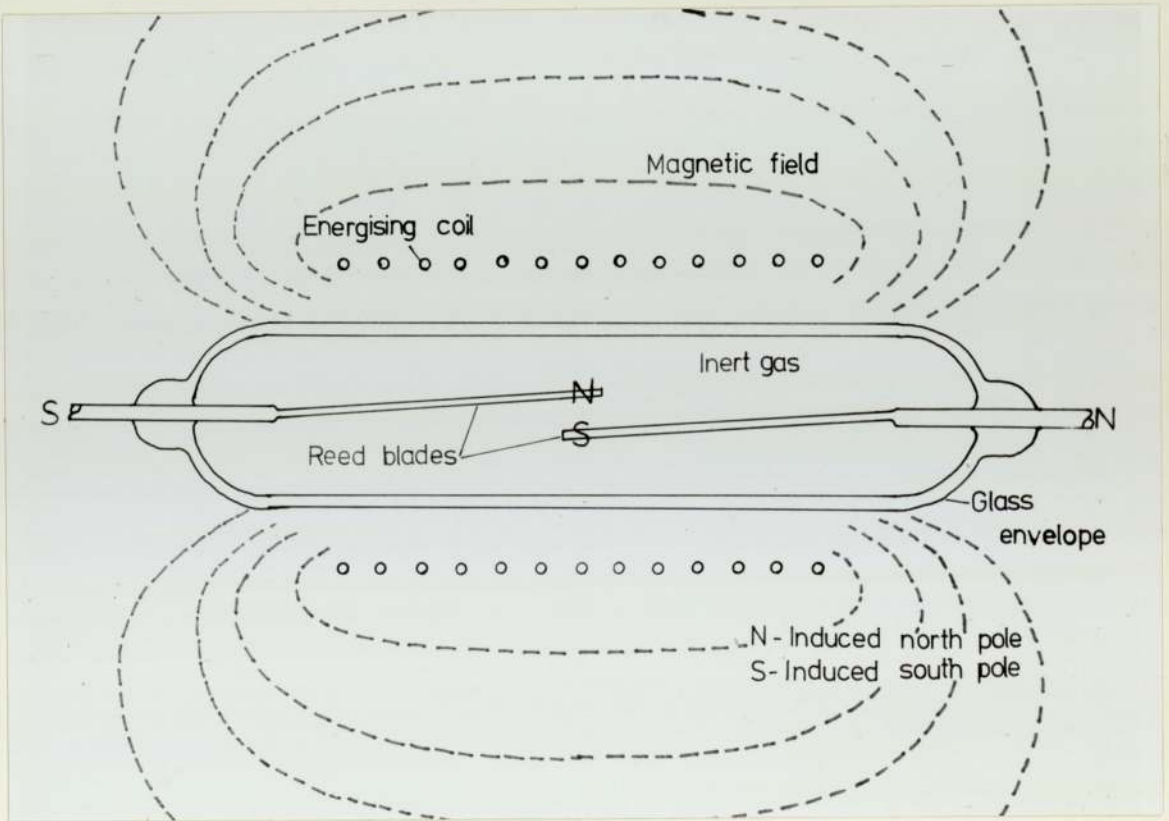
1.1. Reed Switches.

1.1.1. Description and operation. The reed switch is possibly the simplest form of electromagnetic relay, comprising essentially of two cantilevers (reeds) of ferromagnetic metal sealed in a glass envelope. The free ends of the reeds overlap each other, and are separated by a small gap, as in figure 1.1. The reeds are operated by applying an external magnetic field so as to induce opposite polarities in the free tips of the reeds, which causes them to be mutually attractive. This attraction overcomes the stiffness of the reeds and bends them, making contact with each other, thus completing the electric circuit. Modifications to this simple switching action can be made so as to give a 'make' action, a 'break' action or a switching action, operating either on steady fields or on magnetic pulses.

1.1.2. Construction. Practically all reed blades are now made from 51% nickel, 49% iron, an alloy which has the desirable magnetic properties of high permeability and low remanence coupled with the necessary glass-to-metal compatibility.⁽¹⁾ The reeds are usually made from wire, which is straightened and cut to length before one end is flattened to the shape of a paddle which will form the contact end.⁽²⁾ As the nickel/iron does not wear as well as an electrical contact, the tips are coated with a better contact material, often gold, but the choice of material depends on the proposed application of the reed. If, for example, the blade is to be electroplated with soft gold, then it is first cleaned and de-burred, before being electropolished and plated.⁽³⁾⁽⁵¹⁾ The blades are then heat treated in dry hydrogen at about $900^{\circ} - 950^{\circ}\text{C}$,⁽³⁾ which diffuses the substrate into the coating and helps to eliminate the tendency to cold weld, and also anneals the blades to give them the desired magnetic and mechanical properties.



a



b

- 1.1. a) Normal size reed switch.
b) Schematic diagram of a reed relay.

Alternatively, the blades can be heat treated prior to being plated with a hard gold which is not then diffused into the reed blade.

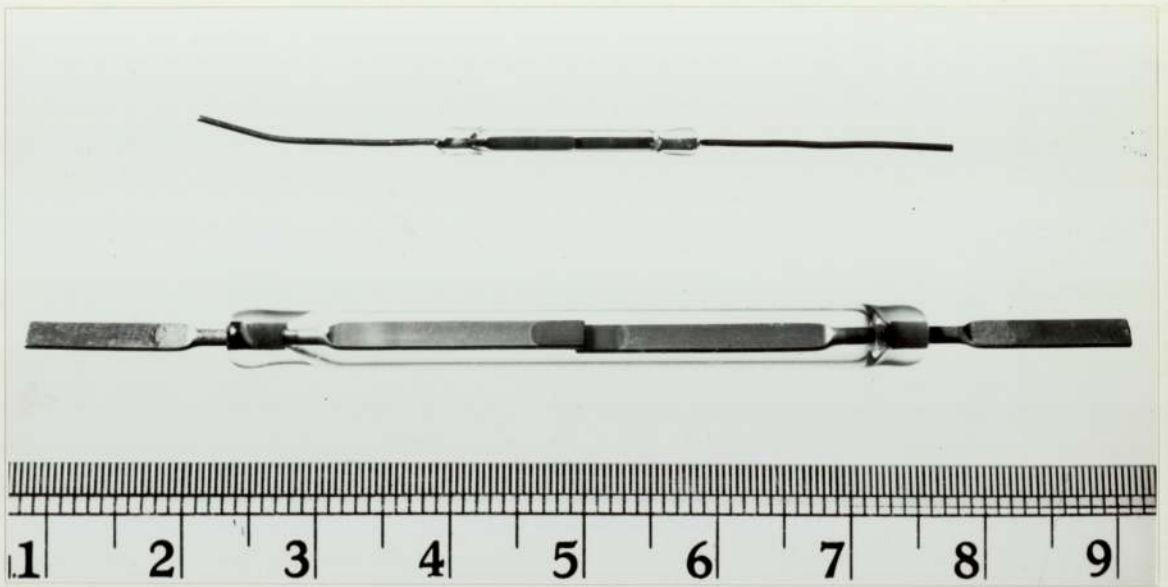
The reeds are then encapsulated in the glass envelope which is made of a soda/lime/silicate type of glass doped with ferrous oxide to increase absorption in the infra-red region.⁽²⁾ This enables the sealing to be carried out quickly by means of focused infra-red lamps, reducing the heat build-up in the reeds. The sealing is done in complex machinery which sets the overlap and gap distances and fills the envelope with inert gas, usually dry nitrogen, with a small percentage of hydrogen present.

Different types of reed are made for specific applications. For example, the contact material can range from gold or rhodium, the commonest types in this country, to silver, used for high frequency applications, and tungsten, used for 'heavy duty' switching. These will be referred to later on (1.1.5.).

1.1.3. Uses. The current carrying capacity of a reed which is limited by its ability to dissipate the heat generated by the conduction and switching of the load. In a given environment, this ability is related to the mass of the reed blade, which is related to the radius, assuming cylindrical reeds of a fixed length. However, if the mass doubles, the radius is increased by a factor of 1.414 which increases the stiffness of the reed by $(1.414)^4$.⁽⁵⁾ Therefore, the energy required to switch large reeds is very high, and this limits the reed to carrying and switching low to medium loads (i.e., a few millivolt amps up to 250VA, depending on contact material⁽⁶⁾).

The reed relay was designed for carrying the voice paths in telephone switching circuits⁽⁷⁾ and this is still by far its largest use, with millions of switches now being made annually.⁽²⁾⁽⁴⁾ These are

called upon to switch currents ranging from zero (no load or 'dry' switching) to 130mA at 50 volts D.C.⁽²⁾⁽⁸⁾ In addition to the switched current, the reed will also have to withstand current and voltage surges caused by the discharge of stored energy held in long lengths (10-15 metres) of cabling and associated equipment. This can cause peak voltage surges of up to 20 times the switched voltage, and short arcs of up to six times the switched currents.⁽⁹⁾ The contact physics of small switches is dealt with later (1.1.4.). An average telephone call has been calculated to use between 50 and 500 reed connections⁽¹⁰⁾, and a 1000 line telephone exchange will contain about 100,000 reed contacts.⁽²⁾ As these exchanges have a design life of 30 years, a high degree of reliability, coupled with small size and low cost are called for. On all these counts the reed relay has advantages. Failure rates of 0.15 failures per thousand per year have been reported,⁽¹¹⁾ and the size of reed switches range from 85mm overall length to 44mm (fig. 1.2.)⁽⁶⁾ With large scale mass production the cost of reed switches is lower than conventional electromagnetic relays,⁽¹⁰⁾ but continued development has lowered the cost of many solid state relays.⁽¹²⁾ This has resulted in the replacement of reeds in logic control units with solid state relays, but reeds maintain their role in switching speech paths due to their low electrical noise and high ratio of open to closed circuit resistance.⁽²⁾ Besides taking over the switching in the central control of telephone exchanges, solid state relays have also displaced reeds in the logic circuits of calculators and computers and the switching of incandescent lamps.⁽¹³⁾ Despite this, the reed switch is still widely used in many applications. It is being used increasingly for switching domestic appliances⁽¹⁴⁾, for such things as proximity switches, and with the development of the ring magnet, it has found use in push button dialling for telephones and level indicators for tanked liquids.⁽¹⁵⁾



1.2. Normal size and miniature reed switches (scale in cm).

1.1.4. Contact physics.

1.1.4.1. Switching 'dry' currents. A 'dry' current is one where the reed is not called upon to make or break currents, and only a small current flows when the reed is closed. This can be the least eroding application for reeds, which will give them an almost indefinite life if used within these specifications.

When the operating magnetic field is applied to a reed switch, the two free reed ends are made mutually attractive (fig. 1.1), with a force proportional to their separation. Thus, the reeds are accelerating towards one another when they come into contact, and as there is no damping in the system, momentum exchanges cause the reeds to bounce or 'chatter'.⁽¹⁶⁾ This results in the contact areas getting a severe hammering many times in excess of the number of switching cycles the reed has made.

When the reed blades have finally come together, the actual metallic contact between the two blades is limited to a few small areas, irrespective of the apparent contact area.⁽¹⁷⁾ This is because even the smoothest surface has a number of irregularities on it which make contact first and hold the surfaces apart. As the total contact force is on these small areas, the local stress will be very high and deformation, both plastic and elastic, will occur until the local contact area is sufficient to bear the applied load. This small area (or collection of smaller areas) also bears the total electrical load, and so quite high current densities can develop locally. These can produce sufficient heat to anneal the contact areas and so get further deformation, and if an even larger voltage drop across the contact is allowed, melting or even boiling of the contact metal can occur.⁽¹³⁾ This will produce welding or loss of metal and if extensive, will cause difficulties when the reed comes to open. For this reason short surges of current, or operation

outside the switches' specifications can shorten the operating life of the reeds.

The passage of these high current densities through such small areas gives rise to an abnormal resistance effect, known as the constriction resistance. This is related to the contact spot diameter, not to its area, and this means that several small spots will have a lower constriction resistance than a single larger one of the same total area.⁽¹⁹⁾ Contacts which have been contaminated will usually have a higher contact resistance, as insulating films will add their own, filmic resistance. In addition, the film may bear some of the mechanical load and so reduce the area of metal to metal contact.

1.1.4.2. Switching currents. As two blades approach one another, the local field between them builds up until/at very small gap distances (around $0.1\mu\text{m}$),⁽²⁰⁾ the field strength will be strong enough to pull electrons out of the cathode by field emission.⁽²¹⁾ This will take place preferentially at high points on the reed surface, because of the high local field at these points, or at areas where low electron work function material is present, where the electrons are easier to remove. This field emission current generates heat, which causes thermionic emission which then causes vaporization of the contact metal. The metal vapour is then ionized, which creates ideal conditions for arcing.⁽²⁰⁾

Although the period of this arcing is short, it causes a crater to be formed on the anode and a corresponding pip to form on the cathode. Owing to the enhanced local field about this pip, it may localise the arc on subsequent closing, thus exaggerating the damage done by the first arc. This causes the pip and crater system to rapidly penetrate the protective contact layer into the iron nickel alloy, where either mechanical interlock of the pip and crater create a short circuit,⁽²²⁾ or other failure modes outlined below occur.

As current carrying reed blades begin to separate, the area of contact gets less and the current density in the remaining areas gets larger until it is sufficient to melt the contact points and a molten bridge is formed. This bridge gets hotter and becomes unstable, eventually exploding and resulting in a net transfer of material from one electrode to the other. The direction and magnitude of this transfer depends on the conditions at the contact, and in many cases the controlling factors are not known.⁽¹⁸⁾⁽²³⁾ It is known that the molten bridge formed between iron/nickel contacts is about 20 times the magnitude of that of gold⁽²⁴⁾ and consequently material transfer, and subsequent failure is much faster in iron/nickel than in gold. In many cases, bridge transfer becomes the most serious erosion mechanism.⁽²⁴⁾

After a molten bridge has exploded, the gap between the separating reeds is filled with metal plasma, an ideal environment for arcing.⁽²⁵⁾ Arcing similar to that on making can occur, causing the same type of damage, but worse, because of larger spark due to the thermionic emission from the still hot reeds. Thermionic emission can cause arcing even with a contact that has not suffered from a molten bridge.

Both 'arc and make' and 'arc on break' are enhanced by the presence of non-resistive elements in the load circuit. Capacitance in the circuit will tend to give a very large current surge on contact closure, whilst a small capacitance and large inductance will give both a current pulse on closure and a voltage surge on opening.⁽⁸⁾⁽¹⁸⁾ These surges can be controlled by protection circuits of resistor and capacitor networks,⁽²⁵⁾ but these increase the cost of the switch and are only fitted when they are needed.

1.1.5. Contact materials.

1.1.5.1. Usual contact materials. The most commonly used contact

material for switching low to medium energy currents is gold; either pure or one of the many high carat gold alloys now on the market. Its low contact resistance, good electrical and thermal conductivity and freedom from surface oxide formation⁽⁸⁾ means that it can switch very low currents without loss. However, this metal to metal contact means that the pure gold is prone to cold welding, and with the small restoring force available in reeds, there is a tendency to fail to open. Because of this, pure golds are often diffused into the reed. Besides the improvement of the gold/substrate adhesion resulting from gold diffusing into the substrate, there is a reduction in the tendency to cold weld resulting from diffusion of iron and nickel into the gold.⁽¹⁴⁾ As well as hardening the gold, they form a thin oxide layer on the gold surface, thick enough to prevent cold welding, but thin enough to allow electrical conduction through it by the tunnel mechanism. Care has to be taken to prevent this layer from getting too thick and forming an insulating film.⁽²⁶⁾⁽³⁾

Because the diffused gold has better adhesion than plated golds, alloys are sometimes produced by multilayer plating followed by diffusion. Among the alloys which have been made by this method are alloys of gold with silver,⁽³⁾⁽²⁷⁾⁽²⁶⁾ with nickel,⁽²⁶⁾⁽²⁷⁾⁽²⁸⁾ with copper,⁽²⁶⁾⁽²⁹⁾⁽⁶⁾ with cobalt,⁽²⁶⁾⁽²⁸⁾ with chromium,⁽²⁸⁾ and with manganese.⁽²⁶⁾ Not all these alloys are equally successful. Copper and silver produce soft alloys and they may not be able to hold a coherent oxide film when under pressure. Both metals corrode fairly easily and silver salts are prone to migrate under electrical stresses,⁽³⁰⁾ although this is not likely to be important except in the smallest reeds. Nickel and cobalt both strengthen the gold and harden it, but only nickel appears to have been used a great deal. This may be due to

the strong effect of cobalt on the conductivity of gold.⁽³¹⁾ Manganese is probably not used because of its similar effect on the contact resistance of gold.⁽²⁷⁾ Besides these hardening effects, multilayer alloys have the advantage that they prevent the formation of iron rich particles on the reed surface, either by acting as sinks,⁽³⁾ or as a barrier layer.

Even in its alloy form, the relatively low melting point of gold and gold alloys causes the contact material to wear rapidly when switching high energy circuits. The most commonly used contact metal in these circumstances is rhodium,⁽⁶⁾⁽⁷⁾⁽³²⁾⁽⁵⁰⁾ as its high melting and boiling points prevent heavy losses at high energy switching, whilst its small tendency to form films allows it to switch quite small currents without serious loss. Rhodium is sometimes diffused into the reed, in a similar manner to gold.

1.1.5.2. Special purpose materials. Neither rhodium nor gold contacts are ideal for all purposes, and for some cases special reed coatings must be used. Where only high voltages are to be switched, tungsten can be used, as the voltage will be high enough to penetrate the oxide layer. The high melting point of the tungsten⁽³³⁾⁽³⁴⁾ will reduce the damage done on switching to insignificant levels. This is true of reeds coated with molybdenum,⁽³⁴⁾⁽³⁵⁾ tantalum⁽³⁴⁾ or chromium⁽⁷⁾ which have also been used for switching high power circuits. For switching very high voltages, up to 100,000 volts, a sprayed-on mixture of silver and tungsten has been claimed to be successful.⁽³³⁾

Silver on its own is used for switching high frequency alternating current where skin effects are important,⁽³⁶⁾ whilst the excellent thermal and electrical conduction characteristics of silver are used in switches where current surges of up to 15 amps are expected.⁽³⁷⁾ An almost

perfect reed is the mercury wetted reed, which has platinum blades wetted by mercury held there by capillary attraction.⁽³⁵⁾ This gives many millions of bounce free switchings with no arcing on opening. However, it is necessary to have external contact protection circuits as any arcing from larger than average surges would damage the wettability of the blades and seriously reduce the reed's life. Because of the pool of liquid mercury on the switch, it is necessary to operate the switch within a few degrees of the vertical, and this, together with its much higher costs than other reeds, has restricted its use to situations where it is essential to have 'perfect' switching (i.e., going from a perfect conductor instantly to a perfect insulator).

1.1.5.3. Composite contact coatings. Composite coatings have been used from early days in the form of underlayers to prevent the diffusion of iron to the surface, the usual underlayer being nickel. More recently, composites of gold with particles of carbon, silicon, phosphorous, sulphur or metal oxides⁽³⁸⁾ have been recommended,⁽³²⁾ whilst others have claimed carbon or air to be of value.⁽³⁹⁾ Solutions depositing a mixture of gold and tungsten carbide⁽⁴⁰⁾ have been suggested to improve reed life, but this seems unlikely at low loads.

Japanese workers have suggested the use of complex multilayer deposits of gold and rhenium⁽⁴¹⁾ as a way of preventing transfer of material by the molten bridge, by balancing heat flows. This method seems too complex for popular use, as is likely of another Japanese suggestion for an aluminium/nickel/gold multilayer.⁽⁴²⁾ Possibly a more practical line of work is the incorporation of a low electron work function element in the gold to enhance the possibility of planar erosion as opposed to the pip and crater method mentioned above.⁽²⁰⁾

Workers in America have been experimenting with a layer of barium⁽⁴³⁾ in the gold. Of more interest is the work that Davies and Watson have been doing on modifying the form of an element already present after gold plating.⁽⁴⁴⁾

1.1.5.4. Other contact coatings. Another attempt to spread the spark erosion over the surface was the use of 'spiky' deposits so as to give many sites with enhanced local fields for field emission on closing. Davis⁽²⁴⁾ used palladium with pyramids 3-6um high on the surface, but found interlocking of the spikes took place. Annealing the palladium to remove the spikes was a failure as undesirable diffusion effects took place.

Attempts to find economic alternatives to gold or rhodium plating have been made but without apparent success. Copper has been claimed to give improved life, with the contact resistance going down after about 10^7 operations.⁽⁴⁵⁾ Corrosion problems between plating and sealing the reeds may have prevented the widespread appearance of this reed on the market. Problems to do with plating the required thickness of ruthenium⁽³²⁾⁽⁴⁶⁾ or osmium⁽⁴⁷⁾ may be responsible for their lack of general acceptance of these contact materials.

It has been suggested that a reed with a gold amalgam contact area would have an improved operational life.⁽⁴⁸⁾ However, heating the amalgam causes it to lose mercury, even when under pressure,⁽⁴⁹⁾ and problems with the interdiffusion of iron and nickel may have prevented its more general use.

1.1.6. Problems with reeds. Whilst much development has taken place there are still problems with the reed switch and the perfect reed has yet to be found. Although gold may be ideal at low switching energies, its

use at higher power is severely restricted. Rhodium has problems with organic films due to its catalytic effect on any organic vapours entrapped in the envelope.⁽⁵⁰⁾ Substrate preparation,⁽²⁴⁾ and housekeeping in the plating shop have both been responsible for many reed failures.⁽⁵¹⁾⁽²⁴⁾ With rising prices, especially of gold and other precious metals, such failures are expensive.

1.2. Project Outline.

1.2.1. Outline of problems. Most of these problems with reeds are closely connected with the electroplating process. Hard wearing gold alloys can be made, as witnessed by developments in the field of wrought contact metals.⁽⁵²⁾ However, the number of alloys of gold which can be electroplated is limited,⁽⁵³⁾ and of these, many are not robust enough for industrial practice. Consequently, the choice of contact alloy tends to depend primarily on its plating (rather than its contact) characteristics.

The area to be plated is not chosen with a view to contact wear problems, but with the aim of maintaining a steady current density whilst plating. Most reeds are plated by immersing their tips in the plating vat to a depth of about 2 centimeters, thus minimising the effects of any slight variation in depth. As this method plates both sides of the reed, the functional area may be as little as 5% of the total plated gold.

Both these problems can be overcome, but not in an industrially acceptable manner. Stopping off or masking the reeds by hand is a very slow and time consuming operation, but automatic plating machines are expensive to develop and install. Plating solution development is a (relatively) straightforward operation, but it is doubtful whether the reed manufacturers show much enthusiasm for yet another 'new' and

'improved' plating solution. In any case, it was thought to be unlikely that this work could compete with the plating supply houses, with their greater manpower and resources.

It was therefore decided to try and develop an alternative coating method for used switches which would allow close control of the coated area, and if possible allow a greater, or at least different, choice of alloy to be produced.

1.2.2. Alternative coating methods. A survey of the possible alternative coating methods showed that most of them were as restrictive as the plating process was. Chemical (electroless) plating would still plate both sides of the reed, but depth control was not so critical. However, the plating rate is slow⁽⁵³⁾ and the range of alloys produced is even more restricted. Chemical coating by the use of organo-metallics⁽⁵⁴⁾ could be contained only on one side of the reed, and mixed resins could produce alloys on firing⁽⁵⁵⁾, but the coating rate to achieve any real thickness would be very slow.

Mechanically fixed composites in the form of bimetallic strips are at present in use⁽⁵⁶⁾ and there seems to be no problem with alloy development, as any wrought alloy could be used. However, the need to replace machinery, geared to using wire, with machines capable of handling strip may be holding up the general acceptance of this method. This method will also produce a fair quantity of scrap from the stamping process, which will contain a small amount of gold. This will need to be recovered, an operation which will tend to raise the overall cost of the process. Mechanically fixing the contact material onto the reed blades after stamping out could be tried,⁽³⁴⁾⁽⁵⁷⁾ but it is not known if any of the present day methods were capable of handling the very small, thin coating that would be required. The production of the very small

contact inserts themselves would present difficulties.

As seen earlier,⁽³³⁾ metal spraying has already been used on reeds, although not for gold contacts. Because of the small area of the reed being coated, there must be a considerable wastage of metal on the masking and surrounds, which could reach important proportions with a metal as expensive as gold. The cost could, of course, be brought down by alloying the gold, which would be very easy to do using this method. The use of hot dipped metal was not considered suitable, mainly because of the high melting point of the gold, and the uneven thickness which would result on drying.

There are many processes which operate in a vacuum, all of which seemed to be hampered by the necessity of loading and unloading the vacuum chamber. Although semi-continuous processes can be devised, the overall coating time may still be too long for a product which is being produced in hundreds of millions a year.⁽²⁾ Some reeds are already being made by evaporation of gold by an electron or ion beam current,⁽⁵⁸⁾ but too much gold must be lost on the mask⁽⁵⁹⁾ and vacuum system to make this an attractive proposition. Cathode spluttering⁽⁶⁰⁾ may be better as the metal is attracted to the reed by a high voltage, and losses to other parts of the system are low. Plating rates of $1\mu\text{m}/\text{min}$ have been claimed⁽⁶¹⁾ and a variety of alloys and mixtures have been produced.⁽²⁰⁾⁽⁴³⁾

Other vacuum coating methods are unlikely to be useful. Vapour deposition, or gas plating, is probably insignificant, due to the nobility of gold and the difficulty in producing it in a gaseous form. Vacuum metallizing of gold is not a commercial proposition as the vapour pressure of gold at usable temperatures is too low.⁽⁶²⁾

Another method considered was the printing of the gold in a suitable carrier, followed by the removal of the carrier. Two types of

carrier were possible, an inert organic carrier of the kind developed by thick film printers in microelectronics,⁽⁶³⁾ or the use of a pasty mercury/gold amalgam. The inert carrier could be removed by either burning or evaporating off at fairly low temperatures, but the mercury could only be removed by evaporation at high temperature under vacuum. This limits the alloys possible to those which will amalgamate with mercury, and have a lower vapour pressure.

1.2.3. Choice of method. The final choice of method rested not only on the conditions outlined above, but also on its industrial feasibility. The method did not have to be so complex as to require skilled or trained men to operate it, nor must it require highly expensive capital equipment. To be industrially acceptable it must have a high throughput with as little wastage of gold as possible. Preferably it should also only use equipment which was available at Aston, or easily obtained or loaned.

These considerations limited the choice of the method to either mechanical fixing or to printing the gold, and because of its novelty in this application, it was decided to work on the last idea - the printing of gold onto the contact faces.

1.2.4. Thick films. The thick films at present in use in microelectronic technology usually comprise of three components.⁽⁶⁴⁾ There is the organic vehicle which gives the paste the correct rheological properties for printing.⁽⁶⁵⁾ The low boiling point constituent of this paste is then usually removed by drying at between 100-200°C leaving a higher boiling point material behind to give the paste some 'green' strength. Another component is the inorganic binder, usually a glass which melts on firing and forms a bond between the metal and the substrate, which is usually alumina.⁽⁶⁶⁾ This glass has recently been replaced by reactive metal oxides said to give better adhesion.⁽⁶⁷⁾⁽⁶⁸⁾

The final component is the metal itself, whose composition varies depending on the properties that are required. Gold, silver, palladium and other metals are used for conducting paths,⁽⁶⁹⁾ whilst resistors are often mixtures of precious metals and metal oxides.⁽⁷⁰⁾⁽⁷¹⁾ After printing and drying, the pastes are fixed, usually in air, on a moving belt type of furnace with a carefully controlled thermal profile. The peak firing temperature is usually between 600°C and 1000°C.⁽⁷²⁾

1.2.5. Thick film problems. Practically all thick films are used on alumina substrates,⁽⁷²⁾ although similar methods are used to fix printed labels onto glass and pottery. Thick film has been applied to metals, but only to those which have a coherent film of oxide present, such as magnesium or stainless steel.⁽⁷³⁾ Such an oxide film, if present on the reed blades, would interfere with the conduction of the current. Other problems which may arise with the use of thick films on reeds, would be mechanical interlocking due to the roughness of the surface finish; the lack of adhesion to an oxide free metal; and the porosity and density of the final fired deposit.

In development of pastes, powder production must be considered. Gold powder can be bought from thick film supply houses, but only in certain sizes and forms. It is also difficult to obtain the desired alloy powders, and so, control over the make-up of the pastes would be somewhat limited. Producing the gold powders at Aston seemed to be the best solution to these problems, but was not without difficulty itself, as almost no information on industrial methods was available.

1.3. Powder Production.

1.3.1. Powder requirements. Before choosing the production route for the gold (and other metal) powders, it is necessary to state clearly in what form they are required. As the life of the reed is, in some cases,

a function of the thickness of the coating,⁽⁷⁴⁾ a dense deposit should be aimed for, and so the powder itself should be dense, and of course, pure. As the powder will be packed together without too much vibration or pressure, there must be little mechanical interaction, and so the particles should be smooth with no re-entrant angles. Also for ease in packing the powders should be all one shape, and as closely graded in size as possible. Owing to technical⁽⁵⁾ and economic constraints on the final deposit thickness, the particle size should be less than 10 μ m.

1.3.2. Production route. Most of the available powder metallurgy production methods were considered,⁽⁷⁵⁾⁽⁷⁶⁾ but were eliminated due to the size and shape conditions outlined above. Crushing and milling were not feasible, due to the malleability of the gold, and the high waste losses which might occur. These high waste losses also excluded shotting or atomising the gold, which would be impractical due to the small size required of the final particles. Methods using molten gold were not considered due to the fairly high temperatures involved, and thermal decomposition or reduction of gaseous products were impractical because of the lack of the necessary equipment. This also excluded reactions which occurred under pressure.

The eventual choice was between chemical precipitation from solution, or electrical discharge from solution. Both require only minimal costs, require no additional equipment, are fully controllable, and are (theoretically) capable of 100% metal recycling. Chemical precipitation was finally chosen as it seemed to be more versatile, with a larger range of precipitation systems being available. Electrical discharge would also have much the same limitations on possible alloys as electroplating.

1.3.3. Theoretical considerations for chemical precipitation. The formation of precipitates in solution is an extremely complex subject, some of the fundamentals of which are not yet fully understood.⁽⁷⁷⁾⁽⁷⁸⁾ The properties of the precipitates are a function of several conflicting reactions, the most important of which are: the generating process, which in this case is the chemical reduction of gold salts; the nucleation of the gold particles; and the growth of these particles to their final size. Variations in the conditions of the reaction, such as the efficiency of the mixing, will alter the rates of all these reactions, giving different final properties.

1.3.3.1. The reduction reaction. The rate of the reaction is controlled by both the thermodynamics and kinetics of the reaction. The thermodynamics determine whether the reaction is energetically possible, and the theory, with metal salts being reduced to metal, is similar to that of corrosion reactions, but in the reverse direction. The thermodynamic driving force is related to the differences of the electrode potential of the cell, the potential of each electrode being given by (for a reversible metal ion-metal electrode) the Nernst equation:-⁽⁷⁹⁾

$$E_{M^{z+}/M} = E_{M^{z+}/M}^{\circ} + \frac{RT}{zF} \ln [M^{z+}]$$

where $E_{M^{z+}/M}$ is the electrode potential under the conditions used, $E_{M^{z+}/M}^{\circ}$ is the standard electrode potential, R is the gas constant, T the absolute temperature, F the Faraday, z the number of electrons involved in the reaction and $[M^{z+}]$ the activity of the M^{z+} ions in the solution. As gold is a very noble metal, with a standard electrode potential of +1.43 volts,⁽⁸⁰⁾ there are many reducing agents available.

However, because of the low temperature of the reactions used (20-100°C) the kinetics of the reaction play a most important part.

For example, under many conditions, nickel should be precipitated from solution by hydrogen at one atmosphere, but the amount of nickel produced is negligible. This is because the molecular hydrogen has a stable electron configuration, with a large dissociation energy which must be supplied before reaction can occur.⁽⁸¹⁾ Reaction will only occur if energy is supplied, by working at high temperatures and pressures, or the activation energy is lowered by use of catalysts or intermediate reaction compounds.⁽⁸²⁾

The kinetics of a reaction are dependent on the phase and energy state of each of the components and on the number of elemental reaction steps and their activation energies. It is thus very difficult to generalise about the reaction kinetics and experiments to determine them have to be carefully designed so as to eliminate the effects of mixing, and precipitation kinetics.

1.3.3.2. The nucleation process. This is similar to the reduction reaction, in that nucleation should start as soon as the concentration of precipitant in the solution exceeds saturation, but due to the kinetics of nucleation, this does not occur until quite high super-saturation ratios occur. (The super-saturation ratio is the ratio of the concentration of material in a solution to its saturation concentration at that temperature. Nucleation should occur when the ratio is greater than one). The kinetics in this case are better understood than those for the reduction reaction (see for example Walton,⁽⁷⁷⁾ and Nielsen⁽⁷⁸⁾). In a super-saturated solution, as a number of atoms come together to form an embryo nucleus, they reduce their total entropy, and release a quantity of free energy related to the volume of the embryo. However, the atoms on the surface layer are in a state of higher potential energy and this surface energy will tend to make the embryo redissolve. This

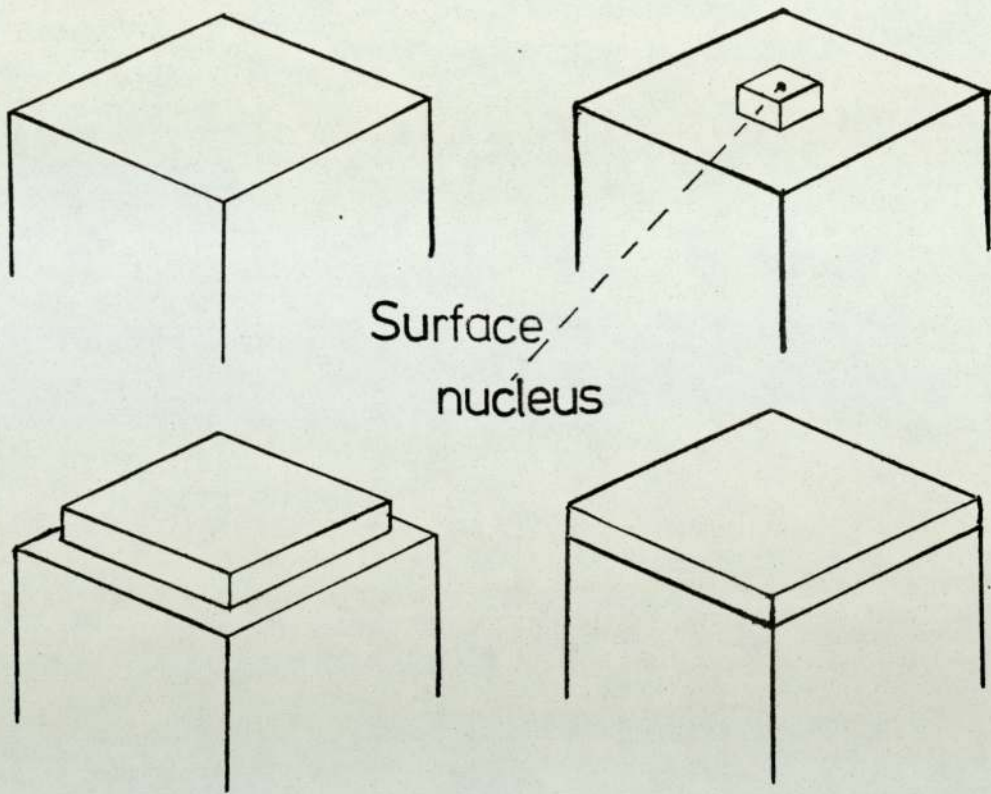
energy, however, which on a macroscopic scale is equivalent to surface tension, is related to the surface area and so for larger embryos the volume term, which encourages growth, will predominate. This gives rise to a critical size of nucleus above which it is stable and will grow, and below which it will redissolve. The size of this critical nucleus is related to the super-saturation ratio, which also controls the frequency of finding an embryo of the critical size.⁽⁷⁸⁾ These effects combine to produce a situation where a super-saturated solution may be metastable, whilst a slight increase in supersaturation may produce an avalanche of stable nuclei. Nielsen⁽⁷⁸⁾ has worked out an example whereby doubling the super-saturation ratio increased the nucleation rate by a factor of 10^{23} .

The metastable super-saturation ratios found in practice are much lower than these shown by calculation to be metastable. This is because particles are nucleating at much lower activation energies either by forming intermediate compounds,⁽⁸³⁾ or by nucleating on to already existing impurities. These heterogeneous nuclei are present in all solutions no matter how well purified, at concentrations varying from $10^{(84)}$ to $10^{8(77)}$ nuclei per millilitre. By nucleating on pre-existing nuclei, the precipitating species avoids most of the surface energy effects which would inhibit nucleation, and growth can occur straight away. The efficiency of the various impurities when acting as nuclei can vary depending on the degree of mismatch between the impurity and the precipitating species lattice. Thus the activation energy for heterogeneous nucleation will range from practically zero - for nucleation on seeds of the precipitating system - up to the activation energy for homogeneous nucleation.

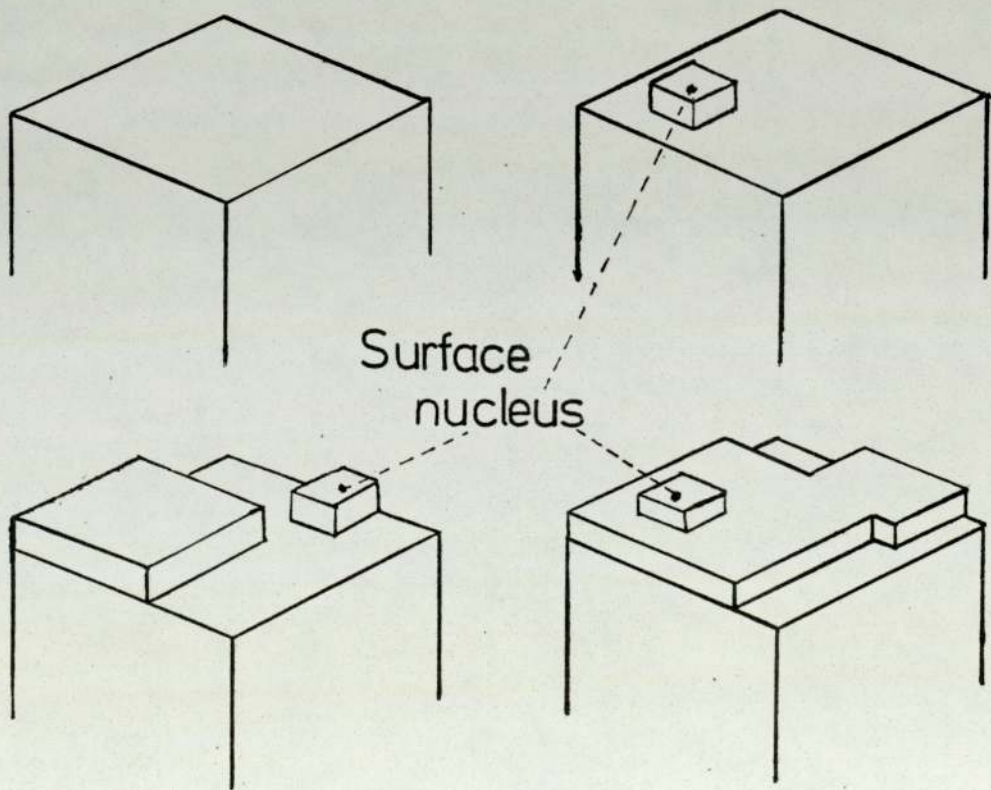
1.3.3.3. Growth reactions. The slight activation energy of 'heterogeneous' nucleation on like material is caused by the necessity of nucleating a growth step on the existing material, if one does not already exist. For most of the lower super-saturation ratios this is the rate controlling step for growth, and there are two ways of overcoming this. The method requiring the smallest activation energy is mono-nuclear layer method, where a single growth point is nucleated on a crystal face and this grows until the face is covered (fig. 1.3.), when the growth step must renucleate. Thus each layer will come from one nucleus. As the rate of surface nucleation is related to the super-saturation (as well as the crystallographic plane⁽⁸⁵⁾), at low super-saturation the nucleation rate will be very small and growth will practically cease, whilst at high super-saturation nucleation will be easy and many nuclei will form on one crystal face which will then grow together. Nucleation can occur on faces which have not yet totally covered the surface. (fig. 1.4.). The nucleation rate will continue to rise as the super-saturation is raised, until eventually this polynuclear layer growth ceases to be the controlling factor, and growth is controlled by diffusion of atoms to the precipitate surface.

The other growth mechanism will occur at dislocation sites. This has a higher activation energy than surface nucleation, but if the dislocation is a screw dislocation, then nucleation need only occur once (fig. 1.5.). Consequently, this growth mechanism is found at lower super-saturation levels than mononuclear layer growth, and will give rise to spiral growth terraces.

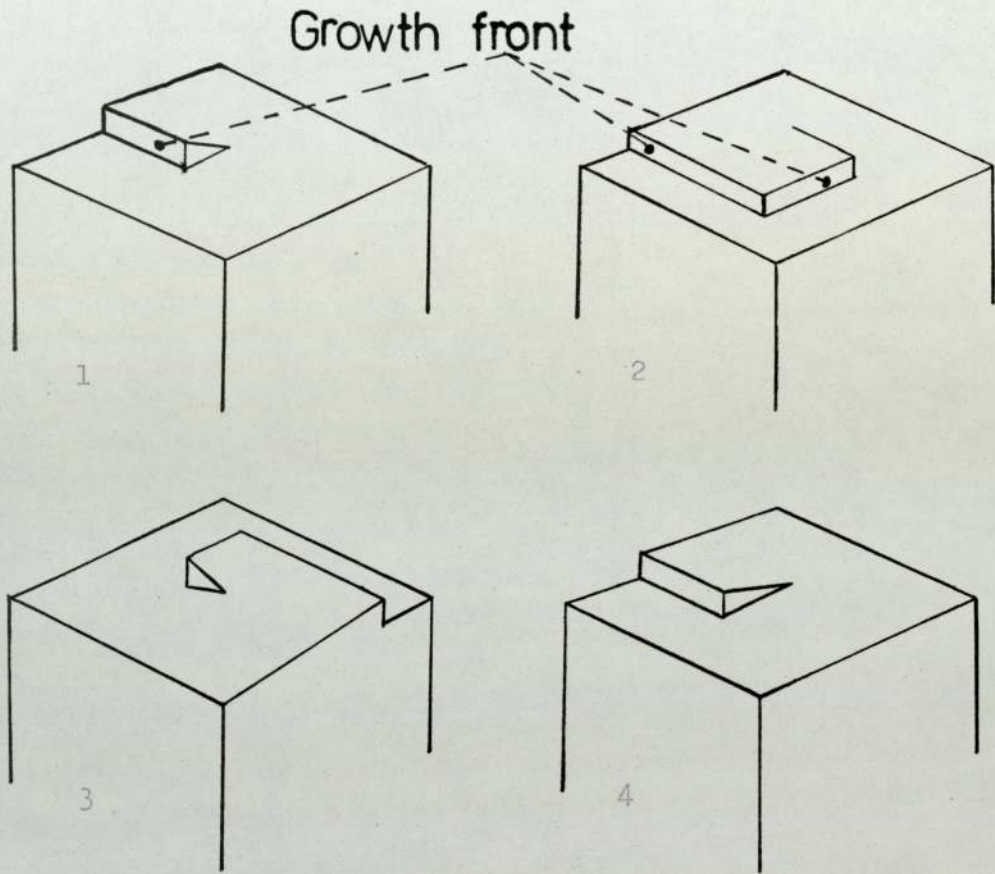
1.3.4. Particle morphology. The overall driving force for a crystal shape under equilibrium conditions is the reduction of the surface free energy of the crystal to a minimum, and so, low indices planes with their



1.3 Stages of growth by mononuclear layer growth mechanism.



1.4 Stages of growth by polynuclear layer growth mechanism.



1.5 Stages of growth by spiral dislocation growth mechanism.

lower surface tension will tend to predominate. This is because the high energy, high indices planes are rougher and therefore grow faster and eventually eliminate themselves.⁽⁸⁵⁾ However, this equilibrium shape is rare as the kinetics of nucleation and growth tend to overshadow it.⁽⁷⁸⁾ At very low super-saturations, nucleation will be on the few most energetically favourable heterogeneous nuclei, and growth will slowly take place by dislocation nucleated growth. The particles formed will tend to be a few large equilibrium structures (as growth will be slow) with pyramidal growths on them which grow steeper with increasing super-saturation.⁽⁷⁸⁾

However, with increasing super-saturation, mononuclear surface nucleation takes over, which is likely to give more 'equilibrium' shaped crystals. Owing to the higher super-saturation, more hetero-nuclei will be brought into operation but whether the particles formed will be larger or smaller than before depends on the spread of efficiencies of the impurities, as hetero-nuclei. This also applies to the polynuclear layer growth mechanism which will follow as the super-saturation ratio is raised. This method will give rise to less crystalline looking particles as the ease of nucleation will allow nucleation on incomplete crystal faces. For homopolar crystals, such as metals, extra growth will tend to occur on the plane centres, not on the edges.⁽⁸⁵⁾ This will continue to break up the smoothness of the crystal shapes, until diffusion of the precipitating atoms to the surface becomes the controlling factor.

The shape adopted by a diffusion controlled particle is difficult to predict, as it will depend strongly on the initial shape of the particle. Some smooth shapes have been shown to be stable in these conditions, whilst other shapes, such as cubes, have been shown to develop

spikes. When these spikes break through the diffusion layer they rapidly develop into a dendrite. The dendrites will become larger in size as the super-saturation is increased, until the super-saturation is large enough to allow homogeneous nucleation to occur. According to Kolthoff and van't Riet,⁽⁸⁶⁾ with increasing ease of nucleation, many very tiny particles are formed, and as the diffusion zones are often the same order of size as the particles, then diffusion control is in operation again.

This scheme of morphology changes with increasing super-saturation, is similar to that found with increasing current density with electro-deposits. At very low current densities, polynucleated layer growth occurs which rapidly becomes diffusion controlled, to give smooth surfaces. Robinson and Gabe⁽⁸⁷⁾ found that with high speed copper deposits, nodules were grown in the diffusion controlled region. If electrocrystalization can be regarded as an essentially one dimensional form of crystal growth, then these results seem to indicate that a sphere would be a stable configuration for diffusion controlled particle growth.

As the current density is increased, breakdown of diffusion control occurs and preferential growth along certain crystal planes give pyramids or dendrites. The onset of the limiting current density and diffusion control is not paralleled in particle precipitation, due to the onset of homogeneous nucleation.

1.3.5. Particle size. The final size of the powders and their range of sizes is dependent mainly on the nucleation process. To obtain a monodispersed powder of very small size range, it is necessary to have only one burst of nucleation followed by growth to the final size. This nucleation can result from either homogeneous or heterogeneous nucleation,

but in both cases it is important that the super-saturation drops below the level where further nucleation is possible. This is fairly easy with heterogeneous nucleation, as the less efficient impurities will require greater super-saturation to bring them into operation. However, with homogeneous nucleation, super-saturation below the maximum may still be sufficient to induce nucleation, albeit at a low rate. This would result in a 'tail off' of smaller particles.

If the super-saturation varied, as when a generating reaction was present, then it would be difficult to obtain a monodispersed precipitate. It may be possible if the precipitation processes were faster than the generating process, but if they were equal, or the rate of generation faster, then nucleation and growth would occur concurrently and a spread of sizes would result.

Work by Turkevich et al.,⁽⁸³⁾ and others⁽⁸⁸⁾ have shown that there is an induction period for nucleation and claim that this caused by the necessity to generate intermediate compounds, which then reduce the gold salts. This means that there is a spread of results arising from both the variations in 'activated' reducing agents, and the variations of reduced atom super-saturation.

All these assumptions are based on perfect mixing of the reagents, but in practice there are different efficiencies of mixing.⁽⁷⁷⁾⁽⁷⁸⁾ This will give rise to local variations of concentration, pH, temperature, etc., which will alter the local rates of nucleation and growth, and give rise to a spread of particle sizes. Even assuming a very fast mixing period of 10^{-4} to 10^{-3} seconds⁽⁸⁹⁾ if the reaction induction period is faster than this, the mixing rate will control the process.⁽⁷⁸⁾ These mixing periods were obtained using special 'T piece' mixing equipment and the mixing periods using beakers and mechanical

stirring would be many orders larger than this, in extreme cases possibly stretching up to hours.

The size range will also be influenced by the amount of agglomeration occurring. Agglomeration is the sticking together of particles after chance collisions, and the particles are held together either by ionic attraction or by mechanical interlock. In both cases the agglomeration may be held together by subsequent deposition of reduced materials. As metal atoms are usually uncharged, agglomeration is unlikely to be important except with very rough precipitates.

Both the size and shape of the particles are strongly influenced by the presence of other ions, either in solution or absorbed onto the growing surface. Precipitation from different solvents produce many cases of different crystal habits and even small additions to the solvent can produce distinct crystal changes.⁽⁹⁰⁾ The effects are complex to interpret as the same ions can have different effects at different concentrations. Morriss and Milligan⁽⁹¹⁾ found that small copper additions stabilised gold colloids whilst larger additions led to precipitation. These effects are due to the alteration of the size of the particles of gold. But for example, with electrodeposited nickel, the effect of the copper ions is to alter the growth characteristics, not the size.⁽⁹²⁾

1.3.6. Gold powders. There is a certain amount of information on the precipitation of gold particles from aqueous solutions, although mainly in the field of gold colloids. When the mechanisms outlined above are applied to this information, it is found that the situation is even more complex.

Turkevich et al.,⁽⁸³⁾ working on a variety of gold colloids, calculated that the diameter of the nucleus was about 30\AA , a value which has been supported by other workers.⁽⁹³⁾ This size implies an embryo of about 10^6 atoms, and Turkevich uses these findings to argue the case for an intermediate compound or 'organiser'. However, Uyeda et al.⁽⁹⁴⁾ claimed, after studying the twin bands in colloidal golds that the nucleus diameter is in the range $10\text{-}20\text{\AA}$, which agrees with the work of Rinde (19\AA)⁽⁹⁵⁾ and Morriss and Milligan (10\AA).⁽⁹¹⁾ Morriss and Milligan calculate that this nucleus contains 18 atoms, which is close to the theoretical number of 19 for a hexagonal face of 10\AA packed by face centred cubic arrangement. This would give rise to (111) faces which is in agreement with Kossel-Stranski's theory of crystal growth for nearest and next nearest neighbour interactions,⁽⁸⁵⁾ which would give rise to a cube-octohedron shape. It is also in agreement with Uyeda's⁽⁹⁴⁾ claim that the nucleus shape is a cube-octohedron, or a tetrahedron of four (111) planes.

Of these two, the smaller sized nucleus seems to be the more likely, as Turkevich's 30\AA estimate was based on growth experiments, whilst Uyeda's $10\text{-}20\text{\AA}$ was based on direct observation. It may be that particles smaller than 30\AA do not grow, or do not act as nuclei for the growth solution that Turkevich used. Also, to produce any considerable numbers of embryos of about 10^6 atoms, some form of organiser would be necessary. Whilst it may be possible to form intermediate compounds with 10^6 gold atoms and with some of the organic reducing agents mentioned by Turkevich, it would be difficult to see this happening with some of the simpler reducing systems, such as hydrogen⁽⁹⁶⁾ or radiation.⁽⁹⁷⁾ However, this is in some respects irrelevant, as all this work was carried out on colloids with low gold concentrations. The solutions used for this work are considerably more concentrated, and will therefore give rise to greater super-saturation with consequently smaller critical

nucleus size.

When attention is turned to the particle shape, it is found that the situation is not so sharply defined. The equilibrium shape for gold reduced from aqueous solution appears to be a flat triangle or hexagon of (111) planes bounded by (100) planes. These are found in a variety of precipitates reduced by different reducing agents⁽⁸³⁾⁽⁹¹⁾⁽⁹⁷⁾ (98) from a variety of salts.⁽⁹⁹⁾⁽¹⁰⁰⁾ This agrees with the theory (1.3.4) in that the (111) is the plane of highest density in the face centred cubic system.

The triangles or hexagons appear to be defect free when viewed by TEM⁽⁹⁴⁾⁽⁹⁷⁾⁽¹⁰⁰⁾ except in these cases where growth has occurred by spiral growth around a screw dislocation.⁽⁹⁸⁾⁽⁹⁹⁾⁽¹⁰¹⁾ Otherwise, growth seems to be a random aggregation of small plates which re-orientate themselves later.⁽⁹⁸⁾⁽¹⁰²⁾ Thus, crystalization tends to be a slow process extending in some reactions up to a week.

These plates are only found in acid solution and this has led to the theory that they are caused by excess hydrogen ions sitting on the growth sites.⁽⁹¹⁾ The presence of screw dislocations suggests that if this is the case, the hydrogen ions prevent nucleation, not growth. However, in most cases there are spherical particles present as well as triangles and hexagons,⁽⁸³⁾⁽⁹¹⁾ and in some cases only spheres occur even at very low pH values. By implication, these must be the unmodified crystal form, when excess hydrogen ions are absent. On some of the plate-like crystals, secondary growths are seen, and these are caused by impurity ions being absorbed into the surface and promoting growth.⁽¹⁰¹⁾ It may be that spheres are special cases of this phenomenon. Alternatively, they may be the result of polynuclear layer growth, which according to Kossel-Stranski's theory,⁽⁸⁵⁾ would preferentially nucleate

on the centre of planes rather than at the edge. With layers nucleating before the previous layer has reached the edge, the crystalline shape is lost, and roughly spherical particles will result.

The two forms can exist at both the low concentration of gold used for colloids (2×10^{-5} molar)⁽⁸³⁾ and at the higher concentrations used for producing gold powder for thick film work (up to 3 molar).⁽¹⁰⁴⁾ This would seem to rule out a connection with super-saturation. The by-products of the reduction process may be involved, but this would not explain why only some of the particles are affected. With many different by-products available, more modifications to the crystal habit might be expected.

Other shapes are found, but these always tend to be irregular. Some of these, such as the ones reduced by carbon monoxide from gold chloride solution, are thought to be due to agglomeration of smaller particles;⁽⁸³⁾ but others, such as the reduction of gold fulminate by hydrazine sulphate⁽¹⁰⁵⁾ probably have irregular particles due to the fact that the gold salt being reduced is in solid form.

1.4. Paste and Film Production.

1.4.1. Mixing and firing. The little published information there is on paste preparation, suggests that mixing is important to break up the clusters of particles and ensure an even distribution throughout the paste.⁽⁶⁵⁾ Most work appears to use three to seven roll mills, but some development work on small quantities of material use a palette-knife and ointment block⁽⁶⁷⁾ for mixing.

Work on closely graded irregular particles have shown that they can be packed to a density of 43-55% solids with the density improving as they become more spherical, until as spheres, they pack to a density of

between 60-64% solids.⁽¹⁰⁶⁾ It is possible to improve this packing by filling the voids left between the spheres with smaller sized spheres, and then filling the voids between these with even smaller spheres. Using this method and four graded sizes of spheres in the ratios of 1:7:38:316, McGeary⁽¹⁰⁷⁾ obtained a packing density of 95% solids. This size range would be impractical in this case, for if the largest particle was 5-10 μ m in diameter, the smallest ones would be only 0.01-0.03 μ m and would prove difficult to produce and handle. However, binary packing mixtures with more realistic size ratios of 1:7-1:10 can produce densities of up to 86% solids.

These packing experiments were carried out on much larger particles than would be used in this work, and this is likely to affect the packing. Fine particles tend to have more interparticle cohesion and this will reduce the efficiency of the packing. It was found, for example, that smooth microspheres of 25-50 μ m diameter will only pack to a density of between 35-42% solid.⁽¹⁰⁸⁾

It is not clear how relevant this information is to the packing of powders by thick film printing. The vehicle used will interfere with the free flow of the particles and so is likely to reduce the density of the dried deposit. In addition to this, the movement allowed in silk screen printing depends upon the viscosity and printing conditions,⁽⁶⁵⁾ but is unlikely to compare with the vibrational energy given to the dry powders in the work above. Thus it seems likely that the density will be towards the low end of the range. This was confirmed by the work of Williams et al.,⁽¹⁰⁹⁾⁽¹¹⁰⁾ on pressureless sintering of nickel powders. Although they were trying to produce porous deposits, they were obtaining only 10% solid density, using a method analogous to screen printing. Methods analogous to printing or dipping were producing lower densities and correspondingly poorer surface finishes.

1.4.2. Surface finish. This property is not of particular interest to thick film manufacturers and users, and so there is little information on the subject. What little there is, tends to confirm the findings from the patents that either spheres or mixtures of spheres and flakes give the better pastes, than flakes alone or irregular particles. Flake silver was found to have a surface profile range of $120,000\text{\AA}$ (CLA= $6\mu\text{m}$),⁽¹¹¹⁾ whilst gold spheres under similar conditions gave a range of $30,000\text{\AA}$ (CLA= $1.5\mu\text{m}$). Glass free reactively bonded pastes were slightly rougher at $50,000\text{\AA}$ ($2.5\mu\text{m}$ CLA) surface profile range, but this is said to be due to the glass acting as a filler for surface irregularities, not to a higher metallic density. The gold powders in these cases seemed to have a particle diameter of approximately $10\mu\text{m}$.

1.4.3. Sintering and firing the deposits. The sintering theory of metals and ceramics is a complex subject, and has been the topic of many papers and reviews.⁽¹¹²⁾⁽¹¹³⁾ Only a simple, qualitative summary will be given here, with the main sintering reactions examined.

Kuczynski⁽¹¹⁴⁾ has studied atomic transport mechanisms and has suggested that there are four possible transport mechanisms, viscous flow, evaporation and condensation of material, volume diffusion and surface diffusion. Of these, viscous flow is possibly the slowest but is likely to contribute to all the other mechanisms, although it has been claimed to be predominant in some cases⁽¹¹⁵⁾. This viscous flow is really the diffusion creep of the Herring-Nabarro mechanism.⁽¹¹²⁾

Vapour phase sintering has been found to be the predominant sintering method for some metal oxides,⁽¹¹²⁾ but the process cannot produce shrinkage. There have been no reports of its being the dominant process for any metals. The usual methods for metal sintering is either volume or surface diffusion, with volume diffusion being the most common at highest

temperatures. Whether diffusion occurs by lattice diffusion or by grain boundary diffusion, seems to depend on the solid solubility of the metals in the lattice. Thus grain boundary diffusion is found with iron, cobalt, and nickel, in aluminium; but lattice diffusion is found with the same metals in gold.⁽¹¹⁶⁾

Surface diffusion has a lower activation energy and will therefore be more prominent at lower temperatures. It will also be more prominent with smaller particles, as they have a larger surface to volume ratio, and studies of submicron particles in the electron microscope have shown that this is so.⁽¹¹⁷⁾ However, the driving forces for both these sintering processes is the reduction of surface energy and any contaminant is likely to lower this, and to affect surface diffusion more than volume diffusion.⁽¹¹⁸⁾ It is also claimed that surface diffusion cannot cause pore shrinkage, and densification will therefore not occur.⁽¹¹²⁾

Equations for the rate of neck growth with time exist for all of the growth mechanisms, but many of the numerical values of these are in question.⁽¹¹²⁾ Even when they are agreed upon, experimental results rarely coincide, and it may well be that more than one mechanism is operating at once.

If there is a multi-component system to be sintered, then in addition to the problems over mechanisms, there are complications from the two or more different types of particle. Assuming solid solubility exists between them, then it is important that the interdiffusion rates between them are fairly similar. If not, then excess vacancies are formed,⁽¹¹²⁾⁽¹¹³⁾ which will encourage diffusion if they remain in the lattice; but if they condense to form a pore, then they can produce undesirable effects. Stablein and Kuczynski⁽¹¹⁹⁾ working on gold and nickel wires, showed that until the mixtures had had time to homogenize the number of contacts between the gold and the nickel was in fact decreasing with time, as excess vacancies in the

gold condensed around the necks and undercut them. As these were fairly large samples (150-250 μ m) at high temperatures (900 $^{\circ}$ C), then volume diffusion was the predominant mechanism, and this neck breaking would be unlikely to occur with surface diffusion.

1.4.4. Sintering of gold and gold alloys. It is not clear by which mechanism gold powders sinter. Pashly et al. used very fine (submicron) particles,⁽¹¹⁸⁾ to show ~~sur~~face diffusion to be more likely, even up to sizes of 1 μ m diameter. However, the low sintering temperature (400 $^{\circ}$ C) makes this result untypical. It would really need more results at different sizes and temperatures, to obtain a realistic idea of the change-over conditions.

With alloy sintering there is less information available. Knowledge of interdiffusion rates is of somewhat limited use, as in most cases only binary diffusion is considered, whilst in practise four or five metals are interdiffusing at once, and this can lead to anomolous results. In addition, none of the work was carried out with particles as small⁽¹¹⁹⁾ as those used in this work, and so the results would not be of direct relevance.

Owing to the natural division of the work into two halves, (1) the production and properties of powdered gold and other metals, and (2) the use of these metals to make up the final products, the thesis is divided similarly at this point. The experimental details of the powder production and the properties of the powders are followed by a discussion of these results, before the work on firing the pastes is reported and discussed. A general discussion on the findings of the work then follows.

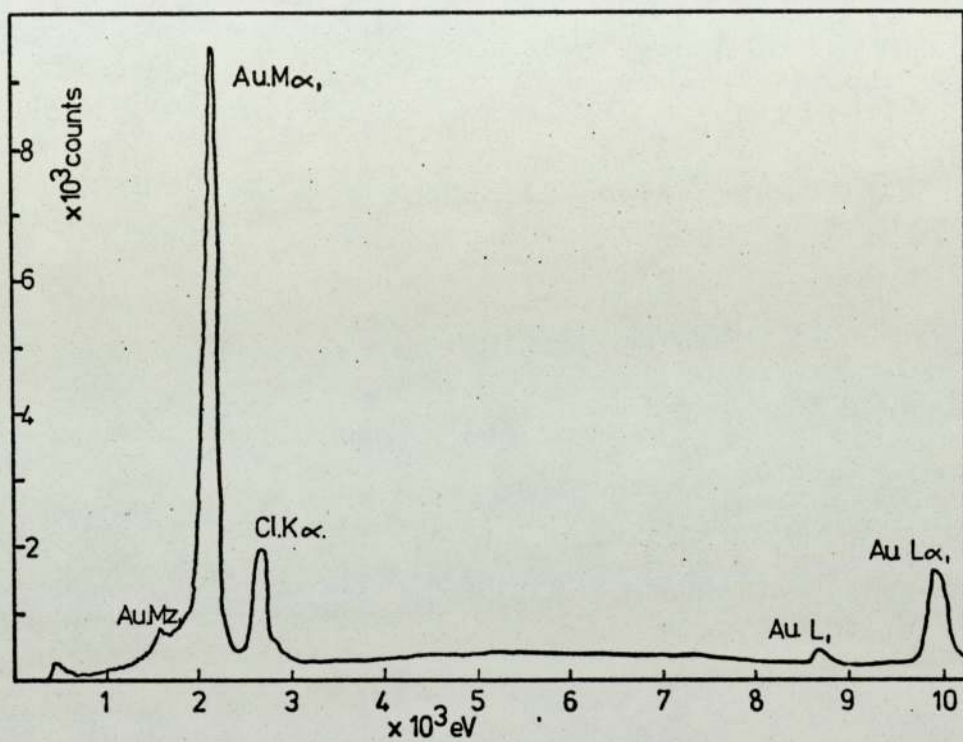
2. EXPERIMENTAL DETAILS OF POWDER PRECIPITATION.

2.1. Materials Used.

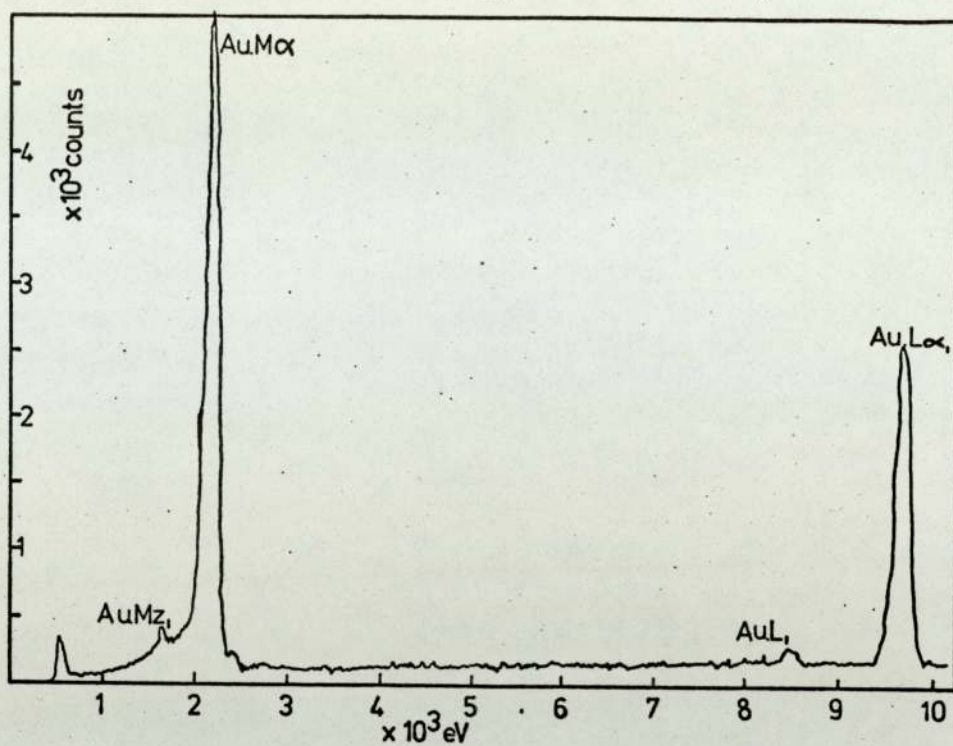
The main source of gold for this work was laboratory grade brown gold chloride ($\text{HAuCl}_3 + \text{aq.}$) supplied by Hopkins and Williams Ltd. This contained about 51% gold and a sample analysed by the 'Kevex' energy dispersive X-ray analyser contained no significant impurities (fig. 2.1.). Palladous Chloride was also obtained from Hopkins and Williams.

As the work progressed the gold was recycled and re-used. The reclaim was carried out by dissolving the gold or gold salts in aqua regia (75% HCl; 25% HNO_3), and reducing the solution almost to dryness in the presence of hydrochloric acid. Repeating this procedure several times, after adding more hydrochloric acid, drove off the oxides of nitrogen and left the gold as gold chloride. The solution of this gold chloride was then reduced to gold by a 5% aqueous solution of sulphur dioxide. The gold was washed before being redissolved in aqua regia and purified, as above, before being reprecipitated by oxalic acid solution. This precipitate was washed and dried, and was then ready for re-use. As the sulphur dioxide separates the gold from all other elements except selenium, tellurium, lead, the alkaline earths, and platinum and palladium when together, and oxalic acid will separate the gold from the palladium,⁽¹²⁰⁾ then this cycle will separate the gold from all the elements likely to be present in the reclaim. This was confirmed by Kevex X-ray analysis (fig. 2.2.).

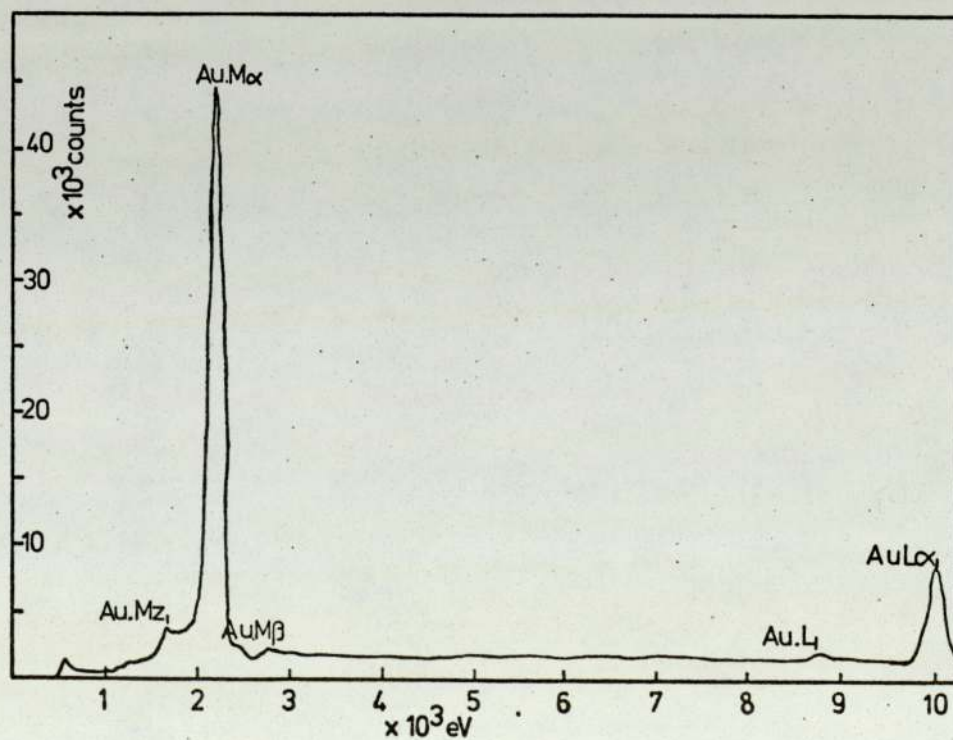
Wherever possible, all chemicals used in this work were 'Analar' or equivalent grades, the exceptions being noted as they occur. The water used was de-ionised with a resistivity greater than $500\text{K}\Omega\text{cm}$.



2.1. Kevex X-ray spectrum of gold chloride from Hopkins and Williams.



2.2. Kevex X-ray spectrum of reclaimed gold.



2.3. Kevex X-ray spectrum of wrought fine gold.

2.2. Experimental Method.

All glassware used was washed in tap water, rinsed in aqua regia and re-rinsed in de-ionised water several times, before being drained or dried with clean paper tissues.

All the chemical work was carried out in open glass beakers using mechanical stirring by glass rod. All mixing of solutions was done as rapidly as possible to eliminate variations of concentration, pH, temperature, etc. Any precipitates which formed were allowed to settle under cover, before the reducing solution was decanted off for testing for the presence of gold. The precipitate was washed with de-ionised water several times, then rinsed with isopropyl alcohol before being dried at room temperature.

The powders formed were evaluated by examination on Cambridge 'Stereoscan Mk.2' scanning electron microscope fitted with a 'Kevex' energy dispersive X-ray analyser. To do this, samples were taken from the powders with a spatula, shaken onto a specimen holder for the microscope and sprayed with antistatic lacquer. Examination of the powders at up to 50,000 magnifications enabled an idea of the size and morphology of a powder to be built up. Photographs of the precipitate were measured, using a projected area diameter type of reading⁽¹²¹⁾ for spherical and roughly spherical powders, and approximate aspect ratios for irregular powders, and histograms of the size distribution constructed. The samples were analysed by the Kevex X-ray micro-analyser. The energy spectra produced were compared with the spectrum produced by a sample of fine wrought gold (fig. 2.3.), and any extra lines identified by reference to tables of the electron energies of the elements.⁽¹²²⁾

2.3. Reduction Systems for Reducing Gold Salts.

2.3.1. Gold salts.

As gold is one of the most noble metals it is very easy to reduce from its salts. Gold chloride (AuCl_3) was used for this work as it is a simple salt to work with and is easy to obtain. In most cases it was used as a 50g/l gold solution (0.2588 molar) at about pH 2. This concentration was chosen as a compromise between a weaker solution, which would mean handling large volumes of solution to obtain a sufficient yield of powder, and the stronger solutions which would be used in industry; these would either require large quantities of gold chloride, or a very small volume of the more concentrated solutions.

From the large number of possible reduction methods for gold chloride,⁽⁹⁶⁾ only 19 were examined in this work. These were chosen because; (1) they produced only one solid product, gold. (2) they were neither offensive nor dangerous to work with, and (3) they used non-solid reducing agents (although some of these were tried for comparison purposes). The effects of variation of temperature, pH and concentration of reagents were examined on most of these systems.

2.3.2. Reducing agents.

The simplest reducing agent used was gaseous hydrogen⁽⁸²⁾⁽⁹⁶⁾ bubbled through both acid and alkaline gold chloride solution for about four hours. Nascent hydrogen was also used, being produced by adding gold chloride solution to excess sodium or lithium hydride (Practical grade, Koch Light Labs.) or by adding water to dry mixture of gold chloride and sodium/lithium hydride. The only other gaseous reducing agent used was hydrogen sulphide⁽⁹⁶⁾ which was passed through an acid gold chloride solution at room temperature.

Hydrogen peroxide⁽⁹⁶⁾ (100 volume) was used to reduce gold under a variety of conditions, acid, alkaline, hot or cold. It was also used to reduce a weak gold chloride solution of 5g/l (0.025 molar) at room

temperature. During some of the additions of sodium hydroxide to gold chloride to alter the pH, a dark red solution was temporarily seen. This was investigated by adding massive amounts of the hydroxide to both hot and cold gold chloride solutions.

Acetone⁽⁹³⁾ was used with gold chloride at both room temperature and 100°C, but the latter tended to spit as the boiling point of acetone is only 60°C. A 5% solution (0.078 molar) of sulphur dioxide⁽¹²⁰⁾ was used to produce a precipitate for powder production as well as for reclaim work. This was tried under acid conditions at various temperatures between room temperature and boiling point. The sodium salt of this acid, sodium sulphite,⁽¹⁰³⁾ was also used to produce precipitates, under most conditions of pH and temperature. Work was also carried out using a 200 g/l (1.59 molar) sodium sulphite solution, to find out the effect of the rate of addition of reducing agent, and the effects of the ratio of reducing agent to gold salts.

The reduction of ferrous salts to ferric salts was tried using saturated solutions of ferrous chloride⁽¹²³⁾ and ferrous sulphate.⁽⁹⁶⁾ Both reducing agents were used at various pH values, the ferrous chloride always hot, whilst the ferrous sulphate was used at a variety of temperatures.

Another inorganic reducing agent was sodium nitrite⁽¹²⁰⁾, used at 200 g/l (2.9 molar) concentration. The effect of change in pH and temperature was examined as well as different concentrations of gold. Formaldehyde⁽¹²⁰⁾ was used as a reducing agent for gold, mainly under basic conditions at a variety of temperatures. Trisodium citrate⁽⁹³⁾ (100 g/l-0.34 molar) also works best under basic conditions, but only at high temperatures. This preference for alkaline environment is also the case with hydroxylamine hydrochloride⁽⁹³⁾ which will not precipitate in acid solution unless seed crystals are present. This property has been

used to make this solution a growth system, growing nuclei produced elsewhere to a larger size. Under basic or neutral conditions it was also used in this work to precipitate gold powder from its own nucleation. Besides using gold chloride, hydrazine hydrochloride was used to reduce gold fulminate⁽¹⁰³⁾ which had been produced by raising the pH of gold chloride solution to 10.5. with ammonia.

Not all the organic reducing work only in alkaline solutions, as a 100 g/l (0.79 molar) solution of oxalic acid⁽¹⁰⁴⁾ was used to reduce boiling gold chloride solutions. A solution of white phosphorus in diethyl ether was used to reduce acid gold chloride solution at room temperature (Faraday's solution)⁽⁸³⁾.

For comparison, gold chloride was reduced with a solid reducing agent, zinc dust,⁽⁹⁶⁾ which was added to an acidified gold solution. Also for comparison, gold chloride was reduced to gold by electrolysis under various conditions.

2.4. Precipitation of Gold Alloys.

Where attempts were made to coprecipitate alloys of gold and other metals, the solution used was a mixture of gold chloride at 50 g/l gold metal and the other metal chloride at 50 g/l metal. They were usually mixed in equal proportions so as to evaluate the efficiency of the reducing system.

Gold/copper and gold/nickel chlorides were treated with oxalic acid under the same conditions as gold chloride was. Gold/cobalt chlorides were reduced with sodium nitrite⁽¹²⁰⁾ solution, as were gold/palladium chloride mixtures. The gold/palladium was also treated with sulphurous acid,⁽⁹⁶⁾ and with ammonia followed by hydrazine hydrochloride.⁽¹⁰³⁾

2.5. Other Metal Powders.

Most work was carried out trying to reduce palladium chloride solution to palladium in the same way as had been done for gold. Among the reagents tried were nascent hydrogen⁽⁹⁶⁾ using lithium hydride, hydrazine hydrochloride, trisodium orthophosphate⁽¹²³⁾, sodium formate⁽⁹⁶⁾ and sodium sulphite. In addition, an attempt was made to produce a palladium-nickel alloy by reducing the palladium with sodium thiosulphate in a solution of mixed chlorides. This freshly precipitated palladium then catalysed the reduction of the nickel chloride.⁽¹²⁵⁾

Attempts were made to reduce nickel chloride directly, using nascent hydrogen from sodium hydride, and hydrazine hydrochloride. The other base metal reductions tried were of copper sulphate, using either iron dust, or iron dust and ferrous sulphate.⁽⁹⁶⁾

Other metal powders were obtained from other sources. Palladium metal was supplied by Hopkins and Williams, whilst a palladium/tin mixture/alloy was obtained as a waste product of the palladium chloride solution used in the activation stage for plating plastics. Nickel and iron powders were obtained which had been produced by the carbonyl process. The nickel was Mond nickel type 4 (batch No. 4/824). Both powders had been sieved to less than 53 microns.

3. RESULTS OF POWDER PRECIPITATION.

3.1. Experimental Errors.

The effect of sampling errors are shown in fig. 3.1., where four 'identical' samples were taken from the same powder and their size distribution measured. Measurement errors are shown in fig. 3.2., where the photographs of the same samples used to give the distribution shown in fig. 3.1., were remeasured. (These, and the following distribution curves are not true distribution curves, in that the area under the curve does not total 100%. These curves were taken from histograms and only intended to give an idea of the size distribution).

An indication of the effect of mixing variations is shown in fig. 3.3. Here two identical solutions of gold chloride were reduced by adding similar amounts of 200 g/l sodium sulphite. In one solution the sulphite had been added as fast as possible, whilst in the other a slow pouring over approximately 5 seconds had occurred. Both solutions had been stirred during mixing.

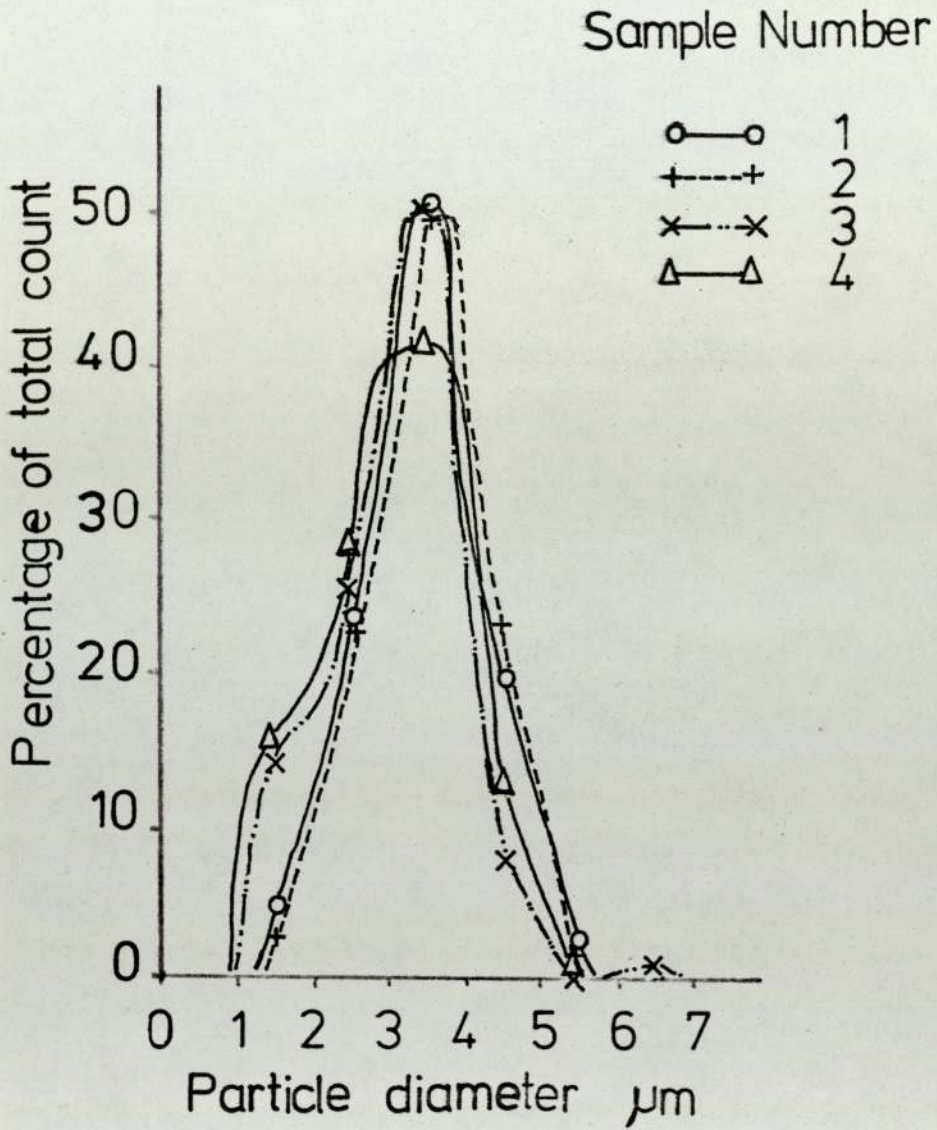
3.2. Gold Powders.

3.2.1. Reduction by hydrogen.

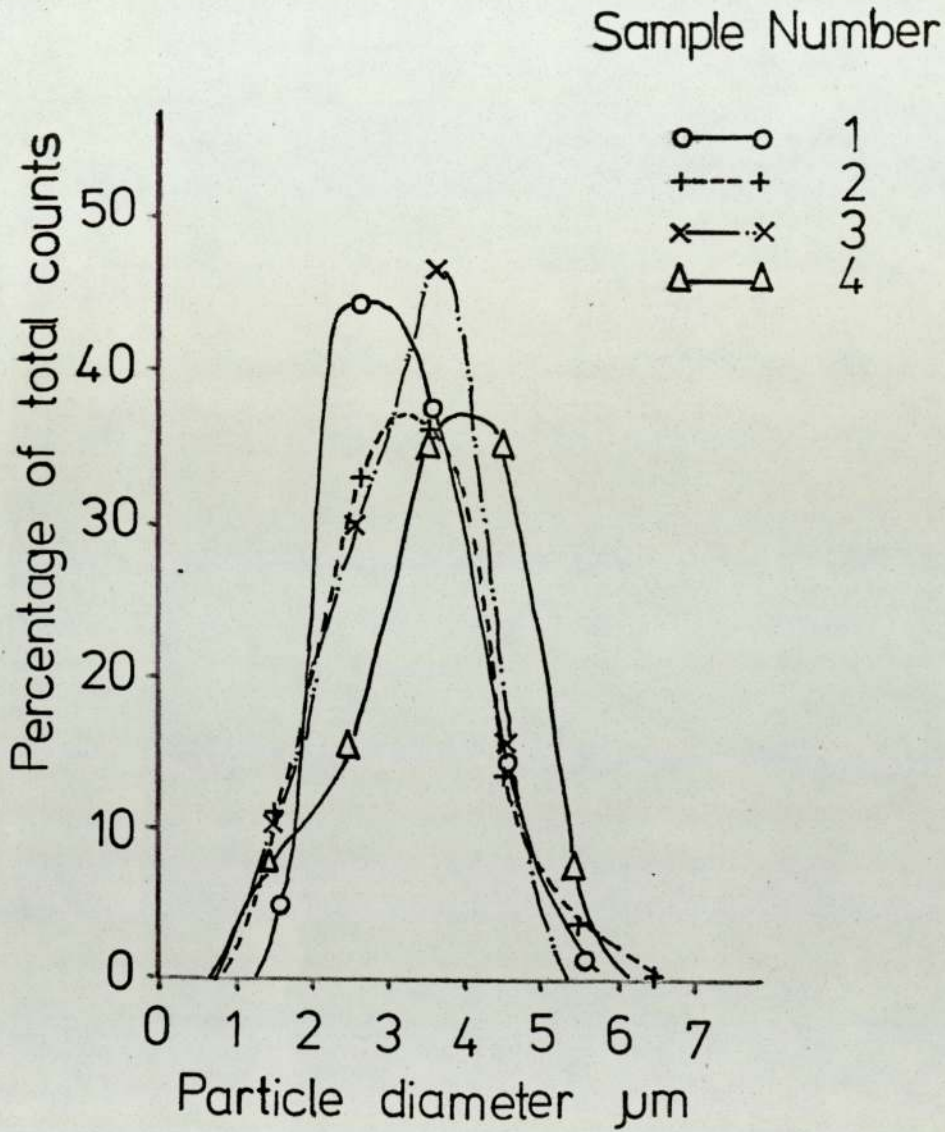
Very little gold was reduced, and that mainly in the alkaline solution. The gold was quite impure (fig. 3.4.) and in the form of small irregular particles of about $0.5\mu\text{m}$ diameter, held together in a large lumpy grain (fig. 3.5.).

3.2.2. Reduction by nascent hydrogen.

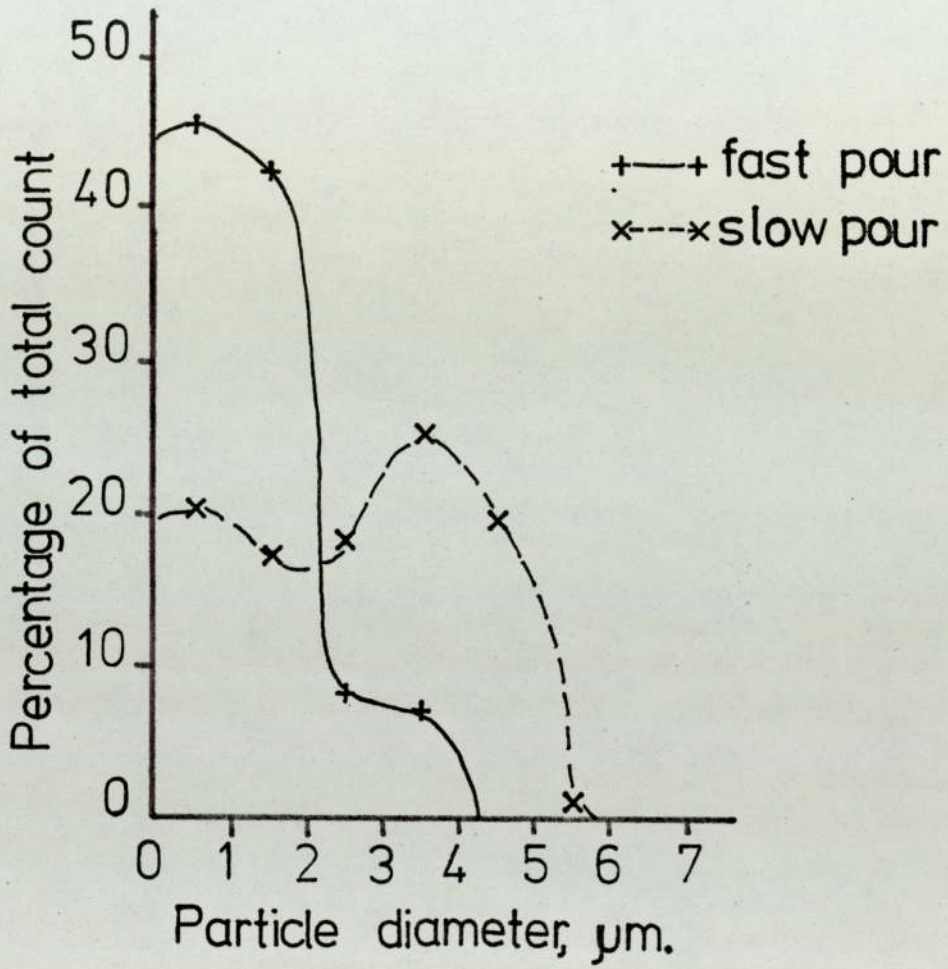
All these reactions were violent, the ones involving sodium hydride excessively so. All the particles formed were very small, mostly less than $0.1\mu\text{m}$ (fig. 3.6.), and held together into a 'foamlike' structure.



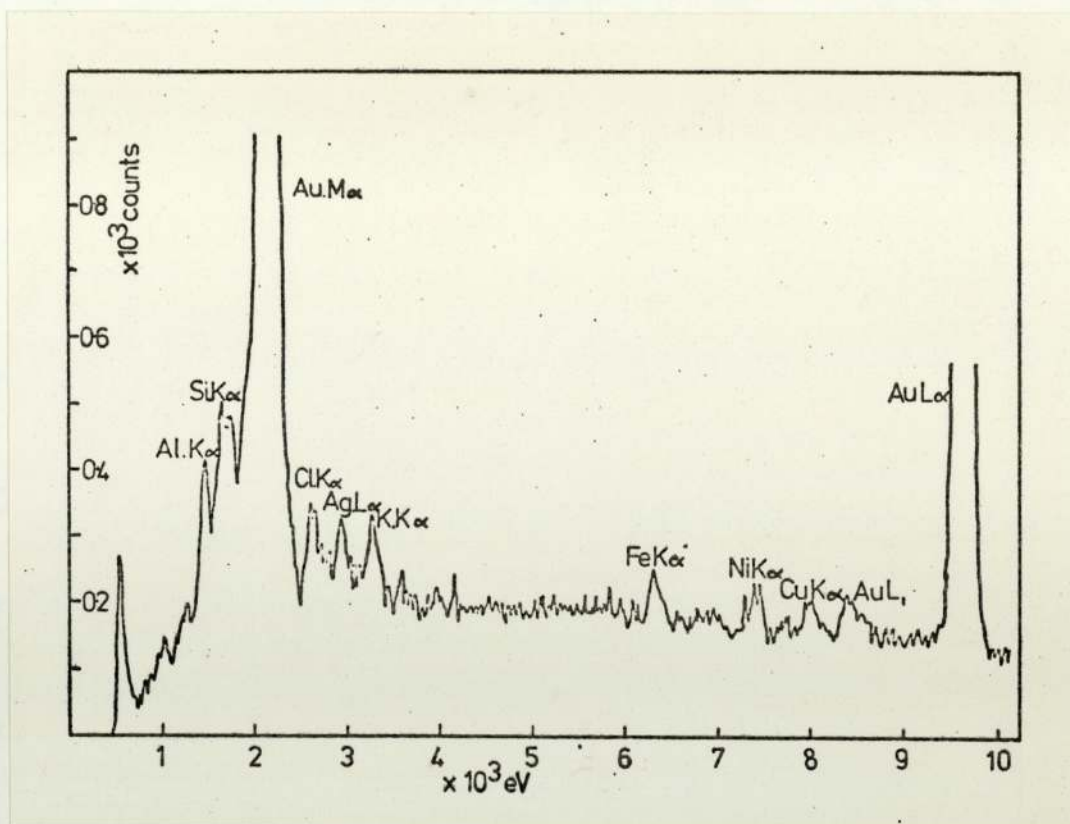
3.1. Particle size distribution of four samples taken from the same powder.



3.2. Particle size distribution of a re-measurement of the same four samples of the same powder used in fig. 3.1.



3.3. Influence of mixing rates on the particle size distribution of gold powder reduced from gold chloride by sodium sulphite.



3.4. Kevex X-ray spectrum of gold reduced by gaseous hydrogen.



3.5. Scanning electron micrograph of gold reduced by gaseous hydrogen. x 10,000



└ 1 μ m.

3.6. Scanning electron micrograph of gold reduced by nascent hydrogen produced from lithium hydride. x 5,400

The golds produced had the same spectra as that of pure gold (fig. 2.2. or 2.3.).

3.2.3. Reduction by hydrogen sulphide.

Hydrogen sulphide rapidly produced a black precipitate which took considerable time to settle, and when dry consolidated into massive particles of a sulphur containing gold (figs. 3.7., 3.8. and 3.9.).

3.2.4. Reduction by hydrogen peroxide.

Hydrogen peroxide produced a mixture of rough irregular spheres mixed with rough triangular and hexagonal plates (fig. 3.10). The size distribution of the spherical particles is shown in fig. 3.11. along with those reduced by the same system at boiling point. In both cases the gold was pure. Reducing the concentration of the gold to 5 g/l had little overall effect on the powder, merely making the 'spheres' more irregular (fig. 3.12.).

None of these acid solutions went to completion, with some gold chloride still being left after the reaction had ceased. Raising the pH however, rapidly carried the reaction to completion, giving a fine foamlike structure to the gold (fig. 3.13.).

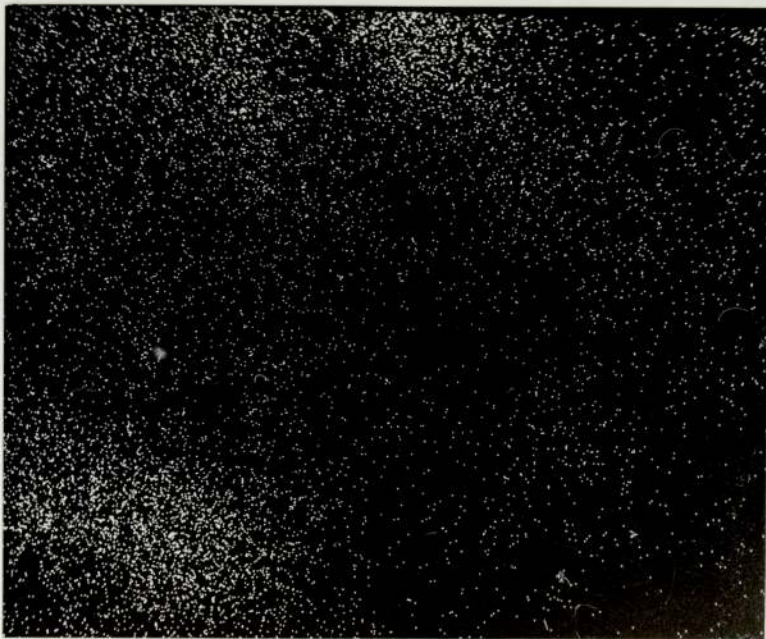
3.2.5. Reduction by sodium hydroxide.

At room temperature, sodium hydroxide gave a precipitate of clumped irregular particles (fig. 3.14.) with some sodium present in the gold (fig. 3.15.). Heating the mixture produced thick long plates of impure gold (figs. 3.16. and 3.17.).



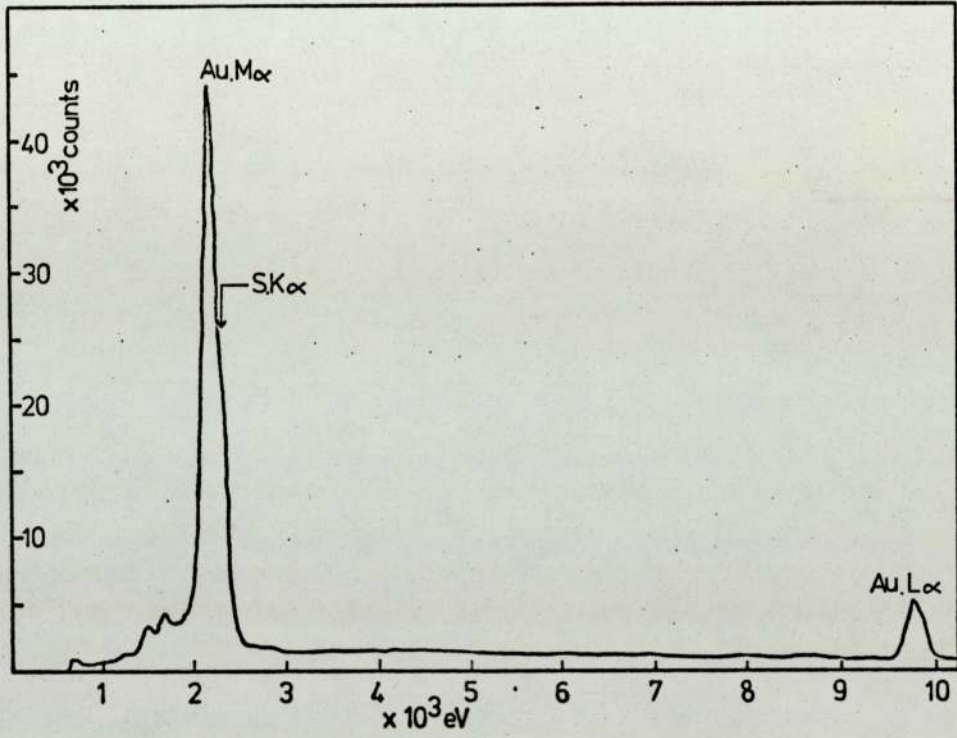
1 μ m

3.7. Scanning electron micrograph of gold reduced by hydrogen sulphide. x 2,100

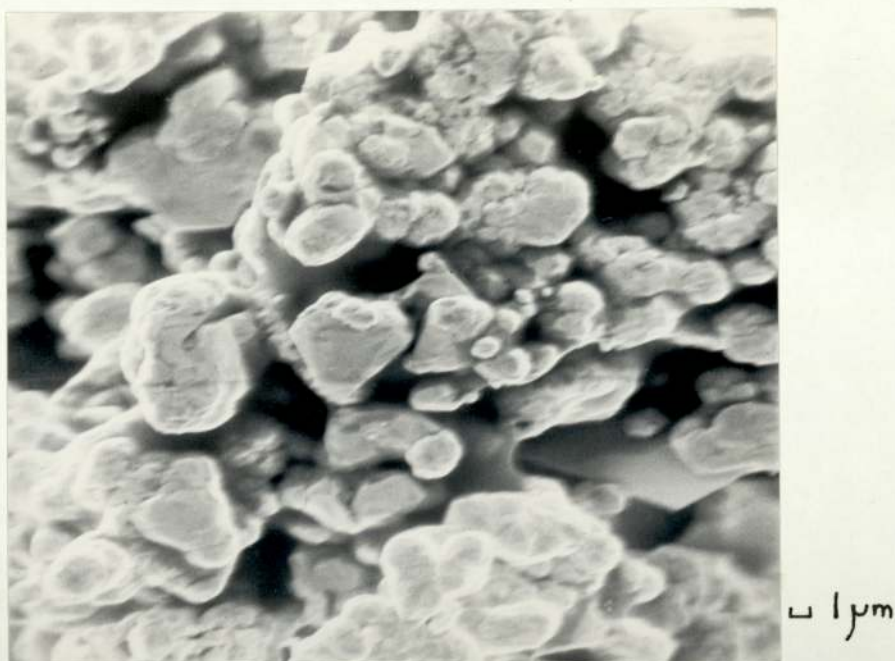


1 μ m

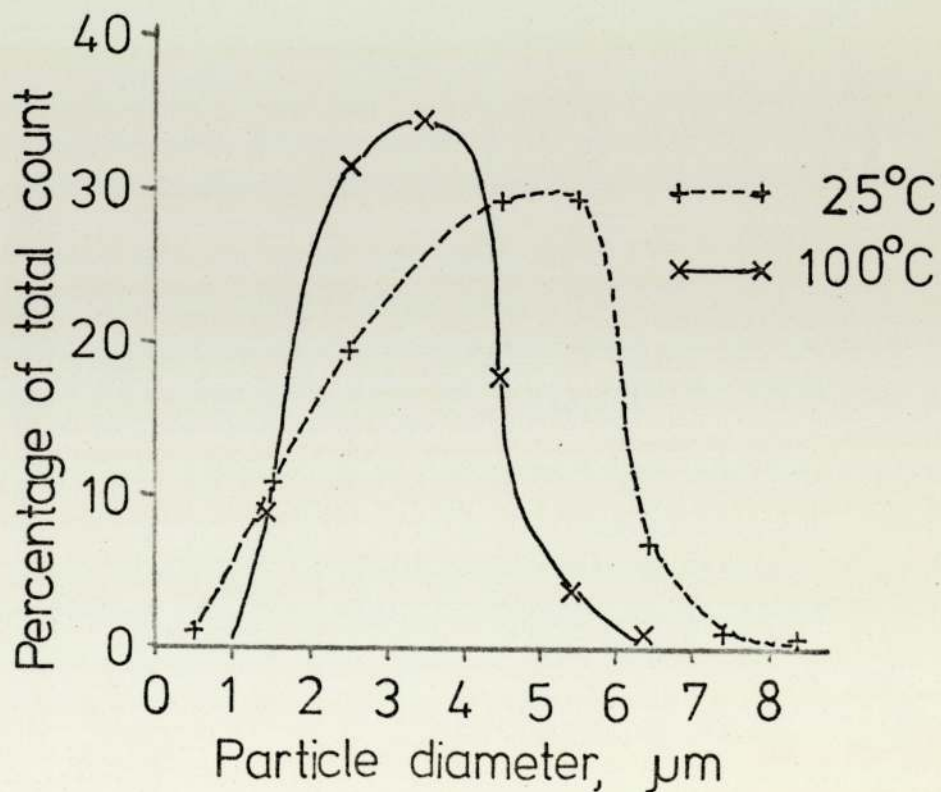
3.8. Sulphur distribution in gold reduced by hydrogen sulphide. (Sulphur $K\alpha_1$ X-rays.) x 2,100



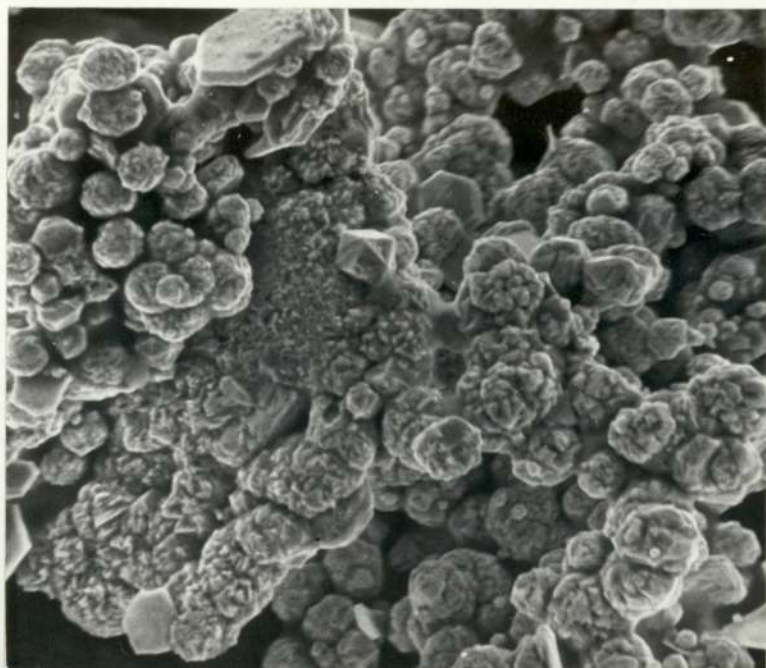
3.9. Kevex X-ray spectrum of gold reduced by hydrogen sulphide.



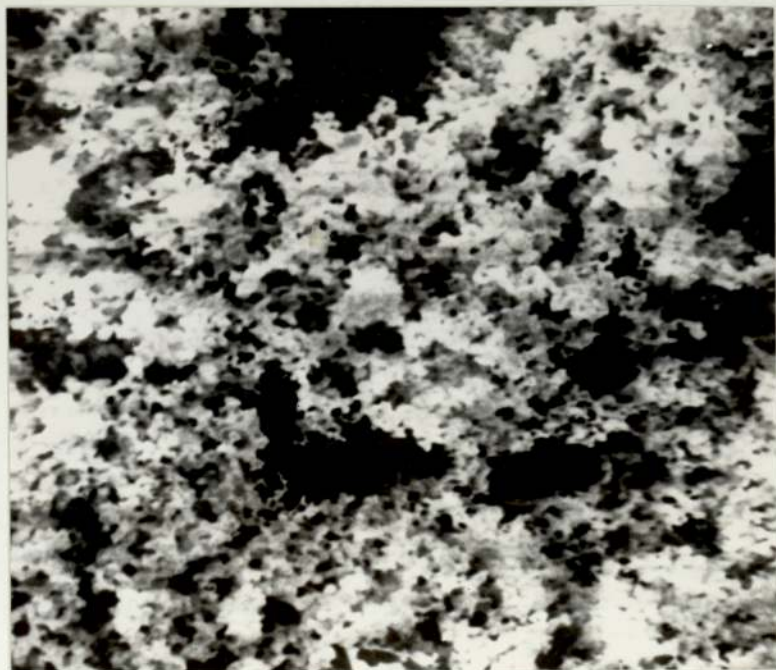
3.10. Scanning electron micrograph of gold reduced under acid conditions by hydrogen peroxide. x 2,250



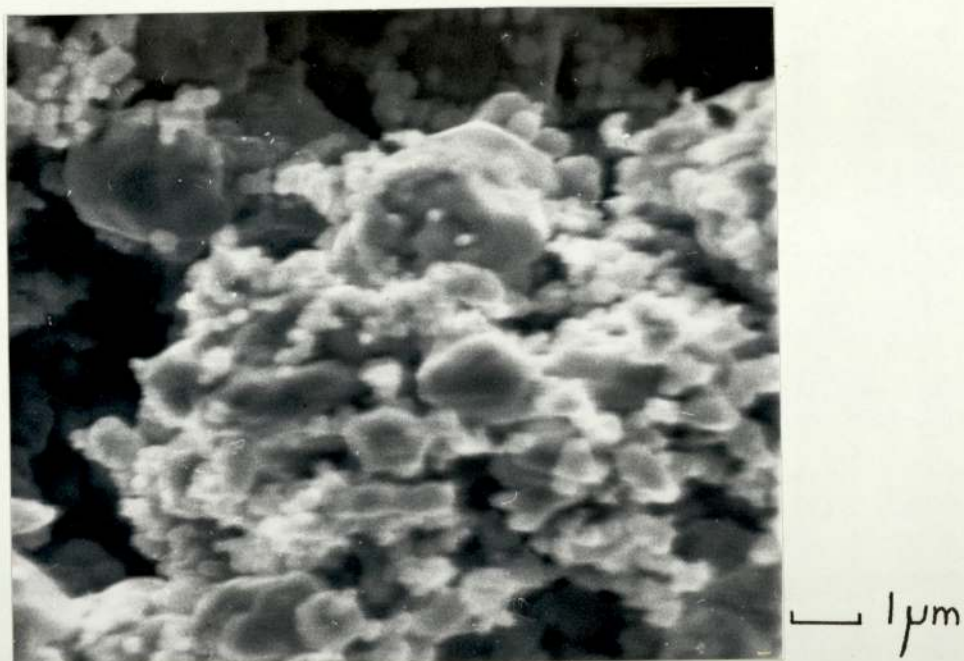
3.11. Influence of temperature on the particle size distribution of gold reduced under acid conditions by hydrogen peroxide..



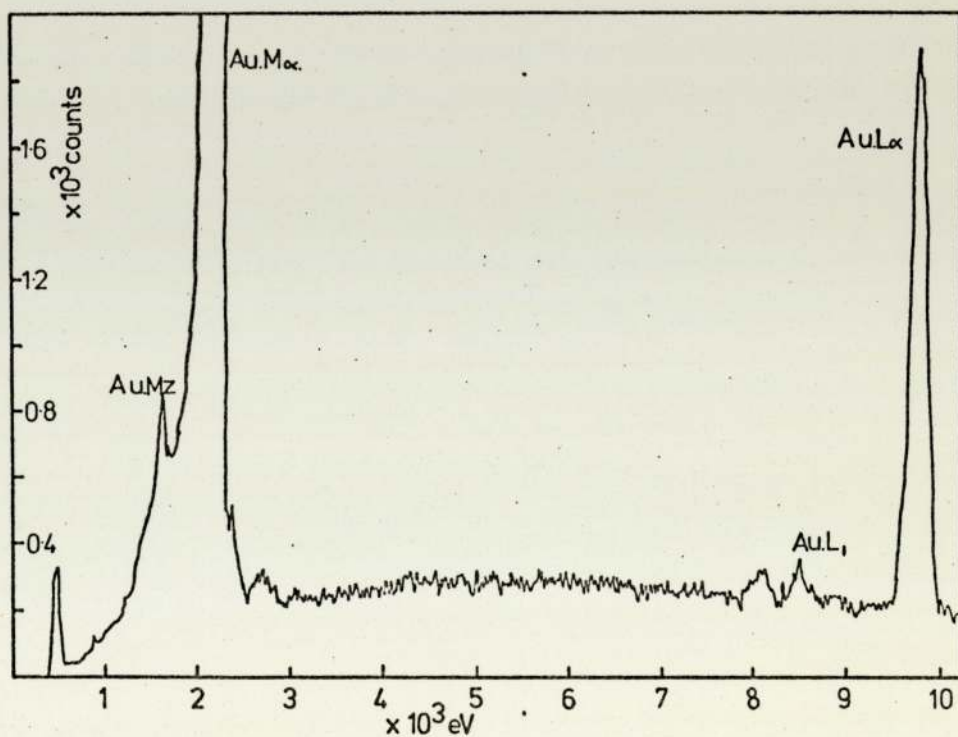
3.12. Scanning electron micrograph of gold reduced from a low gold concentration solution by hydrogen peroxide. x 1,600



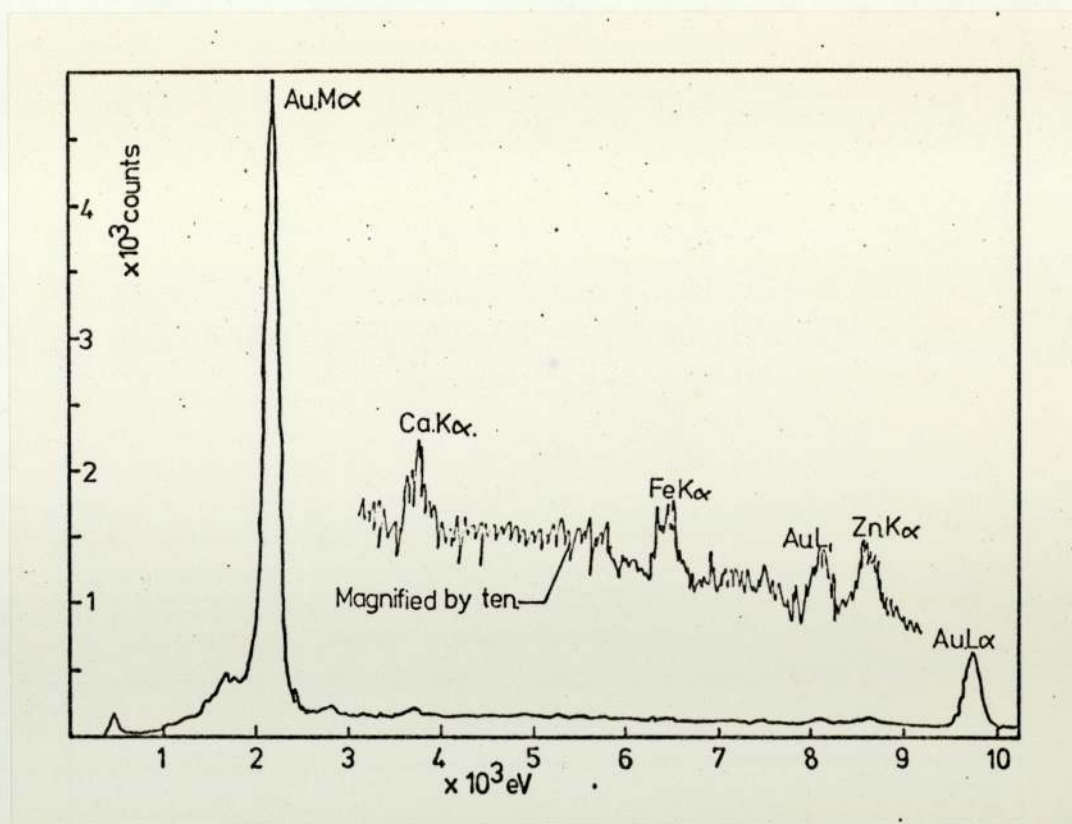
3.13. Scanning electron micrograph of gold reduced under alkaline conditions by hydrogen peroxide. x 5,000



3.14. Scanning electron micrograph of gold reduced at room temperature by sodium hydroxide. x 9,000



3.15. Kevex X-ray spectrum of gold reduced at room temperature by sodium hydroxide.



3.16. Kevex X-ray spectrum of gold reduced at 100°C by sodium hydroxide.



3.17. Scanning electron micrograph of gold reduced at 100°C by sodium hydroxide. x 1,900

3.2.6. Reduction by acetone.

The reduction of gold chloride by acetone at room temperature was very slow and only a small quantity of equilibrium shaped particles and rough spheres of pure gold (fig. 3.18.) were formed after a week. Boiling the gold chloride solution still does not produce a 100% yield, but gave a larger yield of rough pure gold spheres (fig. 3.19.). The size distribution of this powder is shown in fig. 3.20.

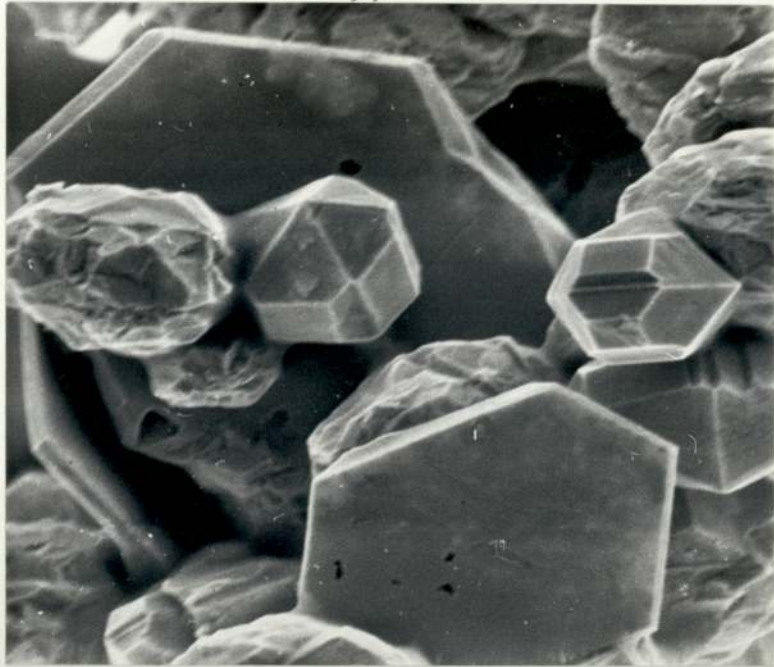
3.2.7. Reduction by sulphur dioxide.

Sulphur dioxide reductions produced a powder of pure gold spheres (fig. 3.21.) with quite a range of particle sizes (fig. 3.22.). Heating the gold chloride before mixing gave much rougher spheres with some spheres approaching dendritic form (fig. 3.23.). Full dendrites were produced by mixing the gold chloride and sulphurous acid at room temperature and then heating (fig. 3.24.). There was a distinct induction period with this system, with a time lapse between the solution losing its colour on mixing and the start of precipitation. The induction period became shorter on heating the solutions.

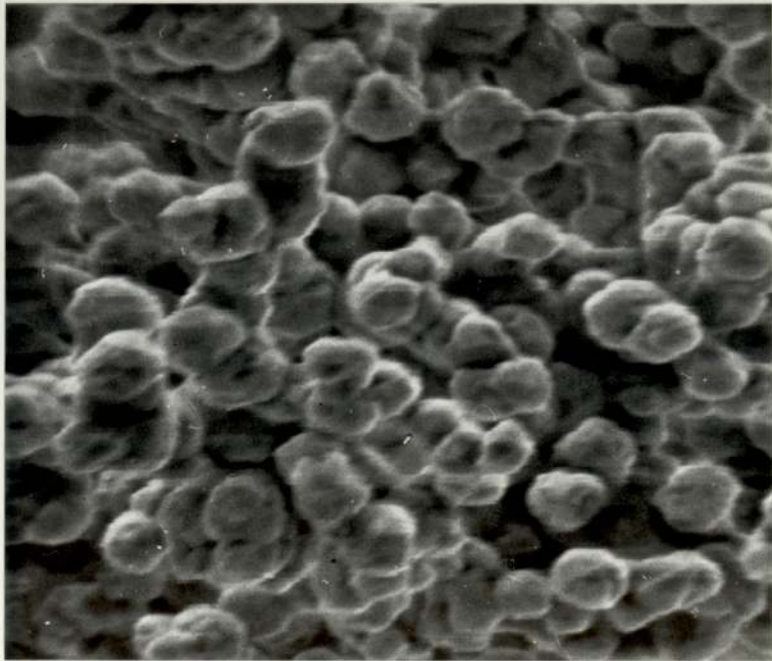
3.2.8. Reduction by sodium sulphite.

Sodium sulphite will only reduce gold chloride solutions in acid conditions and with decreasing efficiencies at pH greater than 2. The powder produced was composed of pure gold spheres, becoming smooth at pH greater than 1.2. (figs. 3.25 - 3.28.). Their size range is given in fig. 3.29.

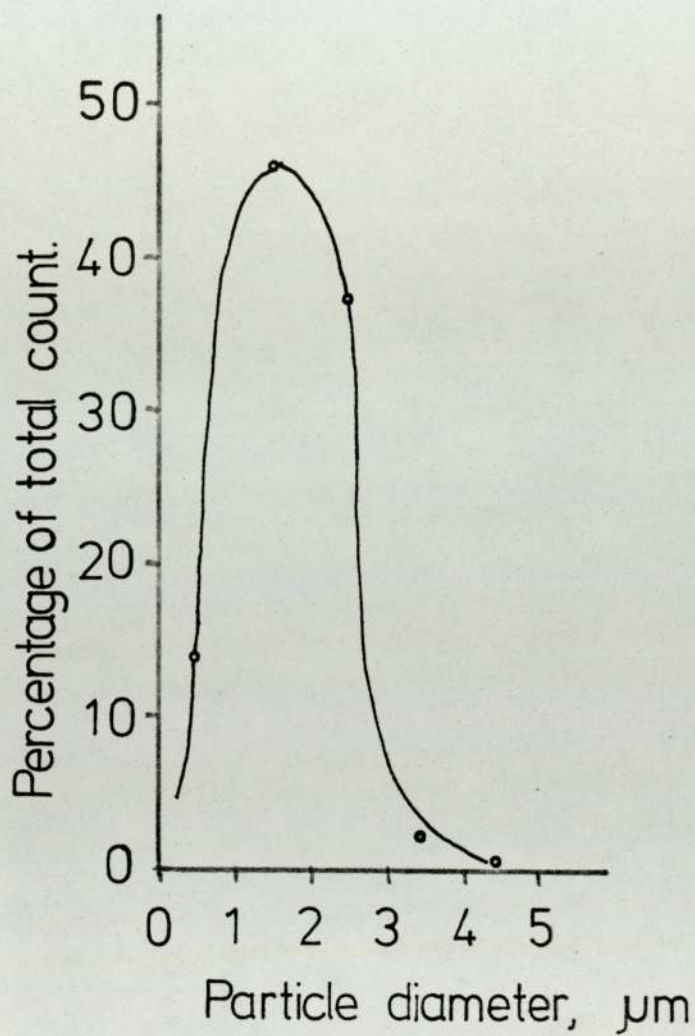
By boiling the mixture it was possible to improve the yield from a solution of approximately pH 6, but the particles formed were a mixture of spheres and a few flat plates (fig. 3.30.). Flat plates were also found, when the ratio of the volume of reducing agent to gold chloride was



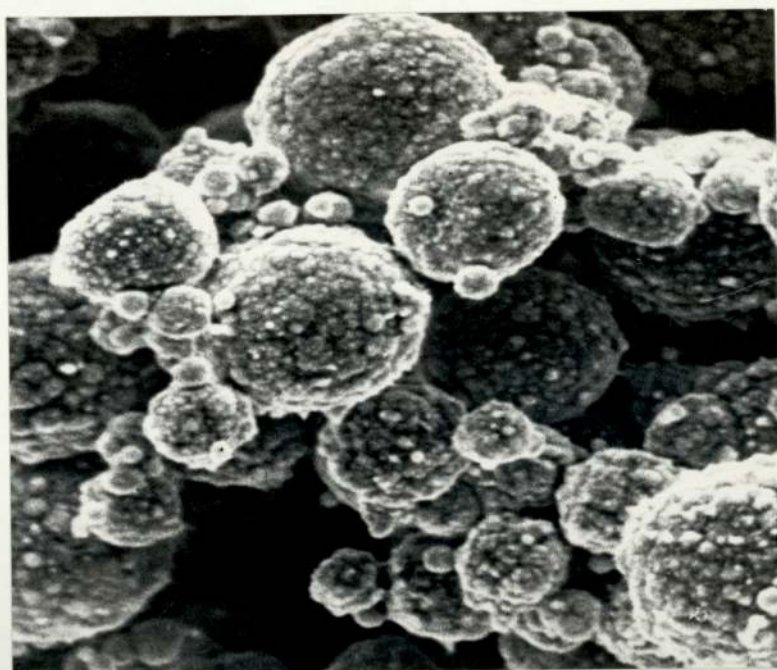
3.18. Scanning electron micrograph of gold reduced by acetone at room temperature. x 2,000



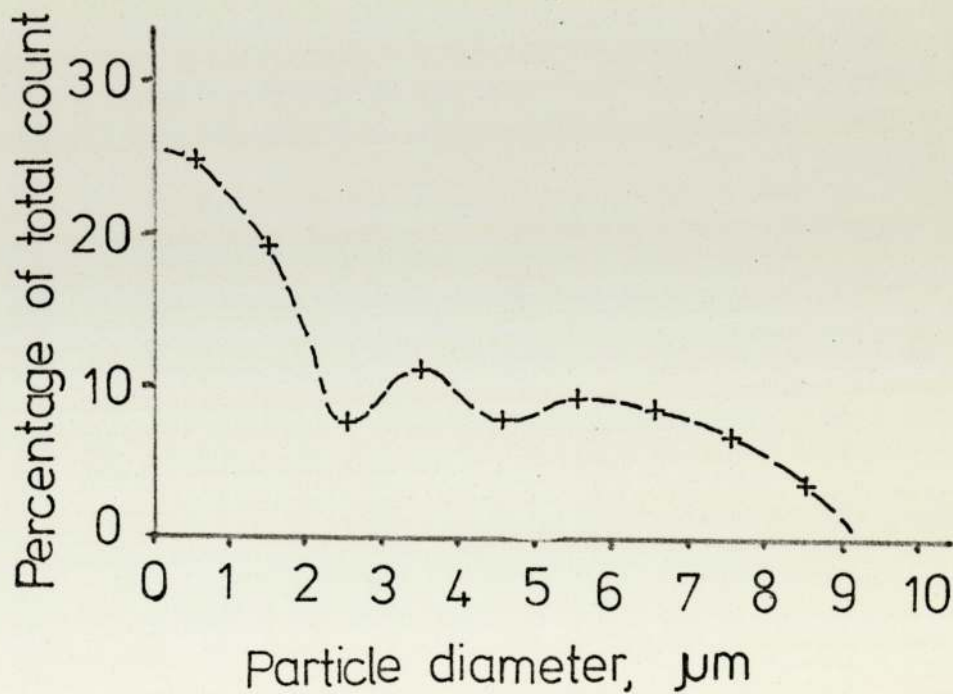
3.19. Scanning electron micrograph of gold reduced by acetone at 100°C. x 5,000



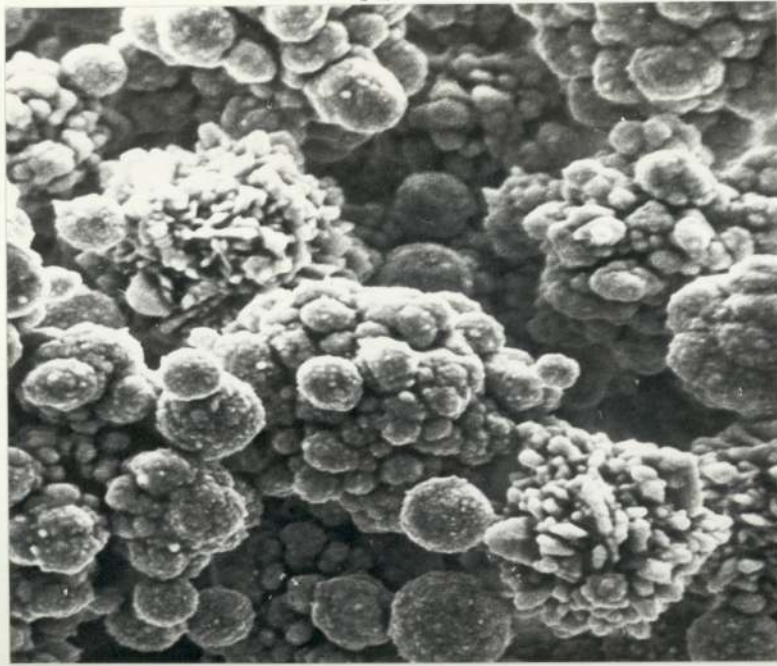
3.20. Particle size distribution of gold reduced by acetone at 100°C.



3.21. Scanning electron micrograph of gold reduced at room temperature by sulphur dioxide. x 4,400



3.22. Particle size distribution of gold reduced at room temperature by sulphur dioxide.



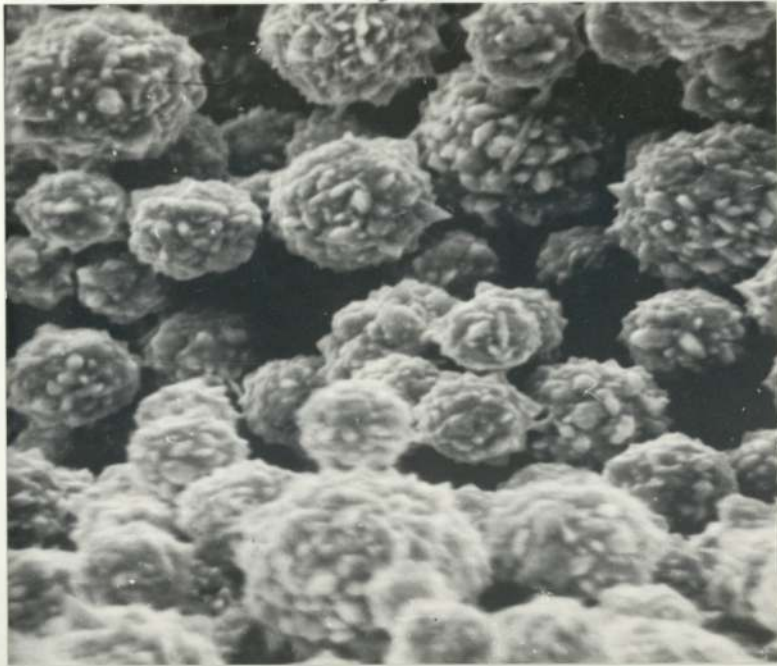
└ 1 μ m

3.23. Scanning electron micrograph of gold reduced at boiling point by sulphur dioxide. x 5,600

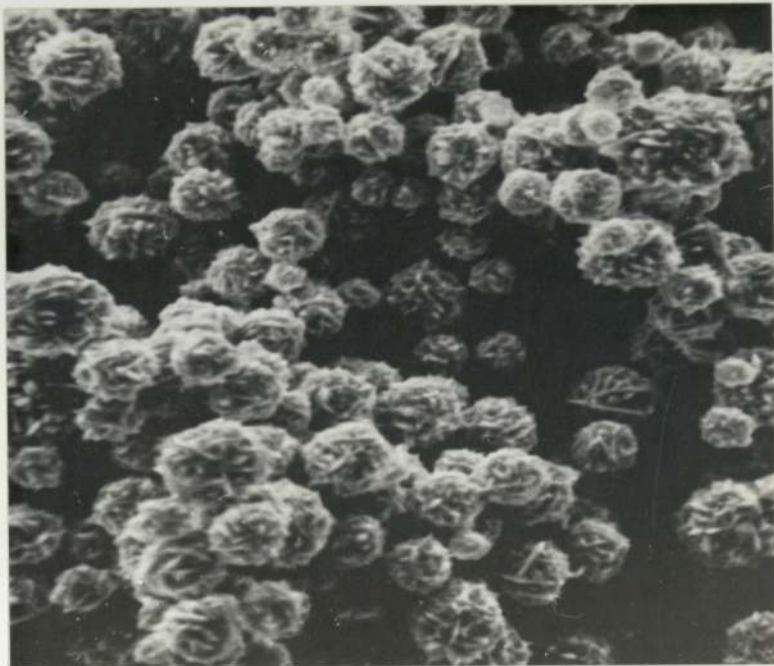


└ 1 μ m

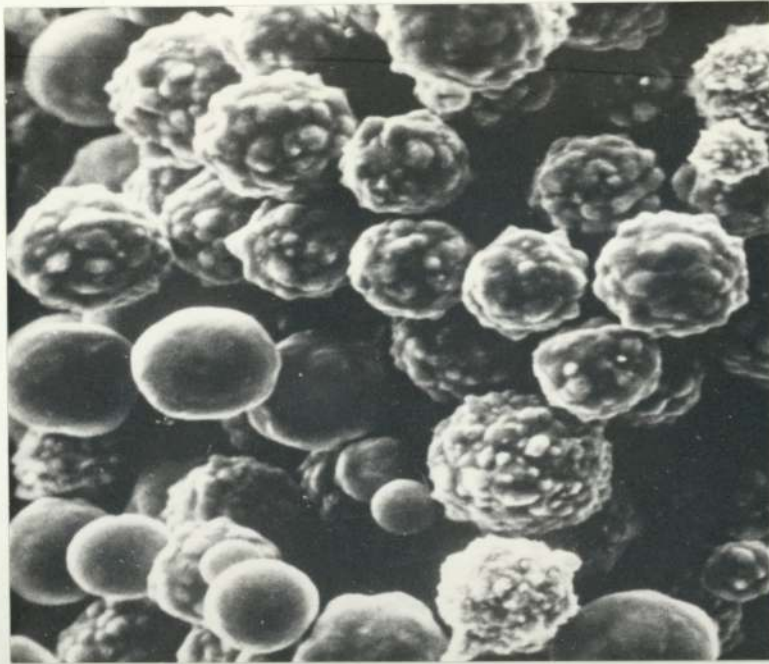
3.24. Scanning electron micrograph of gold reduced at varying temperatures by sulphur dioxide. x 10,000



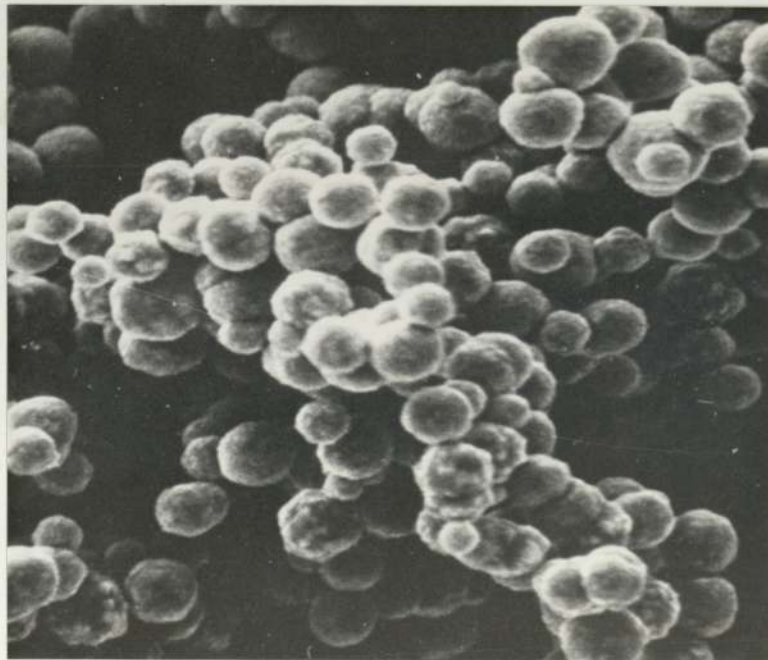
3.25. Scanning electron micrograph of gold reduced at pH 0
by sodium sulphite. x 6,500



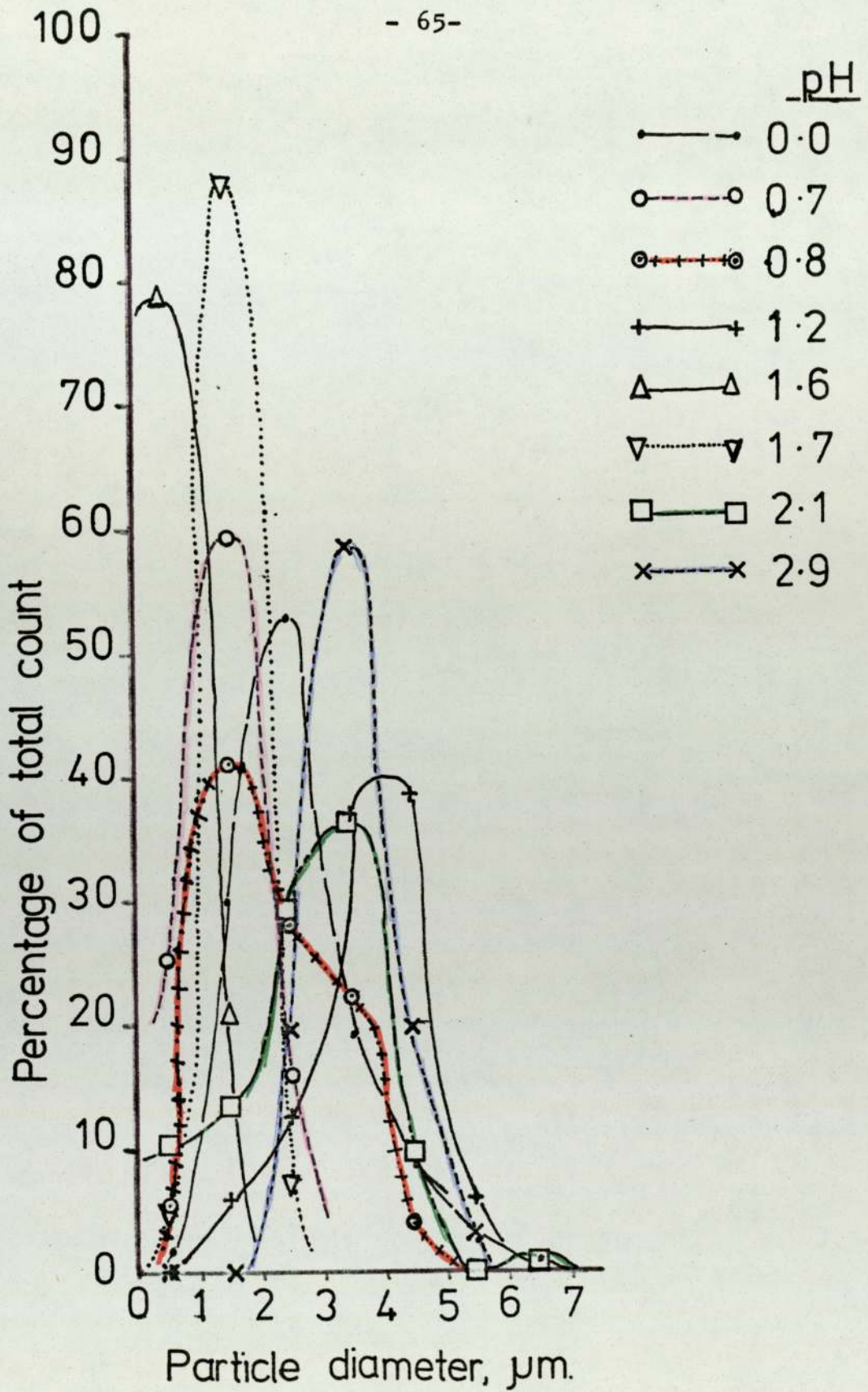
3.26. Scanning electron micrograph of gold reduced at pH
0.7 by sodium sulphite. x 6,500



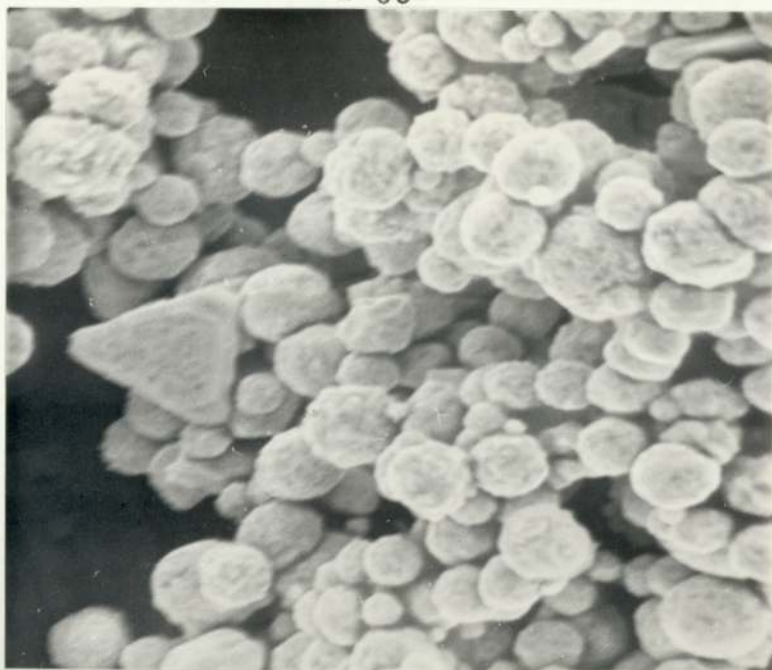
3.27. Scanning electron micrograph of gold reduced at pH 1.2 by sodium sulphite. x 5,600



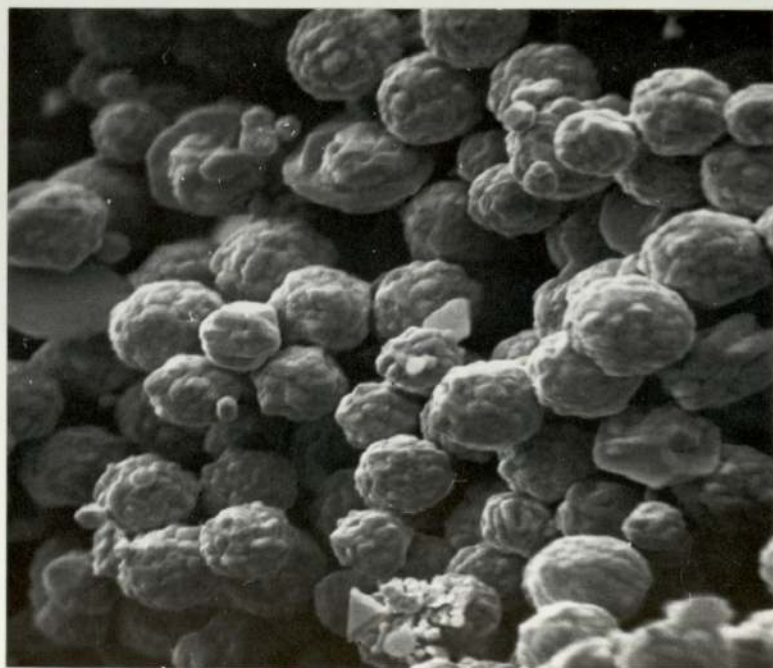
3.28. Scanning electron micrograph of gold reduced at pH 1.7 by sodium sulphite. x 5,800



3.29. Influence of pH on the particle size distribution of gold reduced by sodium sulphite.



3.30. Scanning electron micrograph of gold reduced at pH 6 and 100°C by sodium sulphite. x 5,000



3.31. Scanning electron micrograph of gold reduced at pH 2 with a gold chloride : sodium sulphite ratio of 0.5 x 2,900

reduced from 2.5. to 0.5. (fig. 3.31). The effect of this on the size distribution is shown in fig. 3.32., whilst the effect on the induction period was to reduce it from about 5 seconds for a ratio of 2.5 down to 2 seconds for one of 0.5.

3.2.9. Reduction by ferrous chloride.

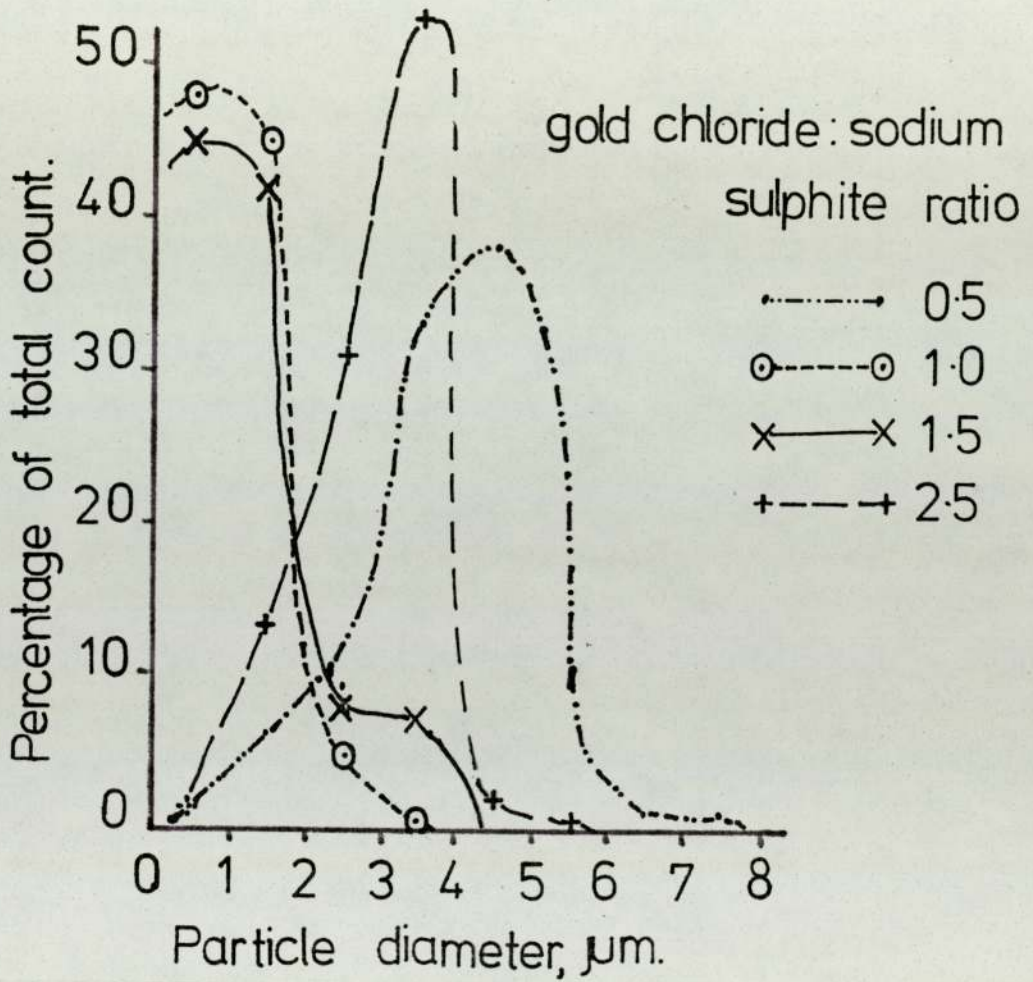
This was a very slow reaction at both high and low pH, and produced only a small quantity of powder. The powder was a mixture of spheres and flat plates (fig. 3.33.) with some chlorine contamination. This appeared to be concentrated in the plates rather than the spheres (fig. 3.34.). The size of the spherical particles seemed to follow an almost normal distribution (fig. 3.35.).

3.2.10. Reduction by ferrous sulphate.

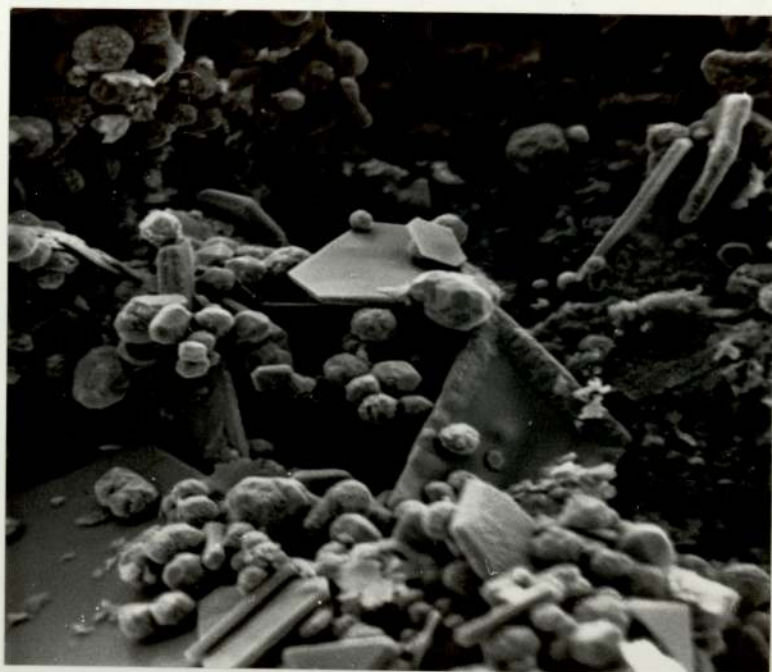
Ferrous sulphate reduces acid gold chloride to pure gold spheres of about $0.9\mu\text{m}$ diameter (fig. 3.36.). As the pH of the gold chloride was raised, the size of the particles dropped to $0.25\mu\text{m}$ in neutral solutions, and to below the resolution of the scanning electron microscope in alkaline solutions. The level of contamination rose with the pH (fig. 3.37.). Reducing the acid gold chloride at boiling point reduced the size of the spheres slightly from $0.9\mu\text{m}$ to $0.75\mu\text{m}$ and introduced a number of plate-like crystals which were rich in iron (fig. 3.38).

3.2.11. Reduction by sodium nitrite.

Reducing gold chloride under acid conditions using sodium nitrite solution produced a pure gold precipitate of very large particles (fig. 3.39.). Raising the pH of the solutions reduced the vigour of the reactions as well as the particle size (fig. 3.40.) until alkaline solutions went green and only slowly settled out as a massive lump with no discernible particles

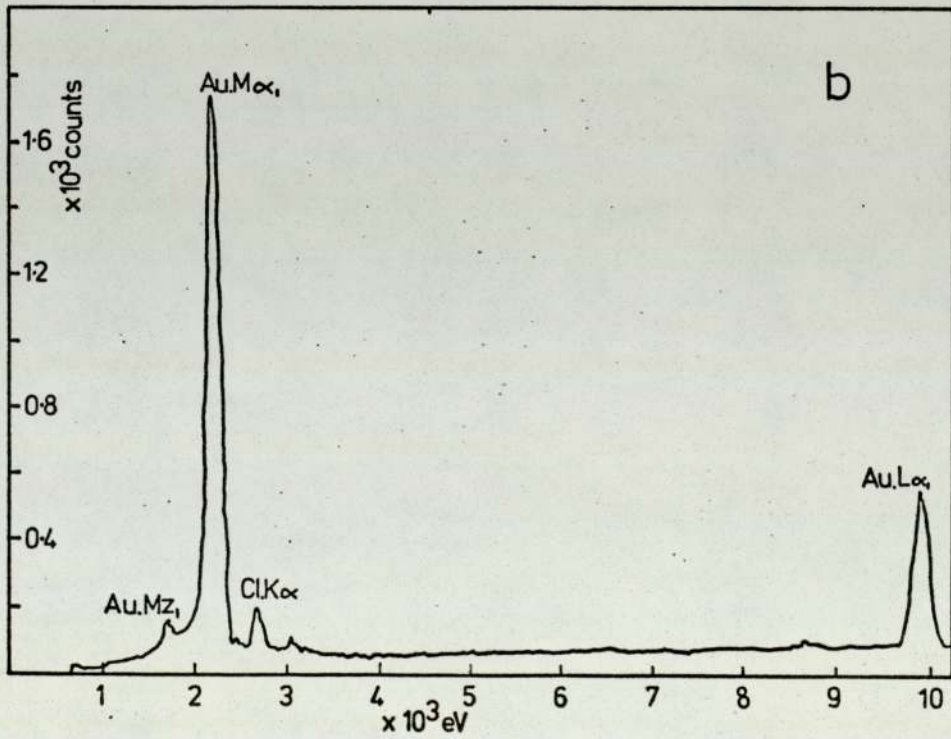
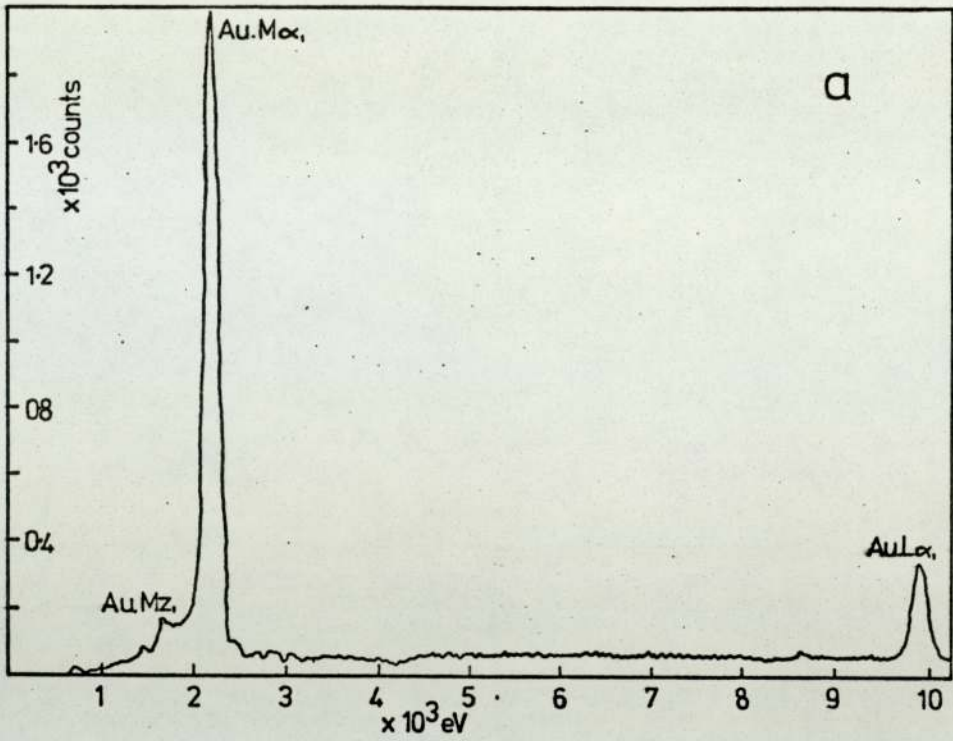


3.32. Effect of the ratio of gold chloride to sodium sulphite on the particle size distribution.

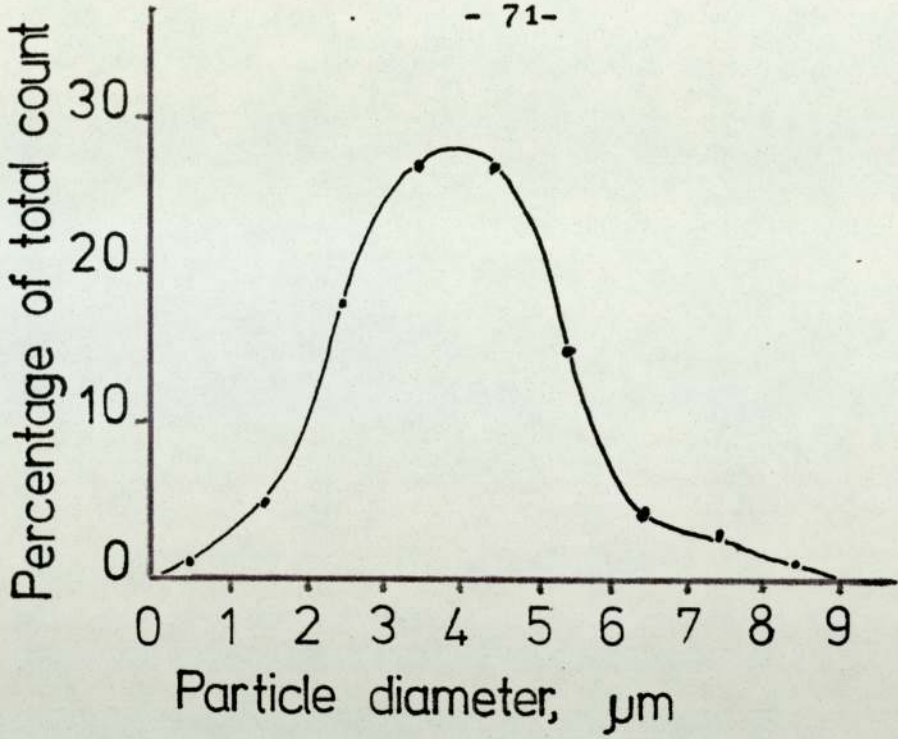


1 μ m

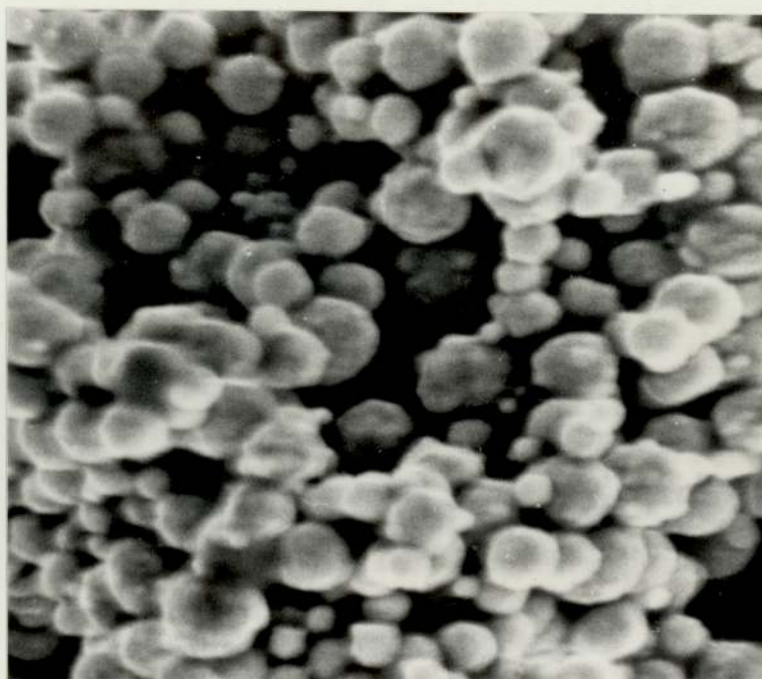
3.33. Scanning electron micrograph of gold reduced by ferrous chloride.
x 1,550



3.34. Kevex X-ray spectra of a) spherical and b) plate-like gold particles reduced by ferrous chloride.

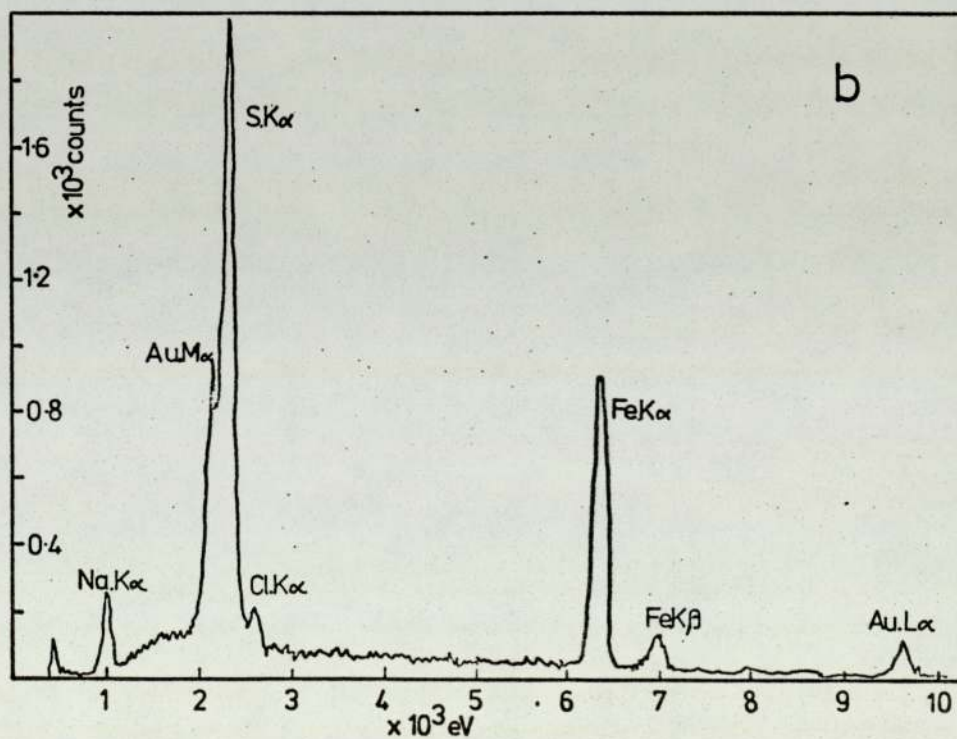
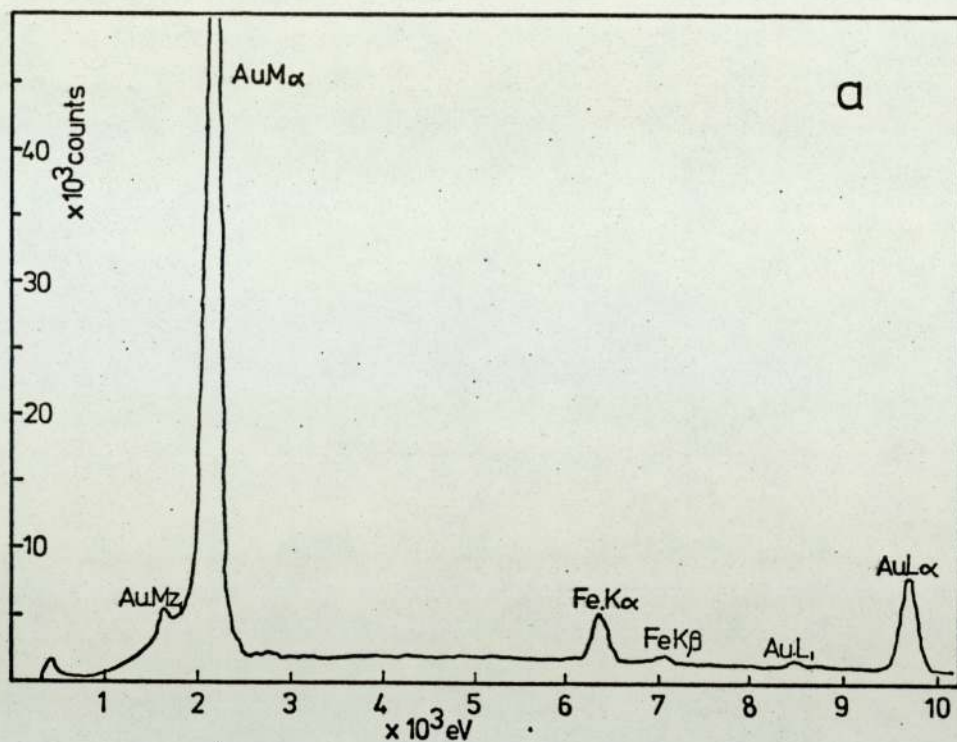


3.35. Particle size distribution of spheres of gold reduced by ferrous chloride.

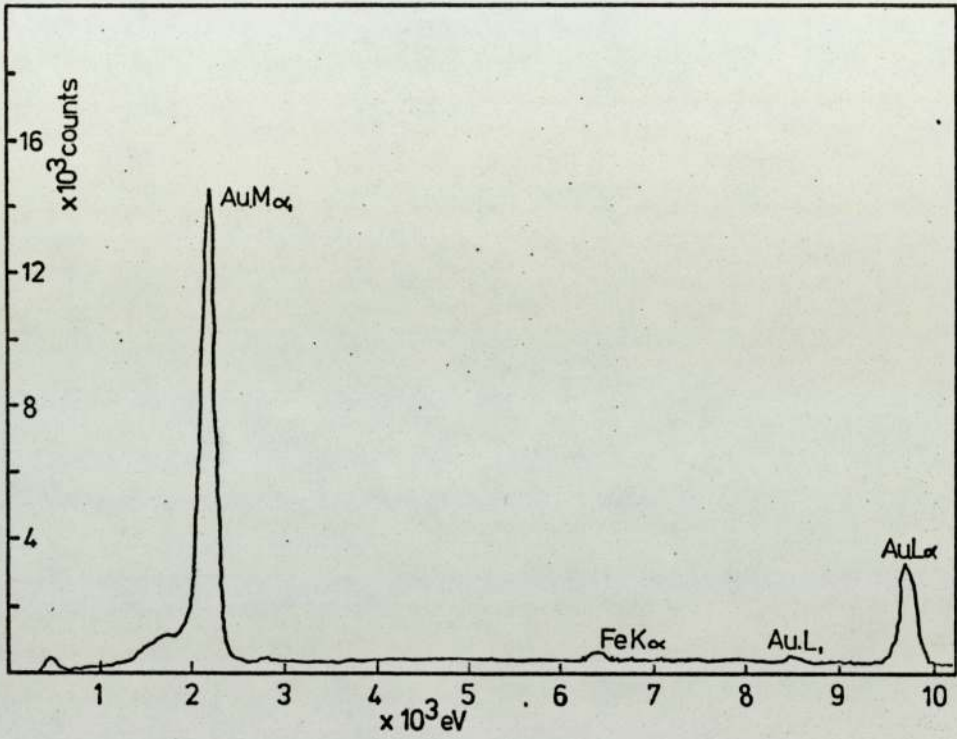


— 1 μ m

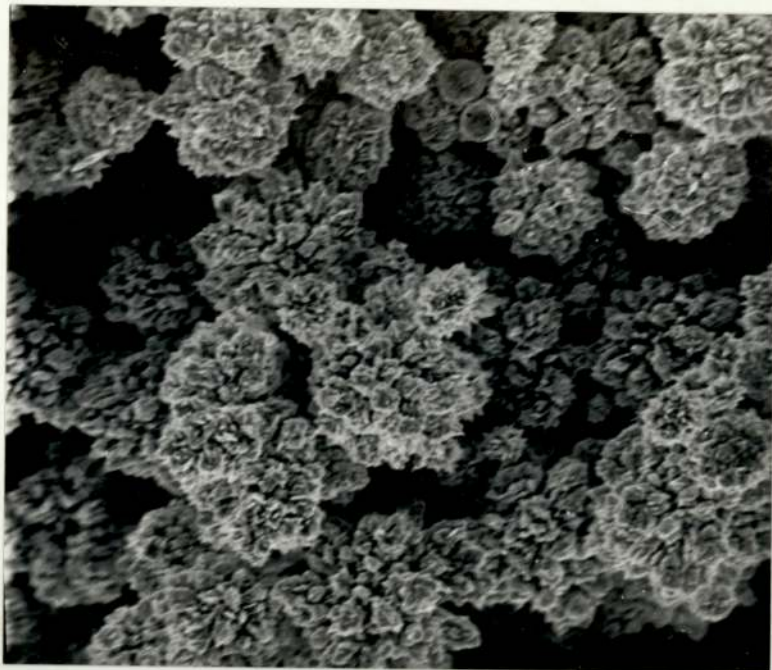
3.36. Scanning electron micrograph of gold reduced under acid conditions by ferrous sulphate at room temperature.
x 10,000



3.37. Kevex X-ray spectra of gold reduced by ferrous sulphate under a) neutral and b) alkaline conditions.



3.38. Keves X-ray spectrum of gold reduced at 100°C by ferrous sulphate.



1 μ m

3.39. Scanning electron micrograph of gold reduced under acid conditions by sodium nitrite. x 1,700



1 μ m

3.40. Scanning electron micrograph of gold reduced under neutral conditions by sodium nitrite. x 1,800

present.

Raising the temperature of the acid solutions resulted in smaller rough spheres of pure gold, the average size of which were 2-3 μ m in diameter. Diluting the gold solution to 5 g/l also reduced the size of the gold powder, but produced more irregular particles (fig. 3.41.). With all these reactions the solution first turned green with some gas evolution, prior to a precipitate forming.

3.2.12. Reduction by formaldehyde.

In alkaline solutions this system produced fine, pure, irregular particles (fig. 3.42.); whilst heating the solution forms larger, more massive grains, in which individual particles cannot be distinguished. Several impurities were present in the precipitate (figs. 3.43. and 3.44.).

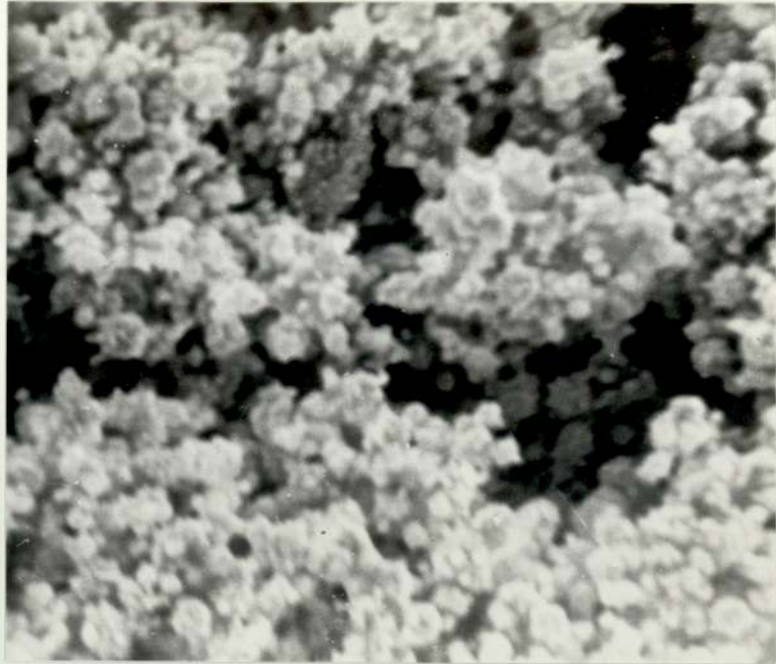
3.2.13. Reduction by trisodium citrate.

Under acid conditions, even when boiling, trisodium citrate would not reduce gold chloride. However, when the pH was raised to about 6 and then boiled, a mixed precipitate of rough spheres and flat plates was formed (fig. 3.45.) of gold uncontaminated with sodium (fig. 3.46.).

Reducing at boiling point and pH 13 produced a foam-like structure of gold particles about 0.2 μ m in diameter. There was a distinct induction period of about one minute with this system.

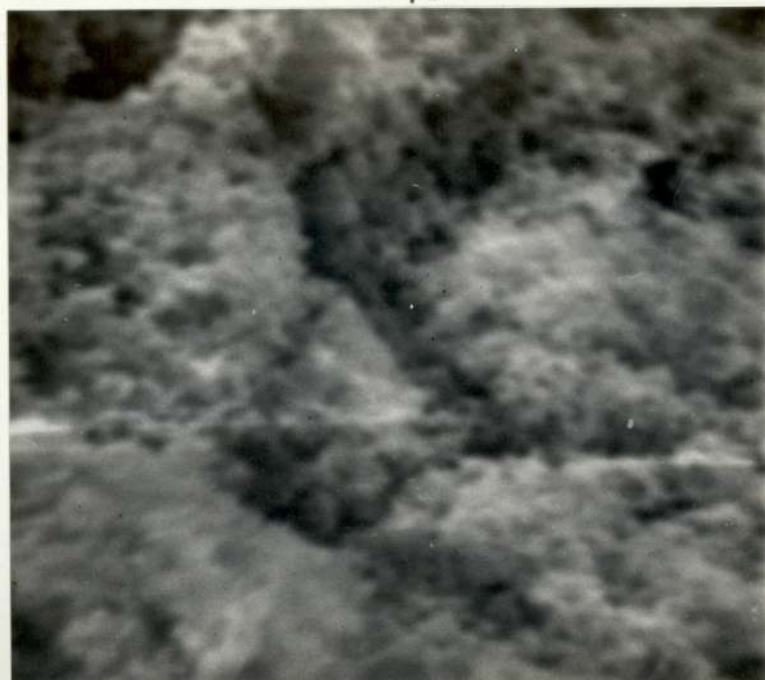
3.2.14. Reduction by hydroxylamine hydrochloride.

Gold chloride in neutral or alkaline solution was rapidly reduced to pure gold by hydroxylamine hydrochloride. Particles from neutral solutions were smooth spheres about 1 μ m in diameter (fig. 3.47.) whilst the alkaline solution gave very small particles about 0.2 μ m diameter (fig. 3.48.).



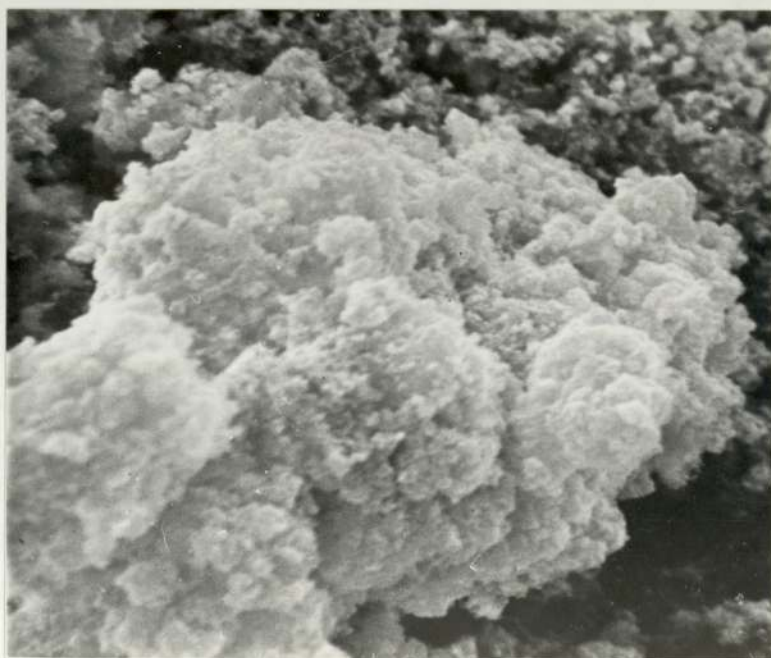
1 μ m

3.41. Scanning electron micrograph of gold reduced from dilute gold chloride solution under acid conditions by sodium nitrite. x 4,500



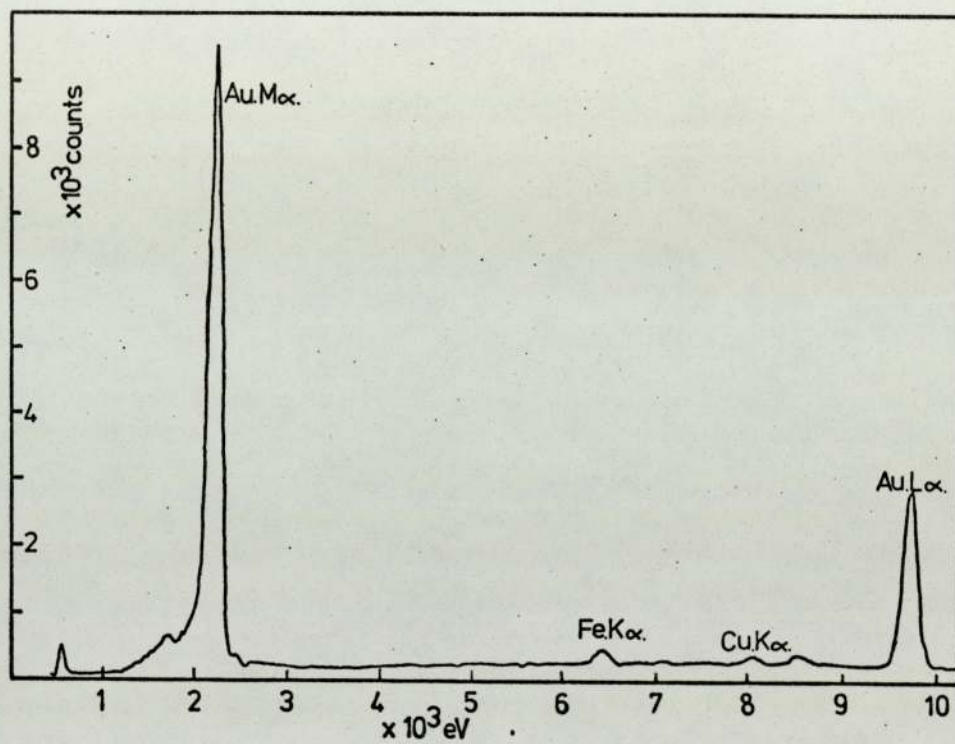
└ 1 μ m

3.42. Scanning electron micrograph of gold reduced at room temperature by formaldehyde. x 5,500

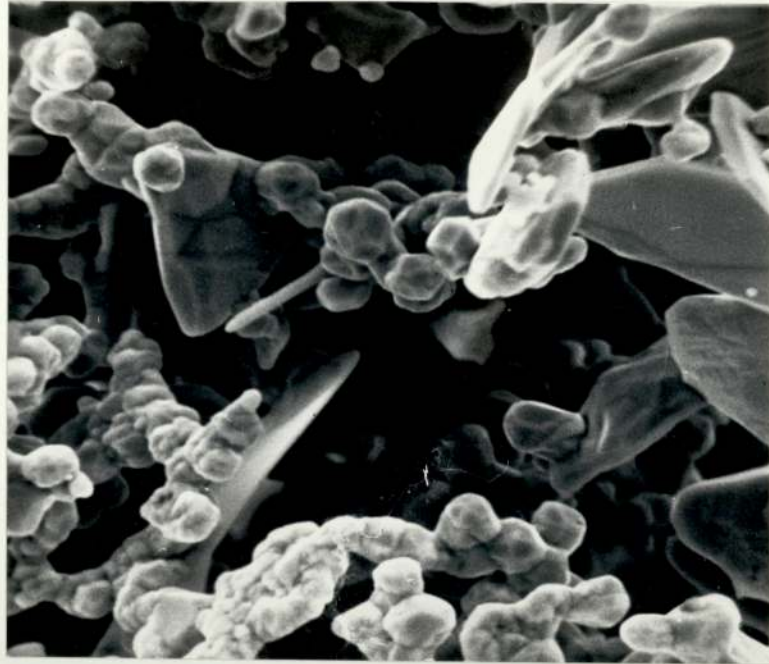


└ 1 μ m

3.43. Scanning electron micrograph of gold reduced at 100°C by formaldehyde. x 5,500

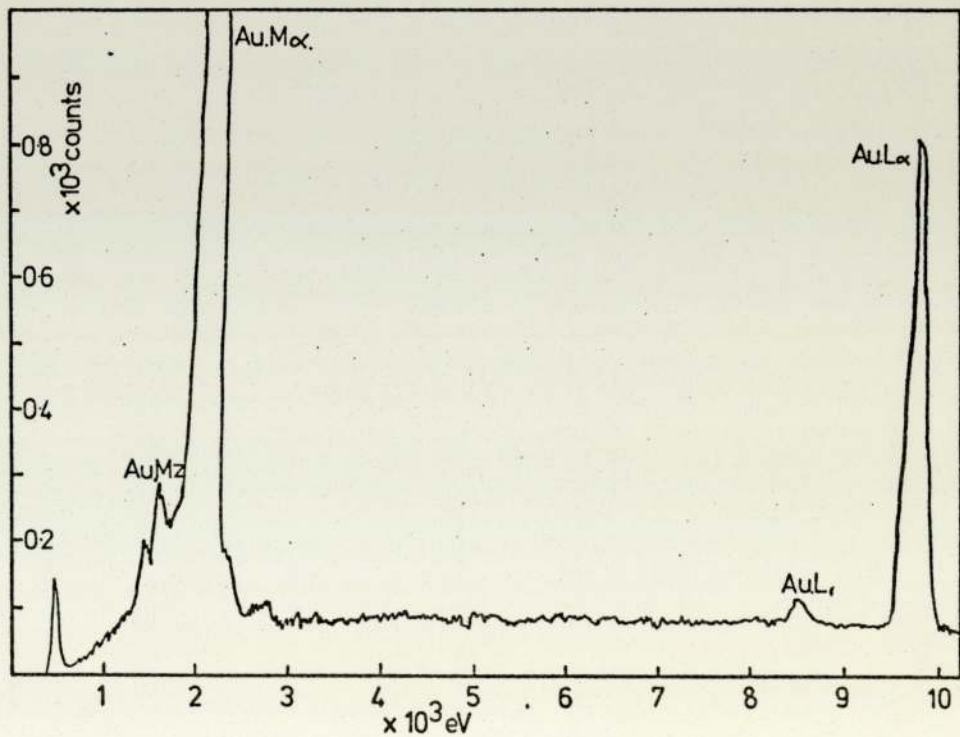


3.44. Kevex X-ray spectrum of gold reduced under hot alkaline conditions by formaldehyde.

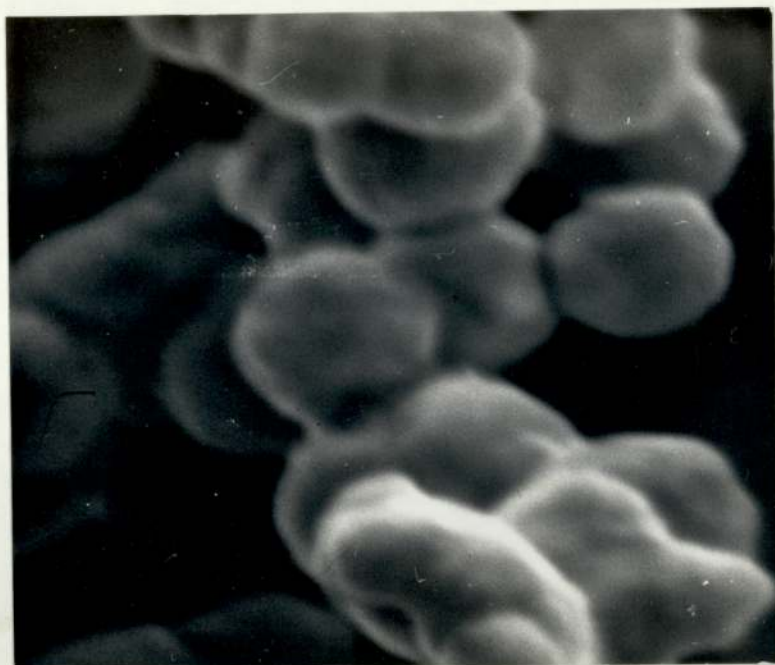


1 μ m

3.45. Scanning electron micrograph of gold reduced from a boiling solution of pH 6 by trisodium citrate. x 5,500

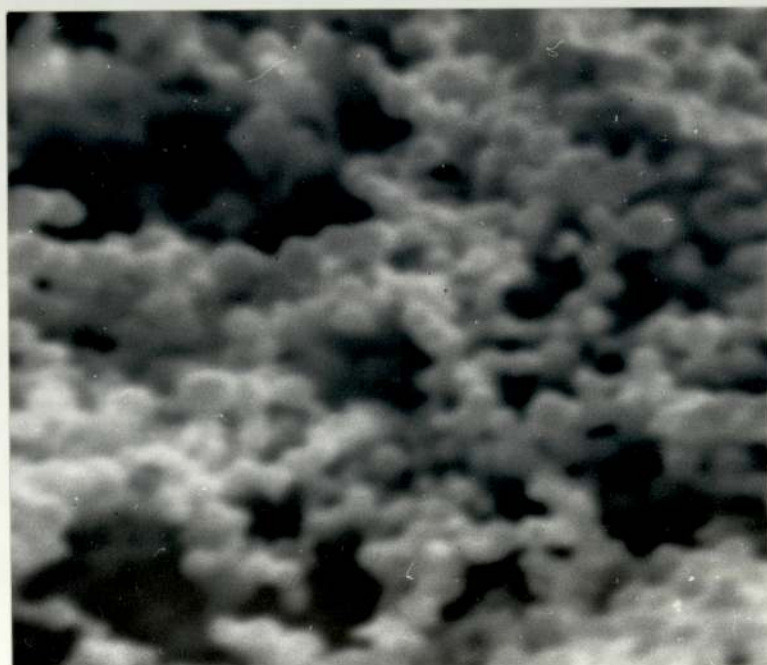


3.46. Kevex X-ray spectrum of gold reduced from boiling solution to pH 6 by trisodium citrate.



1 μ m

3.47. Scanning electron micrograph of gold reduced from neutral solution by hydroxylamine hydrochloride. x 22,000



1 μ m

3.48. Scanning electron micrograph of gold reduced from alkaline solution by hydroxylamine hydrochloride. x 21,000

3.2.15. Reduction by hydrazine hydrochloride.

When added slowly to gold chloride at room temperature, hydrazine hydrochloride precipitated a pure gold powder of rough spheres about $0.3\mu\text{m}$ in diameter (fig. 3.49.).

When the gold chloride was made alkaline with ammonia solution, a yellow-white precipitate of gold fulminate formed, which when washed, was reduced by hydrazine hydrochloride to give a foamlike structure of small gold particles, about $0.1\mu\text{m}$ in diameter (fig. 3.50.).

3.2.16. Reduction by oxalic acid.

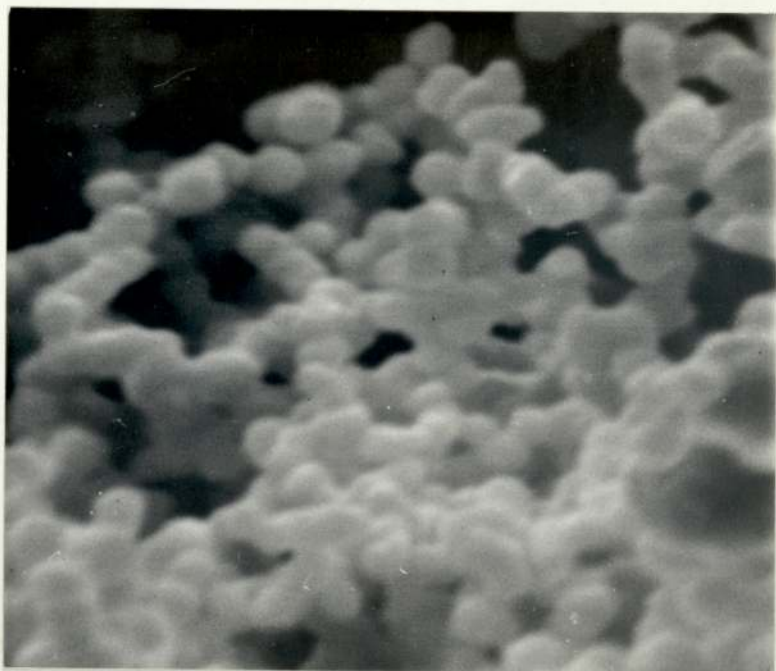
Boiling gold chloride and oxalic acid solutions together produced a pure gold powder of mixed spheres and large flat plates (fig. 3.51.). There was a distinct induction period with this system.

3.2.17. Reduction by Faraday's solution.

Mixing a solution of white phosphorous in ether with gold chloride solution gave an 'oily' precipitate under a green liquid. This liquid may have been a colloid as it did not clear within 18 days. The precipitate was composed of very small spheres about $0.1\mu\text{m}$ in diameter (fig. 3.52.). As the main phosphorous energy peak coincided with the $M\alpha$ line for gold⁽¹²²⁾ it was not possible to determine whether or not phosphorous was present in the gold (fig. 3.53.).

3.2.18. Reduction by zinc.

Zinc dust reduction gave massive irregular particles, (fig. 3.54.) heavily contaminated with zinc (fig. 3.55.).



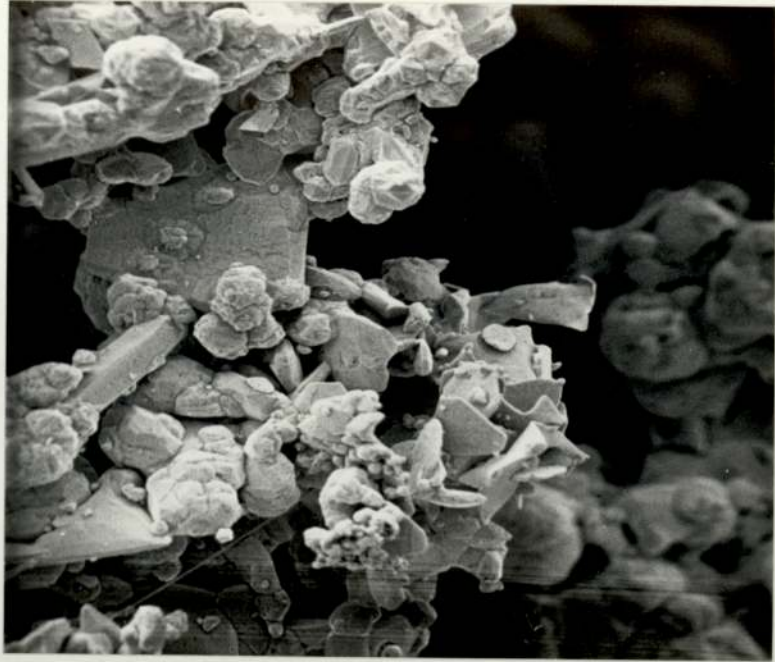
1 μ m

3.49. Scanning electron micrograph of gold reduced under acid conditions by hydroxylamine hydrochloride. x 23,000



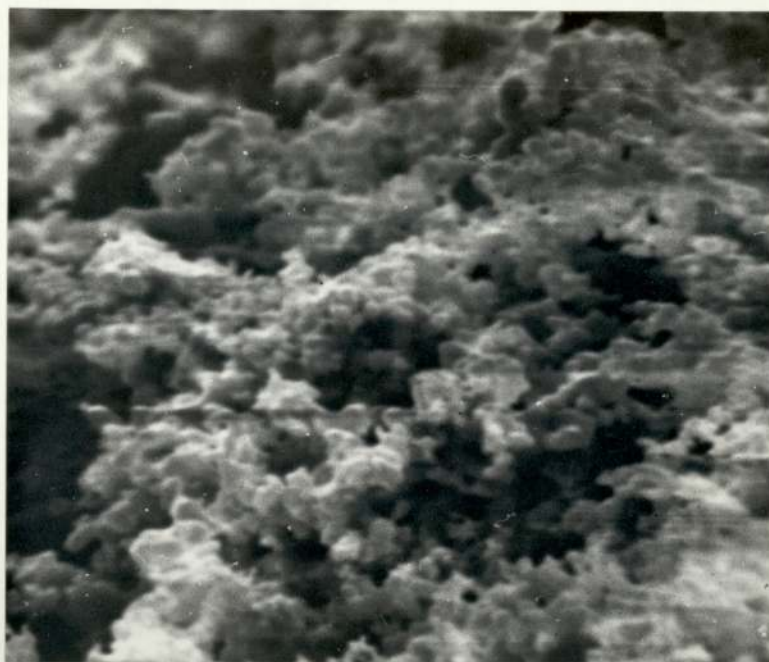
1 μ m

3.50. Scanning electron micrograph of gold reduced by hydrazine hydrochloride via gold fulminate. x 5,500

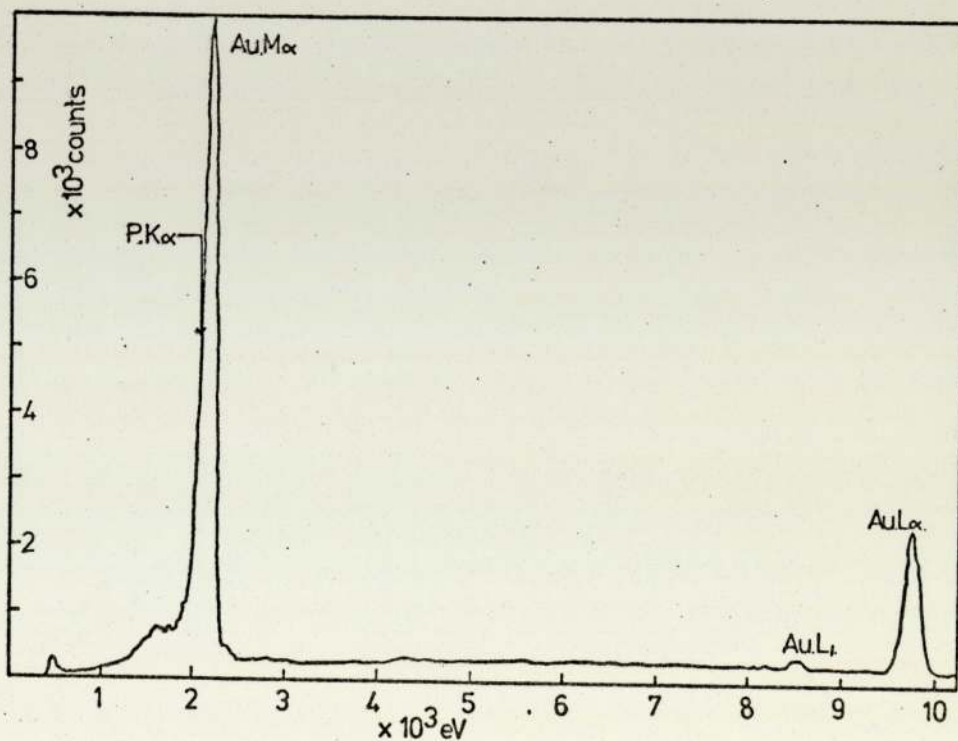


.1 μ m

3.51. Scanning electron micrograph of gold reduced at boiling point by oxalic acid solution. x 690.



3.52. Scanning electron micrograph of gold reduced by Faraday's solution. x 22,000

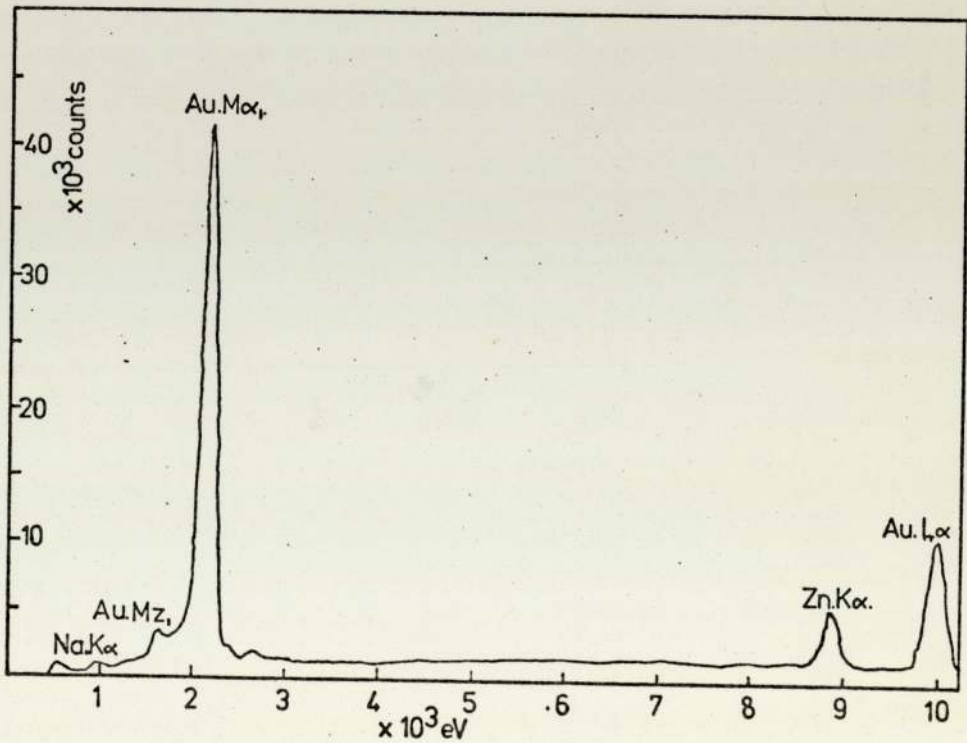


3.53. Kevex X-ray spectrum of gold reduced by Faraday's solution.



1 μ m

3.54. Scanning electron micrograph of gold reduced by zinc dust. x 2,600



3.55. Kevex X-ray spectrum of gold reduced by zinc.

3.2.19. Reduction by electrolysis.

Electrolysis of a 5 g/l (0.025 molar) gold solution at current densities of between 12 and 18 Amps/dm² gave rise to two types of gold, a pure dendritic gold on the cathode (fig. 3.56.) and an irregularly shaped 'dust' floating in the solution (fig. 3.57.). The 'dust' was impure and contained iron, nickel and chloride (fig. 3.58.). The electrodes used were a stainless steel cathode and a carbon anode. Lowering the gold content of the solution to 1 g/l (0.005 molar) produced only a few small irregular growths.

3.3. Nucleation and Growth.

An attempt was made to separate the processes of nucleation and growth of the gold particles, by adding seed nuclei to a growth solution. The nuclei were precipitated by the addition of sodium sulphite to gold chloride solution and the growth solution was an acidified hydroxylamine hydrochloride solution. The particle size distribution of the nuclei and final precipitate are shown in fig. 3.59.

3.4. Alloy Gold Powders.

This was not a success as only two of the precipitates contained anything other than pure gold. One, a gold/cobalt mixture reduced at greater than pH 8, contained some cobalt but this is thought to be entrapped Co(OH)₂. The other alloy was from a gold/palladium chloride solution reduced by hydrazine hydrochloride via the fulminate. This was in the form of a foam similar to that produced by reducing gold fulminate alone (fig. 3.50.), and it contained much less palladium than the original 50/50 mixture (fig. 3.60).

Although the gold/palladium mixture reduced with sulphurous acid produced only pure gold, the spiky particles formed (fig. 3.61.) were all



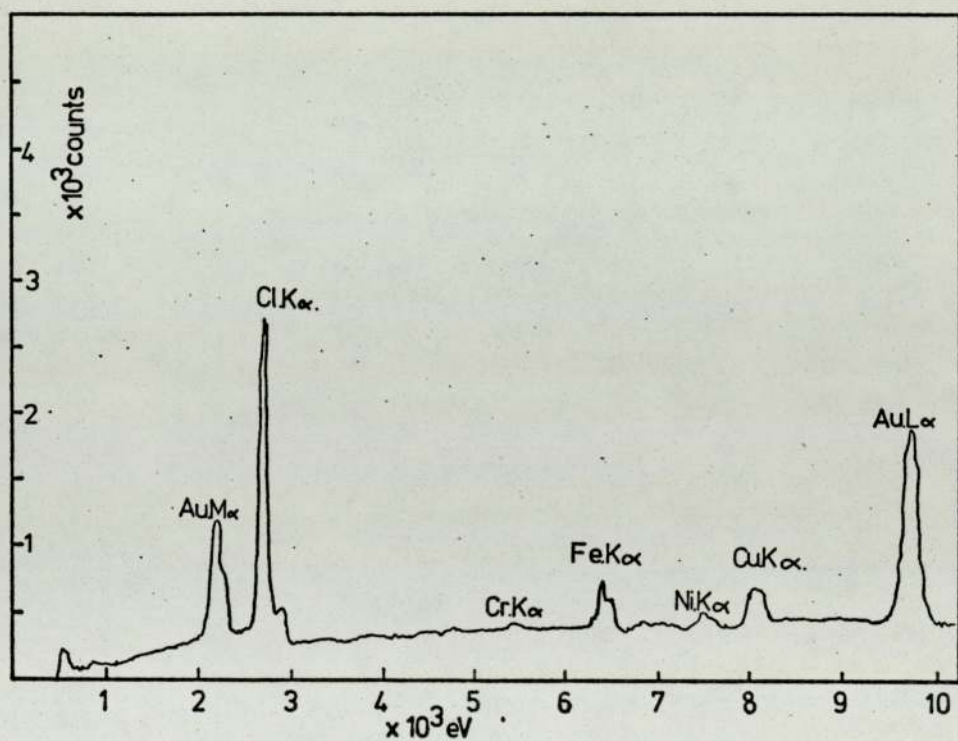
1 μ m

3.56. Scanning electron micrograph of gold found on the cathode after electrolysis. x 2,200

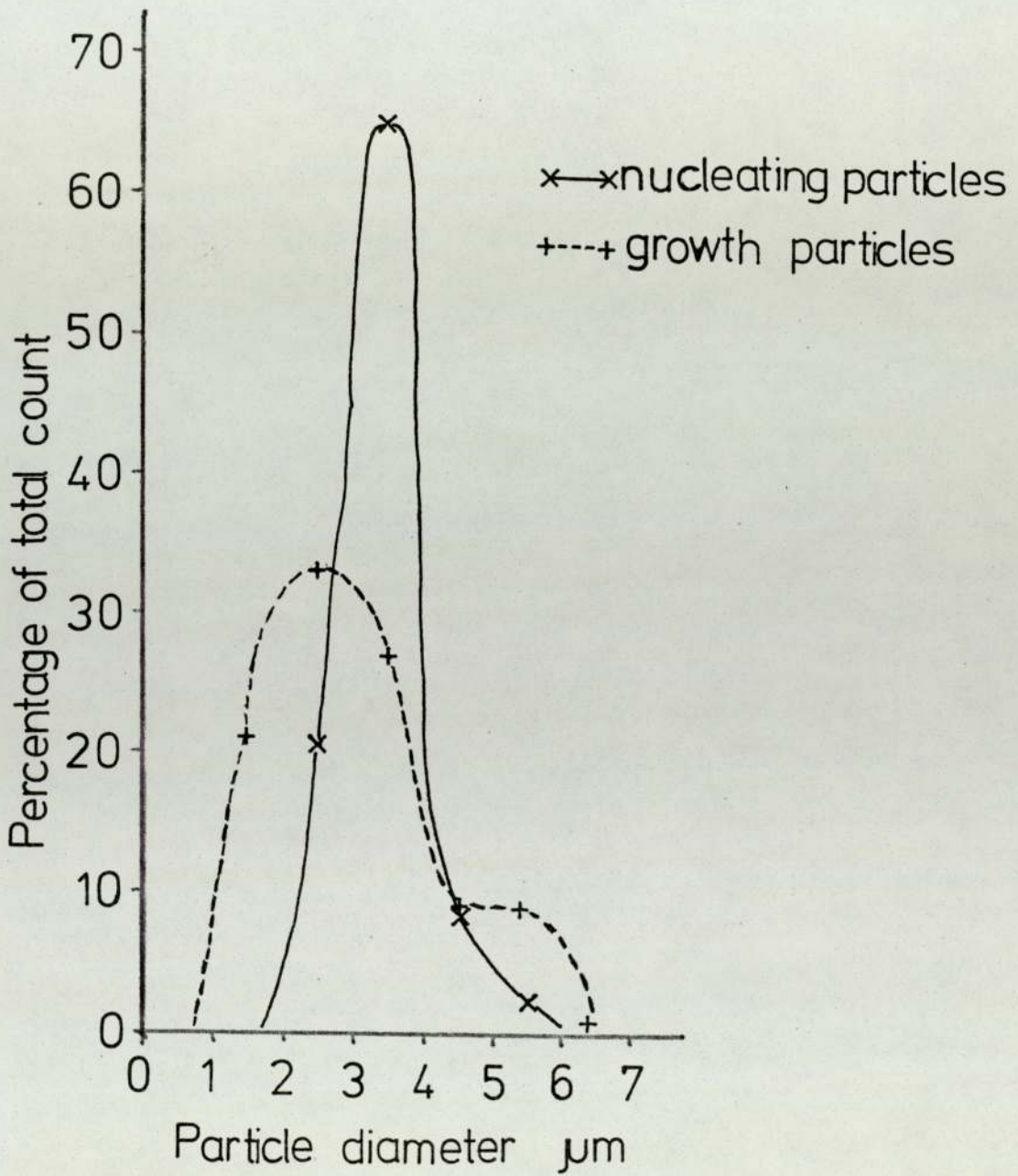


1 μ m

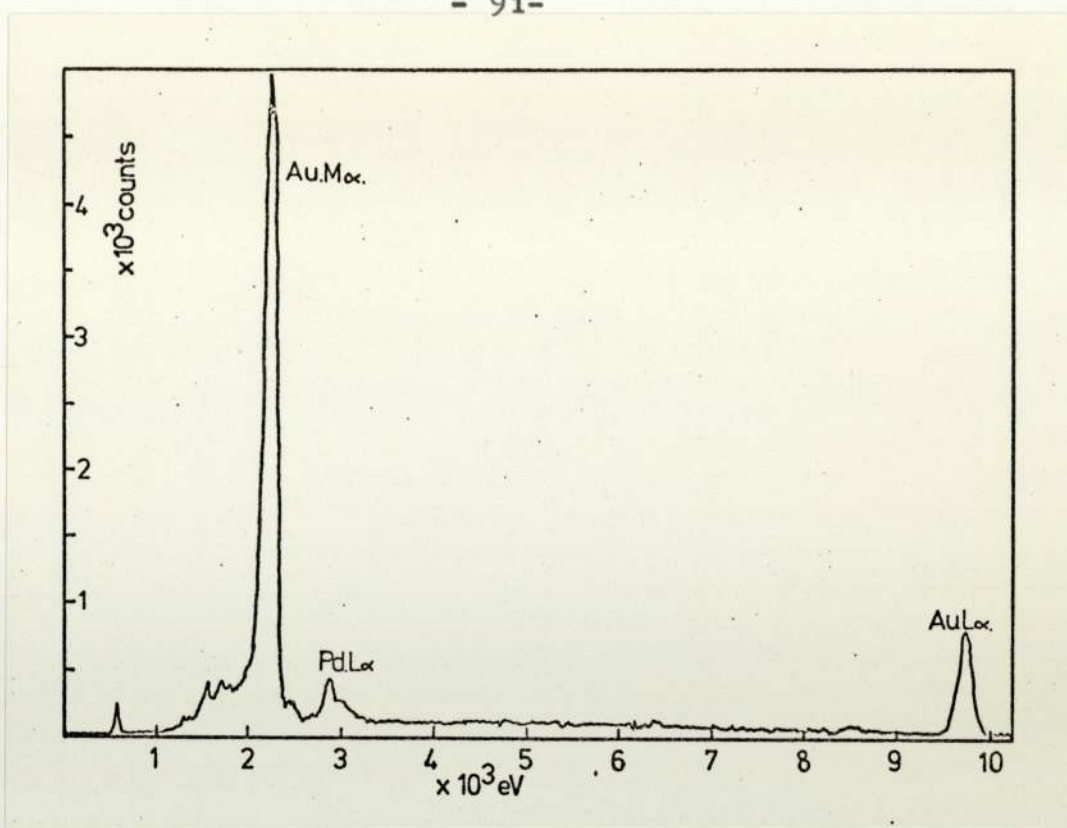
3.57. Scanning electron micrograph of gold found in the body of the electrolyte after electrolysis. x 2,300



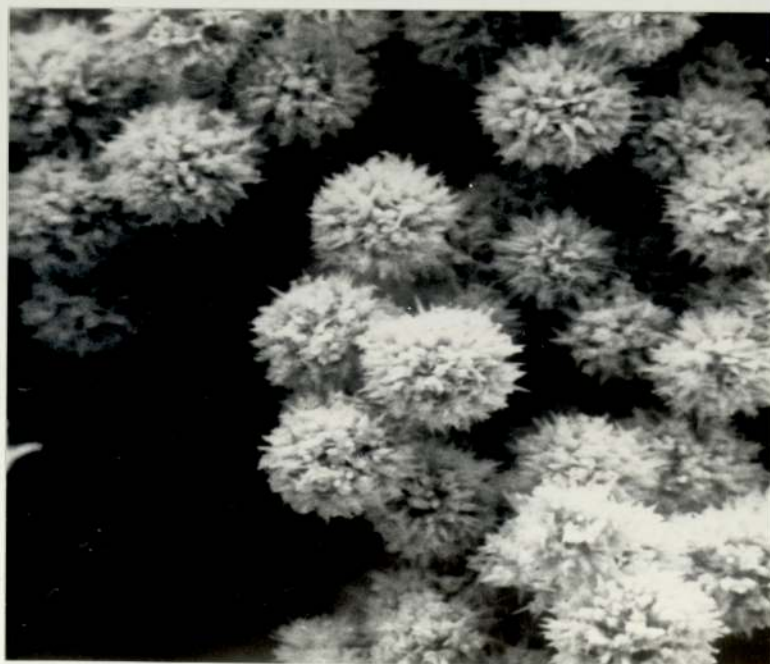
3.58. Kevex X-ray spectrum of gold found in the body of the electrolyte after electrolysis.



3.59. Particle size distribution of nuclei and particles grown from acidified hydroxylamine hydrochloride.



3.60. Kevex X-ray spectrum of gold/palladium reduced by hydrazine hydrochloride via gold/palladium fulminate.



3.61. Scanning electron micrograph of gold reduced from a gold/palladium chloride mixture by sulphur dioxide.
x 7,000.

very uniform in size (fig. 3.62.).

3.5. Other Metal Powders.

Of the palladium reductions tried, only nascent hydrogen (lithium hydride) and acidic sodium formate produced precipitates. Both were pure palladium with particles about $0.1\mu\text{m}$ in diameter or smaller (fig. 3.63.). The palladium produced by hot sodium formate was smaller in diameter than that produced at room temperature.

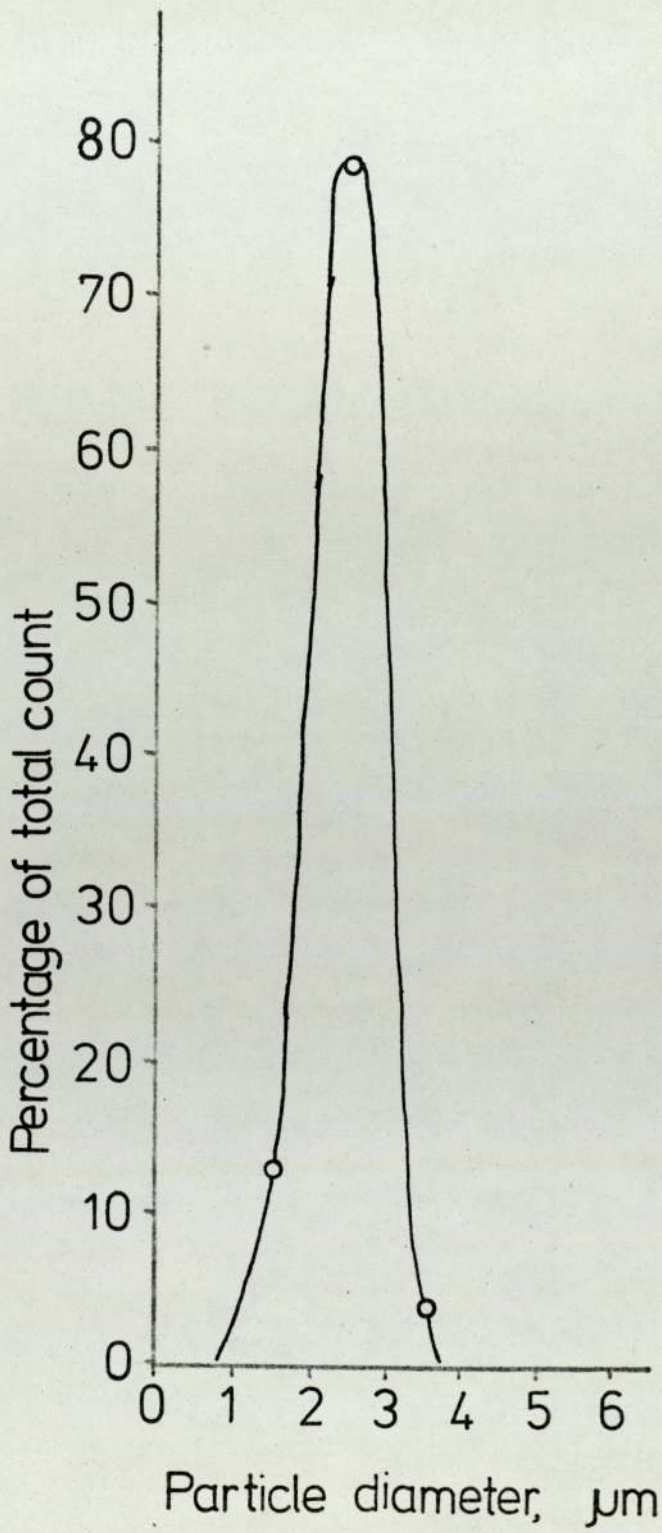
The palladium/nickel alloy formed a black precipitate which took some time to settle into a dried massive form (fig. 3.64.). It contained mainly sulphur as well as palladium and nickel (fig. 3.65.). This powder had to be crushed before it could be used.

The only reduction method for nickel which produced any powder was that using nascent hydrogen, and only then when produced by sodium hydride. Reduction would only occur if concentrated nickel chloride solution was added to excess sodium hydride, and as the reaction was very violent, it was not taken any further. The particles formed were very small and held together in a massive lump (fig. 3.66.).

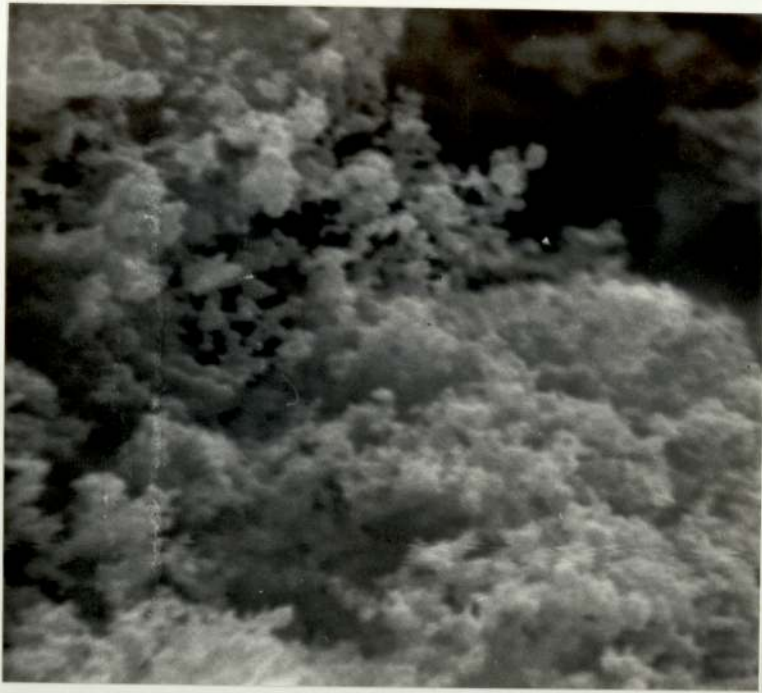
The acidified copper salts were easier to reduce and gave large rough spheres $7-10\mu\text{m}$ in diameter (fig. 3.67.). Those reduced by iron dust plus ferrous sulphate were fairly iron free, but those reduced with the iron dust only were heavily contaminated (fig. 3.68.).

The palladium obtained from Hopkins and Williams was slightly contaminated with chlorine (fig. 3.69.), and in the form of irregularly shaped particles about $1\mu\text{m}$ in diameter (fig. 3.70.). The palladium/tin alloy was finer, about $0.1\mu\text{m}$ (fig. 3.71.), with the majority of the material being palladium (fig. 3.72.).

Both the nickel and iron powder produced by the carbonyl process



3.62. Particle size analysis of gold powder reduced from a gold/palladium chloride mixture by sulphur dioxide.



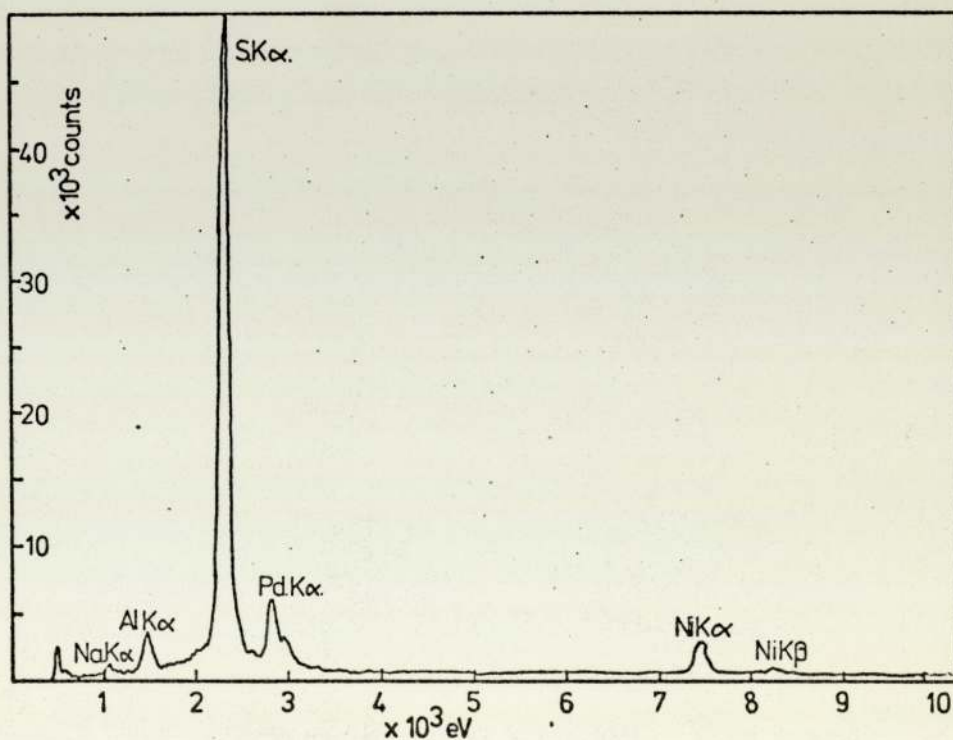
— 1 μ m

3.63. Scanning electron micrograph of palladium reduced by nascent hydrogen. x 10,000



1 μ m

3.64. Scanning electron micrograph of palladium/nickel powder reduced from mixed solution of chlorides by sodium thiosulphate. x 5,400

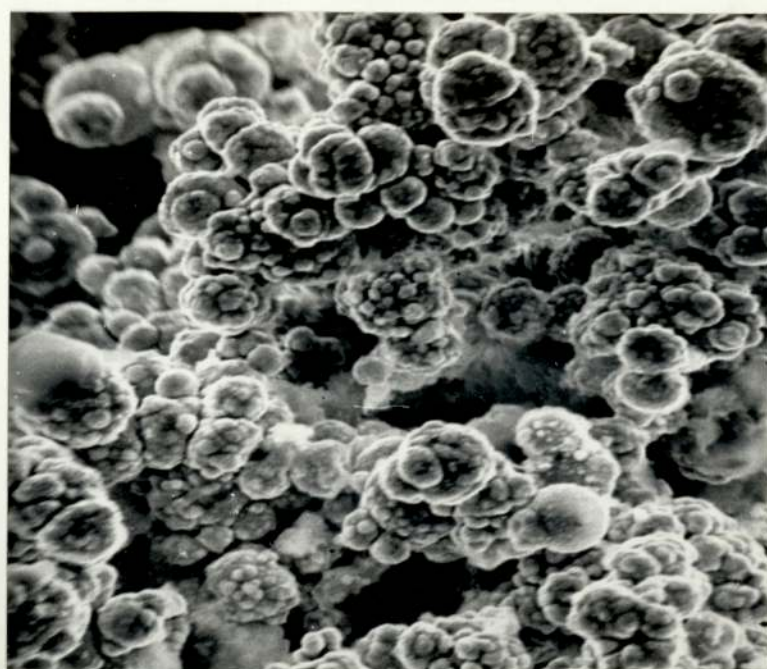


3.65. Kevex X-ray spectrum of palladium/nickel reduced from mixed solution of chlorides by sodium thiosulphate.



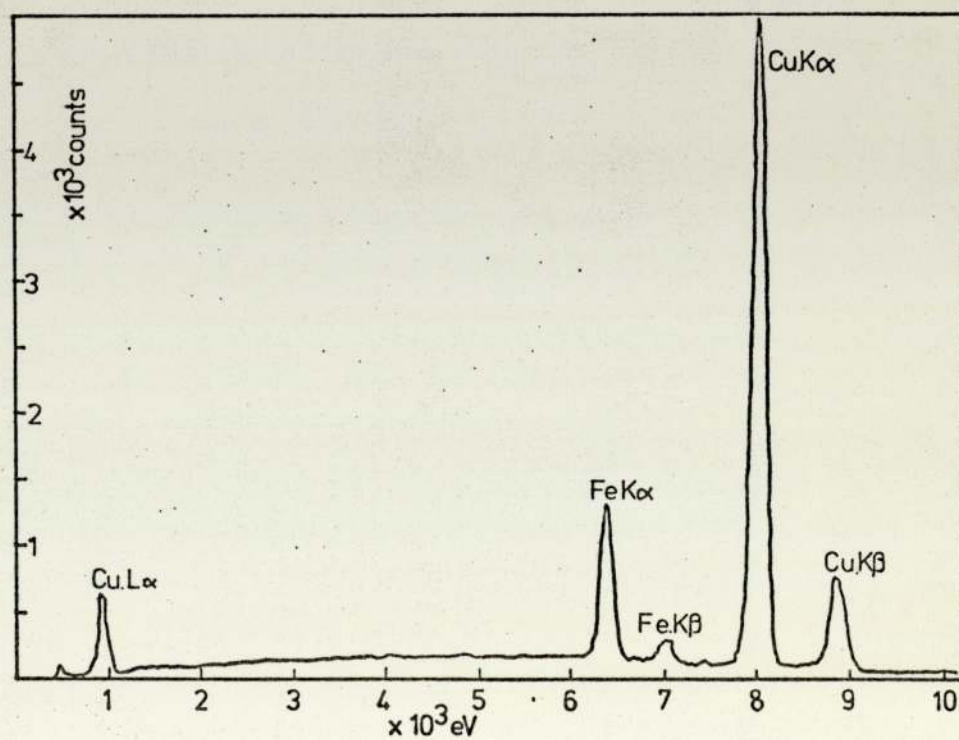
└ 1 μ m

3.66. Scanning electron micrograph of nickel reduced by nascent hydrogen from sodium hydride. x 6,400

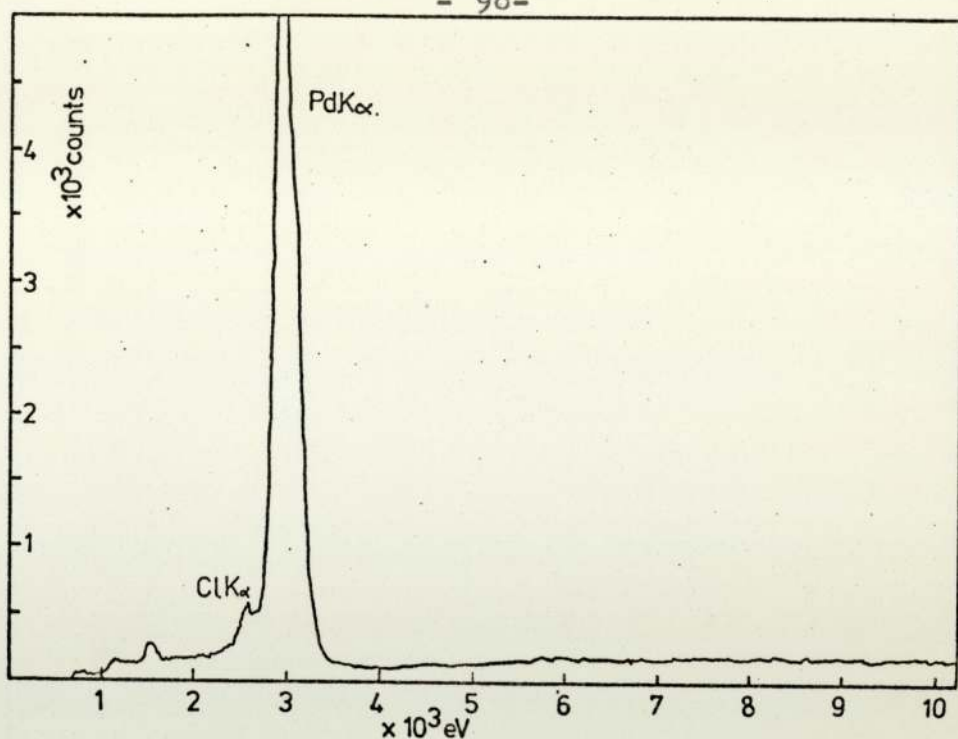


1 μ m

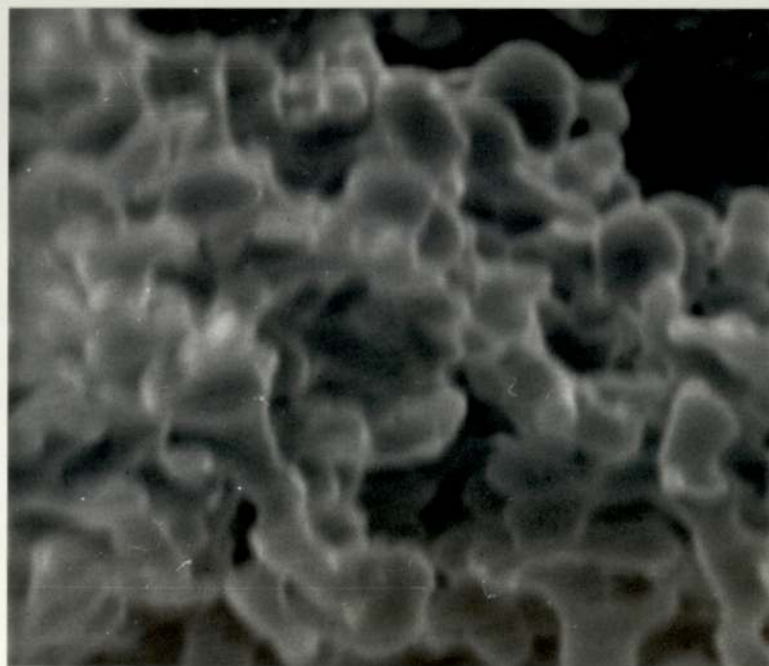
3.67. Scanning electron micrograph of copper reduced by iron powder and ferrous sulphate. x 2,000



3.68. Kevex X-ray spectrum of copper reduced by iron powder.



3.69. Kevex X-ray spectrum of palladium from Hopkins and Williams.

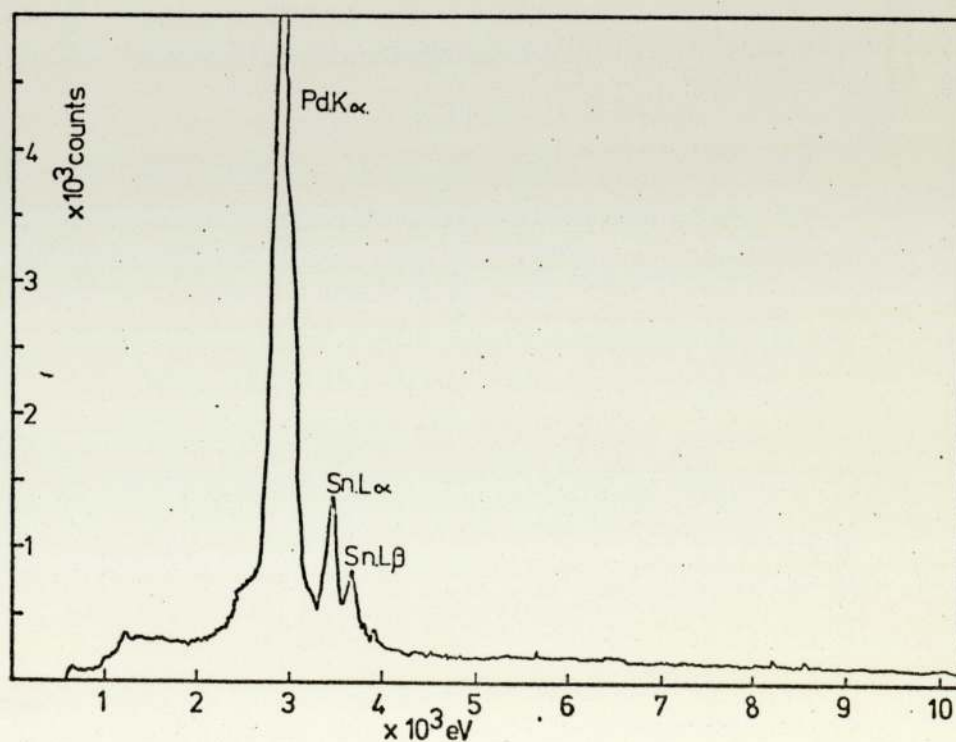


3.70. Scanning electron micrograph of palladium from Hopkins and Williams. x 11,500



— 1 μ m

3.71. Scanning electron micrograph of palladium/tin powder from plating on plastics waste. x 10,500



3.72. Kevex X-ray spectrum of palladium/tin powder from plating on plastics waste.

were composed of smooth spheres of the pure metal (figs. 3.73. and 3.74.). The particle size distribution is shown in fig. 3.75.

3.6. Production of Gold Powders for Pastes.

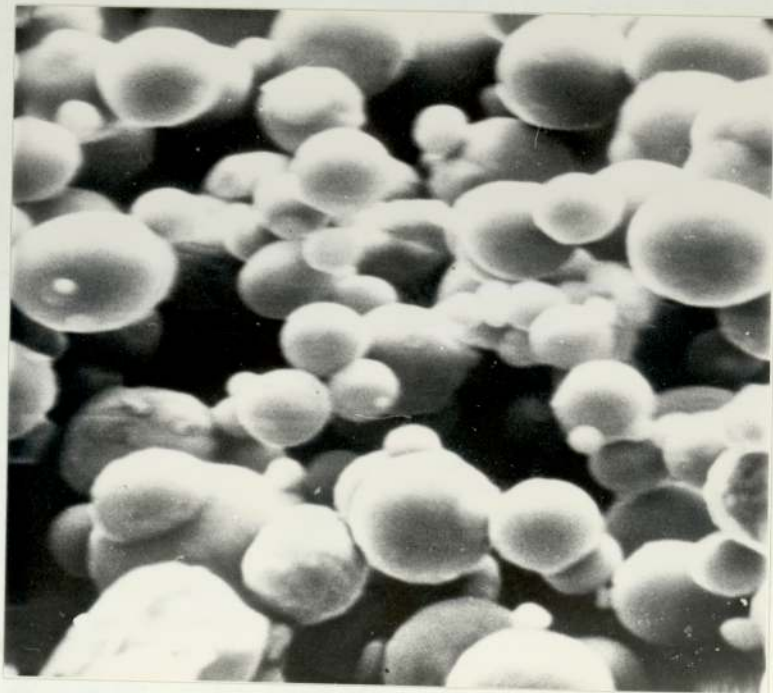
Most of the gold powder used in paste production was reduced from gold chloride solution by sodium sulphite at an approximate pH of 2. To test the reproduceability of this method, five 'identical' batches of gold chloride solution were reduced under 'identical' conditions. The particle size distribution is shown in fig. 3.76.

Most of the powders used for pastes were reduced in six batches, of different sizes, but under similar conditions, i.e., gold chloride 50 g/l, pH 1-2; sodium sulphite 200 g/l, pH 2-3; excess sulphite at room temperature. The details of the batches are given below and particle size distributions are shown in fig. 3.77.

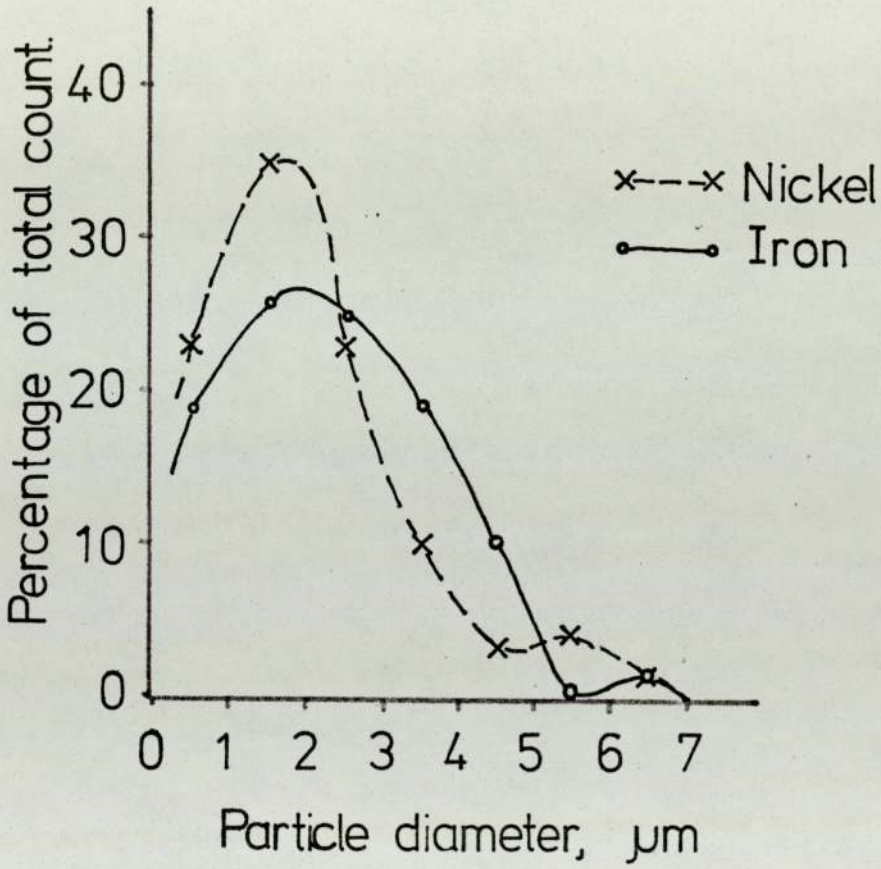
<u>Code.</u>	<u>ml. of 50 g/l gold reduced.</u>	<u>diameter of mode.</u> (μm)
G39	50	3.5
G46	250	0.5
G54	130	1.5
G61	60	2.7
G64	250	1.0
G80/81	140 x 2	2.3



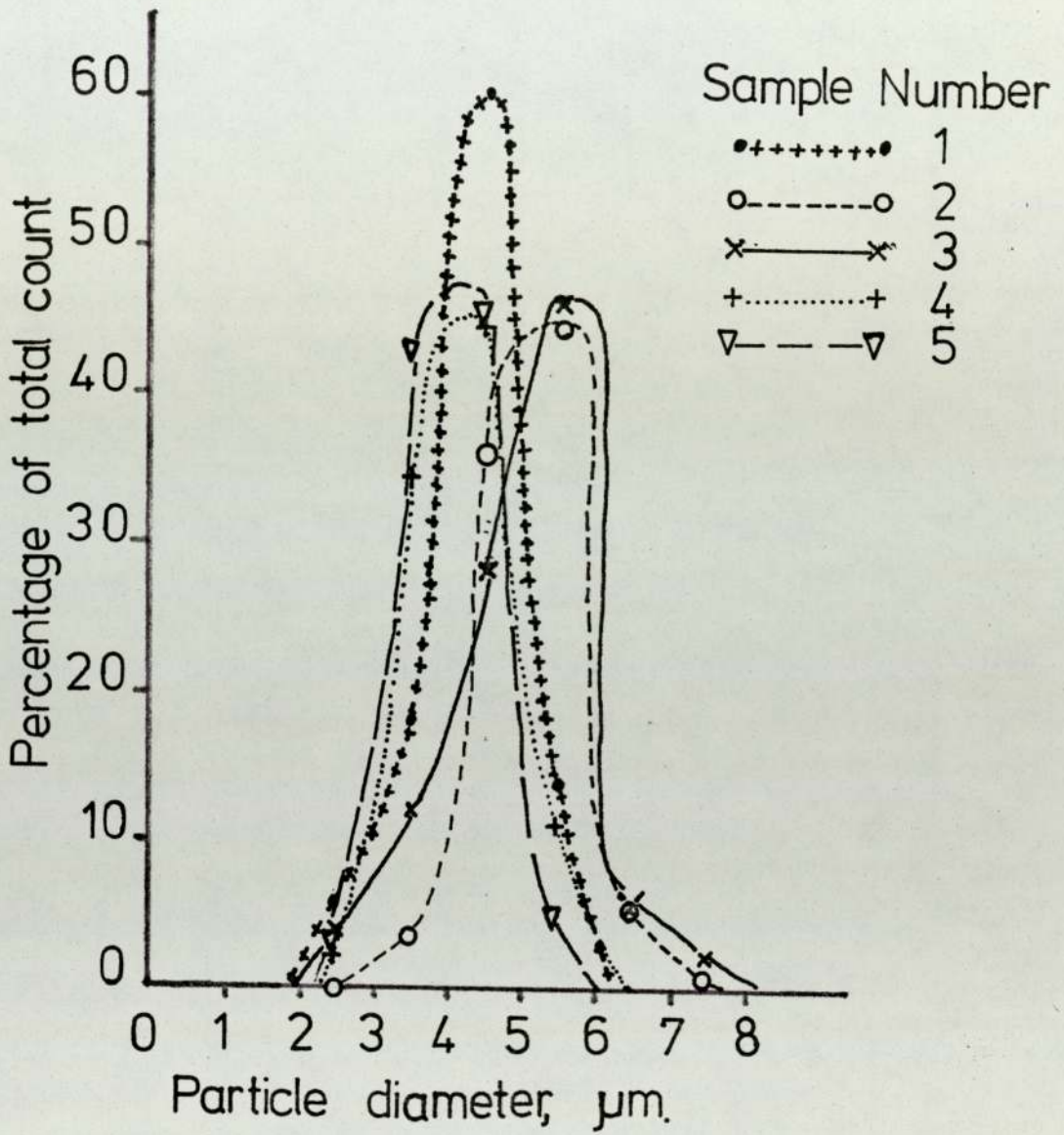
3.73. Scanning electron micrograph of nickel reduced by carbonyl process. x 5,400



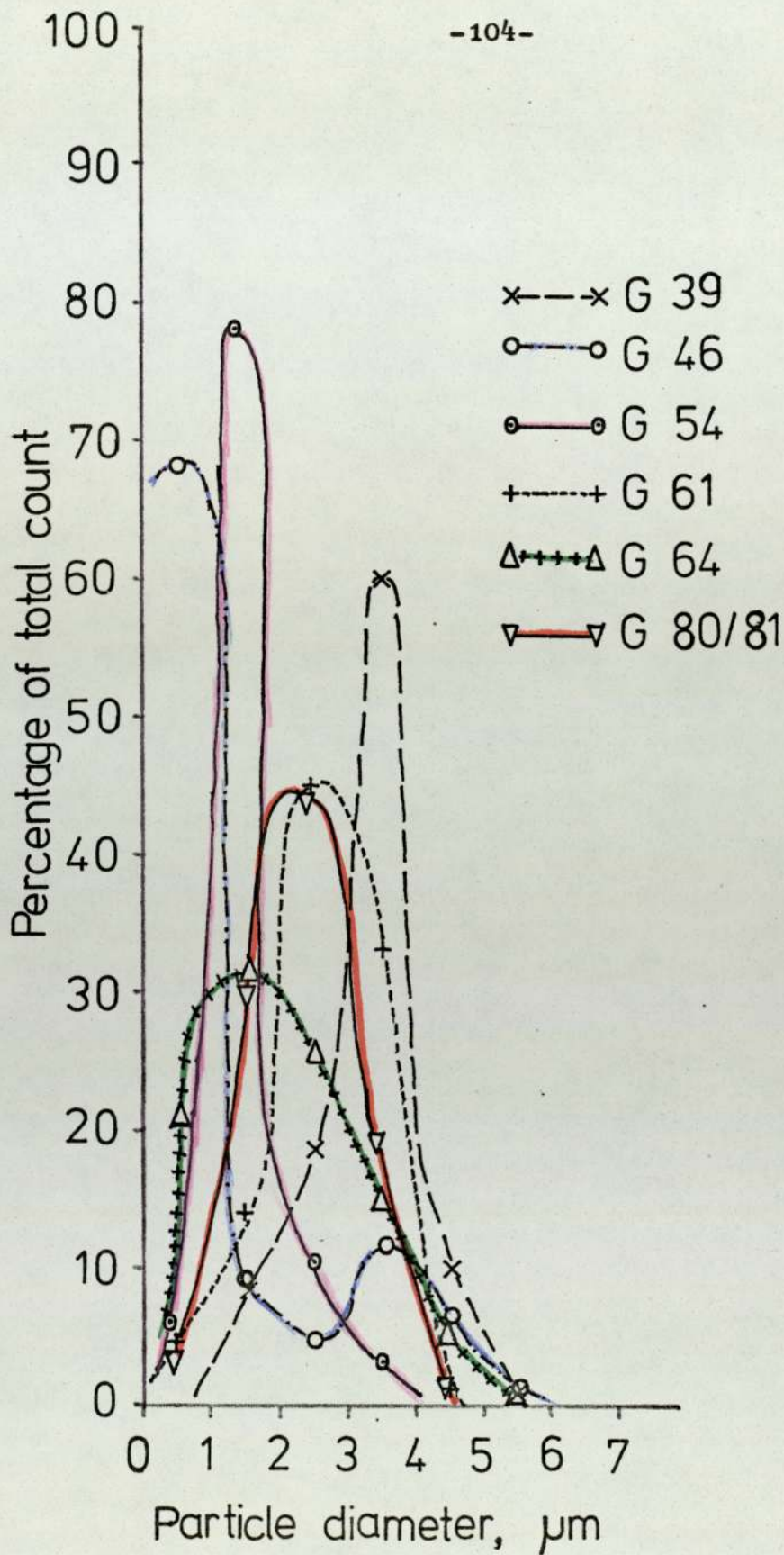
3.74. Scanning electron micrograph of iron reduced by carbonyl process. x 5,400



3.75. Particle size distribution of nickel and iron powders.



3.76. Particle size distribution of five identical samples reduced by sodium sulphite under acid conditions at room temperature.



3.77. Particle size distribution of 'production' batches.

4. DISCUSSION OF POWDER PRECIPITATION.

4.1. Particle Size.

The majority of the powders produced in this work exhibited a wide spread of particle sizes, and in most cases the mode size did not appear to be dependent on any one factor. As few of these powders would fit into the ideal required for close packing,⁽¹⁰⁶⁾⁽¹⁰⁷⁾ it is instructive to examine possible causes of the variations in particle size and range.

4.1.1. Variations in mixing.

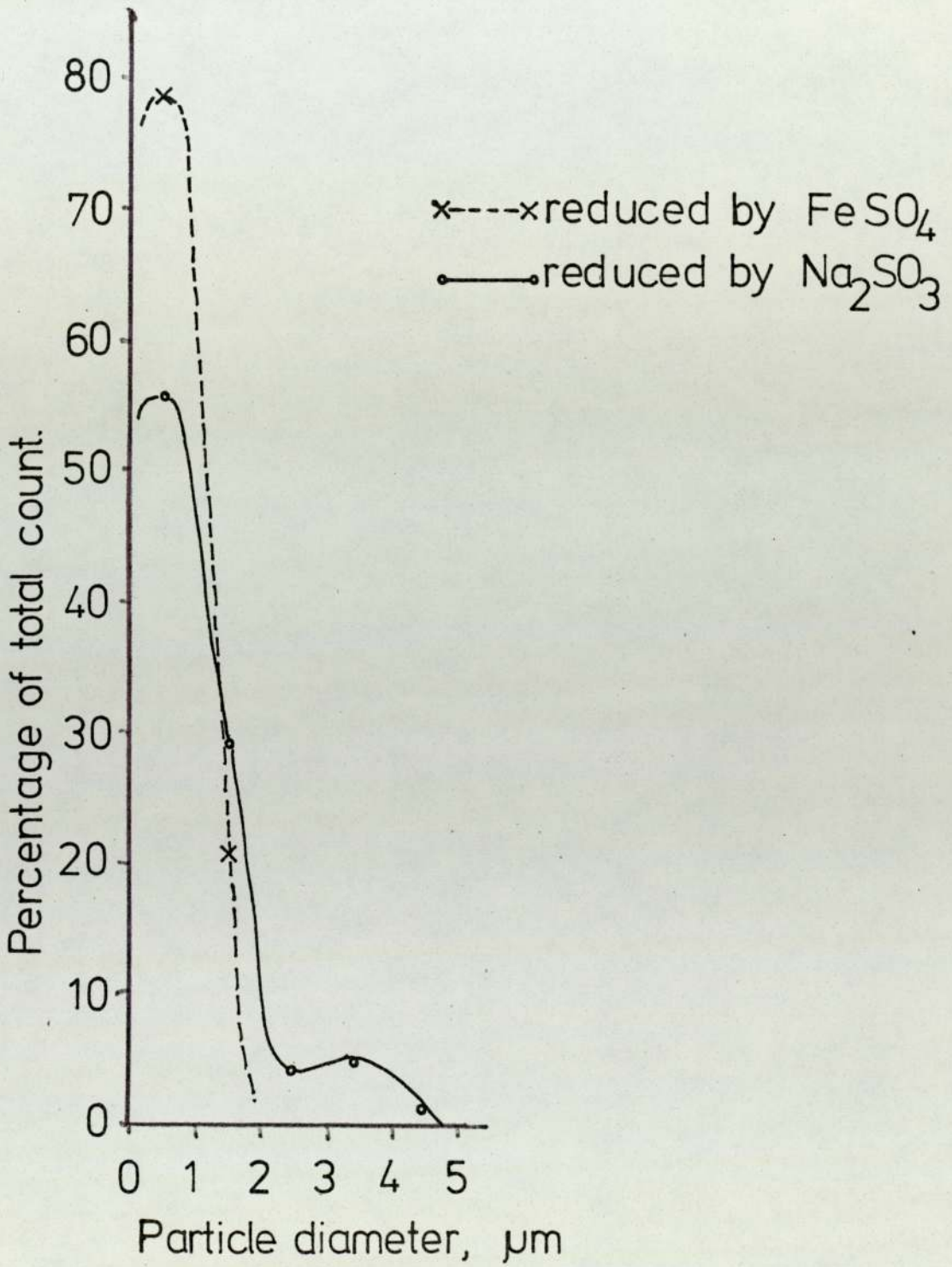
Without designing specific experiments it is difficult to assess the efficiency of mixing within the solutions. The information shown in fig. 3.3. refers only to the rate of addition of the reagents, but shows an increase in size spread with slower additions. It is doubtful whether any of the systems used in this work had addition rates as slow as the slow rate shown in fig. 3.3.

Variations in mixing efficiency may be the cause of the variations in particle size of the 'production' batches of gold powder (fig. 3.77.). With the exception of batch G80/81, which had a different pH 'history', the mode of the particle sizes shows a rough correlation with the volume of gold chloride reduced, and indirectly with the size of the reduction vessel. With smaller batches, there will be a greater proportion of the solution influenced by the friction between liquid and the reaction vessel walls, which could reduce the efficiency of mixing. These smaller volume batches have a larger size mode, and greater size range than the larger batches. This however, may just be coincidental as the production of these powders is much influenced by the generating and precipitation reactions.

4.1.2. Reduction and precipitation reactions.

Again, without specifically designed experiments, it is impossible to distinguish conclusively which of these reactions is controlling the precipitation of the powders. However, with the gold precipitation, some systems, such as those reduced by ferrous sulphate, exhibit no induction periods prior to precipitation; whilst others, such as sodium sulphite, trisodium citrate and ferrous chloride exhibit distinct induction periods. In these circumstances it seems reasonable to suppose that these induction periods are caused by the reduction reaction rather than the precipitation reaction. This is in keeping with the findings of Turkevich et al.,⁽⁸³⁾ who claimed that this induction period was necessary for the breakdown of the reducing agents into more active compounds. In the work of Turkevich et al.⁽⁸³⁾ using trisodium citrate, the active component was acetone dicarboxylic acid, and direct use of this compound removed the induction period. The build-up of this active compound occurs over a finite time and this causes an even slower build-up of the nucleation reaction. Turkevich et al.⁽⁸³⁾ found that there was a slow build-up of the nucleation rate, then a long period of steady nucleation, followed by a fall off of the rate of nuclei formed. This spread of nucleation over a period of time will lead to a spread of final particle size with systems having an induction period showing a wider spread than those which have not. This was found in this work. Ferrous sulphate reduced gold powder, which showed no induction period, had a size mode of about $0.5\mu\text{m}$ and a maximum size of $2\mu\text{m}$, whilst the gold reduced with sodium sulphite solution had the same mode, but a spread of up to $4\mu\text{m}$ (fig. 4.1.). Other systems with induction periods, for example sulphur dioxide, show even greater spread of sizes.

The growth process emphasises these size differences, as Nielsen⁽⁷⁸⁾ has shown that for most solutions, the growth mode (and



4.1. Particle size distribution of gold reduced by ferrous sulphate or by sodium sulphite, with a size mode of $0.5\mu\text{m}$.

consequently the growth rates), changes as the super-saturation ratio drops. As a result, those particles which nucleate first are disproportionately larger than those which nucleate later.

These conditions only apply to liquid/liquid systems where perfect mixing is possible. In liquid/solid and liquid/gas reactions there is always a local concentration of one reagent, and mass transport to the solid or gas is often the limiting factor.⁽¹²⁶⁾ Both these cases are likely to give rise to different size and size range relationships than those found in the liquid/liquid reduction system.

4.1.3. Measurement errors.

The measurement and arranging of the particle size may cause some of the spread of results, as they will introduce errors at almost all stages of sampling and measuring. Samples taken from the gold powder should be fairly random, as the particles themselves tend to be loosely clustered together, and whilst one cluster may not be a fair sample of the population, several clusters should be. It is therefore of little significance if the clusters themselves have segregated into large or small clusters.

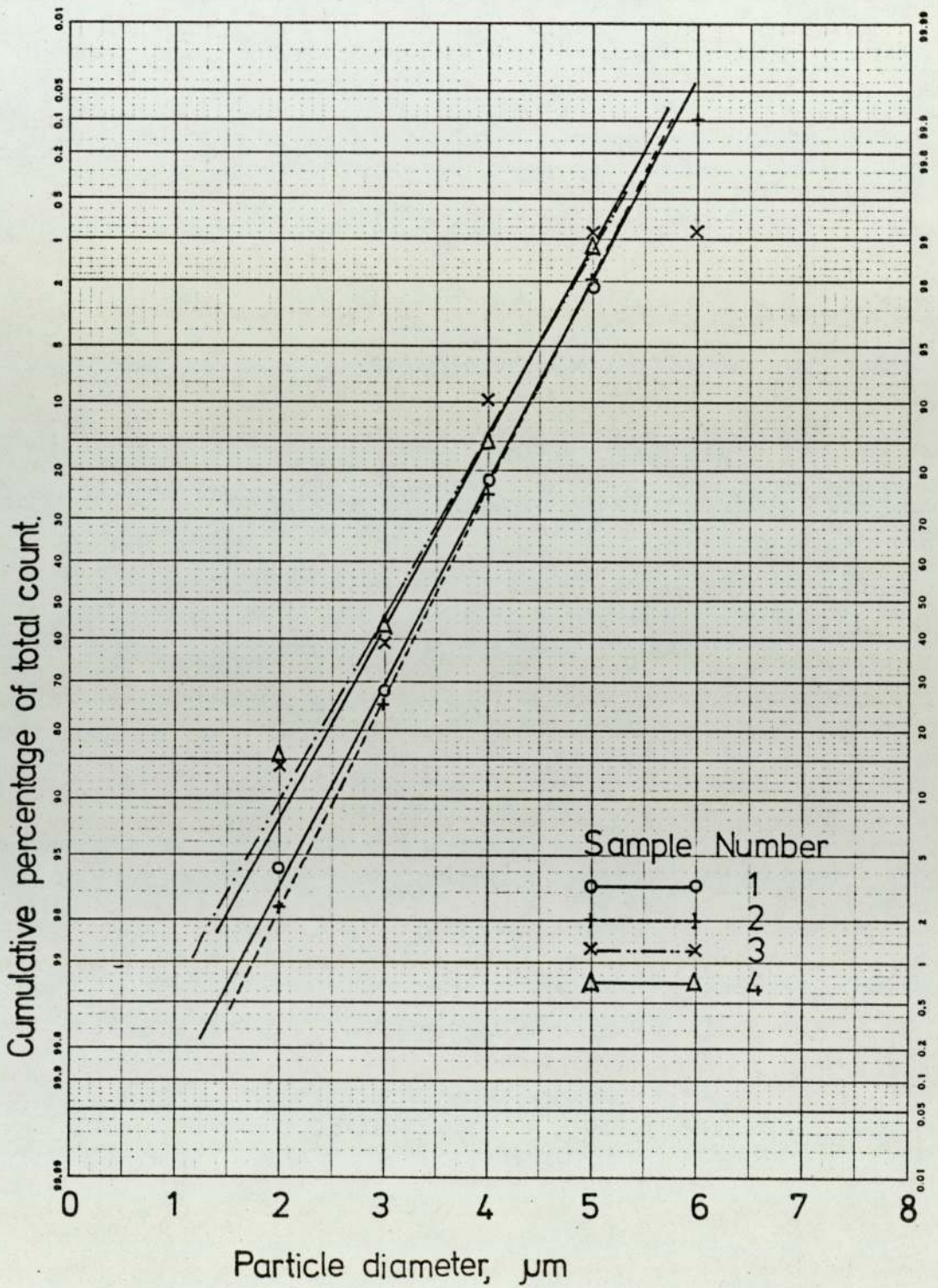
The actual measurement of the particle size from the photographs should be fairly accurate, to within $\pm 0.1\mu\text{m}$, but for the measurement of distributions, the particles are arranged into categories 0-1 μm , 1-2 μm , etc. If only a small number of particles can be seen on the photograph then all of them will be measured; but if there are a large number, then only those particles towards the centre of the photograph, which touch randomly drawn lines will be measured, and this introduces a bias towards the larger particles. The total number of particles measured was usually in the range 50-150 and this is too small to give an accurate representation of the population distribution. About 600 particles⁽¹²¹⁾ would need

to be measured to give an accurate distribution, and this was thought to be impractical for this work. To test how close to this ideal this work was, the sample shown in fig. 3.1. was analysed. The total sample size of 460 particles was considered close enough to 600 to give a reliable result.

Strictly speaking, these results cannot be treated by parametric statistics as the distribution does not represent the repeated measurement of the same particle, but a display of the measurements of a population of individuals whose actual sizes are different.⁽¹²⁷⁾ However, if the distributions shown in fig. 3.1. are plotted on a linear/probability graph (fig. 4.2.), then they form a reasonable straight line and so can be treated as approximately normal. On this basis, it was found that the means of the four samples do not differ significantly from the mean of the total number of counts, but do sometimes differ from each other. The same is true of the variance. This indicates that two samples from the same population would not necessarily look the same, and this may account for the differences found between the five samples which had undergone five 'identical' reduction processes (fig. 3.76.). However, in this case, as the gold powders had been reduced by sodium sulphite rather than ferrous chloride, the distributions did not fit a normal distribution curve (fig. 4.3.), and it is not possible to compare the two sets of curves directly.

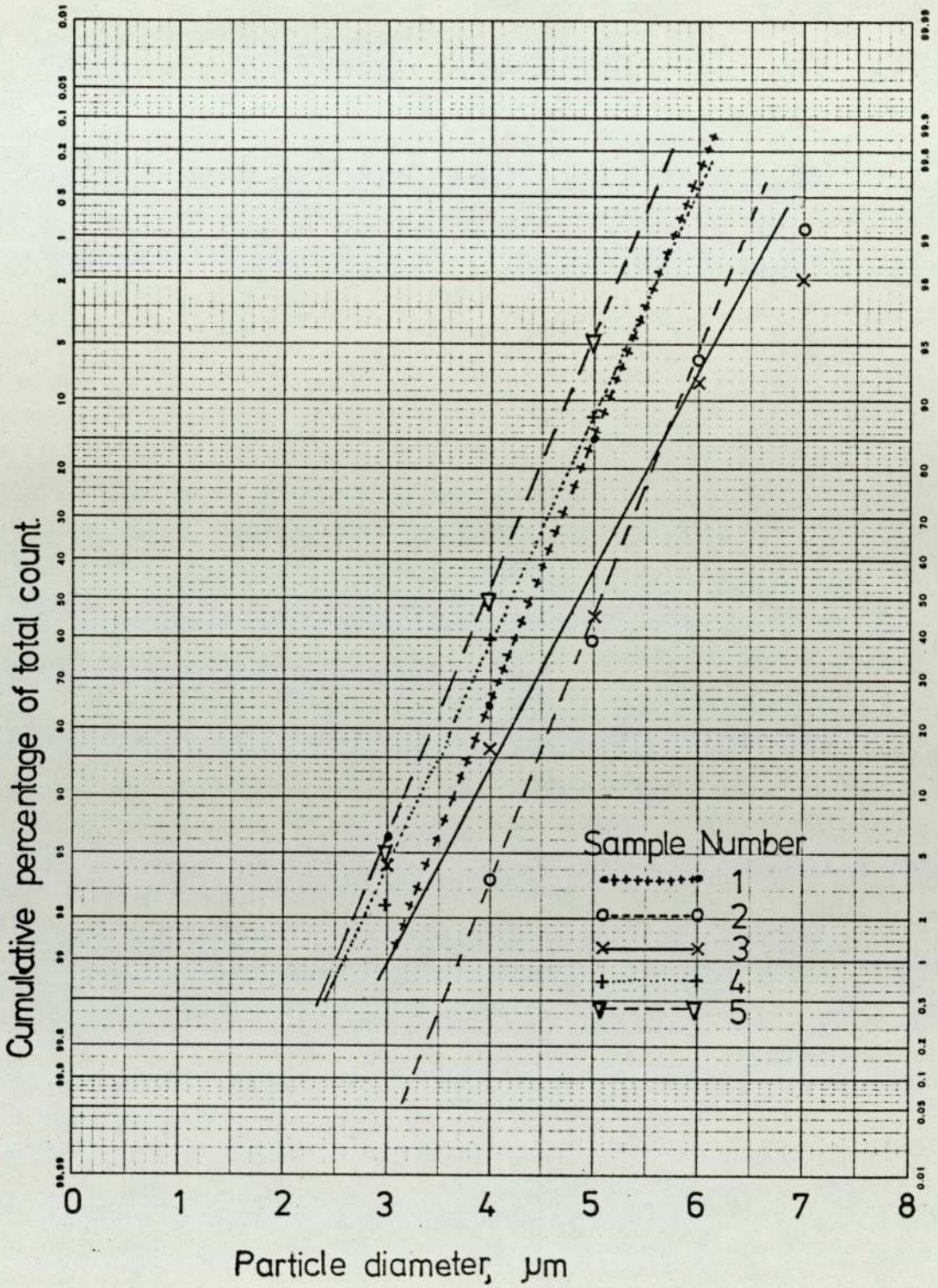
An added complication to the already uncertain size of a particle is the variability of the operator error. Re-measuring the powders which gave the distribution shown in fig. 3.1. gave the different distributions shown in fig. 3.2. Again, the total distribution of all the counts is more accurate and closer to fig. 3.1. than the four individual distributions.

CHART
WELL
Graph Data Ref. 5571
80 Equal Divisions x Probability



4.2. Probability curve for size distribution shown in fig. 3.1.

CHART
WELL
Graph Data Ref. 6571
80 Equal Divisions x Probability



4.3. Probability curve for size distribution shown in fig. 3.76.

4.1.4. The use of distribution curves.

In view of these inherent variations, it does not seem to be sensible to place too much reliance on the values of particle size or distribution. The values that have been given should only be taken to indicate the trends in the shape of the distribution, and sizes should be taken with some latitude, possibly $\pm 25\%$. In practice this is not as restricting as it may seem at first, as most of the gold particles found in this work tended to fall into three fairly easily recognizable groups. There were (1) the large particles from about $10\mu\text{m}$ upwards, which tended to be flat plates or agglomerations of smaller particles; (2) the very small particles from about $0.75\mu\text{m}$ downwards, most of which formed foamlike structures of very small particles. The very small sizes took time to settle and tended to stick together to form massive 'lumps' in which the individual particles could not be distinguished. Between these two sets of particles were (3) those powders which are of interest to this work, those between 1 and $10\mu\text{m}$. Most of the particles found in this work were between 1 and $5\mu\text{m}$ and for reasons given above, variations within this range cannot be detected. As the only use of the size would be for blending into a higher packing mixture, a variation of $1\mu\text{m}$ is of little consequence when blending with particles one tenth of that size. (107)

For these reasons also, the errors introduced by using distribution curves rather than the more accurate histograms will be small, and justified by the increase in clarity when showing several superimposed distribution curves, rather than the superimposed histograms.

4.2. Morphology.

4.2.1. Solubility of gold.

In the published work on the formation of crystals, emphasis is always placed on the driving force for crystalization, whether it is

current density, super-cooling or super-saturation. Super-saturation would seem to be the most relevant to this work, but that implies that some solubility occurs and possibly over a wide range, so as to allow some variation in the super-saturation ratio to occur. However, apart from gold in seawater,⁽¹²³⁾ which is likely to exist as gold chloride, no reference to the aqueous solubility of gold could be found. The uncharged gold atom is unlikely to be solvated to any degree, and only a 'pseudo-solubility' is likely to occur, of randomly distributed gold atoms spread throughout the 'solvent'. The number of atoms will be such that the probability of enough atoms coming together to form a stable nucleus, will be small enough for it to be ignored over considerable periods of time. Such a 'pseudo-solubility' is unlikely to produce the changes in morphology seen in this work. An alternative controlling reaction is needed, and this could be the rate of reduction of the gold. This could account for some of the conflicting evidence, such as the effect of pH, which in some systems, such as sodium sulphite, stops the reaction as it is raised, whilst in others, such as trisodium citrate, raising the pH encourages precipitation. These changes in reaction rates are reflected in the morphology of the particles found.

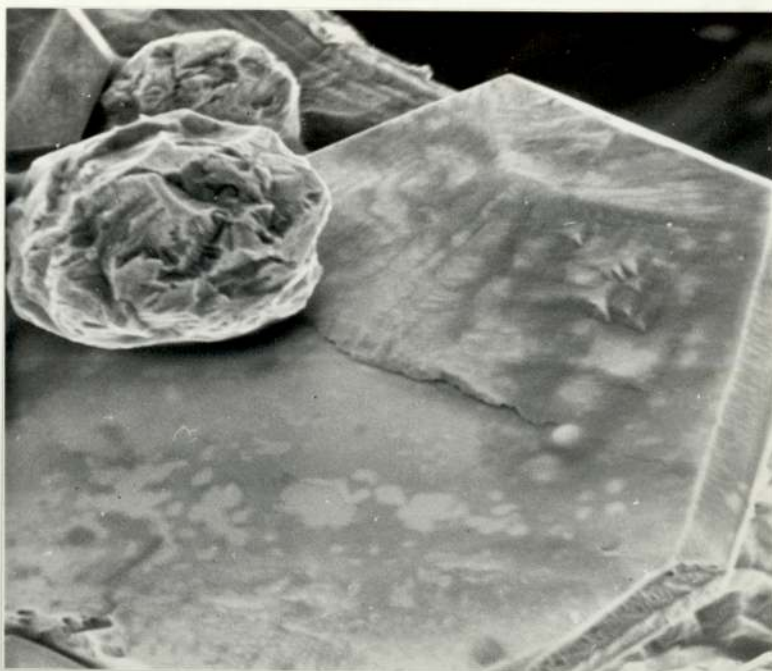
4.2.2. Effect of reaction rates on morphology.

As explained in section 1.3.4., increasing saturation will give rise to particles of different morphologies. Initially these will be large 'equilibrium' shaped particles often with spiral growth on them, which will tend to become more 'equilibrium' shaped as the super-saturation increases. At greater super-saturation they start to lose their crystalline shape, and eventually diffusion control sets in, only to give way to dendritic growth at higher super-saturation levels. As this goes even higher, homogeneous nucleation occurs and many small particles are formed, which become smaller as the super-saturation rises. If the

reaction rate is the controlling factor, then very slow reactions should exhibit the equilibrium shape for gold precipitated from aqueous solution, which is a flat triangle or hexagon of (111) planes. The only reaction which was allowed to continue for a week was the room temperature reduction of gold chloride by acetone, which produced a high percentage of flat plates (fig. 3.18.), some with growths on the surface, which could have been generated by screw dislocations (fig. 4.4.). If the cone seen in fig. 4.4. is grown on a dislocation, then the size of the base angle would seem to indicate a super-saturation ratio in excess of 10,000.⁽⁷⁸⁾ This seems feasible in view of the very low 'pseudo-solubility'.

Raising the temperature of the reduction system should improve the kinetics of the reduction and change the mode of precipitation to one that occurs at a higher super-saturation. The particles formed on treating boiling gold chloride with acetone are irregular, and this morphology is probably due to the acetone being in a gaseous state at that temperature. Heating gold chloride solution at pH 6 with sodium sulphite increases its reaction rate from being so slow as to be negligible, to one which precipitates flat plates and spheres. As sodium sulphite solution normally reduces gold chloride under acid conditions to spheres, the flat plates seen here cannot be explained by excess hydrogen ions sitting on the growth site, and must be explained as a reaction rate causing precipitation at a rate where surface nucleation controlled growth has not completely been converted to diffusion controlled growth.

From the work of Robinson and Gabe⁽⁸⁷⁾ it could be inferred that spheres are the diffusion controlled form of gold precipitation. Work on colloids⁽⁸³⁾⁽⁹⁴⁾ has shown that spheres exist from the start of the precipitation, and Uyeda⁽⁹⁴⁾ has suggested one way in which spheres can be formed. If this is so, then increasing the reaction rate should change the precipitate morphology from a sphere to a dendrite. As raising the pH of



4.4. Scanning electron micrograph of gold reduced by acetone
at room temperature. x 2,000

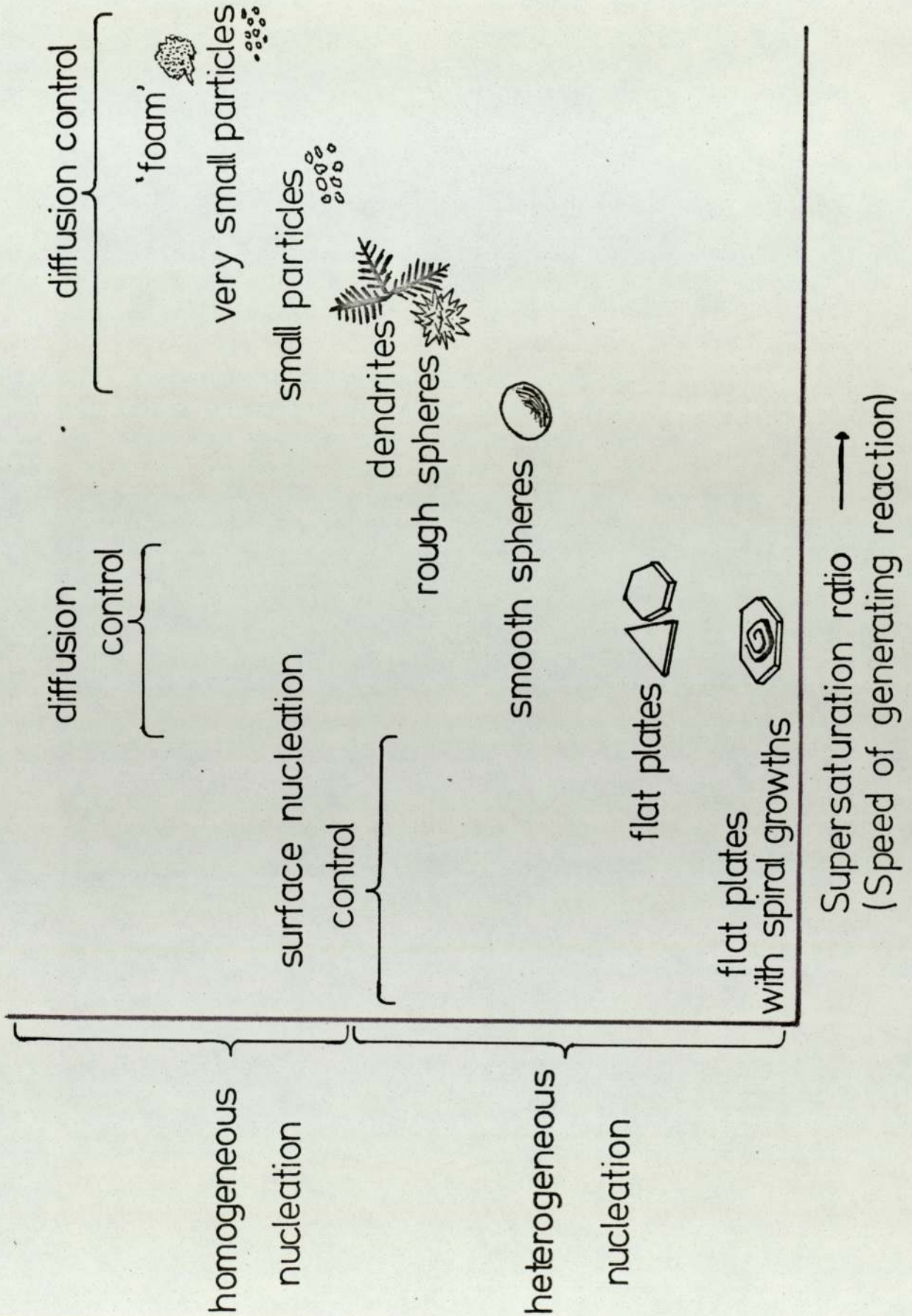
the solution effectively stops the reduction of gold chloride by sodium sulphite, lowering the pH should increase the rate of the reduction reaction and change the spheres found at pH 2-3 to dendrites. In fact rougher spheres are found in the lower pH powders, and these could be regarded as semi-dendritic (compare for example figs. 3.25. and 3.28.). The same effect can be seen by increasing the temperature when reducing with sulphur dioxide.

Increasing the reaction rate still further should start homogeneous nucleation and the presence of many small particles, and many of the reduction systems used, show this transition. Trisodium citrate will not precipitate at all in acid solutions and will only produce a few flat plates and spheres in neutral solutions. In alkaline solutions the reaction rapidly goes to completion, possibly due to the better environment for the formation of acetone dicarboxylic acid, and a mass of small spheres are formed. Thus the relationship between speed of reaction and particle morphology may be shown as in fig. 4.5.

4.2.3. Gold powders.

The mechanisms in the previous sections do not apply to the reduction of gold chloride by hydrogen, as the reducing agent was gaseous, and like reduction by nascent hydrogen and hydrogen sulphide, all produced irregular particles. The hydrogen reduced gold was very impure (fig. 3.4.), and this was presumably due to the difficulty in reducing metal salts with hydrogen. Nickel, iron,⁽⁸²⁾ and copper⁽¹²⁸⁾ are known to act as catalysts for this reduction and so any impurities in the water, or brought over in the gas stream, will be concentrated in the very small amount of gold which would be precipitated around them.

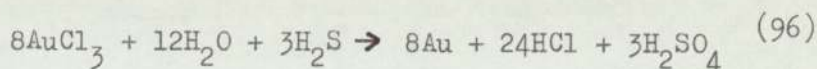
The sulphur in the gold reduced by hydrogen sulphide could be from the reaction -



4.5. Relationship between morphology and reaction speed.



although it is claimed that the reaction is -



Alternatively, Mellor⁽¹²³⁾ reports that this reaction at room temperature produces aurosoauric sulphide, Au_2S_2 , but this compound should break down in the presence of excess gold chloride to give metallic gold and sulphuric acid. This could be the source of the sulphur, as X-ray examination shows that it is distributed throughout the gold, and not located in discrete particles (fig. 4.6.).

The improved reaction rates of the hydrogen peroxide reduction in alkaline solutions is due to the neutralization of the acidic products of the reaction, and this also applies to many of the organic reducing agents. This results in a rapid transformation from surface nucleation controlled growth (figs. 1.3. and 1.4.), to the homogeneous nucleation of many fine particles, with only a (relatively) small change in pH. Such transformations occur in formaldehyde reductions, trisodium citrate reductions, and reduction by hydroxylamine hydrochloride. These reductions are further encouraged by the instability of the gold salts in alkaline solutions. Adding sodium hydroxide to gold chloride may produce sodium aurate, NaAuO_2 , but some reports have claimed that it also precipitates metallic gold.⁽¹²⁹⁾⁽¹³⁰⁾ However, most other reports of this reaction do not mention the precipitation of metallic gold; this precipitation could be due to the presence of impurities or foreign nuclei in the solution. Such impurities could account for the particles produced in the growth solution, which were smaller than the 'nuclei' introduced.

Particles produced by the reduction of gold chloride by hydrazine hydrochloride were very small, indicating a fast reaction rate, and this seemed to be the case as the reaction was rapid and vigorous. This is unexpected, as the reduction reaction -

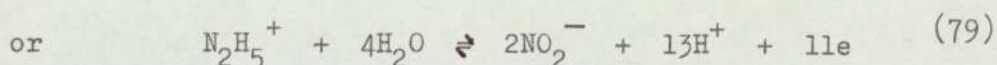
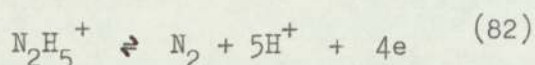


1 μ m



1 μ m

4.6. Scanning electron micrograph of sulphur content of gold reduced by hydrogen sulphide. x 2,100



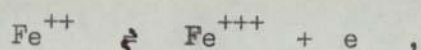
produces many hydrogen ions and this should impede the reaction rate in acidic solution. Of these two above reactions, the first seems to be the more likely as it evolves gas, as was found in practise, and would be the least impeded of the two in acid solutions. The situation may be different in alkaline solutions where the second reaction would tend to have the greater driving force. Certainly, the structure of the gold reduced from alkaline solutions was very fine, compatible with being precipitated from a very high super-saturation (fig. 3.50). This may also be due to the instability of the gold fulminate, which is known to be highly explosive when dry.⁽¹²³⁾ However, the fulminate is in the solid form when reduced, and this could alter the morphology as mass transport effects will come into play. This will also account for the morphology of the gold precipitated by zinc and by Faraday's solution; the zinc dust being solid, whilst the Faraday's solution is composed of an emulsion of phosphorous in water. In the latter case, as reduction can only take place at the interface, a particle must remain in contact with the phosphorous if it is to grow, and this would account for the colloid which also formed alongside the precipitate. The green colour of the colloid indicates that the particles are either smaller than 160Å or larger than 1500Å,⁽⁸⁸⁾ with the speed of the reaction favouring the smaller size.

Of all the reducing agents which gave some flat plates, oxalic acid was the only one to take the reaction to completion. Taking about an hour at boiling point, it is fairly fast for a reaction giving flat triangles and hexagons, but is still slower than those reactions which gave spheres or 'foamlike' structures.

The reduction of gold chloride by the sulphite ion follows the

relationship between morphology and reaction rate very well, with the only two normal particle shapes being rough and smooth spheres. The dendrites found in the gold reduced with sulphurous acid (fig. 3.24.) may be regarded as exceptional as in this case the solutions were mixed cold, and after the initial stirring, only convection currents occurred as the solution was heated up. This would allow large diffusion gradients to build up with the subsequent opportunity for larger dendrites. The only other anomaly in this system is the appearance of flat plates when the gold is reduced with only a small quantity of reducing agent (fig. 3.31.). As the concentration of reducing agent in the mixed solutions is very low, the concentration of reduced gold will also be very low, and by the time the ratio has dropped to 0.5., the concentration is low enough for surface nucleation control of growth to occur. The plates found are fairly thick (compare 3.31. with 3.33.), and this is compatible with polynucleated layer growth (fig. 1.4.).

The reduction of gold chloride with the ferrous ion shows the importance of other ions in the system. Both ferrous chloride and ferrous sulphate reduce gold chloride by the reaction -



but the chloride reaction is very slow, producing only a small yield of mixed spheres and plates over a number of hours, whilst the sulphate very rapidly produces a mass of spheres. This may be due to the ease in which ferric chloride is oxidised in air to ferrous chloride, leaving only a low concentration of ferric ions to reduce the gold chloride. The slow rate of this reaction is not increased even in high pH solutions which should encourage the formation of ferric ions. The ferrous sulphate reduction on the other hand, at high pH, produces even smaller particles, indicating precipitation in the homogeneous nucleation region. This is in agreement with published results for the size of gold particles reduced by ferrous

sulphate at room temperature.⁽¹²⁴⁾

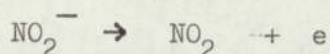
The increase in impurity present in ferrous sulphate precipitation may be due to the use of saturated ferrous sulphate solutions, and the possible presence of undissolved particles of ferrous sulphate in the reduction system. These would act as nuclei, and would be coated with gold. The crystal structure of ferrous sulphate (heptahydrate) is monoclinic⁽¹³¹⁾ and this could give rise to the distorted hexagons which were found in this system. The high level of iron contamination at high pH values is probably due to entrapment of iron hydroxide.

The electrolytic reduction does not fit into the morphological scheme as outlined, due to its different driving force. The dendrites formed at a higher current density to that where diffusion control would produce nodules.⁽⁸⁷⁾ The 'dust' is possibly broken-off particles of dendrites, or it may be the result of plating on the low current density area at the back of the cathode. Bipolarity of the back of the cathode could result in the leaching out of elements from the stainless steel, which are replated with the gold on the low current density areas. This would account for the high level of contamination in the dust.

4.2.4. Problems.

Unfortunately, not all the systems examined in this work fit this theory exactly. Sodium nitrite reduces gold chloride under acid and alkaline conditions, the reaction being less vigorous as the pH rises, with the precipitate at high pH values taking some time to settle. The size of the particles formed goes down with the pH, and the vigour of the reaction. Flat triangles and hexagone are not found at all in this system.

The problem is complicated by the large number of reactions which the nitrite ion can undergo.⁽⁷⁹⁾ The overall reaction seems to be -



but at high hydrogen ion concentrations, the number of competing reactions is very large. It could be that despite signs of activity at low pH, the actual reduction of gold is proceeding only slowly. Raising the pH stops most of the side reactions and allows the main reduction to proceed a little faster, producing a smaller precipitate. It must be admitted that this is not a very satisfactory answer, and more work is needed on this system. The effects of concentration changes, and the action of related reducing agents, might throw some light on the actual reduction reaction at the various pH values. A study of the kinetics of these reactions may then explain the anomalies found in this system.

Another difficulty in fitting facts and theory is the general occurrence of spheres with the triangles and hexagons. These are not due to the high gold concentration used, but occur in practically all gold reductions⁽⁸³⁾⁽⁹¹⁾⁽¹⁰⁰⁾ even at very low concentrations. Only very slow reactions such as irradiation of gold chloride⁽⁹²⁾, or its reduction by salicylic acid⁽⁹⁸⁾⁽¹⁰¹⁾⁽¹⁰²⁾ show only flat triangles and hexagons with no spheres, and it may be that only these reactions reduce gold at a low enough rate to permit only surface nucleation control to take place. All other reactions have at least some form of diffusion controlled precipitation. Although these spheres are difficult to explain in a simple theoretical model, they are an advantage in practise because of the improvement they gave to the packing and surface finish.⁽¹¹¹⁾

4.2.5. Other metal powders.

Applying this theory to the other metals used, it was found that all the palladium precipitated appeared to have been formed in this homogeneous nucleation region, with particles rarely above 0.1 μ m in size. This is confirmed by examples in the literature⁽¹³²⁾⁽¹³³⁾ which give the

size of the palladium particles formed as being 0.1 μ m, and that flat plates are rarely found. This would seem to suggest that the 'pseudo-solubility' of palladium is less than that of gold.

It is more difficult to apply the theory to the other powders precipitated, as solid reducing agents were used for both nickel and copper. The large spheres of copper powder suggest that the reduction process is fairly slow, or the copper has a large 'pseudo-solubility'. The nickel powder, on the other hand, is very fine, as would be expected from a system reduced by sodium hydride.

4.2.6. Alloy precipitation.

The use of co-precipitated alloy powders is desirable, due to the more intimate mixing of the elements in the alloy powder, than that achieved by mixing two or more elemental powders. Segregation of the elements is also unlikely, as the metals cannot be separated either through settling or through poor mixing. However, the co-precipitation of alloys is a complex process and the lack of success is not really too surprising. The chances of success were not raised by the attempts to co-precipitate gold with copper or nickel, using the reducing agent that is used elsewhere to separate gold from these metals !

The use of sodium nitrate to reduce gold/cobalt and gold/palladium was based on a statement that in almost neutral solutions, this reagent will contaminate the gold with base metals.⁽¹²⁰⁾ The lack of success may be due to the poor control of pH.

Sulphurous acid is stated to reduce palladous chloride,⁽⁹⁶⁾ but did not do so in this work in the presence of gold chloride. As this reaction gave an almost monodispersed precipitate (fig. 3.62.), some interaction between the chemicals caused a single burst of nucleation of the gold particles, with no subsequent nucleation of palladium particles.

More work is needed on this system.

The gold/palladium alloy which did form, reduced from the fulminate by hydrazine hydrochloride, was probably formed by entrapment of palladium fulminate within the gold fulminate precipitate, as palladium fulminate is soluble.⁽¹²³⁾ This method is clearly unsuitable for commercial practice.

The reduction reaction for the precipitation of palladium by sodium thiosulphate is probably -



which would account for the large amount of sulphur found (fig. 3.65.).

The nascent palladium would then catalyse the reduction of nickel by a similar reaction to that above. The precipitate may have had a considerable water content as the volume of the precipitate shrank appreciably on drying.

4.3. Choice of Materials.

4.3.1. Gold powder.

The choice of gold powder for mixing into a paste is restricted not only by the paste requirements, but also by the production requirements. This excludes from the choice very fine particles which take time to settle, and slow reduction reactions which also take time. Both these problems could be overcome in an industrial practice where the appropriate equipment could speed up events.

Technical requirements as to the thickness of the final deposit restrict the size of the particle, and what little information on surface finish is available, suggests that spheres, or flakes and spheres, are better than flakes alone.⁽¹¹¹⁾⁽¹³⁴⁾ Some workers suggest that particles under 5µm in diameter would be best.⁽¹³⁵⁾ Consideration of other technical requirements exclude powders that are impure, especially if the

impurity lowers the melting point of the gold.

These requirements limit the reducing reagents to hydrogen peroxide, sulphur dioxide, sodium sulphate, ferrous sulphate and possibly, oxalic acid, although the latter **reducing agent** may produce too many flat plates for easy packing and sintering. Owing to the better packing of spheres, only those which produce spherical or roughly spherical particles were considered. The final choice between sulphur dioxide, room temperature sodium sulphite and ferrous sulphate, was in favour of the sodium sulphite, due to the lack of contamination and consistently spherically shaped particles, usually within the range 1-4 μ m diameter.

The final reduction route chosen was the room temperature reduction of gold chloride solution at pH 1-1.5., 50 g/l gold metal, by excess sodium sulphite at pH 2-2.5., 200 g/l sodium sulphite (0.2588 molar). This reaction was fast enough to produce a super-saturation level when nucleation on the surface of a gold particle was easy, and diffusion of the reduced gold to the growing particle was the controlling factor. Irregularities on the particle surface would attempt to break through the diffusion layer, and rough spheres would result. Nucleation of the initial particles would be by heterogeneous nucleation on all the available impurities capable of acting as nuclei.

4.3.2. Other metal powders.

The choice of other metal powders is restricted not so much as by what is desirable, but by what is available. The palladium precipitated from the chloride is at the bottom end of the usable range, whilst the metal bought from Hopkins and Williams is of a better size. The palladium/nickel alloys were not really of a usable size, even when they had been crushed, and the same could be said of the nickel precipitated out of nickel chloride.

The final choice of metal powders used was the copper reduced from copper sulphate, the palladium from Hopkins and Williams, and the iron and nickel powders produced by the carbonyl process. The palladium alloys with nickel and with tin were also used, but not with any real hope of producing a successfully firing paste.

5. EXPERIMENTAL DETAILS OF PASTE PRODUCTION AND FIRING.

5.1. Materials.

As well as the gold powder produced by the methods outlined above, two sets of gold paste were obtained from Messrs. Engelhard Ltd. Both contained the same kind of gold powder (fig. 5.1.), but one also contained a glass flux as well as the organic binder.⁽¹³⁶⁾ These were printed as a pattern of squares by Engelhard Ltd., on substrates of 51% nickel, 49% iron. These substrates, which were used for all the pastes in this work, were in the form of hot rolled strip, 2mm thick which had been prepared by Henry Wiggin & Co. Ltd. The grain size was A.S.T.M. No. 7, larger than the specification of A.S.T.M. No. 8.⁽¹³⁷⁾ The surface finish of the rolled strip was rougher than that of a reed blade (figs. 5.2. and 5.3.), with surface finishes of 0.75 μ m CLA for the rolled strip, and 0.5 μ m CLA for the reed blank. The cast analysis for this material was⁽¹³⁸⁾ (in percent) -

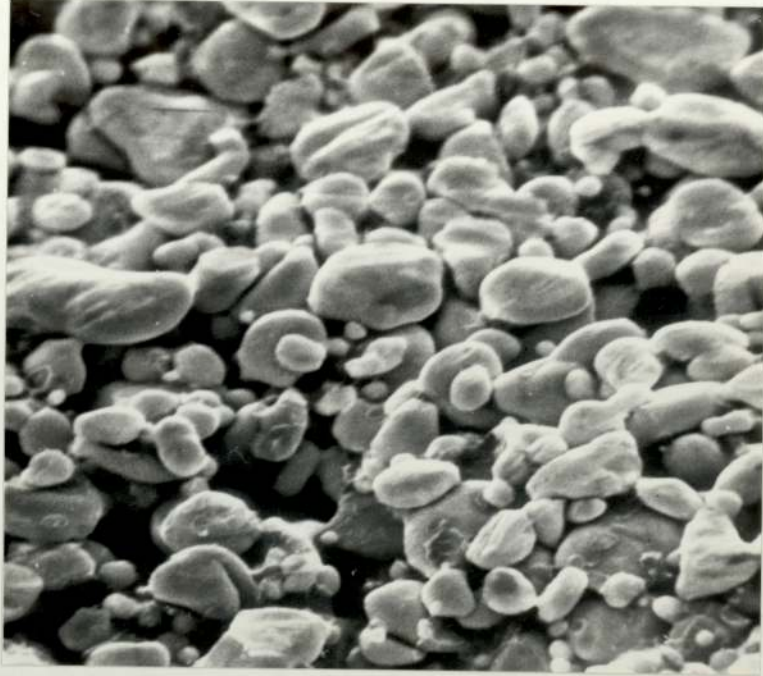
Ni	Co	C	Si	Cu	Mn	Al	S	Mg	Fe
50.8	0.19	0.004	0.01	0.19	0.46	0.04	0.007	0.011	bal.

The manganese was added as a sulphur 'getter' and this, combined with the aluminium de-oxidant, can form glass particles on the surface of alloy if it is overheated.⁽²⁴⁾

The vehicle used to change the powders into pastes, was a mixture of 2% ethyl cellulose in terpinol. These substances were similar to those used in commercial practice. The terpinol provided the correct printing properties, after which it was dried off leaving the ethyl cellulose to give the deposit 'green' strength. Occasional printing was carried out using a water based vehicle containing up to 8% ethyl cellulose, to examine the effect of using a different vehicle.

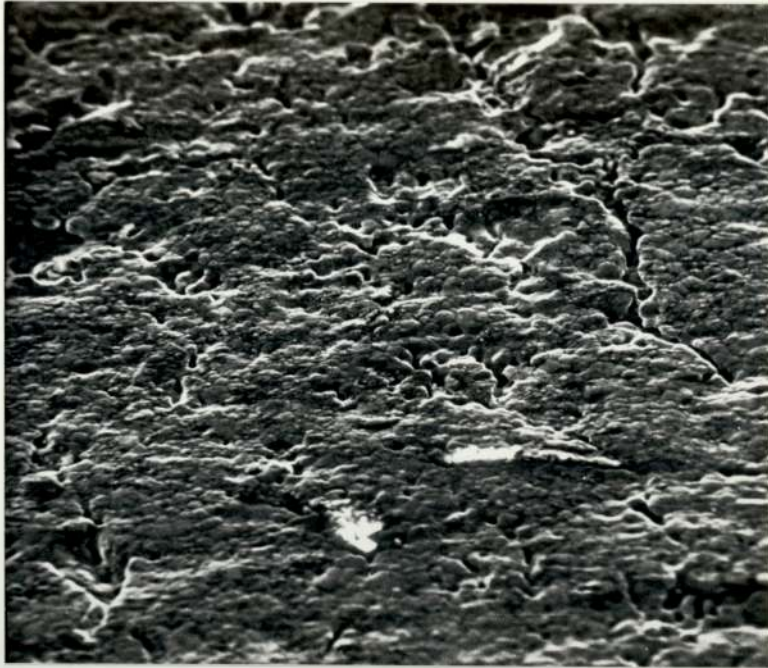
5.2. Mixing.

Mixing on a three roll mill was desirable for its uniform and



└ 1 μ m

5.1. Scanning electron micrograph of gold powder used in Engelhard pastes. x 6,500



.1 μ m

5.2. Scanning electron micrograph of nickel/iron substrate surface finish. x 650



.1 μ m

5.3. Scanning electron micrograph of reed blank surface finish. x 460

reproducible action, but because of the fairly large quantity of paste required (15-20g) for the efficient use of the mill, mixing by palette knife and ointment block was used. Quantities down to approximately one gram could be mixed in this way, and the varying distances between the knife and the block effectively simulated the shearing action of the rolls.

Where alloys were made, the components were shaken together prior to the vehicle being added and mixed.

5.3. Substrate Preparation.

Initial printing was done on substrate which had been cleaned by polishing to 600 grit, de-greased and painted with a protective lacquer until required. As firing progressed, this was dispensed with and most of the printing was done on samples which had been washed and de-greased, but were basically as they were received.

5.4. Printing.

Apart from the gold pastes printed by Engelhard with a silk screen printer, all the pastes used in this work were painted on, using a fine camel hair brush. These were then dried in air, either at 250°C for an hour, or 150°C for ten minutes. The Engelhard printed samples had received this latter treatment.

5.5. Firing the Samples.

The dried samples were fired in a vertical wire-wound vacuum furnace under a variety of atmospheres for between 5 minutes and several hours, at temperatures between 800°C and 1000°C. The samples were placed in a wire cradle at the centre of the furnace, which was then evacuated down to 10^{-6} torr, before the covering gas was admitted. The furnace was

then pumped down again and the covering gas (if used) re-admitted. Heating to the desired temperature was as rapid as possible, and the samples were furnace cooled. A typical thermal history of a firing is shown in fig. 5.4.

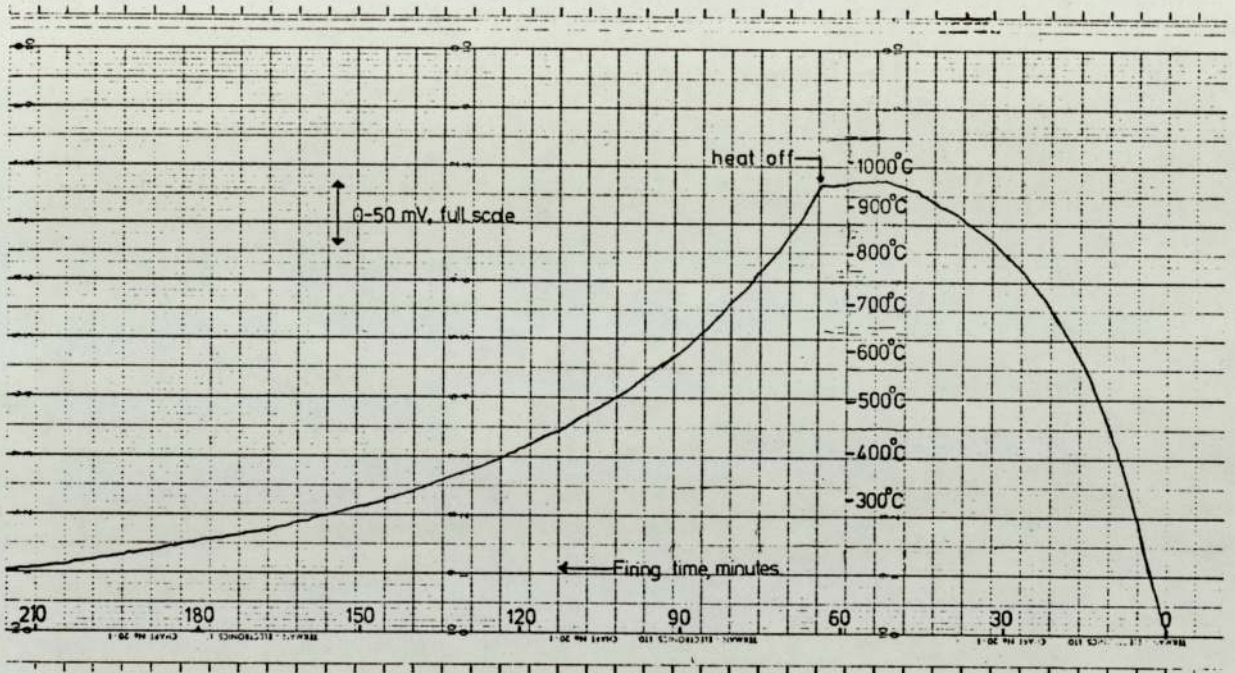
5.6. Testing.

5.6.1. Visual examination.

This was used to assess the surface roughness, and would also give an indication of any surface attack, and pick out examples of poor adhesion. Continuation of this examination using the scanning electron microscope would also allow an estimate of the porosity to be made, the extent of the sintering to be measured, and the surface finish at micro levels to be examined. The simultaneous analysis of the top 1 μ m layer of the deposit by the Kevex X-ray analyser enables an estimate of the surface diffusion to be built up, as well as giving the composition of any surface anomalies. X-ray mapping gave a clear picture of the distribution of any alloying elements present. The overall analysis of the deposits was obtained by the Cambridge Microscan Mk. 5 X-Ray Microanalyser, which was also used to examine cross sections of the deposit and substrate, as was the scanning electron microscope.

5.6.2. Surface finish.

Most assessments of the surface finish of the fired deposits were done by comparison of photographs from the scanning electron microscope at magnifications of 100X - 500X. Sufficient differences usually existed between the samples to enable them to be assessed in order, between best and worst. Occasionally, samples would be measured on the Rank-Taylor-Hobson "Talysurf" and the results given as a centre line average (CLA).



5.4. Thermal history of a typical paste, fired in nitrogen.

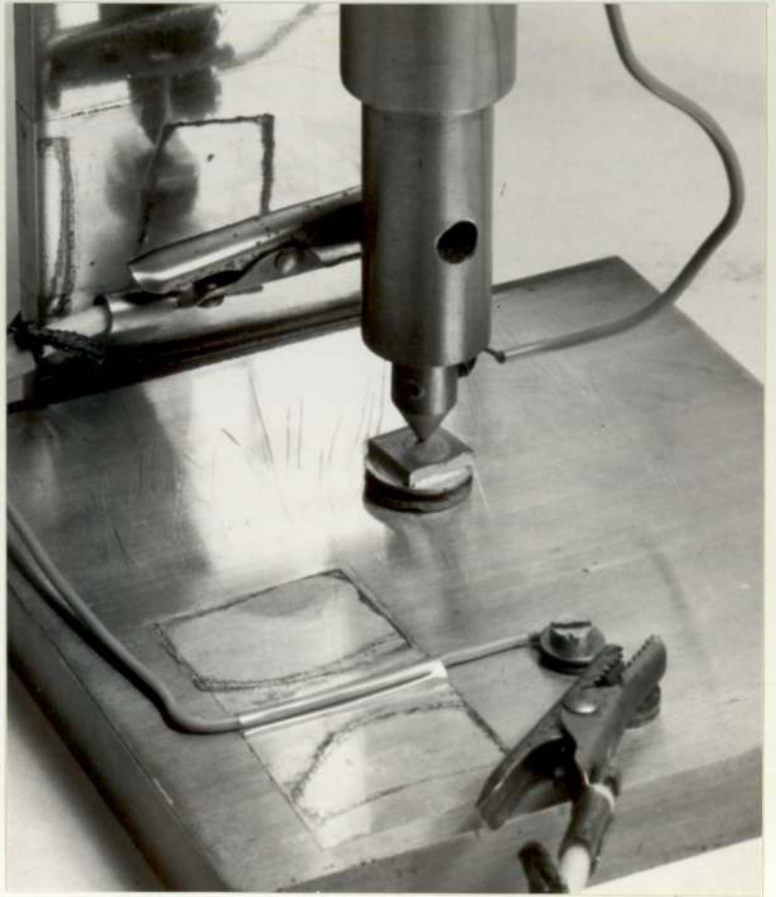
5.6.3. Electrical resistance.

An attempt was made to assess the electrical properties of the deposits using the equipment shown in fig. 5.5. A steady d.c. current of 10mA was passed by the current source through the probe and sample, and the voltage drop across the sample measured. The current source used was a Keithly Instruments Inc. type 225 current source, whilst the voltage drop was measured on a Pye Scalelamp galvanometer, type 1901/5. The probe tip was plated with 10 μ m of pure gold and was loaded using a spring of 250g compliance. Before use, the probe was cleaned by swabbing with cotton wool containing aqua regia, rinsed and dried.

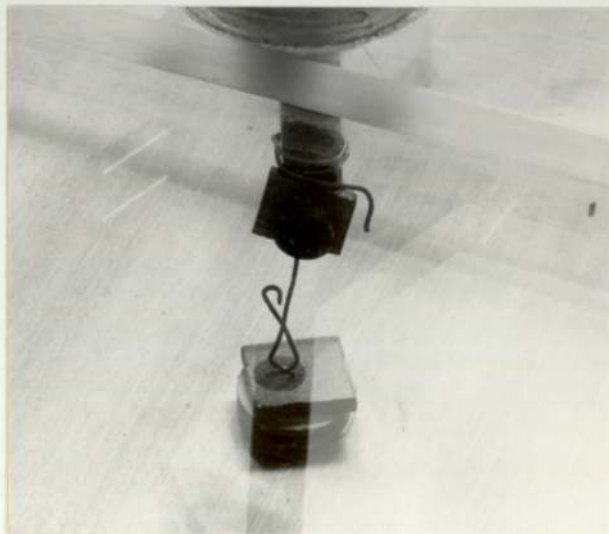
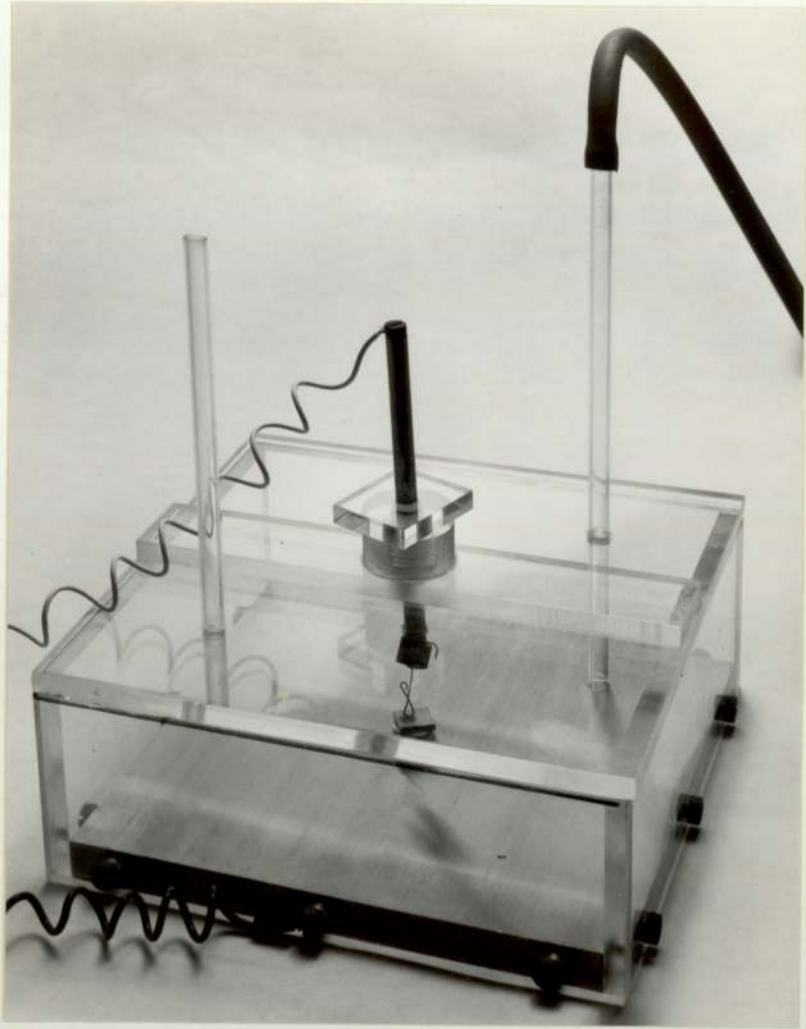
The sample, which was about 10mm square, had had the four sides of the substrate ground on 600 grit before being fixed to a Stereoscan sample stub. Silver Dag was applied to all four freshly ground sides, which was then left to dry overnight. The dry sample was held in the jig by a screw which was tightened until deformation of the stub occurred. The cleaned probe was then lowered until the spring showed movement, when the current was passed through the jig, in both the positive and negative directions. The two voltage drops were then averaged, and the resistance calculated.

5.6.4. Spark resistance.

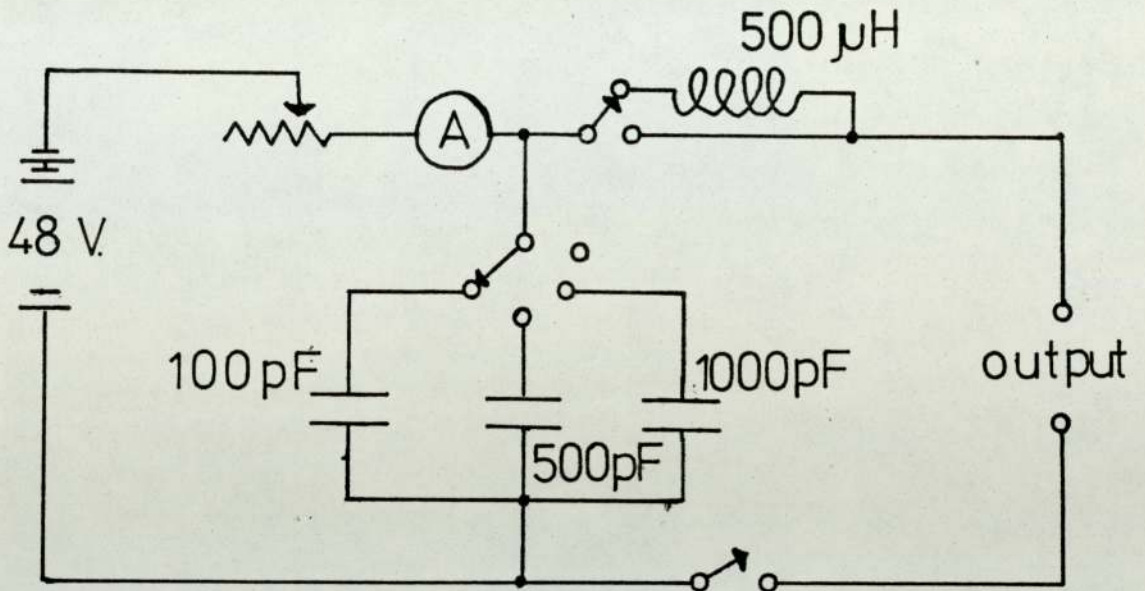
The rig showed in fig. 5.6. was built to attempt to assess the deposits resistance to spark erosion. The sample, which was held in the same manner as the resistance jig, was held within the perspex box which was then flushed out with the required atmosphere. Current, passed through the circuit shown in fig. 5.7., was broken by rapidly pulling away the contact from the sample. Alternatively, the contact could be dropped onto the sample to give a 'make' situation. The effect of these sparks on both the fired deposits and polished substrates, were then assessed on the



5.5. Electrical resistance testing rig.



5.6. Spark testing rig.



5.7. Circuit diagram of spark generator.

scanning electron microscope.

5.6.5. Adhesion.

Several unsuccessful attempts were made to obtain a value for the adhesion of the fired deposit to the substrate. Some techniques, such as ultrasonic energy, or the energy of a spark discharge from a spark machine, produced no results at all. Others, using solder, adhesives, or electroplate to fix a handle on to the deposits so that they may be pulled off, are suspect in that they alter the nature of the deposit and so may change the adhesion value. These did, however, produce some results (except those using adhesives). The sample using solder was a copper wire soldered on to a 2mm square gold land and pulled, in tension, on an Instron mechanical testing apparatus.

The electroplated sample was a strip of the nickel/iron substrate, 75mm x 25mm, which after painting and firing the deposit, was overplated with approximately 50 μ m of copper. Two grooves were then cut down the sample about 10mm apart, and the central strip of copper plate peeled back for about 10-20mm. The sample was clamped to the bench and the rest of the copper strip was peeled off at right angles to the substrate by use of applied weights.

6. RESULTS OF PASTE FIRING

6.1. Test Methods.

6.1.1. Electrical resistance.

Initial tests with this method showed the importance of each of the interfaces on the electrical path. A poor sample/sample holder interface via the silver Dag raised the total resistance by a factor of 20; whilst even such a small change as Dag resistance after one hour's drying and twelve hours' drying alters the overall resistance by 10%. The resistance of a sample held in place by a hand tightened screw, is four times that of the same sample when the screw has been tightened with a screwdriver.

Not only were there variations arising from the different interfaces, but the substrates themselves showed variation. The table below gives the resistance of nine substrates cut from the same sheet of material. The resistance was re-checked after washing with isopropyl alcohol and wiping dry, after the renewal of the silver Dag, after having the surface layers removed by scraping, and after being polished down to 600 grit (resistance in millichms).

	Initial state.	Washed.	re-Dagged.	Scraped.	Polished.
1.	34.4	38.2	28.3	10.4	
2.	11.0				
3.	21.4				
4.	32.2	44.9	23.9	21.4	27.6
5.	14.5				
6.	43.4	63.6	41.6	6.6	
7.	18.2				
8.	18.1				
9.	45.8	79.5	28.1	11.3	

The rise of the resistance after washing was presumably due to removal of the silver Dag, as re-application of the Dag lowered the resistance to below what it was before.

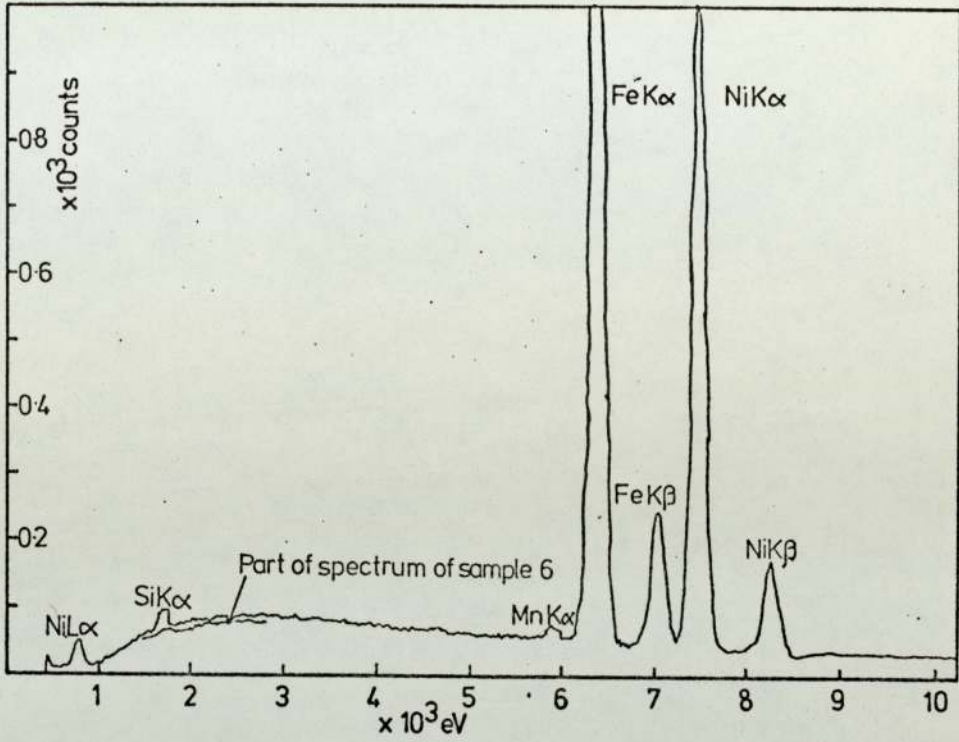
The high resistance of some of the substrates was possibly due to differences in the oxide layer beneath the probe. This could account for the high resistance of sample 4, which showed a higher than average silicon content when analysed on the Kevex (fig. 6.1.). To test the reproducibility of the method, a plain freshly cleaned sample of nickel/iron substrate was placed in the test jig, and its resistance was measured eight times with both positive and negative current flow. It was then removed from the jig, replaced, and the measurements repeated, and this cycle was repeated four times. The results showed that the readings at any one session were within 0.25% whilst results after removing and replacing the sample were within 1.6% of each other.

6.1.2. Neck growth.

An approximate measure of the amount of sintering which had taken place was obtained by a comparison of the neck between two particles and their diameters. This gives only an approximate result, as often the particles are not of the same diameter, and the plane of the particles is not always parallel to that of the photograph. There is also considerable variation in the extent of neck growth shown by a particular sample, presumably due to differences in the contact conditions at the start of sintering.

6.1.3. Spark resistance.

The conditions used in these tests were meant to simulate those used in telephone switching, (2) and currents of between 0.1 and 1.5 Amps were switched at 48-50 volts. It was discovered that sparking did not



6.1. Kevex X-ray spectrum for substrate sample No. 4, showing high silicon content.

occur when the capacitance or inductance were switched into the circuit, presumably because the inherent capacitance of the circuit acted as a contact protector and suppressed the arc. As a result only (nominally) resistive switching was used. Results of resistive switching (break only) at various current values are given below (voltage 48-49 volts):-

Current	Diameter of burnt area.	Size of craters seen.
1.5 A	0.44mm	9-10, 20-25 μ m
1.0 A	0.22mm	9-10, 20-25 μ m
0.5 A	about 50 μ m	9-10 μ m
0.4 A	-	0.5, 5 μ m

Unfortunately, repeated tests on identical substrates failed to give reproducible results. Of nine 1 amp resistive 'breaks' on one substrate, only five produced visible sparks. Examination of the substrate afterwards produced three areas of about the same size, two smaller burnt areas, and the rest could not be found (figs. 6.2., 6.3., 6.4.).

6.2. Mixing Variables.

6.2.1. Influence of mixing method.

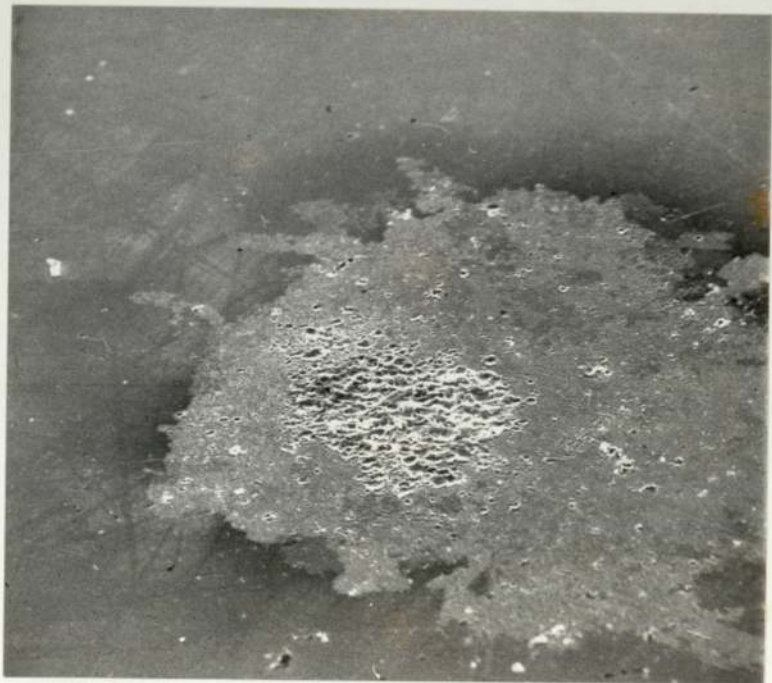
It is difficult to compare the results of mixing with a palette knife and mixing with a three roll mill, as those mixed by the mill were also screen printed which will give a better surface finish and printed density. Bearing this in mind, the two methods seem to be comparable (figs. 6.5. and 6.6.) with CLA's of 2 μ m for palette knife mixed pastes, and lum for roll mixed pastes.

6.2.2. Influence of the vehicle.

The use of water based vehicles, either pure or mixed with ethyl cellulose, was not a success, as the pastes were very difficult to mix and



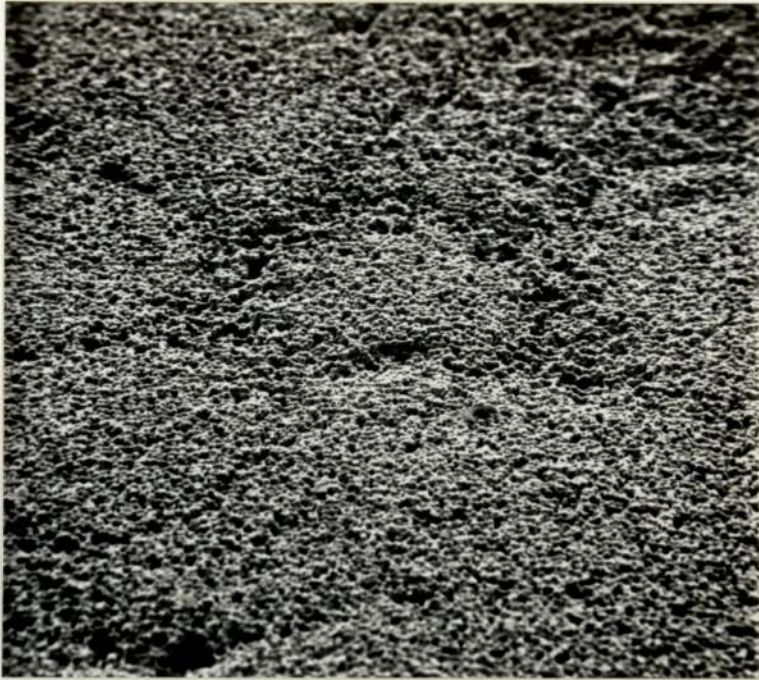
6.2. Scanning electron micrograph of spark damage on polished nickel/iron substrate. x 220



6.3. Scanning electron micrograph of spark damage on polished nickel/iron substrate. x 240



6.4. Scanning electron micrograph of spark damage on polished nickel/iron substrate. x 250



6.5. Scanning electron micrograph of paste mixed with a palette knife. x 230



6.6. Scanning electron micrograph of paste mixed with a three roll mill. x 280

remained lumpy despite prolonged treatment with the palette knife. The resultant pastes fired badly with little sintering and poor adhesion (fig. 6.7.).

Vehicles using terpinol with 2% ethyl cellulose mixed and printed much better than the water based pastes. Normally, pastes contained between 12 and 15% (by weight) vehicle, but pastes outside this range were made up, to examine the effect of viscosity on the fired product. However, the tests proved inconclusive, either because the viscosity had little effect on the surface finish, or more likely, the irregularity of the painting method swamped any differences there might have been between the samples.

6.3. Printing.

6.3.1. Influence of printing method.

Although painting could achieve results comparable to those produced by silk screen printing (see above, figs. 6.5. and 6.6.), the irregularity inherent in painting meant that reliable results could not be obtained. Variations in evaporation rates of terpinol, or the room temperature at the time of painting meant that the same paste could give deposits with either smooth or irregular surface finishes, depending on the conditions. It was therefore difficult to pick out differences due only to the change of paste.

6.3.2. Influence of drying temperature.

A mistake over the temperature of drying resulted in most of the earlier samples being dried at 250°C, at which temperature the vehicle boiled off rather than evaporating. This resulted in a very rough surface (fig. 6.8.), which was improved by drying at the lower temperature (fig. 6.9.)



1 μ m

6.7. Scanning electron micrograph of fired paste mixed with a water based vehicle. x 2,200



6.8. Scanning electron micrograph of paste dried at 250°C
x 24



6.9. Scanning electron micrograph of paste dried at 150°C.
x 23.

Firing the deposits whilst still wet, i.e., no drying, did not change the surface finish appreciably, presumably because the rate of temperature rise was slow enough to allow the vehicle to evaporate. For convenience of handling, all subsequent samples were pre-dried.

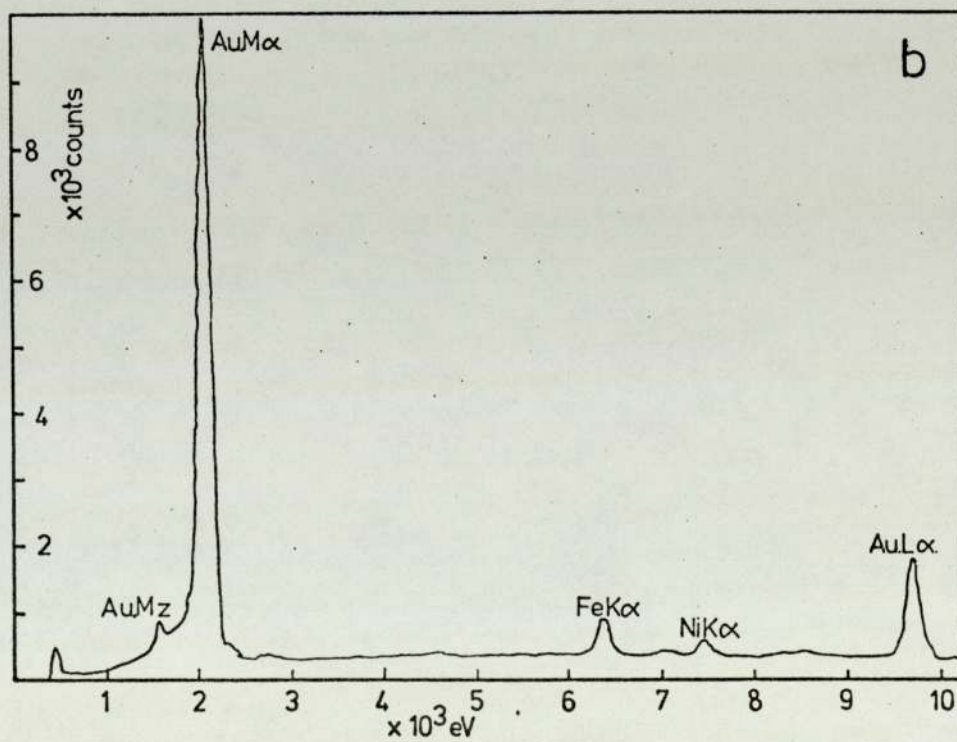
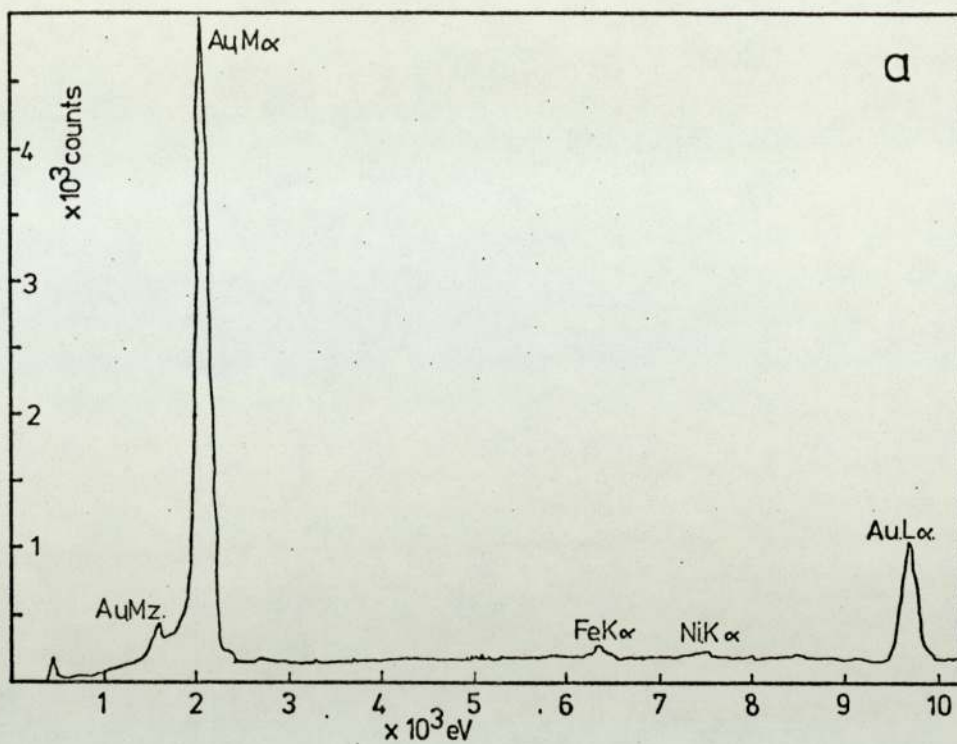
6.4. Firing.

6.4.1. Influence of substrate preparation. This proved to be very inconsistent, with results from some pastes giving the highest iron/nickel interdiffusion to cleaned samples, whilst other pastes gave this the lowest readings (fig. 6.10.). Neither did these results tie in with the resistance results, with results of 13.0, 10.1, and 15.6 milliohms for the Engelhard golds, printed onto cleaned and protected, cleaned but unprotected, and uncleaned substrates respectively. There did not appear to be any effect on the surface finish of the deposits, even on those pastes which were printed by silk screen printer.

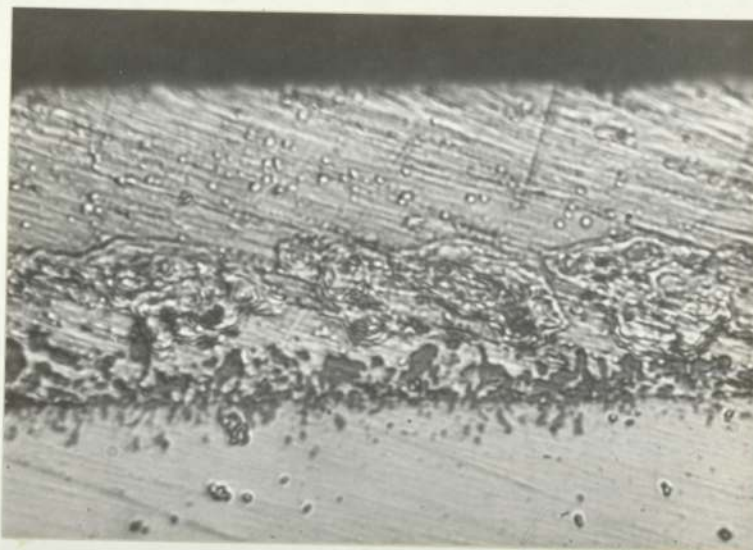
6.4.2. Influence of firing atmosphere.

Commercial thick film pastes are designed to be fired in air, and firing a sample printed by Engelhard Ltd. in air produced a bright gold deposit. Unfortunately, the oxidation of the substrate at 850°C, the firing temperature, produced a thick oxide layer which passed below the gold (fig. 6.11.). This would obviously be detrimental to its performance as a contact material for reeds.

Firing the pastes in inert atmospheres, nitrogen or argon, gave good sintering, with no sign of attack on the substrate. The resistance of pure gold pastes was low, being 12 milliohms in nitrogen, or 11 milliohms in argon, but on the Engelhard printed golds there was a film on the surface which varied in thickness from sample to sample (fig. 6.12.). This film could be removed by cleaning the sample; Kevex analysis before and after



6.10. Kevex X-ray spectra of Engelhard gold printed on
a) cleaned substrate b) uncleaned substrate.



1 μ m

6.11. Cross-section of paste fired in air, showing oxide layer beneath the gold deposit. x 1,000



1 μ m

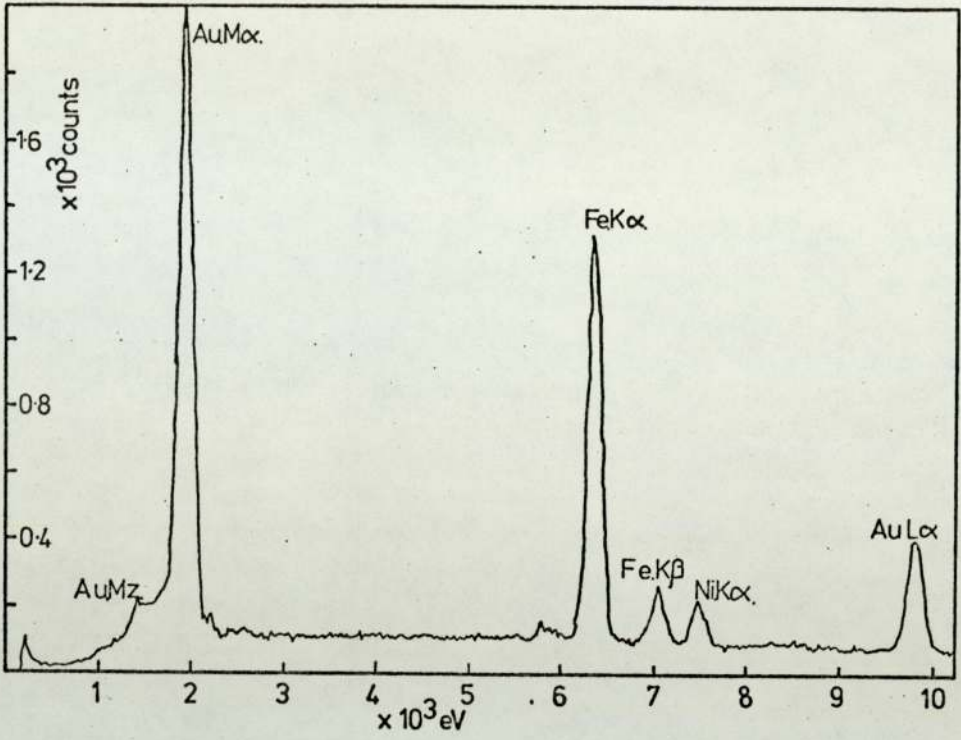
6.12. Scanning electron micrograph of Engelhard gold, showing film on deposit surface. x 2,600

showed that the deposits lost most of the iron and manganese from the surface layers (figs. 6.13. and 6.14.). The cleaned surface was golden in appearance, but the surface finish was rougher than before cleaning, with large cracks in the surface (figs. 6.15. and 6.16.). The cleaning cycle used was:-

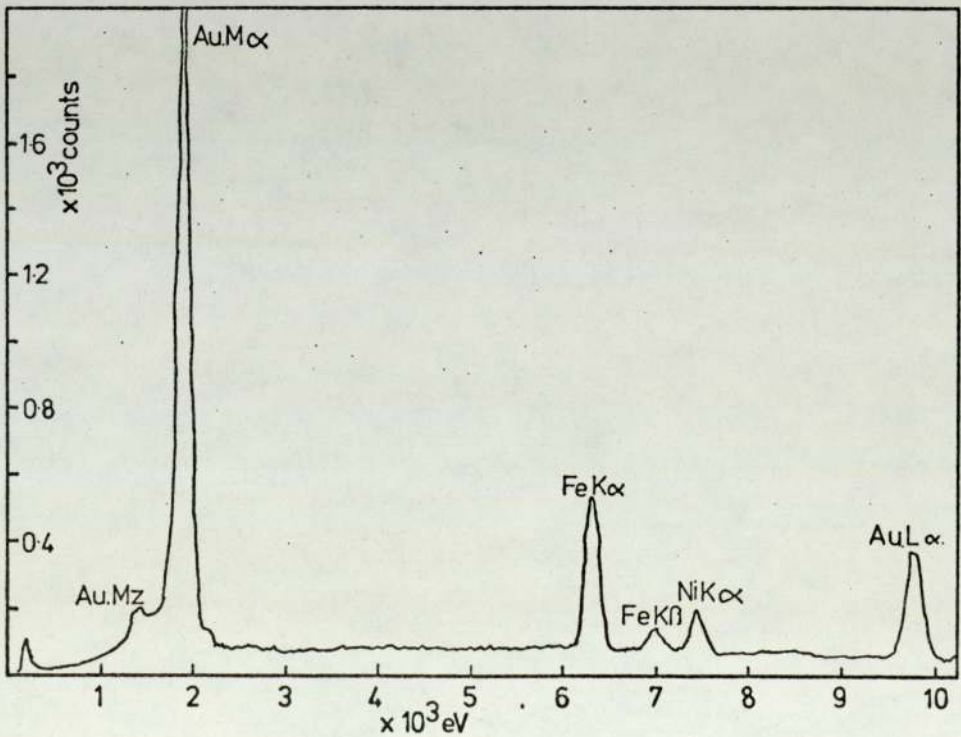
90 seconds electrolytic cleaner (proprietary alkaline);
Rinse with water;
90 seconds electrolytic cleaner (sodium cyanide solution);
Rinse with water;
Dip, 50% sulphuric acid;
Rinse with water.

The film only arose with the gold pastes printed by Engelhards, and it may be that either the vehicle required an oxidising atmosphere before it would be totally removed, or the gold used may require an out-gassing. Tests with a terpinol/ethyl cellulose solution showed that these solutions leave a stain, but not to the extent found on the fired golds. In view of the high level of iron found to be removed with the cleaning process, it may be that diffusion from the substrate surface occurred, but only in the Engelhard samples, to such an extent that iron rich layers formed on the surface. Such improved diffusion could be a result of the closer packing of the printed samples.

Firing the Aston produced pastes in a reducing nitrogen/10% hydrogen mixture, in some cases produced fired deposits very similar to those produced under nitrogen, with similar resistances. However, a significant number of these samples (45%) showed poor adhesion, due to the absence of any appreciable sintering (fig. 6.17.). This absence of sintering was also found in samples of both Aston and Engelhard produced gold, which had been fired under vacuum.



6.13. Kevex X-ray spectrum of Engelhard gold after firing.



6.14. Kevex X-ray spectrum of same Engelhard gold after cleaning.



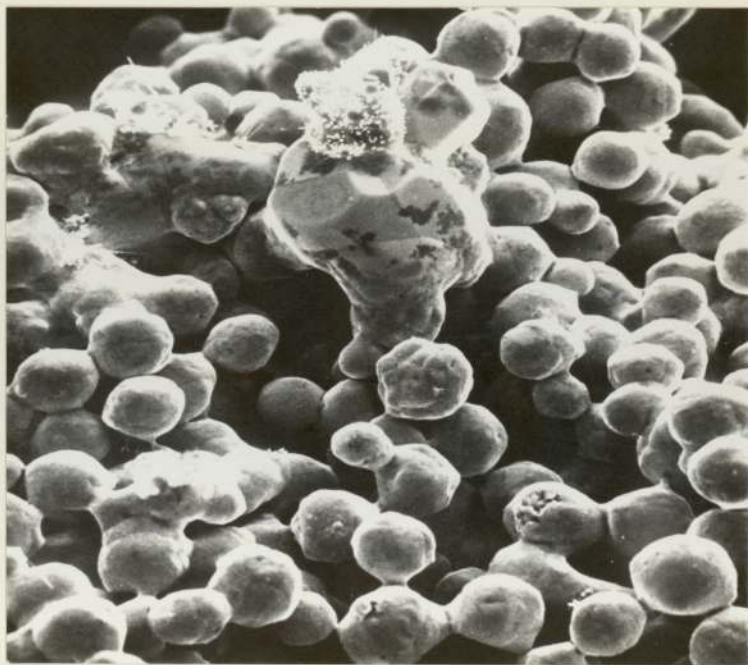
1 μ m

6.15. Scanning electron micrograph of Engelhard gold after firing. x 2,800



1 μ m

6.16. Scanning electron micrograph of same Engelhard gold after cleaning. x 2,800



1 μ m

6.17. Scanning electron micrograph of gold paste fired under nitrogen/10% hydrogen, showing zero neck growth.

x 2,100

6.4.3. Influence of firing time.

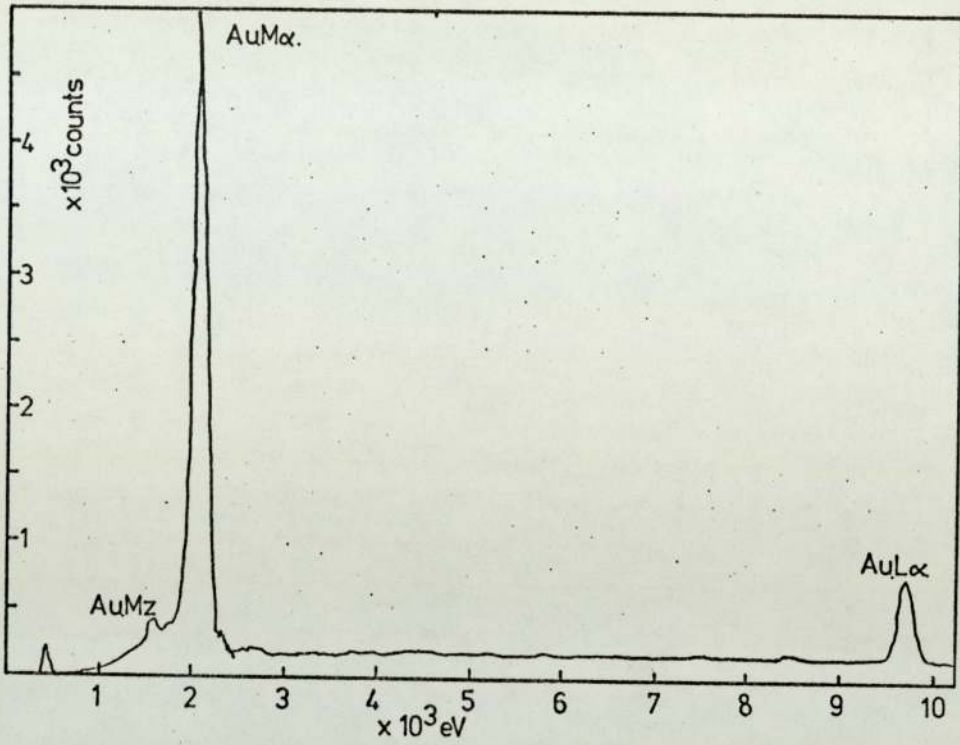
Owing to the presence of the film on the samples printed by Engelhard, it was difficult to interpret the effects of the time of firing on these samples. The glass containing samples fired at 850°C in nitrogen gave resistance values of:-

Time at 850°C	5	10	15	20	minutes.
Resistance	34	13	72	10	milliohms.

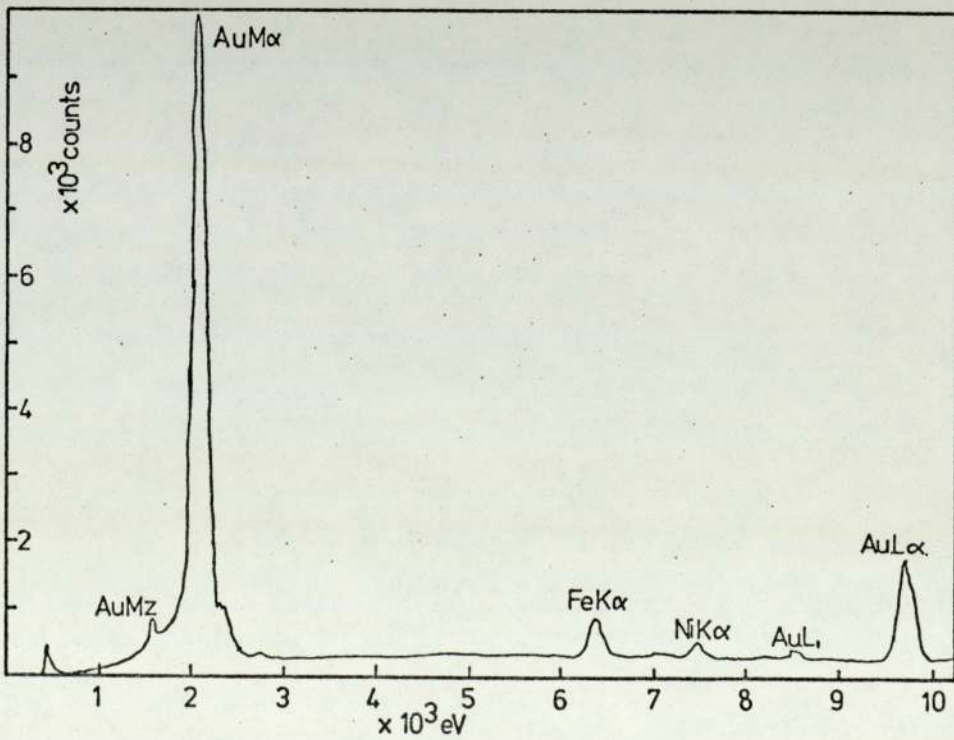
The analysis of these samples showed that there was a correlation between impurity content (figs. 6.18.- 6.21.) and resistance, but no correlation with time, unless the fifteen minute sample was discounted. In that case the resistance dropped with increasing firing time.

Prolonged heating up to 25 hours, increased the contact resistance (to greater than 2 ohms), but this was due to the build up of iron rich particles on the surface (figs. 6.22.- 6.25.). These might have been due to the presence of an oxidizing atmosphere on the surface, as the furnace tube broke during this firing.

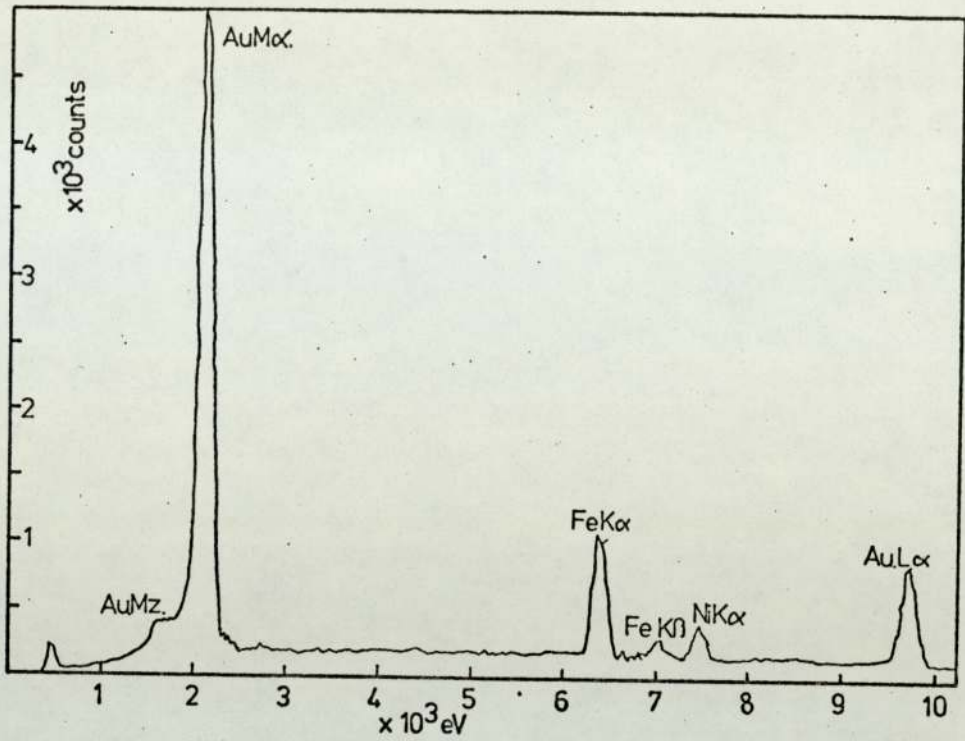
The Aston produced samples were fired in a different firing cycle in which they were heated up from cold with the furnace. This resulted in much longer firing cycles, so that five or ten minute differences at peak firing temperatures tend to be meaningless. Therefore, only a limited number of time changes were tried. For example, increasing the time at 900°C for a pure gold in argon from 10 to 60 minutes, produced a resistance drop from 24 to 5 milliohms. There does not appear to be any large change in the structure of the deposit, except that the particles seem to be a little closer on the deposit fired for one hour (figs. 6.26. and 6.27.). In both cases the necks between the particles were almost as thick as the particles themselves, with the grain boundary grooves clearly visible (fig. 6.28.).



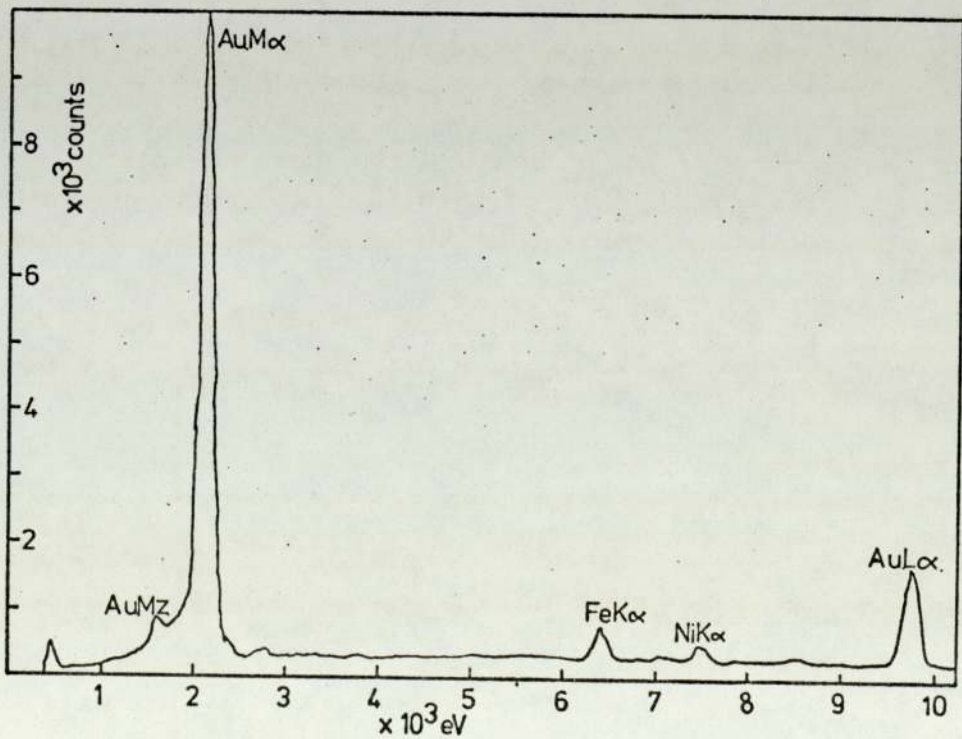
6.18. Kevex X-ray spectrum of gold paste fired for 5 minutes at 800°C in nitrogen.



6.19. Kevex X-ray spectrum of gold paste fired for 10 minutes at 850°C in nitrogen.



6.20. Kevex X-ray spectrum of gold paste fired for 15 minutes at 850°C in nitrogen.

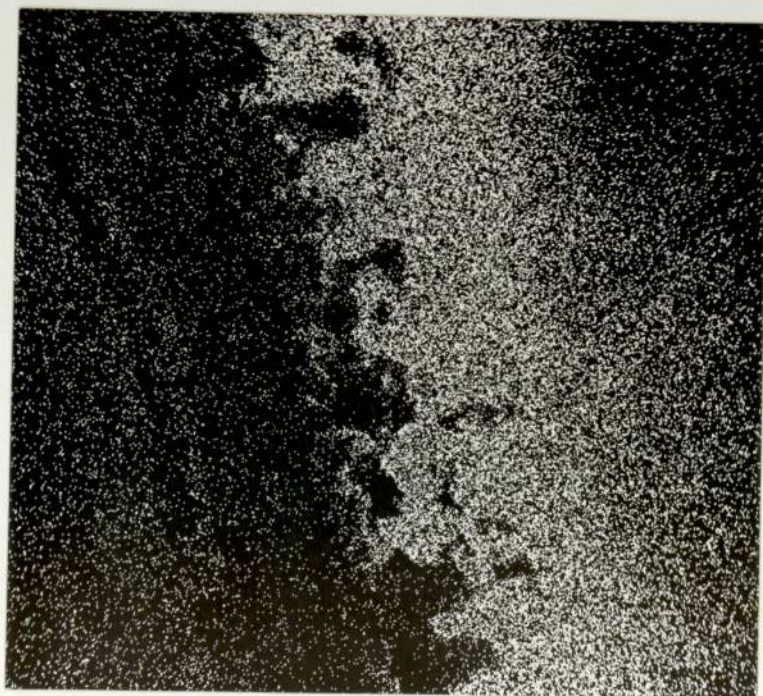


6.21. Kevex X-ray spectrum of gold paste fired for 20 minutes at 850°C in nitrogen.



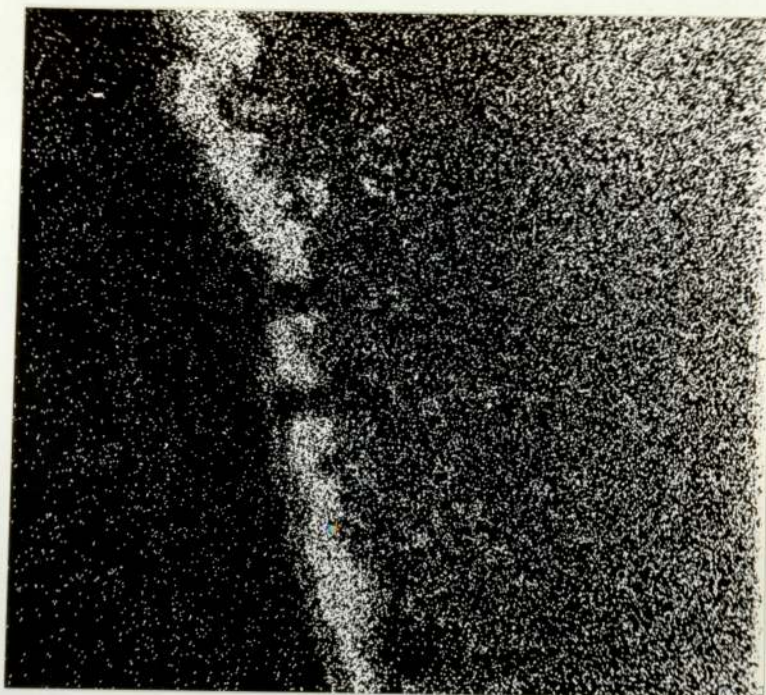
1 μm

6.22. Scanning electron micrograph of a cross-section of a gold paste fired for 25 hours in argon. x1,200

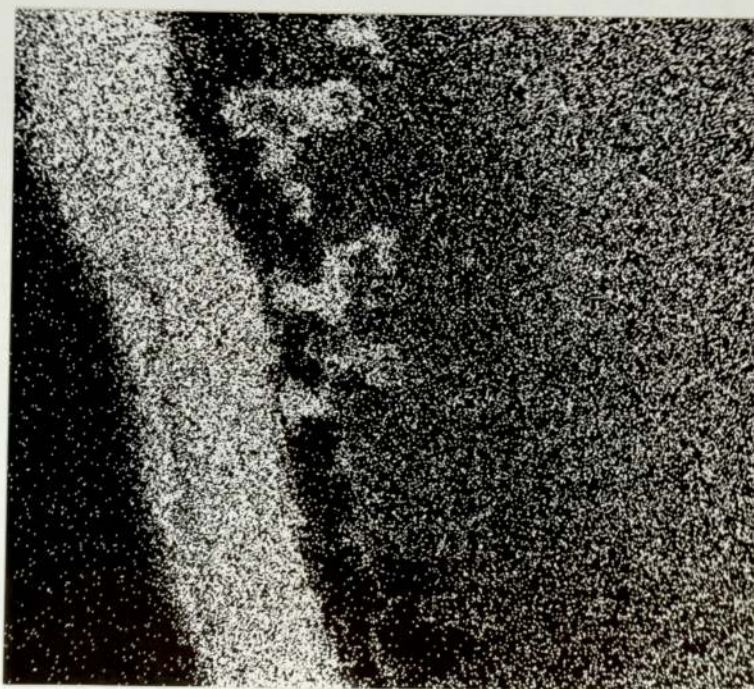


1 μm

6.23. Distribution of gold in fig. 6.22. (Gold $M\alpha$ line). x 1,200.



6.24. Distribution of iron in fig. 6.22. (Iron $K\alpha$ line).
x 1,200.

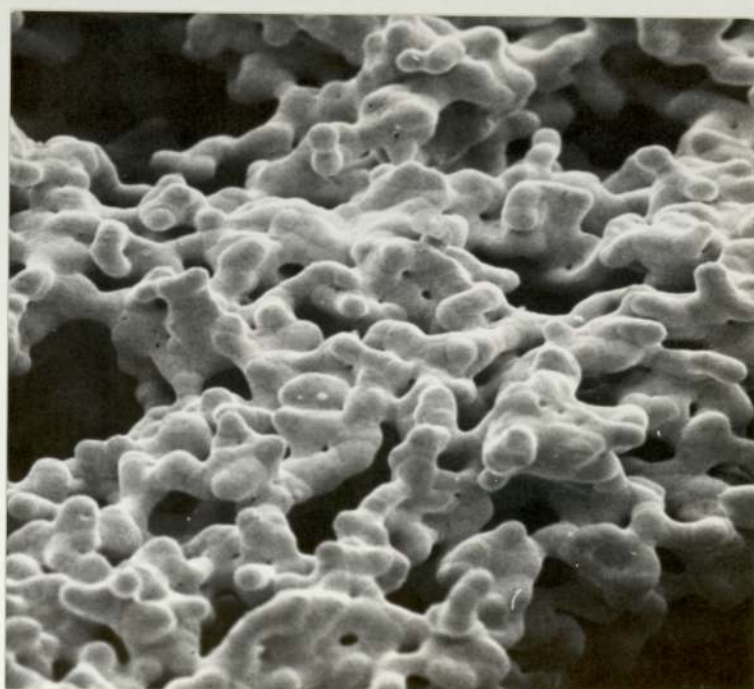


6.25. Distribution of nickel in fig. 6.22. (Nickel $K\alpha$ line).
x 1,200.



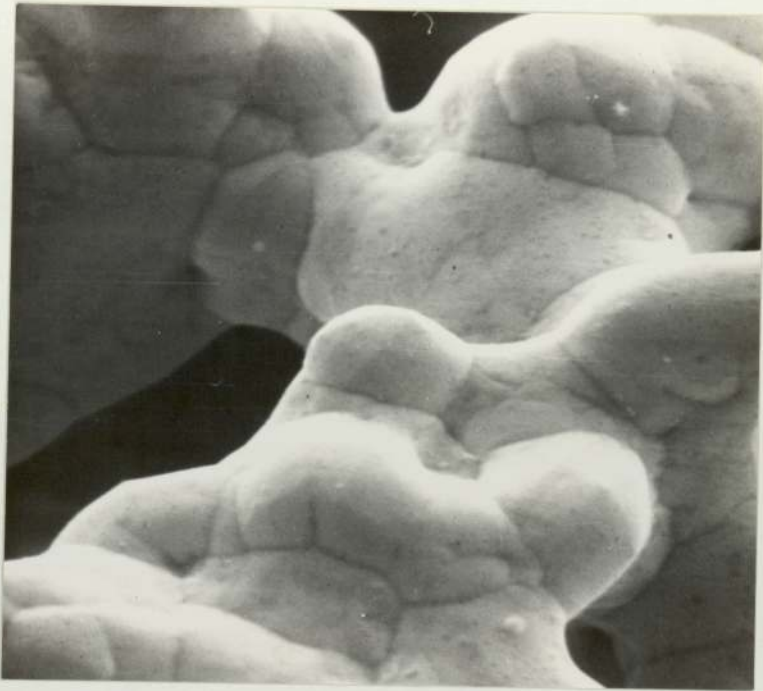
$\mu 1 \mu\text{m}$

6.26. Scanning electron micrograph of gold fired in argon at 900°C for 10 minutes. x 1,300



$\mu 1 \mu\text{m}$

6.27. Scanning electron micrograph of gold fired in argon at 900°C for 60 minutes. x 1,280



└ 1 μ m

6.28. Scanning electron micrograph of gold fired in argon at 900°C for 60 minutes. x 6,500

6.4.4. Influence of firing temperature.

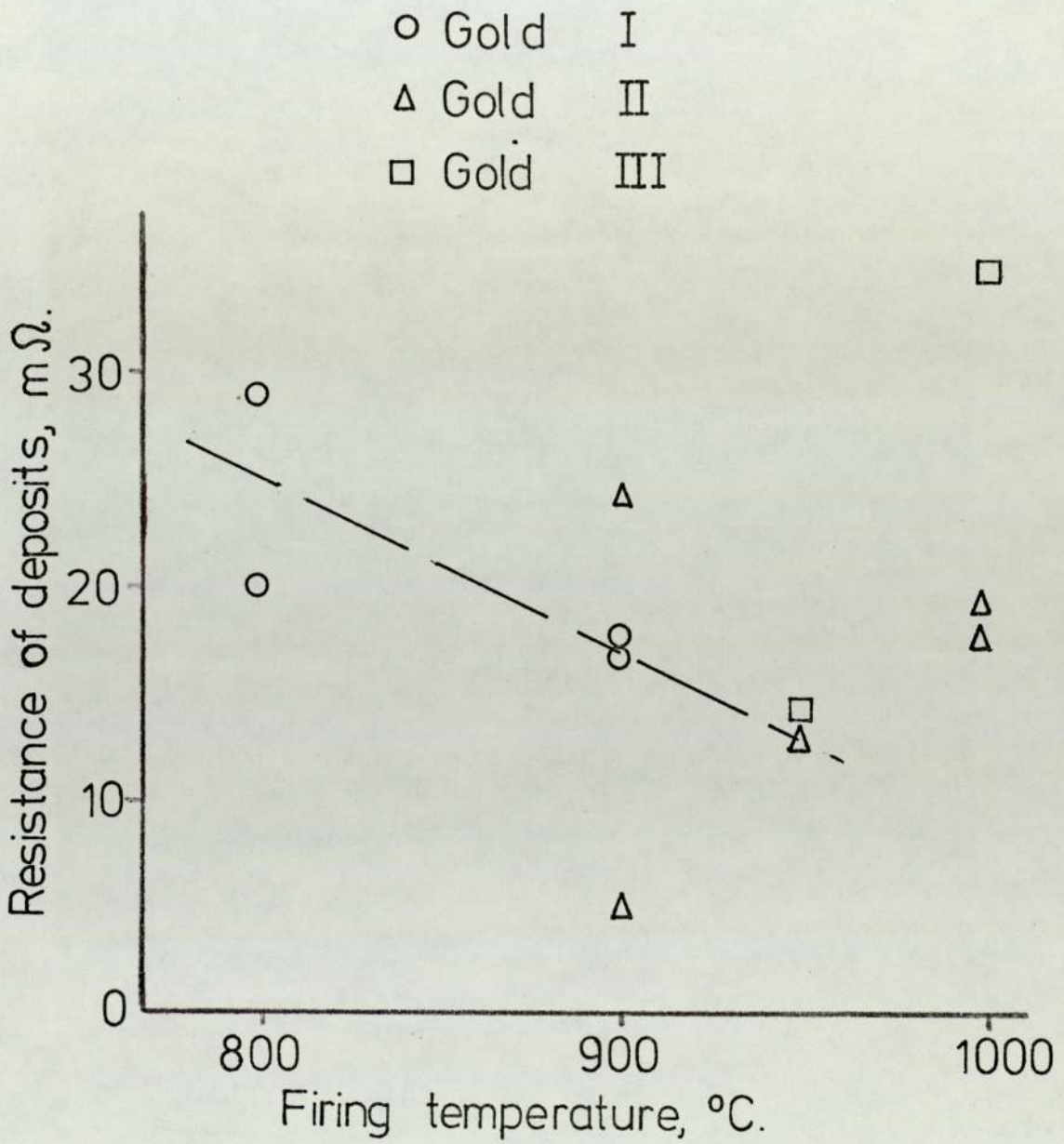
The resistance of all the pure gold deposits fired for 10 minutes at various temperatures is given in fig. 6.29., and shows a steady drop in resistance from 800°C to 950°C, followed by a rise in resistance at 1000°C. The degree of neck growth also follows this trend, going from about 10% particle diameter at 800°C up to 90% diameter at 950°C (figs. 6.30. and 6.31.). However, the sample fired at 1000°C has all the appearances of having melted, being smooth and silvery, and having a visible grain size similar to that of the substrate material (fig. 6.32.). It also had a very high level of impurities (fig. 6.33.).

6.5. Paste Composition.

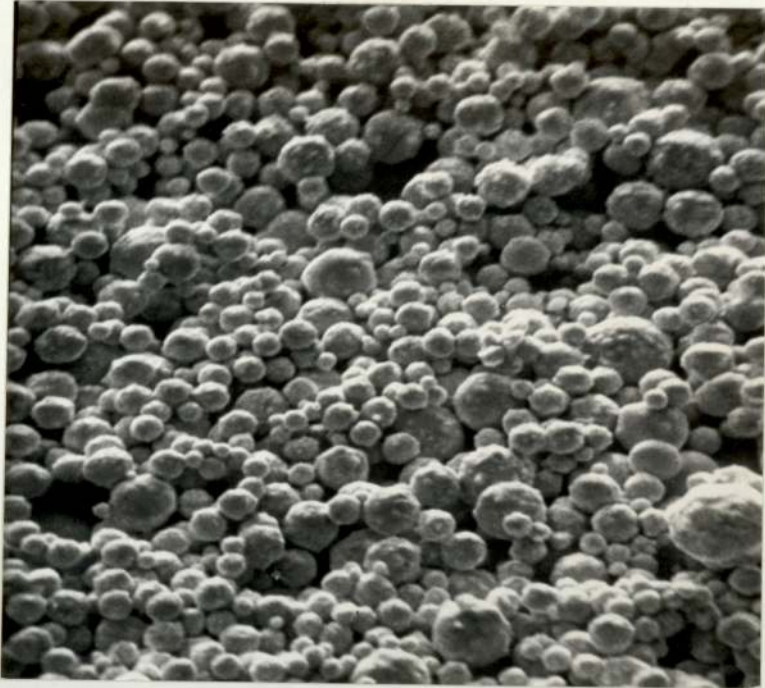
6.5.1. Influence of particle morphology.

There appears to be little influence of size on particle growth, as can be seen from fig. 6.29. The samples marked 'gold I' were made up from the golds shown in fig. 3.29., giving a fairly uniform spread of sizes up to 3µm (pH 2.1. and 2.9. gave only low yields). The gold shown as 'gold II' was made up from the gold powders shown in fig. 3.76., which gave a paste of particles bunched between 3 and 6µm. The third powder, 'gold III' was made up of golds G39 and G46 on fig. 3.77., giving a mixture of large particles about 3-4µm in diameter, filled in with small particles of about 0.5µm diameter. This ratio fits in closely with the 1:7 ratio for good binary packing,⁽¹⁰⁷⁾ but neither this nor any of the other mixtures showed noticeably better packing than any of the others.

Powder from oxalic acid reduced solutions containing many flat plates (fig. 3.51.) was mixed into a paste and fired at 950°C. The paste required much more vehicle to make it suitable for brushing, and eventually 50% by weight of vehicle was added. The fired sample showed very poor adhesion and very few signs of sintering (fig. 6.34.). However, rough



6.29. Variation of electrical resistance with firing temperature for pure gold.



1 μ m

6.30. Scanning electron micrograph of gold fired for 10 minutes at 800°C. x 2,600

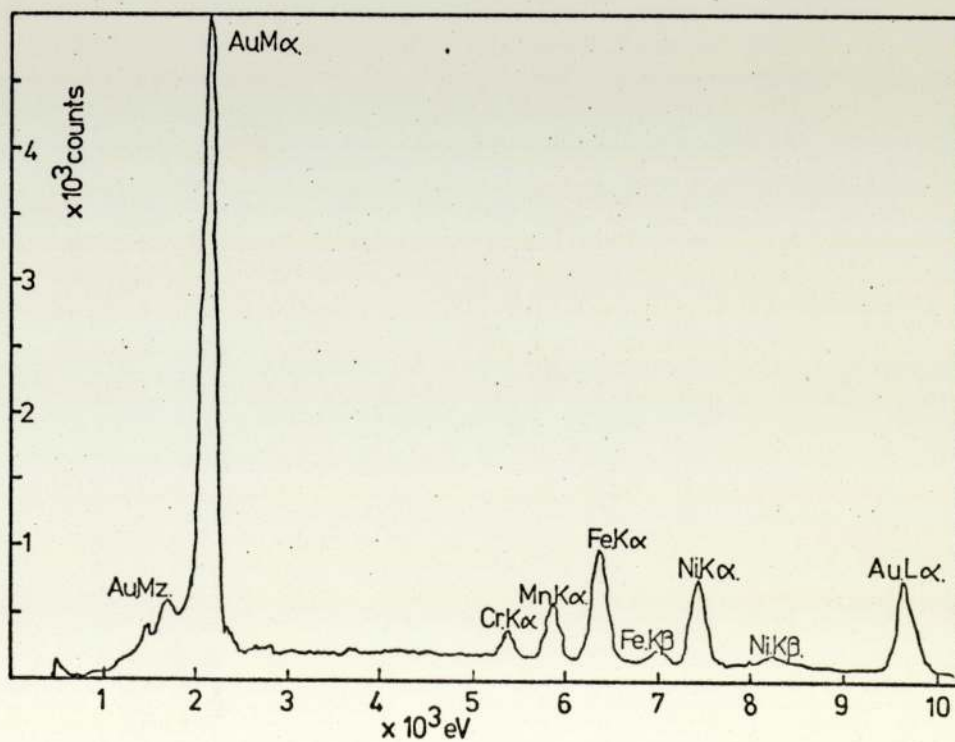


1 μ m

6.31. Scanning electron micrograph of gold fired for 10 minutes at 950°C. x 2,100



6.32. Scanning electron micrograph of gold fired for 10 minutes at 1000°C. x 1,000



6.33. KeveX X-ray spectrum of gold fired for 10 minutes at 1000°C.



$\approx 1 \mu\text{m}$

6.34. Scanning electron micrograph of gold powder in the form of flat plates after firing. x 1,200

gold spheres were found to sinter very rapidly to smooth spheres, compare for example figs. 6.35., and 6.36. which show the gold before and after sintering.

6.5.2. Effect of glass frit.

The presence of the glass frit appeared to make little difference to the electrical properties of the deposits, the resistance being 13 milliohms without the frit and 11.9 milliohms with it. The surface finish did not appear to be changed either by the presence of the frit (figs. 6.37. and 6.38.).

6.5.3. Gold/palladium alloys.

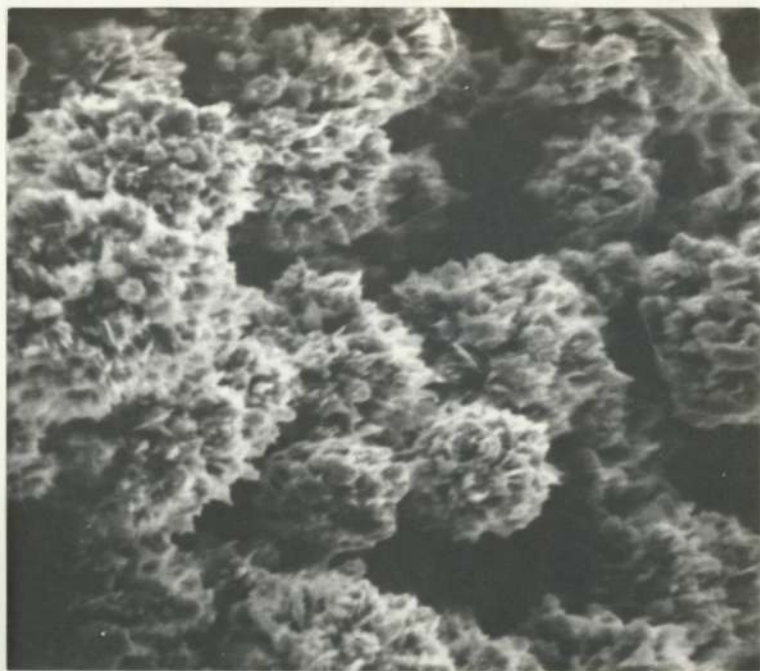
Gold/10% palladium alloys were made up from gold reduced by sodium sulphite (fig. 6.36.), and the palladium supplied by Hopkins and Williams (fig. 3.69.). The fired samples were analysed by X-ray microanalysis and found to contain 9.25% palladium.

These samples had very poor surface finishes (fig. 6.39.), with the palladium badly distributed over the surface (fig. 6.40.). The palladium remained separate from the gold, despite raising the firing temperature from 900°C to 1000°C or increasing the time at peak temperature from 10 to 60 minutes. The effect on the resistance is shown below:-

Temperature -	900°C	950°C	1000°C
Time at temperature			
10 mins.	32mΩ, 25mΩ.	15mΩ, 13.6mΩ.	8mΩ, 9.6mΩ.
60 mins.	4.7mΩ, 10mΩ.		

(Two values are given for each set of conditions as the firings were duplicated at a later date).

The drop in resistance with increased time or temperature may be



└ 1 μ m

6.35. Scanning electron micrograph of gold powder showing rough spheres before firing. x 4,700



└ 1 μ m

6.36. Scanning electron micrograph of the same gold powder as in fig. 6.35, after firing at 900°C for 10 minutes. x 3,700



6.37. Scanning electron micrograph showing the surface finish of a fired gold paste containing no glass. x 30.



6.38. Scanning electron micrograph showing the surface finish of a fired gold paste containing glass frit. x 23.



6.39. Scanning electron micrograph of a gold/palladium paste after firing at 900°C for 10 minutes. x 150.



6.40. Distribution of palladium in figure 6.39. (Palladium $L\alpha$ line). x 150

due to the slight increase in sintering of the gold powders in the mixture (figs. 6.41. - 6.44.). Firing in the reducing nitrogen/hydrogen mixture, however, prevented practically all the sintering, even at 1000°C (fig. 6.45.).

6.5.4. Gold/palladium/tin alloys.

These alloys were similar to the gold/palladium alloys, being mixed from the same gold and 10% (by weight) of palladium/tin from the plating on plastic waste products (fig. 3.71.). After firing, however, it was found that the palladium/tin had segregated to the surface and formed a smooth surface layer, which had subsequently fissured (figs. 6.46. - 6.48.). This was confirmed by X-ray microanalysis which gave palladium and tin contents of 11% and 13% respectively. The gold beneath the surface appeared to have sintered together well (fig. 6.49.), but there did not seem to be any sintering of the palladium/tin at this temperature, even after one hour at 900°C.

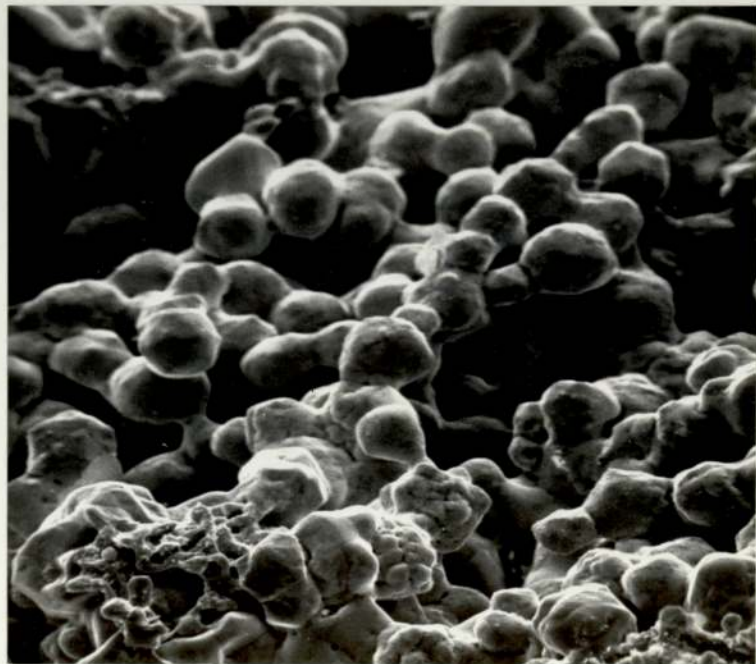
Raising the temperature of firing to 950°C improved the sintering of the gold, but changed the form of the palladium/tin to rough spheres about 9µm in diameter on the surface of the gold (figs. 6.50. and 6.51.). The deposit was very badly fissured (fig. 6.52.). Raising the temperature again to 1000°C produced a very rough deposit which showed signs of melting at the edges, and a subsequent increase in the amount of impurities present (figs. 6.53. and 6.54.).

The effects of time and temperature on the electrical properties of gold/palladium/tin alloys are given below.

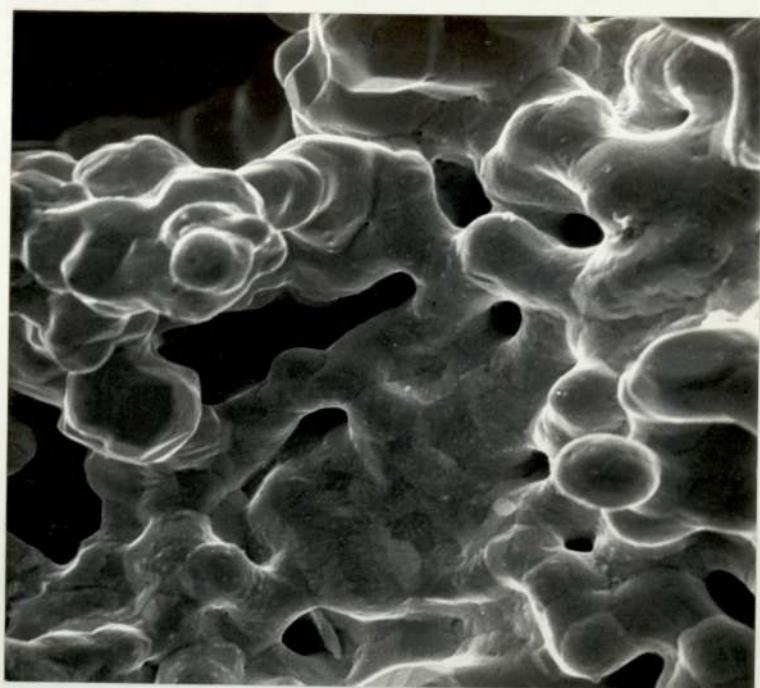
Temperature -	900°C	950°C	1000°C
Time at temperature			
10 mins.	35mΩ.	37mΩ.	31mΩ.
60 mins.	6.4mΩ.		



6.41. Scanning electron micrograph of a gold/palladium paste after firing at 900°C for 10 minutes. x 3,700



6.42. Scanning electron micrograph of a gold/palladium paste after firing at 900°C for 60 minutes. x 2,100



6.43. Scanning electron micrograph of a gold/palladium paste after firing at 950°C for 10 minutes. x 2,100



6.44. Scanning electron micrograph of a gold/palladium paste after firing at 1000°C for 10 minutes. x 2,400

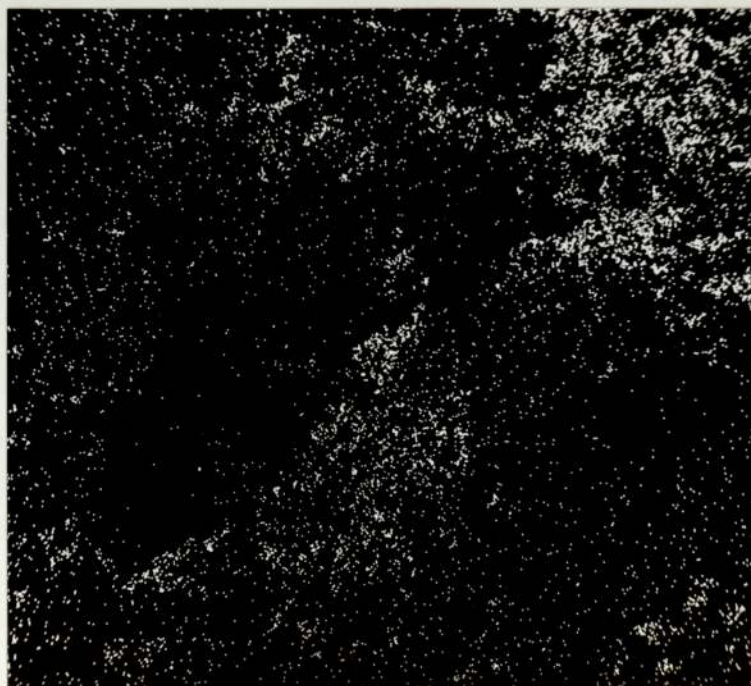


— 1 μ m

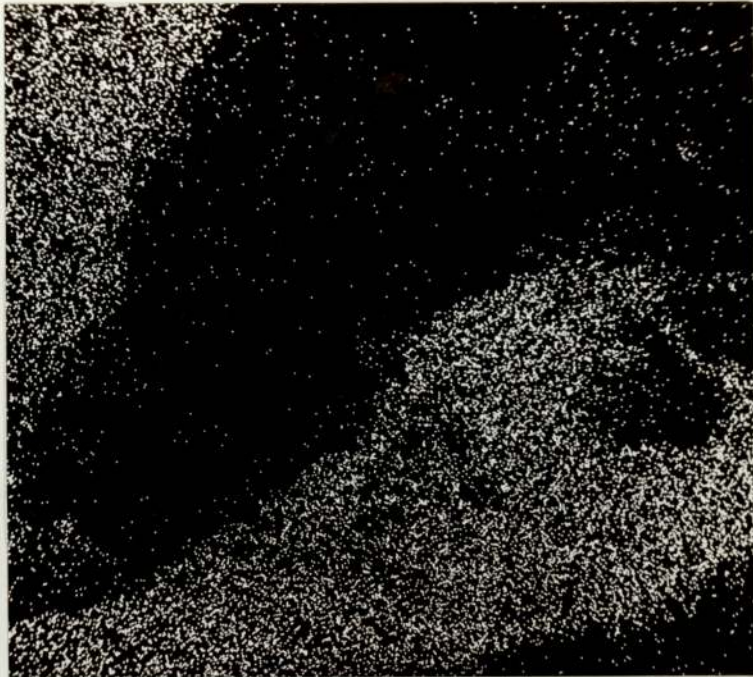
6.45. Scanning electron micrograph of a gold/palladium paste after firing at 1000°C for 10 minutes in a nitrogen 10% hydrogen atmosphere. x 5,400



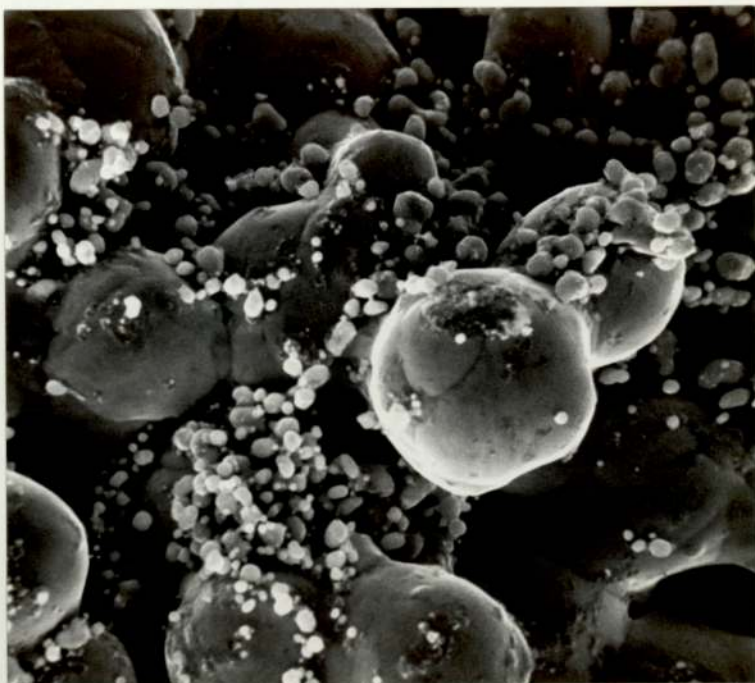
6.46. Scanning electron micrograph of a gold/palladium/tin paste fired at 900°C for 10 minutes. x 375.



6.47. Distribution of gold in fig. 6.46. (Gold M α line). x 375.

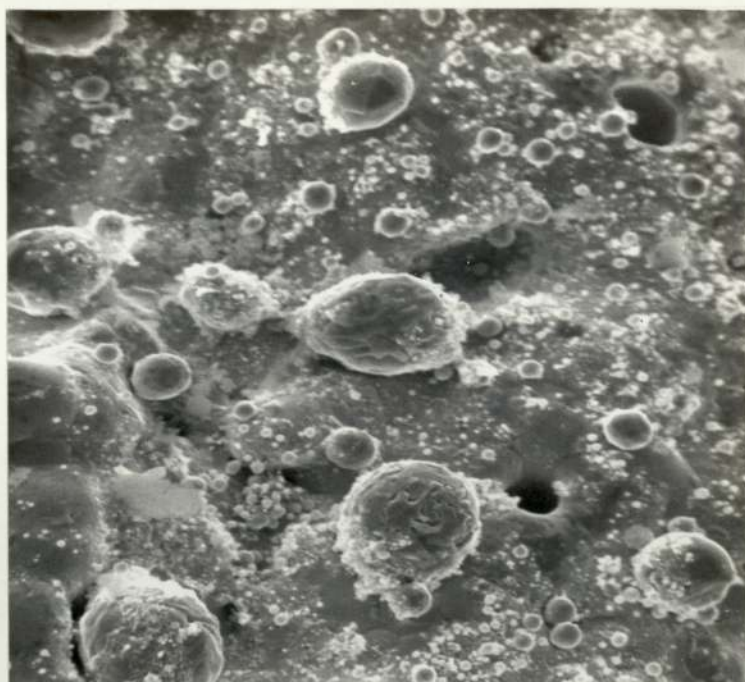


6.48. Distribution of palladium in fig. 6.46. (Palladium
L α line). x 375.



1 μm

6.49. Scanning electron micrograph of gold/palladium/tin
paste fired at 900°C for 10 minutes. x 3,750



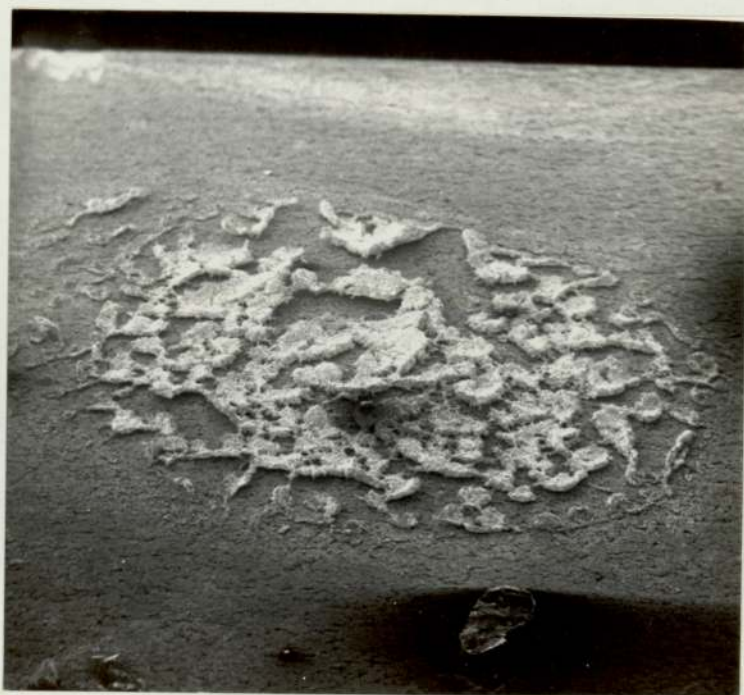
1 μ m

6.50. Scanning electron micrograph of a gold/palladium/tin paste fired at 950°C for 10 minutes. x 2,100

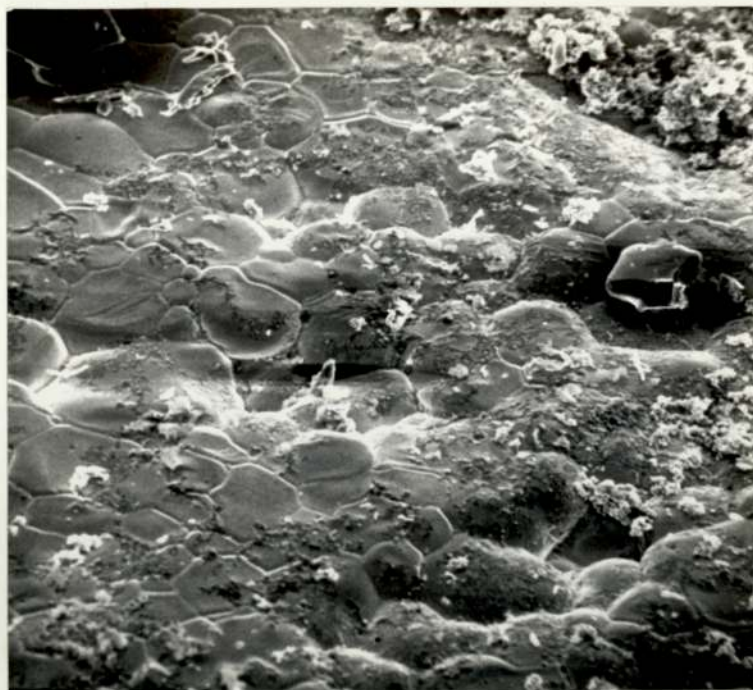


1 μ m

6.51. Distribution of palladium in fig. 6.50. (Palladium $L\alpha$ line). x 2,100

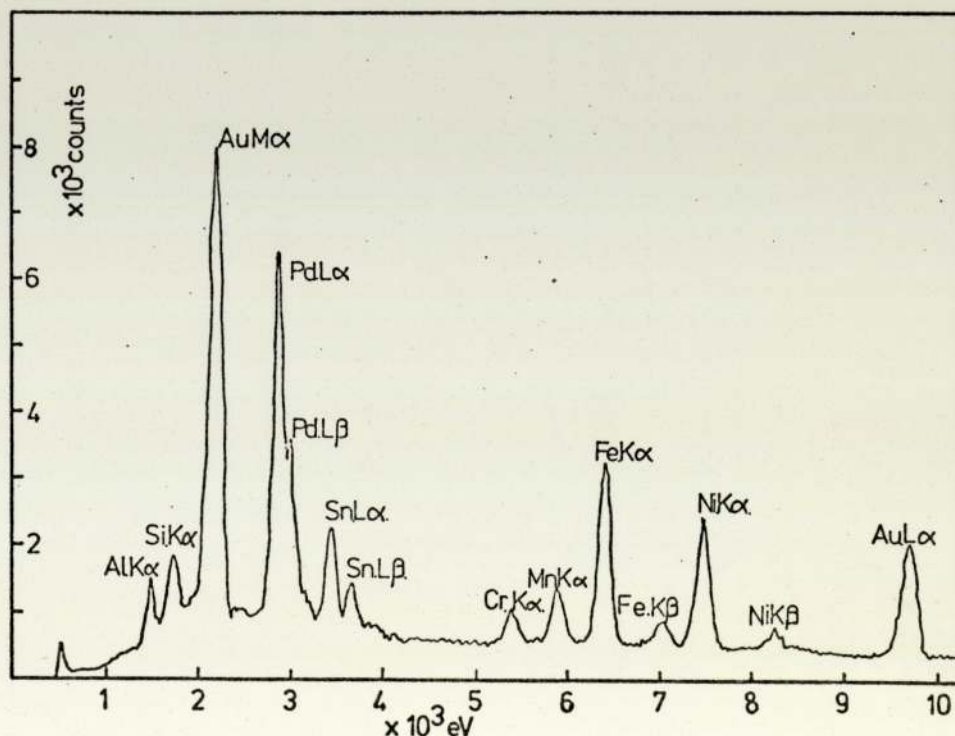


6.52. Scanning electron micrograph of a gold/palladium/tin
paste fired at 950°C for 10 minutes. x 21.



1 μ m

6.53. Scanning electron micrograph of gold/palladium/tin paste fired at 1000°C for 10 minutes. x 520.



6.54. Kevex X-ray spectrum of melted area of gold/palladium/tin paste fired at 1000°C for 10 minutes.

6.5.5. Gold/palladium/nickel alloys.

Despite being mixed from the crushed palladium/nickel alloy (fig. 6.55.), this alloy gave a mixture of gold particles and smaller alloy particles (fig. 6.56.), the size and distribution of which showed a vast improvement on the original alloy powder. Unfortunately the surface finish of these alloys was very poor, with many small holes visible (fig. 6.57.). Changing the alloy content from palladium 3.45%, nickel 3.45%, to palladium 5.2%, nickel 3.5% (results by X-ray microanalysis) did not produce any noticeable changes, neither in the sintering nor the electrical resistance.

The resistance changed from 25 milliohms to 27 milliohms with the increase in alloy content.

6.5.6. Gold/nickel alloys.

Four gold/nickel alloys were made up with the carbonyl nickel (fig. 3.73.) and gold from batch G54 of fig. 3.77. The details of the pastes are given below:-

Nominal composition	% added.	Fired Analysis.	
1	1.04	1.33	
5	4.98	5.45	
10	9.75	11.05	all in weight %
20	20.30	22.40	

Firing the pastes at 900°C for 10 minutes produced a grey surface on all except the 1% alloy which was light yellow in colour. All had reasonable surface finished (fig. 6.58.). Examination on the scanning electron microscope showed that all except the 1% alloy had a neck growth of approximately 100% particle size, with the nickel separate and proud of the surface (figs. 6.59. and 6.60.). Some nickel solution must have taken



1 μ m

6.55. Scanning electron micrograph of palladium/nickel/
(sulphur) precipitate after crushing. x 2,100



1 μ m

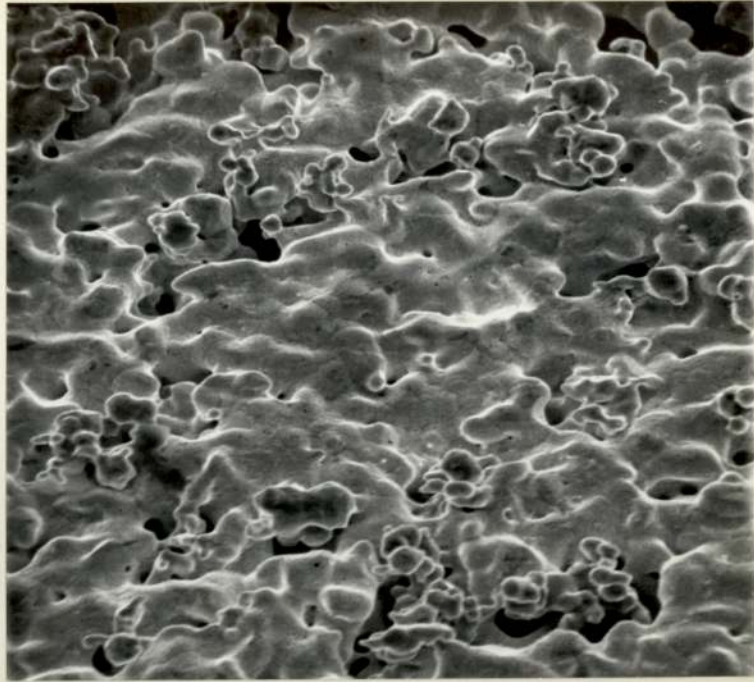
6.56. Scanning electron micrograph of gold/palladium/nickel
paste after firing at 950°C for 10 minutes. x 2,100



6.57. Scanning electron micrograph of gold/palladium/nickel paste after firing at 950°C for 10 minutes. x 21.



6.58. Scanning electron micrograph of a gold/nickel paste after firing at 950°C for 10 minutes, showing the surface finish. x 110



1 μ m

6.59. Scanning electron micrograph of a gold/20% nickel paste after firing at 900°C for 10 minutes. x 1,100



1 μ m

6.60. Distribution of nickel in fig. 6.56. (Nickel $K\alpha$ line). x 1,100

place as the background nickel radiation became progressively higher with increasing nominal nickel content (fig. 6.61.). The 1% nickel alloy on the other hand, showed almost no sintering at all, except in isolated areas which appeared to have melted or sintered to 100% neck growth (fig. 6.62.). There was no connection between these areas and any nickel concentrations (fig. 6.63.).

Increasing the firing temperature to 950°C did not change the appearance of the 1% and 5% alloys, but both the 10% and 20% alloys appear to have melted, displaying the flat bright areas similar to those seen in fig. 6.53. The electrical properties of these alloys are shown below:-

% nickel -	1%	5%	10%	20%
Firing temperature:				
900°	12mΩ	20.5mΩ	19mΩ	12.4mΩ
950°	23mΩ	27mΩ	22mΩ	12mΩ

6.5.7. Gold/iron alloys.

The details of the analysis of these alloys are given below, and in most respects they follow a trend similar to that of gold/nickel alloys.

Nominal composition.	% added.	Fired analysis.	
1	1.0	0.84	
5	5.8	5.4	all in weight %
10	-	12.5	

The 1% alloy shows the same isolated patches of 100% neck growth, but in this case the other areas show some signs of sintering (figs. 6.64. and 6.65.). The 5 and 10% alloys both show the similar structure of 100% neck growth, although in this case the iron is not standing proud of the surface and does not appear to be particular (fig. 6.66.). The change of electrical properties with composition is given below:-

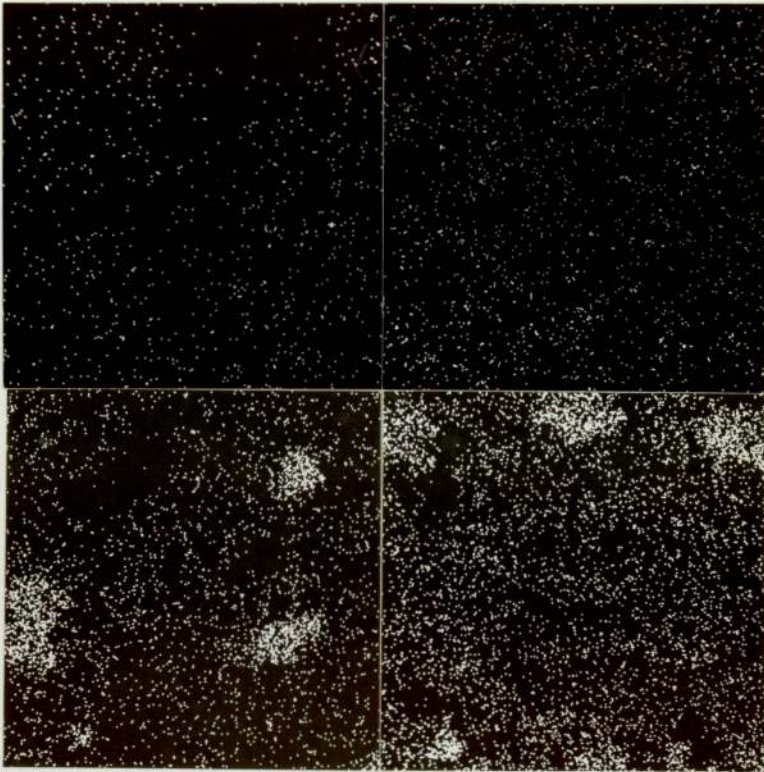
% iron -	1%	5%	10%
Firing temperature:			
950°	28m Ω .	104m Ω .	44.5m Ω .

6.5.8. Gold/copper/alloys.

Only two alloys of gold and copper were mixed, the details of which are given below:-

1 % Ni

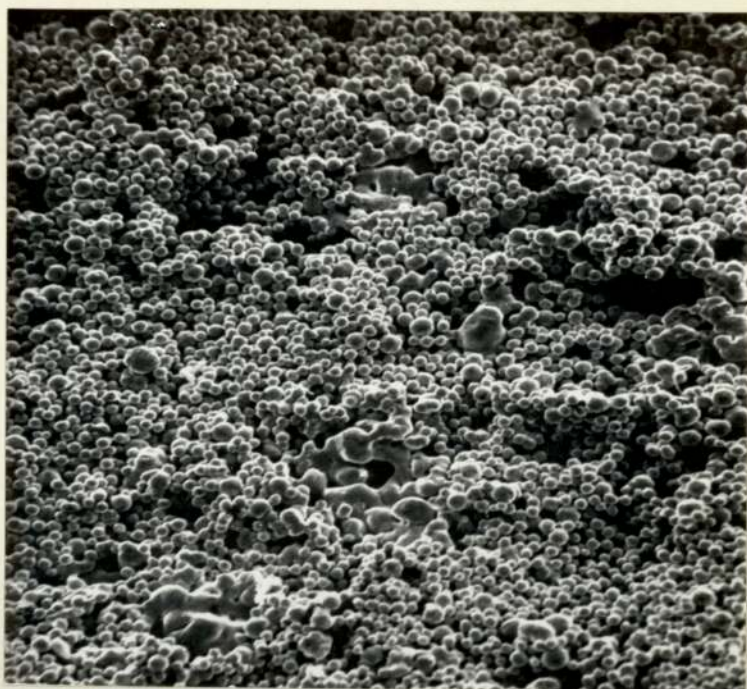
5 % Ni



10% Ni

20% Ni

6.61. Nickel background radiation for gold/nickel alloys.
(Nickel $K\alpha$ line).



1 μ m

6.62. Scanning electron micrograph of gold/1% nickel alloy fired at 900°C for 10 minutes. x 1,100



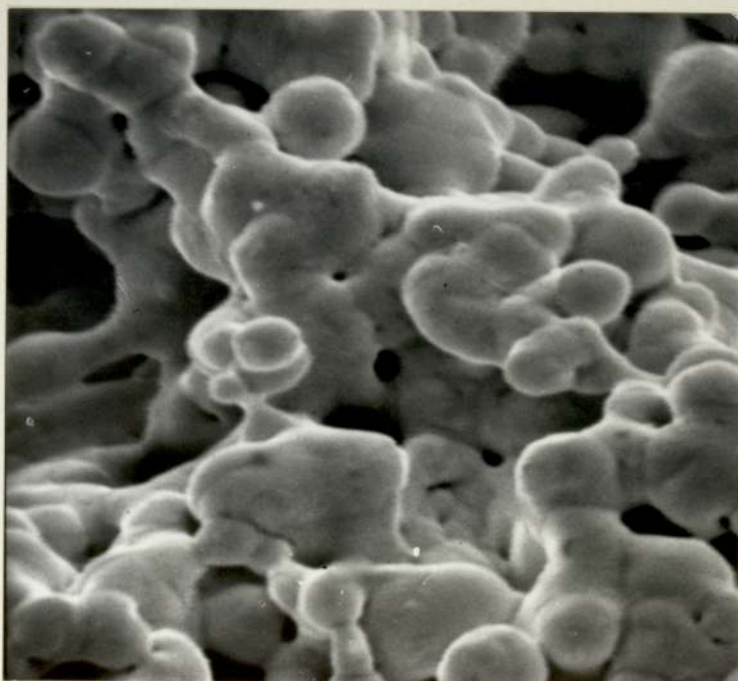
1 μ m

6.63. Distribution of nickel in fig. 6.62. (Nickel $K\alpha$ line). x 1,100



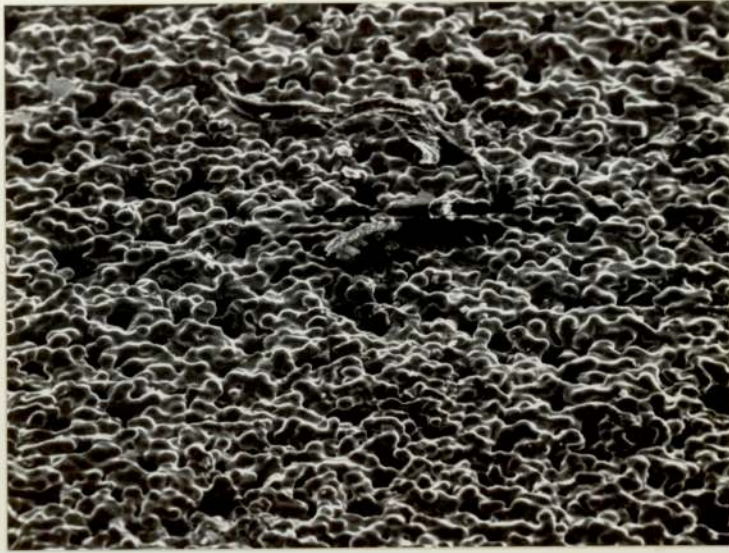
1 μ m

6.64. Scanning electron micrograph of a gold/1% iron alloy fired at 950°C for 10 minutes. x 1,100



1 μ m

6.65. Scanning electron micrograph of gold/1% iron alloy fired at 950°C for 10 minutes. x 5,500



μm

6.66. Scanning electron micrograph of gold/10% iron alloy
fired at 950°C for 10 minutes. x 1,100

Nominal composition	% added.	Fired analysis.	
1	1.1	2.25	
5	4.7	5.7	all in weight %

After firing at 950°C for ten minutes, both samples exhibited the isolated sintering structure (figs. 6.67. and 6.68.), with a larger area of sintering on the 5% alloy. The electrical resistance of the 1% copper deposit was 54 milliohms, dropping to 24 milliohms for the 5% copper alloy.

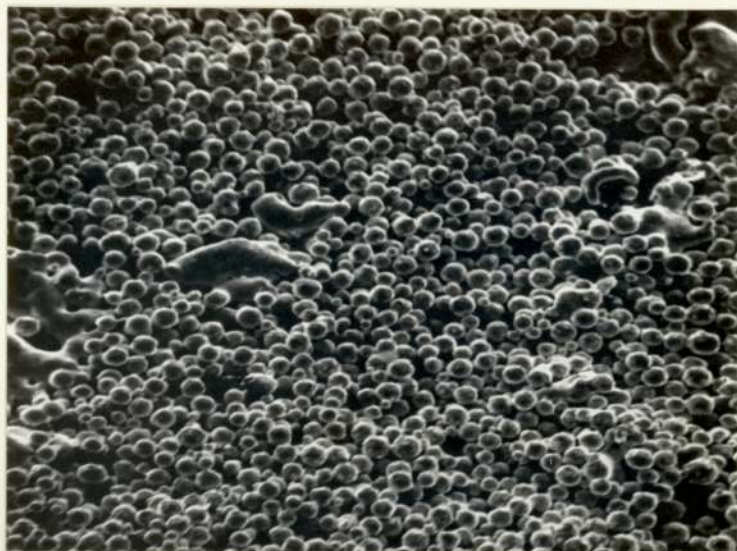
6.6. Deposit Properties.

6.6.1. Adhesion.

Several deposits were found during the work to have poor adhesion, and fell off the substrate during handling. These were found to be the samples with almost no interparticle neck growth (e.g. fig. 6.45.). There appeared to be no common factor between them, being pure or alloyed golds, at all temperatures and under most protective atmospheres. However, by far the greatest portion of them fired in either a vacuum or a reducing nitrogen/10% hydrogen mixture.

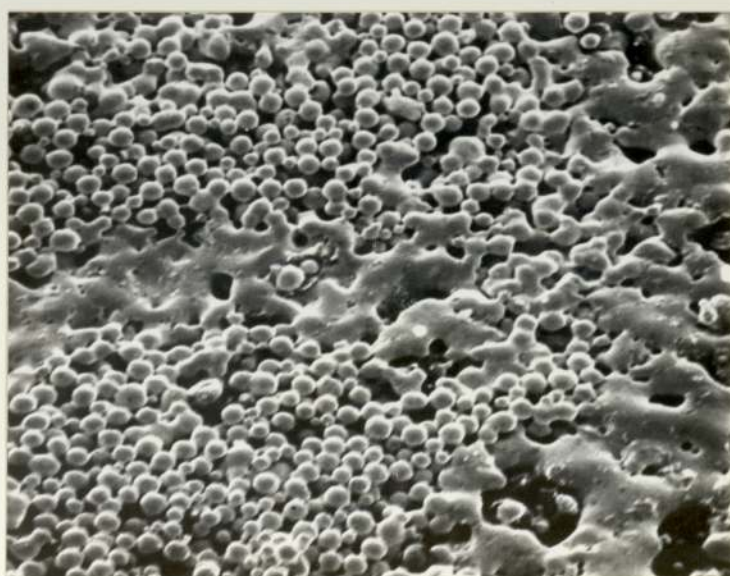
The direct pull test on the sample of gold paste fired in air, failed under a load of 4.87 Kg, equivalent to 1.22 Kg f/mm². The break appeared to be between the gold and the substrate (figs. 6.69. and 6.70.).

The peel test gave limits to the adhesion of the deposits to the substrate of between 50 - 200g/mm lower limit and 226g/mm upper limit. This was due to the fact that the first test failed between the copper overlayer and the gold, whilst the second test failed between the gold and the substrate. One gold broke cleanly from the iron/nickel, although there was a considerable amount of dynamic loading on that deposit (fig. 6.71.).



1 μ m

6.67. Scanning electron micrograph of gold/1% copper alloy fired at 950°C for 10 minutes. x 1,000



1 μ m

6.68. Scanning electron micrograph of gold/5% copper alloy fired at 950°C for 10 minutes. x 1,000



6.69. Scanning electron micrograph of the substrate after adhesion testing using a soldered wire. x 28.



6.70. Scanning electron micrograph of the underside of the soldered area pulled off the substrate shown in fig. 6.69. x 32.



6.71. Scanning electron micrograph of the underside of a pure gold deposit peeled off a nickel/iron substrate. x 100

A gold/palladium/nickel alloy, which had static loading, broke in patches leaving areas of gold still on the substrate, and copper showing through the holes in the gold (figs. 6.72 and 6.73.).

6.6.2. Density.

The fired density of a properly mixed and dried gold deposit with no out-gassing may be as high as 80% of solid density. This figure was based on cut and weigh techniques used on scanning electron micrographs of deposit cross-sections (e.g., fig. 6.74.). They were also confirmed by analysis by the image analysis computer (Quantimet). In both these methods, attempts were made to eliminate the effects of the electroless nickel thickness on the apparent density of the gold.

6.6.3. Deposit/substrate interdiffusion.

Examination of gold deposits fired for ten minutes or an hour showed that diffusion was predominantly gold into the substrate, with very little iron or nickel diffusion in the opposite direction (figs. 6.75-6.78.). (The high nickel count was due to the use of electroless nickel plating to protect the edges during microsectioning). Only after prolonged heating (up to 25 hours) was iron and nickel diffusion seen in the gold (figs. 6.79.-6.82.). In these cases, a build-up of iron was seen on the surface. This was confirmed by microprobe analysis (fig. 6.83.).

6.6.4. Electrical resistance.

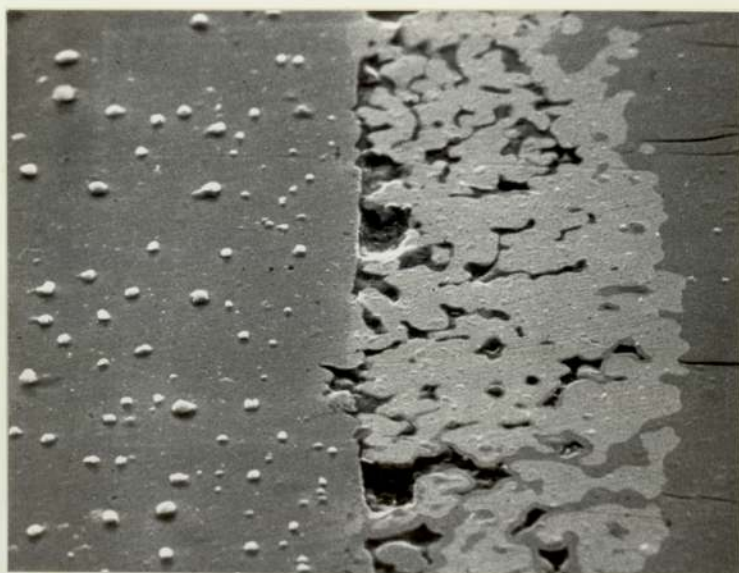
The resistance values quoted were the total of several component resistances, some of which were not important to the work. These were lead resistances, the lead/probe interface resistance, the probe resistance, the substrate/sample stub interface, sample stub resistance, the sample stub/base plate interface resistance, and the base resistance. These



6.72. Scanning electron micrograph of the underside of a gold/palladium/nickel deposit peeled off a nickel/iron substrate. x 21.



6.73. Scanning electron micrograph of the holes in the gold/palladium/nickel deposit peeled off a nickel/iron substrate, showing the copper overplate at the base of the holes. x 110



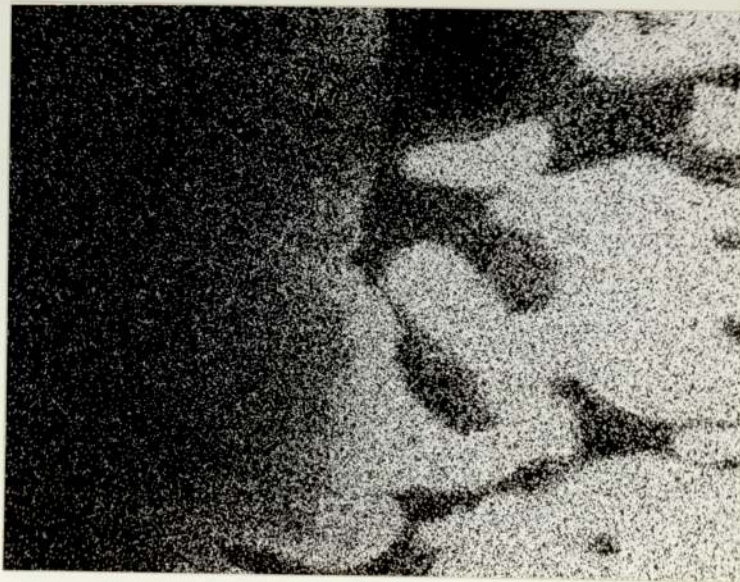
.1 μm

6.74. Scanning electron micrograph of a cross-section of a pure gold deposit fired at 900°C for 10 minutes in argon.
x 650.



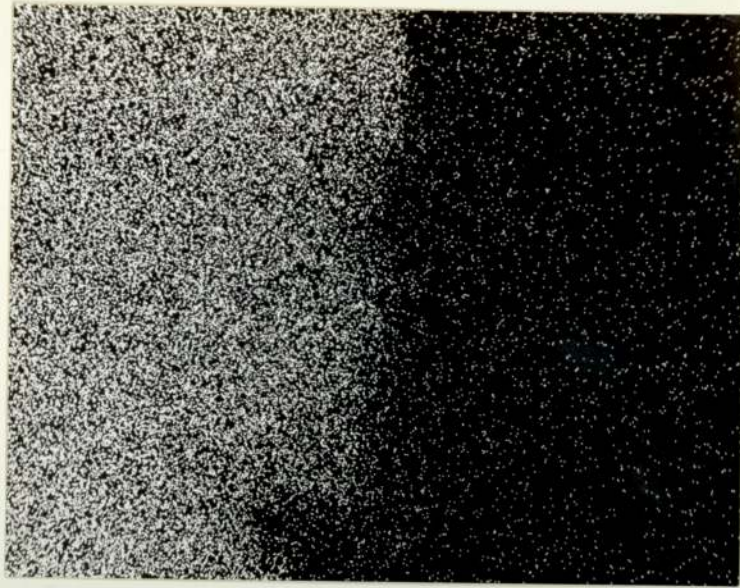
□ 1 μm

6.75. Scanning electron micrograph of a cross-section of the gold shown in fig. 6.74. x 2,600



□ 1 μm

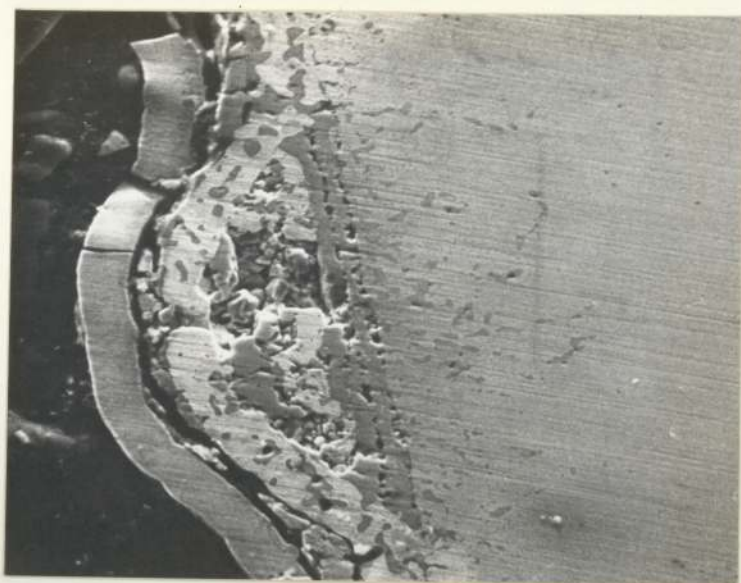
6.76. Distribution of gold in fig. 6.75. (Gold $M\alpha$ line). x 2,600



6.77. Distribution of iron in fig. 6.75. (Iron $K\alpha$ line).
x 2,600



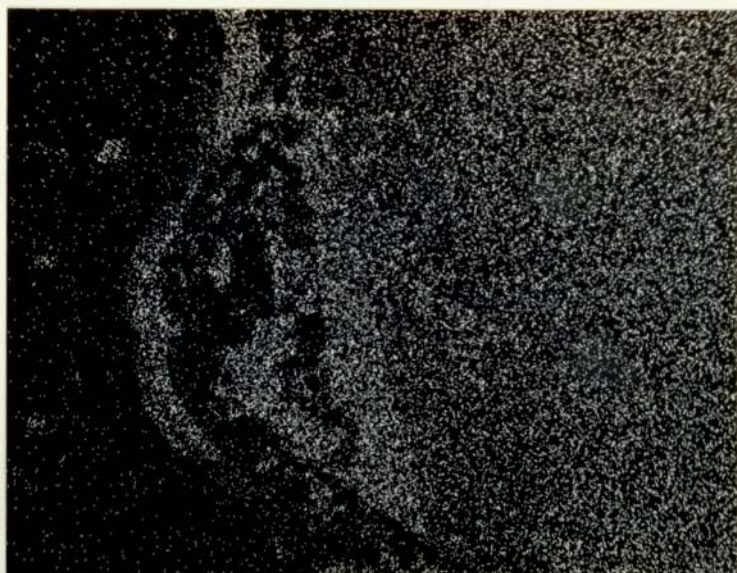
6.78. Distribution of nickel in fig. 6.75. (Nickel $K\alpha$ line)
x 2,600.



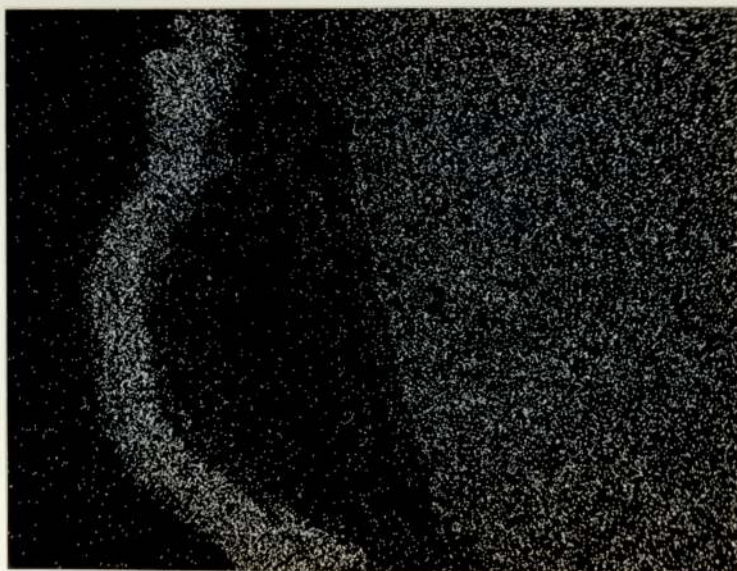
6.79. Scanning electron micrograph of a pure gold which has been fired at 850°C for 25 hours in argon. x 600.



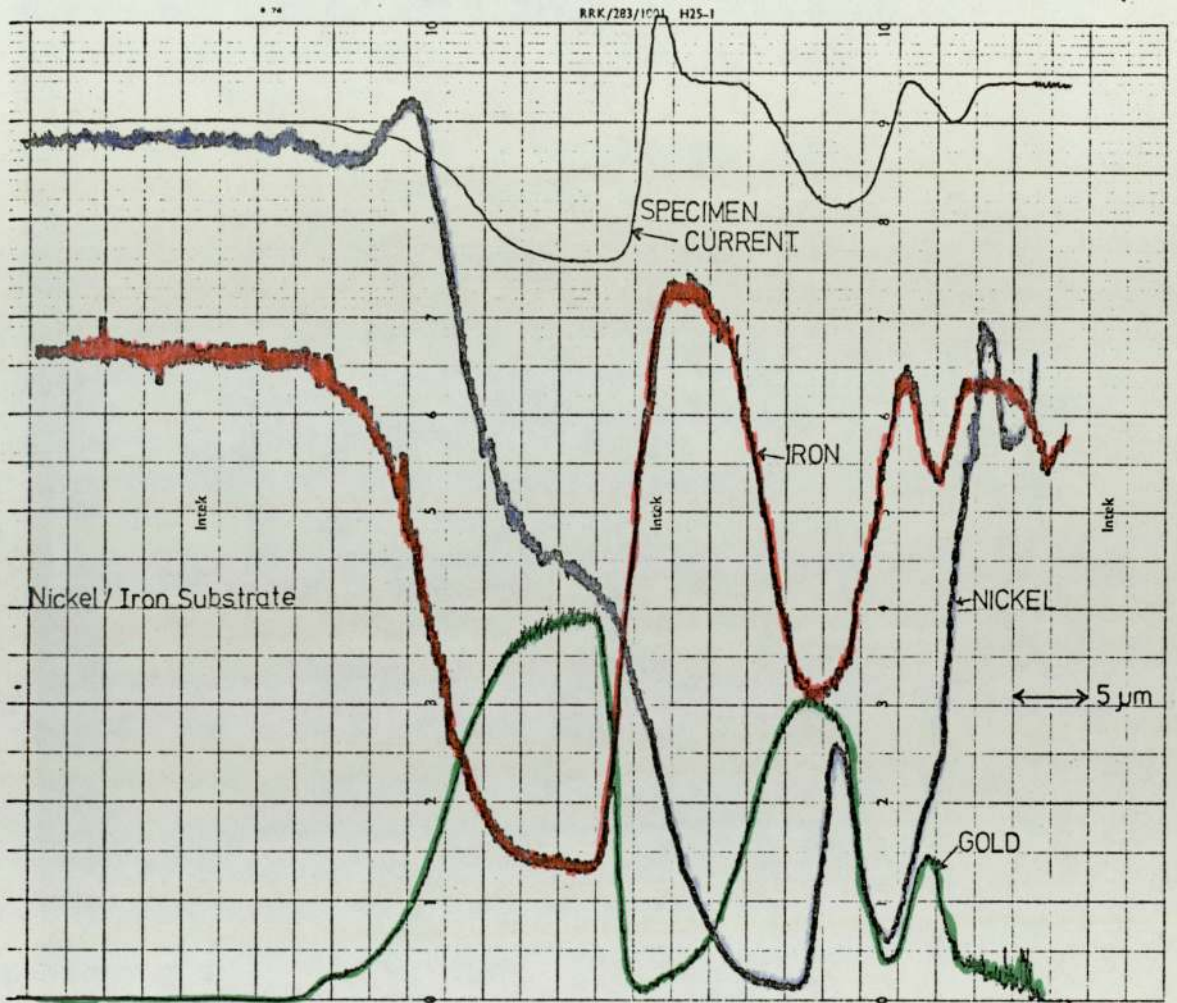
6.80. Distribution of gold in fig. 6.79. (Gold M α line)
x 600.



6.81. Distribution of iron in fig. 6.79. (Iron $K\alpha$ line)
x 600.



6.82. Distribution of nickel in fig. 6.79. (Nickel $K\alpha$ line).
x 600.



6.83. X-ray microprobe analysis trace for gold shown in fig. 6.79.

should remain constant throughout the work, but their magnitude may exceed the sought resistances of the deposit and the substrate. Attempts were made to evaluate these various resistances to obtain an absolute value for the substrate/deposit resistances.

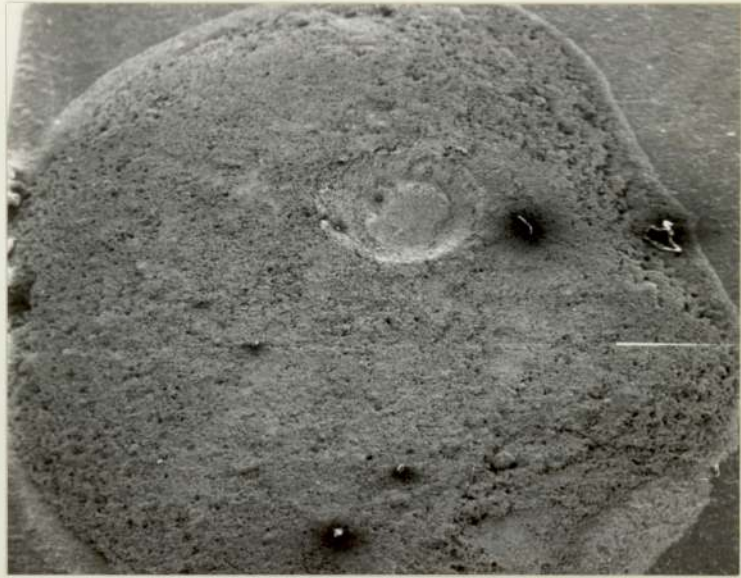
Shorting the probe out on the brass base produced a result of 1.8 milliohms, which unfortunately includes a fresh probe/base plate interface resistance. Applying the probe directly to a freshly scraped aluminium specimen stub gave a resistance of 6 milliohms, the same as that obtained from a clean iron/nickel substrate.

These results showed the importance of the contact resistance, as a pure gold deposit produced a resistance of 0.37 milliohms. In this case severe deformation of the gold had occurred (fig. 6.84.), and metal to metal contact would have been inevitable. Increasing the amount of iron/nickel diffusion in samples which were deformed in this manner, increased the resistance to 0.63 milliohms and 1.65 milliohms, for gold 'b' and 'c' respectively (fig. 6.85.).

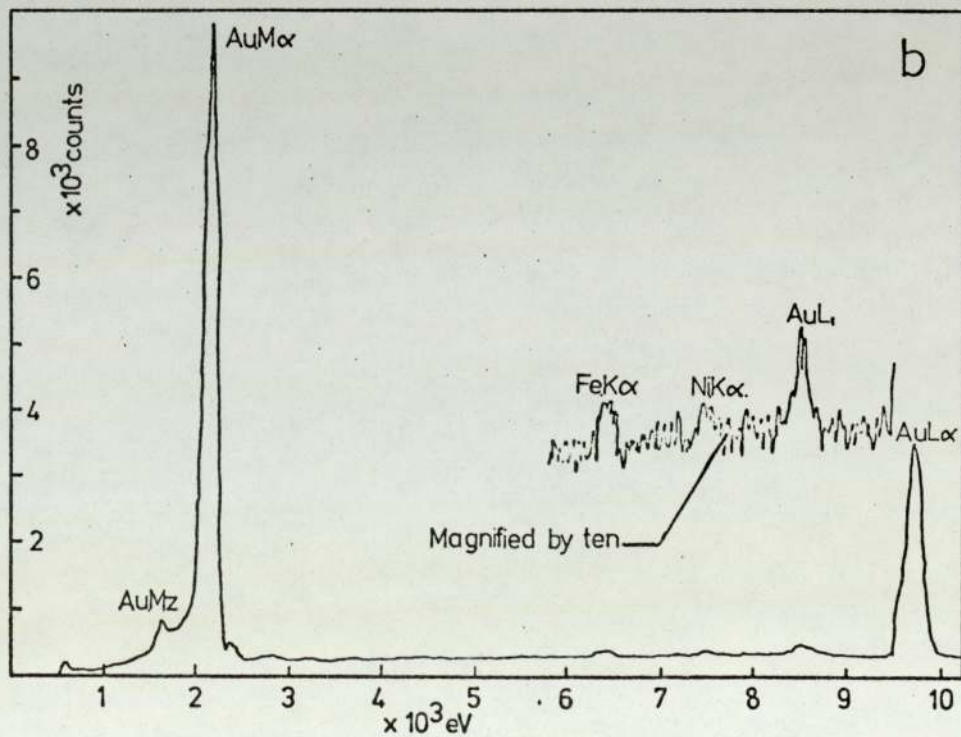
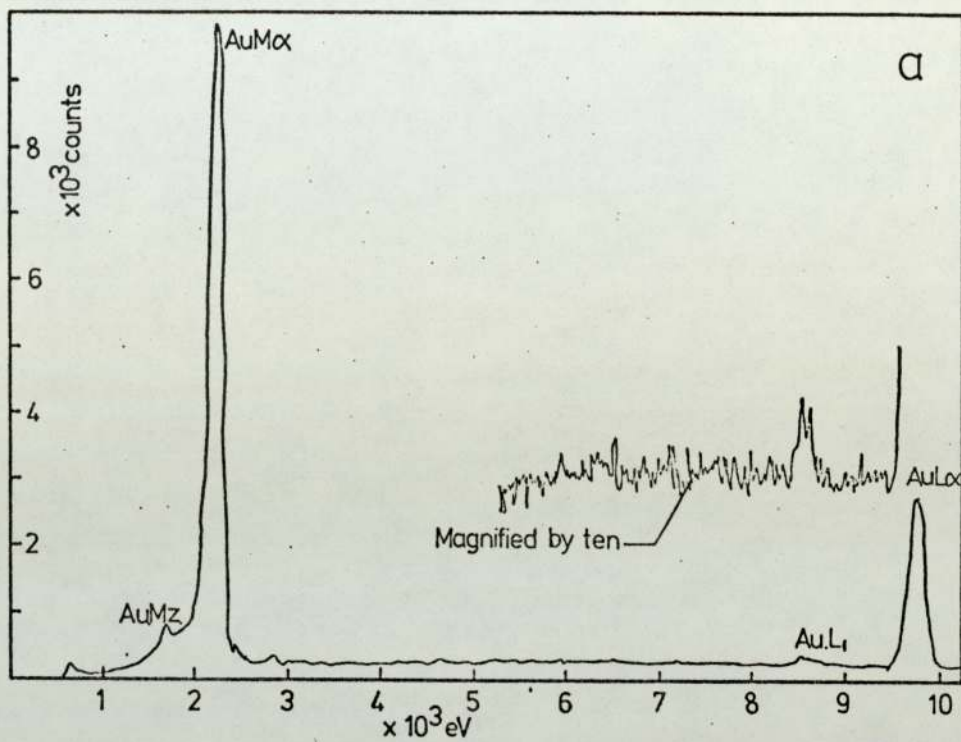
6.6.5. Spark resistance.

The major difficulty in testing the fired deposits for resistance to sparks of a size met in service, was that the damage areas were of the same order of magnitude as the variation in the surface roughness of the deposit. Most of the damage areas on the gold deposits which were tested could not be found, so comparison of the different deposits' resistance to sparks could not be made.

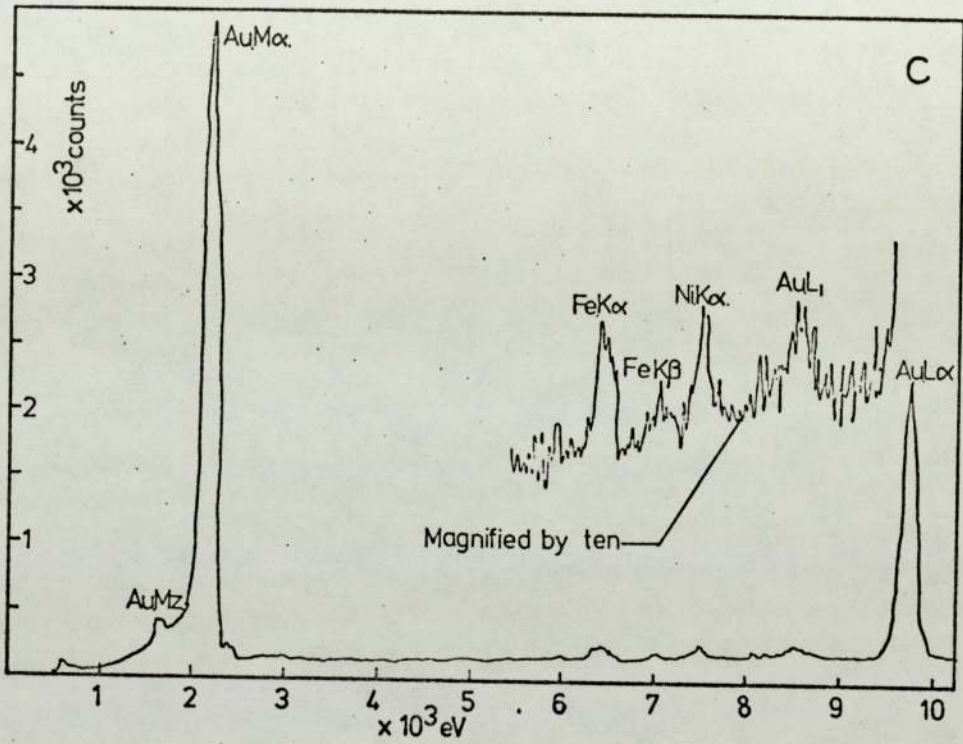
The damage area which could be found showed craters about 10-15 μ m across, a little below the general deposit surface (fig. 6.86.). On the denser, printed gold deposits, the spark damage tended to consolidate the deposit (fig. 6.87.).



6.84. Scanning electron micrograph of a pure gold deposit showing damage caused by electrical resistance probe tip. x 22.



continued over page.



6.85. Kevex X-ray spectra of pure golds fired at 950°C for 10 minutes in nitrogen. The three pastes had different viscosities.



1 μ m

6.86. Scanning electron micrograph of the spark damage on an Aston painted deposit. x 1,150



1 μ m

6.87. Scanning electron micrograph of the spark damage on an Engelhard silk screen printed deposit. x 770

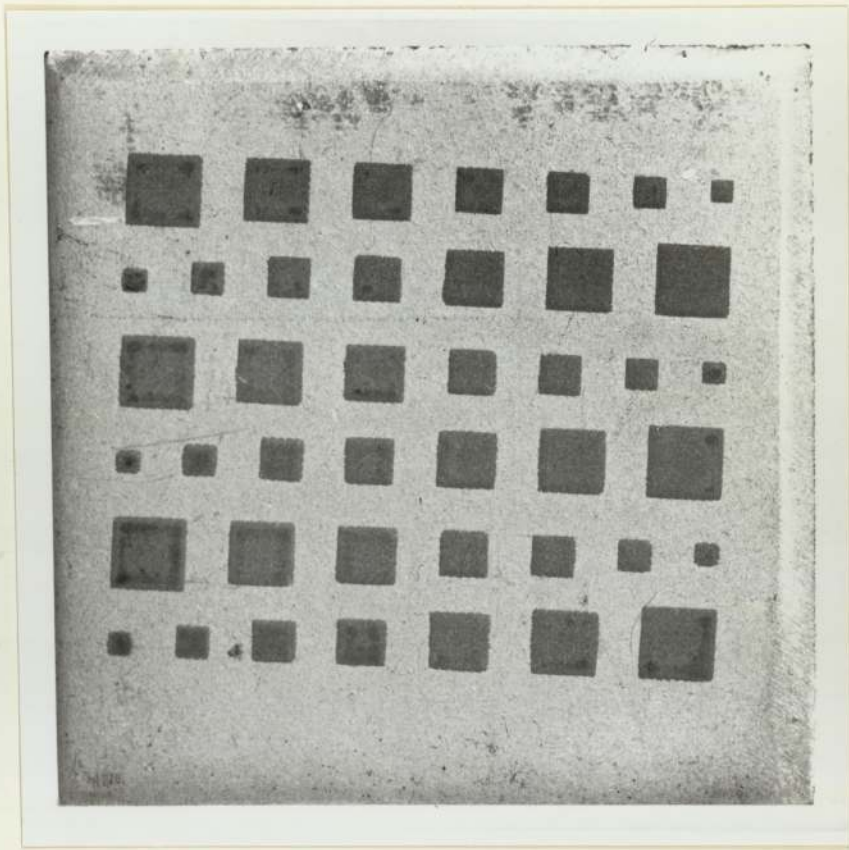
6.6.6. Deposit thickness.

The effects of varying thickness was difficult to assess, as there were differences arising from the packing of the gold at different thicknesses. In general, for pure golds fired for 10 minutes at 900°C, the thickness deposits appeared to have had the lower resistance, going from 12 milliohms to 4 milliohms, as the thickness rises from 50 μ m to 75 μ m. This was confirmed by the fact that the samples which gave the lowest resistance of 0.36 milliohms were appreciably thicker than most of the other deposits produced.

However, with longer firing times and thinner deposits (1 hour @ 900°C, 20-50 μ m thick deposits), the opposite effect was seen with the resistance rising from 4.5 milliohms to 9.1 milliohms with increasing thickness.

6.6.7. Surface finish.

The surface finishes of the fired deposits were about 2 μ m CLA, and even allowing for a reduction to 1 μ m CLA with printing instead of painting, this was still rougher than the finish of a plated reed, which was about 0.5 μ m CLA. Various ways of improving the surface finish were tried. Compressing the deposit before firing was tried, using a polished iron/nickel substrate as a tool face. A total loading of about 1.5 Kg/mm² was applied and the impression of the gold was subsequently found on the face of the tool. However, only about half the gold seemed to have been compressed (fig. 6.88.). On examination of the fired sample on the scanning electron microscope, there appeared to be no sign of tool damage and little improvement in the surface finish (figs. 6.89 and 6.90.). Application of this technique to the golds printed at Aston produced even less success, as they did not possess the 'green' strength to remain on the deposit during the operation.



6.88. Engelhard printed gold deposit after compressing to a loading of 1.5 Kg/mm^2 . Dark areas have been compressed.



1 μm

6.89. Scanning electron micrograph of a compressed area of fig. 6.88. x 750.

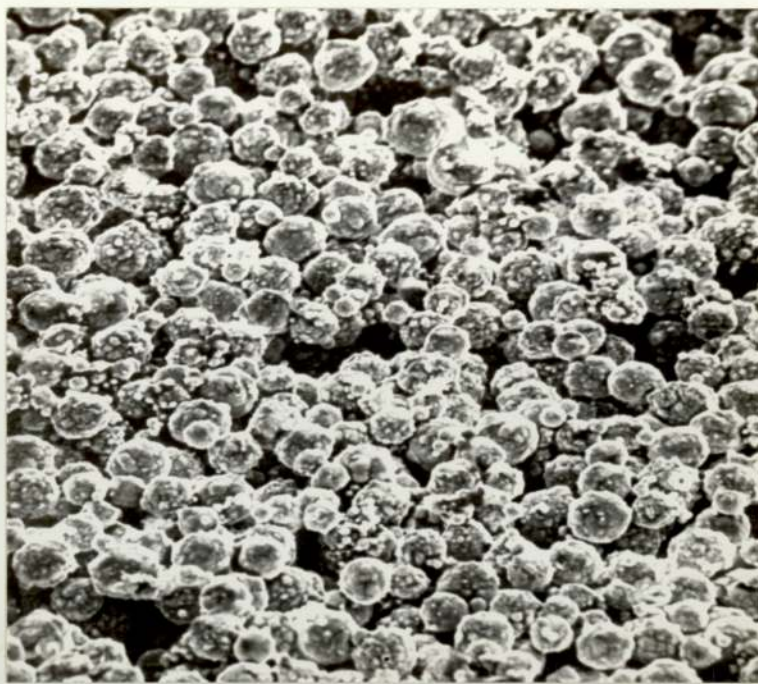


1 μm

6.90. Scanning electron micrograph of an uncompressed area of fig. 6.88. x 750.

Another technique tried was the printing on to a flat surface, which was then inverted on to the reed to show the bottom side uppermost. This was in effect a decal or transfer, and the surface which was in contact with the smooth paper showed better surface finish and packing than was usual (fig. 6.91.).

Surface markings were noticed on several gold and gold alloy pastes which had been fired in a variety of atmospheres (figs. 6.92-6.94.). The only common factor seemed to be that they appeared at the higher end of the firing range, 950°C - 1000°C . The marks ranged from small lines or ridges (fig. 6.92.), to complex patterns and shapes (fig. 6.93.), some of them geometrical (fig. 6.94.).



□ 1 μ m

6.91. Scanning electron micrograph of the underside of
a transfer painted onto art paper. x 1,800



—
1 μ m

6.92. Scanning electron micrograph of the lines seen on a gold/palladium/tin deposit fired at 1000^oC for 10 minutes in argon. x 12,000



—
1 μ m

6.93. Scanning electron micrograph of the lines seen on gold/palladium/tin deposit fired at 950^oC for 10 minutes in nitrogen. x 10,500



— 1 μ m

6.94. Scanning electron micrograph of the lines seen on a pure gold deposit fired at 950°C for 10 minutes in argon. x 11,000

7. DISCUSSION OF RESULTS OF PASTE FIRING.

7.1. Relevance of Test Methods.

One of the problems in working with industrial products and processes is the assessment of the results of the work. By far the best test is the use of the product in service conditions, which in the case of this work, would involve considerable time and expense. Not only would reed blanks have to be coated and built into reeds, but the reed relays would have to be 'life tested' on complex and expensive machines.⁽¹³⁹⁾ As these, or any other complex equipment for this project could not be financially justified by the usage they would receive, cheaper and simpler tests would have to be applied. As the tests become simpler, the less realistic they become, and their relevance to the problem becomes more difficult to evaluate.

7.1.1. Visual assessment.

Visual examination, even without the use of the scanning electron microscope is both a simple yet relevant test, giving considerable information about the extent of the sintering, the surface finish and the porosity of the deposit. These factors are not easily misunderstood.

7.1.2. Electrical resistance.

The original intention when measuring the electrical resistance was to obtain an idea of the size of the contact resistance of the deposits. Plots of contact resistance against loading would have given some indications as to the nature of any surface film present, and the nature of the contact area beneath the probe. However, to obtain results in the loading region of interest (1-10g), precautions against vibration would be needed⁽¹⁴⁰⁾ and the absence of these prevented studies at this level. In addition, the weight of the probe, and strength of the spring holding it, meant that the

smallest detectable movement of the spring occurred at about 250g, greatly in excess of the contact forces on reeds. This caused deformation beneath the probe tip (fig. 6.84.), which resulted in fresh metal being exposed. Not all deformation was as extreme as that shown in fig. 6.84., as most of the deposits resisted deformation by a similar mechanism to that which prevented the improvement of surface finish by prior compression (section 6.6.7.). This resulted in the continued existence of a surface resistance effect, the magnitude of which can be assessed by comparison of the resistance of a gold which underwent extensive deformation (fig. 6.84.) 0.36 milliohms, with the resistances of most of the other gold pastes, which did not deform. These fell in the range of 5 milliohms to 30 milliohms.

The other components of the resistance are the conduction through the deposit, and the deposit/substrate interface. All the other resistances are present in other samples and have been discussed before (section 6.1.1.). The nature of the 'conduction' resistance will vary as the sintering continues. At low levels of sintering, when neck growth is less than 10% particle diameter, constriction between the particles is important, and resistance can be related to the overall porosity.⁽¹¹⁵⁾ At higher levels of sintering, the resistance decreases as the contacts grow more perfect and defect free.^{(102)(110).}

The resistance from the iron/nickel surface layer can be quite high, as much as 200 milliohms in some cases. This is presumably due to thicker than normal oxide layers, as the normal contact resistance for nickel/iron is about 20 milliohms.⁽¹⁴¹⁾ Even if this was not the case, no fired gold deposit exhibits a resistance as high as this; so either the oxide layer is removed during firing, or more likely, the current bypasses the high resistance spots, by conduction through the gold to breaks in the oxide film where gold/metal contact occurs.

With all the other variations in the resistances (above), the electrical resistance seemed to be a very poor test. However, treated as an indication of trends, it produced some useful work, although it was never as informative as had been hoped.

7.1.3. Spark resistance.

Although the spark generating system proved to be too unreliable to be used for sorting out the spark resistance of various alloys, it did give some idea of the damage that would be caused by passage of a spark on to the deposit. There was not a tremendous amount of difference between the size of the spark damage found on plated reeds (fig. 7.1.), and that found on deposits which had been printed (fig. 6.87.), or painted on (fig. 6.86.). What differences there were could be attributed to the various energies of the sparks, but the damage done to the plated reeds was initially more damaging as it stood out from a flat area, whereas the surface of a printed or painted reed was already as rough as a spark damaged area.

There may be more damage on a less densely printed deposit, as the heat build-up from the spark will not travel away from the point of arcing. Better printing should improve that. However, with a less densely printed deposit, melting of the particle tends to lower the surface of the gold at that spot as the molten metal cools and consolidates. This will reduce the chance of the next arc striking that area, and will increase the possibility of planar erosion.

7.1.4. Adhesion.

There are very few adhesion tests which give results that are not in some way modified by the test itself.⁽¹⁴²⁾ Of the tests tried in this work, ultrasonic testing was the best from the point of view of not modifying the adhesion, but unfortunately sufficient power was not available.



1 μ m

7.1. Scanning electron micrograph of a worn electroplated reed after switching more than 10^6 cycles. x 1,400

The use of solder to attach a wire for the tensile test modifies the deposit by heating it, allowing diffusion to take place, by filling in the pores and by chemical modification. With a gold deposit this is dangerous, as a brittle gold/tin intermetallic may form. Failure, however, does not seem to have occurred through that, but through the iron oxide layer, which ran below the gold in this sample (fig. 6.11.). This gave an adhesion value of about 1% to 10% of those obtained from electrodeposited coatings.⁽¹⁴²⁾

The peel test is more complex; peel adhesion values depend upon a combination of factors: (a) the thickness of the printed deposit and overplated electrodeposit; (b) the Youngs moduli of these deposits; (c) the thickness of the yielding strip in the substrate; (d) the strength and Youngs modulus of this strip.

Using the results given in the work by Saubestre et al.,⁽¹⁴³⁾ and correcting for the thickness of the copper overplate used in this work (50um), it was found that the values of adhesion found in this work are of the same order of magnitude as electroplated metals, but lower in values. This was to be expected in view of the discontinuous nature of the gold/substrate interface.

7.2. Nature of Adhesion.

In commercial thick film practise, the fired pastes are held on the substrate either by a fusing of the glass frit to the alumina substrates, or by reaction between base metal oxides and the alumina.⁽⁶⁷⁾ Bonding of the glass frit could certainly have occurred on the sample fired in air, and seems to have been the method of bonding of the pastes fired on to stainless steel and magnesium. However, the vast majority of pastes used in this work did not contain glass, and bonding had to be by some other method. This other method is the forming of a continuous metallic bond by

interdiffusion of the gold and iron/nickel, which is confirmed by the poor adhesion of those deposits which exhibit zero neck growth. This is far better from an electrical point of view and seemed to have occurred, at least with long diffusion periods (figs. 6.79. - 6.82.). Shorter diffusion time samples seemed only to show gold diffusing into the nickel/iron, which is at odds with the published information.⁽¹⁴⁴⁾ (figs. 6.75. - 6.78.). However, this apparent one-way diffusion is enough to give the deposit better bond strength than a frit bonded paste, fired on to alumina substrates, even if it is not as good as that obtained by electroplating. The improvement of this bond may be responsible for the low resistance of golds which have melted (some of those pure golds fired at 1000°C), even though the impurity levels have risen considerably.

7.3. Sintering Mechanism.

As mentioned earlier, the exact mechanism of the sintering of gold powders of this size and at these temperatures, is not known. Although this work was not designed to illuminate this problem, some hints as to the various mechanisms predominant at different times may be found.

7.3.1. Material transported by vapour phase.

The evidence for this occurring comes from the lack of sintering and neck growth which was apparent in the golds fired in vacuum and some of those fired in nitrogen/10% hydrogen. Identical samples fired under argon or nitrogen exhibit considerable neck growth and sintering. If vapour phase transportation is occurring, the gold is evaporating from the particle surface and condensing on the neck region between the particles. If the sintering atmosphere is rarefied, the mean free path of a gold atom will be lengthened, and the gold vapour will be spread over a wider area. This will mean a thinner gold deposit on the neck area and slower sintering. Replacing

some of the nitrogen with smaller atoms of hydrogen would also lengthen the mean free path of the gold atoms and inhibit sintering. As this would not lengthen the mean free path by as great an extent, this does not inhibit growth to the same extent, and over half the samples fired in this atmosphere exhibited considerable neck growth.

The presence of vapour phase transport mechanisms in other atmospheres is shown by the presence of the markings shown in figs. 6.92. - 6.94. These bear a resemblance to the marks left by thermal etching, which occurs by a process of evaporation and condensation.⁽¹⁴⁵⁾ This also occurs in the sintering of copper and copper oxide particles, which also gives rise to marks very similar to these found here.⁽¹⁴⁶⁾

Vapour phase transportation cannot be the main sintering mechanism, as it is not possible to produce shrinkage by this method, and shrinkage of thick films on firing has been noted.⁽¹¹¹⁾ However, the presence of only two states of sintering in pastes which have been fired in nitrogen/10% hydrogen (either no neck growth, or almost complete neck growth), suggests that vapour phase transport is only important at the start of sintering. If the sintering process starts, either by better initial particle packing or for some other reason, then sintering occurs practically unhindered. This seems reasonable in view of the initial state of the gold particles at the start of firing. The lack of pressure or vibration will result in a poor density of gold particles, which will be held apart by a coating of ethyl cellulose mixed with them to impart 'green' strength. As this binder is burnt away, the gold is left with gaps between the particles. The only way that these could be bridged is either by particle rearrangement by mechanical means or by vapour phase transportation. As neck growth by this method is slow,⁽¹¹²⁾ and the vapour pressure of gold, even at 900°C, is low,⁽¹⁴⁷⁾ the gaps between the particles must be very small, and presumably must bear some relationship to the molecular size of ethyl cellulose. Once

these gaps have been bridged then other, faster methods of neck growth can occur.

7.3.2. Surface diffusion.

Surface diffusion is known to be predominant when firing very small gold particles at low temperatures⁽¹¹⁸⁾, but it is not known if this is important at the temperatures at which these larger gold particles were fired. The only evidence to suggest that this may be important is the presence of an iron rich layer, on the outside of the gold fired for longer than average periods (fig. 6.81.).

Admittedly, this may be exceptional due to the oxidation of this sample, but the production of a particle with a much higher iron content than the gold matrix, suggests that surface diffusion of the iron over the particles may be the explanation. However, an analysis on the cross-section of a gold deposit did not find any increase in the iron concentration on the gold particle surface, despite the ability of the Kevex X-ray analyser to analyse particles down to a weight of 10^{-17} g.

If this surface diffusion mechanism was predominant, then it may explain why no nickel or iron diffusion into gold was seen on short firing of the deposits. The far greater surface area of the gold compared to that of the nickel/iron substrate would mean that the substrate would be rapidly covered with a layer of gold, which would then start to diffuse into the nickel/iron. The nickel and iron, on the other hand, would soon have to start to diffuse through this gold layer before it could reach the gold particles. Their greater surface area would mean that considerably larger quantities of iron or nickel would be needed to obtain similar diffusion profiles to that of the gold. In addition, there would be the added complications of multicomponent diffusion with a maximum possible build-up on the gold surface of only 50% iron or nickel, compared with the 100%

build-up for gold on iron/nickel.

The main objection to the predominance of surface diffusion as the sintering mechanism is its inability to cause shrinkage of the pores in the powder compact. The only two mechanisms which could cause this to happen are volume diffusion, and viscous flow.

7.3.3. Volume diffusion.

Although there is no direct evidence of volume diffusion of iron and nickel into the gold, there is no evidence to suggest that it does not occur. Stablein and Kuczynski⁽¹¹⁹⁾ showed that because of the differences in volume diffusion rates between gold and nickel, more gold diffuses into the nickel than the other way round. This produced excess vacancies in the gold, which held up diffusion until homogeneity was established. This could explain the initial absence of nickel or iron in the gold after short periods of sintering. The process of homogenizing would be held up, or slowed down, by the fact that all diffusion material would have to pass through the contact points between gold particles and the substrates.

7.3.4. Viscous flow.

Again, there was no evidence to suggest that this occurred, but it has been claimed⁽¹¹²⁾ that this is likely to occur concurrently with most other sintering processes.

7.3.5. Overall sintering reactions.

Although nothing definite can be said on the progress of sintering in this gold/nickel/iron system, a provisional schedule of mechanisms can be outlined. Initially, after the ethyl cellulose has evaporated away, leaving small gaps between the gold particles, vapour phase transport of gold builds up contacts between them. As these contacts form, surface

diffusion starts to build up the contact thickness. This is due to the low temperature (it is assumed that this occurs before peak firing temperature is reached), and to the smallness of the neck growth at that time. As the neck grows bigger, volume diffusion will become more prominent. At the same time gold is diffusing into the nickel/iron substrate by lattice diffusion, increasing the deposit adhesion and lowering the resistance. Throughout all this, viscous flow may be occurring simultaneously with the other diffusion mechanisms.

7.4. Influence of Preparation of the Pastes and Substrates.

7.4.1. Substrate preparation.

It was surprising that the presence or absence of an oxide layer on the substrate surface, had so little and so inconsistent an effect on the resistance of the fired deposits. This must be due either to the removal of the oxide film during firing, or the inability to remove the film initially on cleaning, or possibly the gold deposit provides a short circuit path round the high resistance oxide layers. In this case the adhesion would suffer and this would prove to be a more sensitive test. Unfortunately this variable was not tested in this work.

7.4.2. Influence of the vehicle.

Very little was found out about the ability of the vehicle to control the properties of the pastes, mainly because of the overshadowing effects of the painting method. This is not too serious an omission, as the thick film industry has considerable experience with the effects of vehicles on pastes.

7.4.3. Influence of printing/painting.

The lack of a convenient small printer was possibly the greatest

drawback to this work, as the influence of variables in printing the deposits tend to overshadow so many other properties. Printing the deposits, whilst permitting the use of very small quantities of paste, could not control the density or packing of the pastes, nor the thickness, nor to a large extent the shape of the deposit.

7.4.4. Influence of particle morphology.

Although the size of the gold particles was only varied over a small range, the lack of any noticeable effect was surprising. This was possibly due to the large amount of sintering which had taken place and had swamped the effects due to the size differences. As the density tended to get lower with smaller particles, the shrinkage might have been greater, but this was difficult to detect without a control on the printed thickness.

The reluctance of the flat plates to sinter may be due to the poorer packing, with fewer contact points, of this paste. On the other hand, such plates have large areas of convex surfaces, and it is known that there is a decrease in the number of vacancies under convex surfaces.⁽¹¹³⁾ Such a reduction would slow down the sintering process. This mechanism could account for the rapid removal of the spikes on sintered gold powder. Here the volume of material under convex surfaces is much less than that volume at the bottom of the spike, which is under a concave surface, and hence has greater than average vacancy concentration.

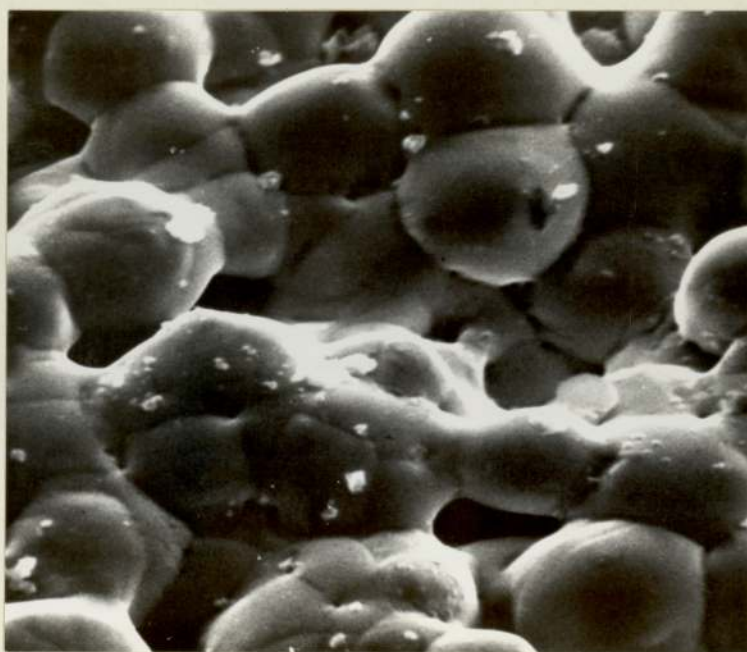
7.4.5. Influence of precompressing the printed surface.

As the local loading of the gold was above the compressive strength of the metal, it is surprising to find little sign of the compression of the deposit. This could be due to the size and surface finish of the particles. Gane,⁽¹⁴⁸⁾ working with submicron particles of gold up to 0.6 μ m in diameter,

found that they had compressive strengths approaching the theoretical value. The best strengths were found when the particles were contaminated with amorphous material, which helped to prevent the ingress of dislocations into the defect free particles. Thus little dislocation movement could occur and high strengths were obtained. The particles used in this work were larger than the $0.6\mu\text{m}$ maximum size used by Gane, but were all thoroughly contaminated with ethyl cellulose. Gane's particles were chemically precipitated and were found to be defect free, as were all other transmission electron micrographs of chemically precipitated gold particles,⁽⁹⁴⁾⁽⁹⁷⁾⁽¹⁰⁰⁾ so that it is feasible that the particles produced in this work are also defect free. It is also likely that they are single crystals, as the grain boundary grooves on fired deposits only run between the particles (fig. 7.2.). Although there will be grain boundaries present, which could generate dislocations, this mechanism could account for the lack of deformation caused by the resistance probe on fired deposits.

7.4.6. Influence of deposit thickness.

As shown above, the diffusion of nickel and iron into gold is slow, and this may account for the lower resistance of the thicker (greater than $50\mu\text{m}$) golds. Owing to the length of the diffusion path, the surface layers are still practically pure gold and so the interface resistance between the probe and the deposit will be low. However, these thicknesses are of little practical use as there is a limit to the thickness of the deposit, above which contact force drops, and the bounce time increases. For the reeds shown in fig. 1.2., the maximum thicknesses are $25\mu\text{m}$ and $8\mu\text{m}$ ⁽⁷⁴⁾ for the larger and smaller reeds respectively. At these thicknesses, the nickel and iron concentrations are likely to be fairly uniform and the resistance will increase with the longer current path of the thicker deposit.



1 μ m

7.2. Scanning electron micrograph of pure gold deposit showing grain boundary grooves. x 5,500

7.5. Pure Gold Pastes.

As a result of this work, the best deposit properties came from those deposits which were fired at the highest temperature without actually melting. These had better sintered particles with low electrical resistance and good adhesion. The time of firing did not appear to be so important, partly because of the long heating and cooling cycles. However, Williams et al.⁽¹⁰⁹⁾⁽¹¹⁰⁾ found that in pressureless sintering of nickel, the deposit was much more sensitive to temperature changes than to time changes, and this could apply in this case. It would be an advantage as it would allow the deposit to fit into the existing heat treatment cycle of reed blades.⁽²⁾ The atmosphere must be inert and have a large molecular size, to help initiate sintering. On account of its cheapness, nitrogen would be ideal, but there may be a problem in firing the deposit at the same time as heat treating the reeds, as these are normally heated in dry hydrogen.

Although this part of the work considers pure gold pastes, the material in fact comprises of a gold/iron/nickel alloy. This alloy, at high gold content, has a melting point lower than that of gold⁽¹⁴⁹⁾ and this may account for the number of pure gold samples which melted at 1000°C. This may have been helped by the development of hot spots within the furnace, which occurred after the furnace had been calibrated. It is unfortunately not known at what stage in the work these hot spots developed, so that all the temperatures must be treated with caution.

7.6. Alloy Pastes.

7.6.1. Possible range of alloys.

Pure gold is too soft and has too great a tendency to cold weld to have much use on electrical switches. Pure gold plated reeds, in practise and in the work above, are alloyed with iron and nickel, which

gives a thin layer of base metal oxide on the surface which prevents sticking and the alloy beneath is strengthened so that it is strong enough to bear the load without cracking the oxide skin.⁽³⁾ Other materials are useful in achieving this, and they have a further attraction in that they cheapen the expensive gold by diluting it. When choosing an alloying element, a compromise between the mechanical strengthening and a weakening of the electrical properties is required. The necessary strength can be obtained by a number of ways - from solid solution hardening, to hard particles in the gold, either mixed with it as powder, or generated from intermetallics. However, every element added to gold raises its electrical resistance,⁽³¹⁾ and this will increase the temperature of the molten bridge. If the alloy has a lower melting point as well, then the increase in damage will be considerable. In addition to this, the alloys may have different corrosion, frictional, or magnetic properties from pure gold, or their mechanical properties may leave something to be desired.

The range of possible alloys for electrical contacts is very wide (section 1.1.5.), and many others have been recommended for different electrical conditions.⁽⁵²⁾ Most of these rely on electroplating to produce their useful characteristics, and do not appear to have inherently desirable properties which would be of use in alloys produced in other ways. Recently recommended alloys⁽¹⁵⁰⁾ include a gold/copper⁽¹⁵¹⁾ alloy and a gold/copper/cadmium⁽¹⁵²⁾ alloy.

The use of low work function⁽²⁰⁾⁽⁴⁴⁾ metals was not attempted, as it would require a better mixing method than was used in this work to ensure a uniform mixture. It was also thought to be unnecessary because of the localized field effect⁽⁴³⁾ due to the roughened surface of the deposit, and the compacting effect of the arc damage on the surface of the printed deposit (figs. 6.86. and 6.89.).

With these and the previous factors in mind, a number of possible

alloys were considered. Excluding such alloys as gold/bismuth and gold/chromium because of their brittleness⁽¹⁵³⁾, and excluding all those alloys whose melting point drops below (approximately) 900°C, one is left with the alloys of gold with silver, cobalt, copper, iron, nickel, palladium and platinum. Platinum can be deleted from this list because of its cost, and silver because gold/silver alloys tend to be soft. All the remainder, except for iron and cobalt, do not seriously affect the resistivity of the gold alloy. Higher concentrations of cobalt causes brittleness, so only low concentrations would be likely to be used. Iron has a large effect on the resistivity of the gold⁽³¹⁾ and was used partly to test whether this effect was detectable, and partly because a good source of iron powder was available.

7.6.2. Gold/palladium alloys.

Sintering of mixtures is complicated not only by the difference in interdiffusion rates (section 1.4.4.), but also by the differences of the free energy of the alloys compared with those of the component metals. The conditions for multicomponent sintering were set out by Pines⁽¹⁵⁴⁾, and sintering will only occur between different metal particles if the interfacial energy of the alloy is less than the total free surface energies of the component metals. If this is not the case, then only sintering between like metals will occur, and this appears to be the case with the gold/palladium alloys. This is despite the solid solution which occurs between all mixtures of gold and palladium.⁽¹⁵⁵⁾

7.6.3. Gold/palladium/tin alloys.

These show this effect more clearly, with the palladium/tin remaining separate from the gold even when molten. If the analysis of the surface layer of palladium/tin is correct at 46% palladium, this mixture

should have melted at between 850°C and 900°C ⁽¹⁵⁶⁾ and there would be the added complication of liquid phase sintering.

The palladium/tin appears to have segregated to the upper surface of the deposit, possibly under the influence of gravity before the paste had dried. This constant layer of palladium/ ~~tin~~ may account for the fairly constant electrical resistance of this alloy, although with the large variations in the surface finish of this deposit it is difficult to make a definite statement.

7.6.4. Gold/palladium/nickel alloys.

This again shows little sintering between the alloy and the gold powder, although the alloy powder appears to have become better dispersed throughout the deposit (fig. 6.56.). As there was considerable sulphur present in this alloy (fig. 3.65.), this must have been driven off; this could account for the holes seen on the surface. The newly formed particles of palladium/tin were smaller than the original constituents of the powder, and their spherical shape and position below the gold suggests that they have at some stage been molten. The lowest melting point of a palladium/nickel alloy is 1237°C ⁽¹⁵⁵⁾ and this suggests that the particles melted whilst still containing sulphur. The position of the palladium/nickel alloy below the gold explains why the amount of alloy material does not affect the electrical resistance.

7.6.5. Gold/nickel alloys.

The firing of gold/nickel alloys proceeded as predicted by the work of Stablein and Kiczynski⁽¹¹⁹⁾ in that the nickel particles do not sinter into the mass of the gold, but stand proud. The nickel segregates onto the surface as seen by the high analysis of nickel found by the micro-probe analyser. This is not diffusion of nickel from the substrate, as the

copper alloy also shows a higher analysis than the mixed weights would allow, and there is no copper in the substrate (below).

The melting of the 10% and 20% nickel alloys at 950°C (155) is not surprising in view of the closeness to the liquidus minimum and the uncertainty of the furnace temperature. The maximum resistance of the 5% nickel alloys may be due to the presence of solid state immiscibility at low temperatures, causing an increase in resistance due to the precipitation of two phase material. Higher composition alloys, starting the transformation reaction at higher temperatures, would have a longer period for the reaction to go to completion. The 5% alloy, starting at a lower temperature, with lower diffusion rates, would not go so far to completion, and the precipitate may be left in a state of strain, giving higher resistance. There is difficulty in calculating the effect accurately, as the composition of the matrix is not known due to the segregation of nickel on the surface of the deposit.

7.6.6. Gold/iron alloys.

These sinter in a similar manner to the gold/nickel alloys except that the iron is taken into the body of the matrix. The resistance of this alloy is high, but not as high as would be expected from the work of Linde.⁽³¹⁾ This seems to indicate that the conduction of the deposit is not a major cause of resistance.

7.6.7. Gold/copper alloys.

Both 1% and 5% gold/copper alloys exhibited the phenomena previously seen on gold 1% nickel, and gold 1% iron alloys. All the alloys have a structure of showing minimum interparticle neck growth, with occasional scattered regions of almost 100% neck growth. The 1% nickel alloy showed practically no neck growth (fig. 6.62.), whilst the iron alloy

showed some sintering between the particles (fig. 6.64.). The 5% alloys of both iron and nickel showed complete sintering, but the 5% copper alloy showed a similar structure to that of the 1% alloys, except that more areas with 100% neck growth were visible. As the sintered regions did not coincide with any detectable concentration differences, this phenomenon could not be attributed to sintering enhancement due to the alloying elements.

It appears that small additions of alloying element inhibit sintering whilst large additions, and no additions at all, promote sintering. This is not due to the higher base metal containing alloy being nearer to its melting point than the lower content alloy. The 1% nickel alloy fired at 950°C showed only isolated sintering despite being at 92.5% of the alloy's melting point (in °K), whilst the 5% alloy sintered to 100% when fired at 92.0% of its melting point (fired at 900°C).

From the photographs (figs. 6.62., 6.64., 6.67.) the most inhibited samples are the copper alloys, followed by the nickel alloy and finally the 1% iron alloys. There are many properties which would cause these three metals to be listed in this order;⁽¹⁵⁷⁾ for example the melting point, the atomic number, the vapour pressure,⁽¹⁴⁷⁾ ferromagnetism, etc. In view of what was said earlier (section 7.3.3.) vapour pressure would seem to be the most likely cause of this phenomena. However, it is difficult to see how small additions of elements which lower the vapour pressure inhibit sintering, when large additions do not. It is at least consistent with this that the least inhibition is a result of adding an element with the lowest vapour pressure. This would imply that a high vapour pressure has an inhibiting effect, but this would also inhibit the sintering of pure gold. More work is needed on this problem before an explanation can be offered.

7.6.8. Selection of alloy pastes.

Although there has been insufficient work done on these pastes to make a final decision, some indications as to their future usefulness are beginning to emerge. Some, such as gold/palladium and gold/nickel are suspect due to the lack of sintering between the alloy components. The gold/nickel paste is even more suspect because of the danger of the loose nickel particles breaking away and forming a short circuit in the reed gap. The gold/palladium/nickel alloys seem to be hindered by the presence of sulphur in the alloy. This seems to be responsible for the poor surface finish of this alloy, and there is a danger that any sulphur remaining in the alloy on firing will cause the melting of the palladium/nickel component. The danger of a low melting point alloy is also present in the gold/palladium/tin alloy, with a further complication in the brittle intermetallic, gold/tin.

The three best deposits seem to be gold/copper, gold/iron, and pure gold, which is in fact a dilute gold/nickel/iron alloy. There are problems in the poor sintering of the gold copper alloys, and the possible high resistance of gold/iron alloys, but further development work on these alloys may either solve these problems or help to alleviate them.

8. GENERAL DISCUSSION.

The experience of firing the powders produced in the first sections showed that whilst the size seemed to be unimportant, the shape of the particles was significant. Within the range tested in this work, 0.5 μ m to 6 μ m, the effects of sintering were greater than those caused by the differences in size, although when better control of the printing is achieved, effects may be detected. The effects of different shaped gold particles were detected in this work, where it was found that only spheres sinter to the extent required. It seems that there is little difference in this respect between rough and smooth spheres as the rough rapidly lose their roughness, but the initially smooth spheres should give better packing with less shrinkage on firing.

The use of alloys has not really been examined but better mixing of the particles is required, which would be carried out on mechanical mixing machines. A more uniform mixture could be obtained - especially at low alloy content - by co-precipitating the alloy from a mixed solution, but more work is required on this to produce the correct alloy powder.

Before any real assessment of the worth of this method for coating reeds is possible, samples have to be printed by a silk screen printer. Otherwise control of thickness, packing density, surface finish, etc., cannot be obtained and their variations will swamp the effects of other parameters. From the point of view of reed switches, the most important factor to be controlled is the thickness, as this affects the contact force of the reed, influences the bounce characteristics and the likelihood of cold welding.

Despite these reservations it is possible to consider the deposits fired in this work for the contact areas of reeds. The surface finish of these deposits (after correct drying) was probably sufficient for use on reeds, although they were not as smooth as a plated reed. This is no

problem with contact resistance, as the many contact points will give the same resistance as a smaller number from a smooth deposit.⁽¹⁷⁾ The many high particles will also have localised field effects⁽²⁰⁾ which will enhance the localised field emission of electrons and present many arcing points, thus spreading the arc damage areas. As the raised areas are rounded, they are less likely to mechanically interlock, which caused Davis to abandon work in this area.⁽²⁴⁾ The surface finish of the reeds is certainly no worse than that shown by an arc damaged reed which had experienced over 10^6 cycles without mechanical interlock, and the spark damaged surface must have existed for most of these cycles (compare fig. 7.1. with, for example, fig. 6.66.).

The adhesion of these deposits does not seem to be as high as that of electrodeposits, but could be improved with silk screen printing, giving better packing and more gold/substrate contact. There is no direct evidence of the adhesion levels required by reed contacts, where most of the stress comes from the differential cooling rates of arc damaged areas. There were no reports of reed failure due to adhesion defects, so that the adhesion of these deposits may be high enough for reed contact usage. Only life testing will tell.

The major problem in applying these coatings to reeds is the porosity of the deposits, as shown by the ease of access of the electroless nickel overplating on the cross sections. Much work has been carried out on the problems of porosity in electroplates,⁽¹⁵⁸⁾ mainly due to the danger of entrapment of plating solutions which would subsequently contaminate the reed switch.⁽²⁾ This would not be a problem with printed deposits as there is no solution to be trapped, but oxidation of the substrate during manufacture could cause difficulties. Some work on electroplated deposits for reeds claims that entrapped air is good for lateral erosion enhancement,⁽³⁹⁾ but it is doubtful if that work considered air entrapment on the

scale that has been achieved in this work.

Another problem could arise with the thermal dissipation of the printed reed deposit. Initially this would be poorer due to the lower mass of the deposit, but would be alleviated by the improved 'gas cooling' of the porous deposit. After a certain amount of sparking, the deposit would have become compacted by the localised melting of small areas, and its thermal properties should then be similar to that of a plated reed in the same condition.

After superficial examination, the printed deposit seems to be a feasible proposition on reed switches, but this will only be known after life testing deposits printed on reeds by silk screen printing or some other process, giving a uniform and controlled thickness.

9. CONCLUSIONS.

- (1) Gold can be precipitated from aqueous solutions of gold chloride with controlled morphology. The morphology is controlled by the speed of the reducing reaction. A range of particle shapes can be obtained depending on the conditions, ranging from flat triangles and hexagons, through spherical and dendritic powders, to very small irregular particles.
- (2) Sodium sulphite solutions under acid conditions at room temperature produces spherical particles of the size range $0.5\mu\text{m}$ to $6\mu\text{m}$ diameter.
- (3) The particles can be mixed into pastes, painted onto nickel/iron substrates and fired in inert atmospheres to give bright, coherent deposits which adhere to the substrate. The best deposits are found after firing at 950°C to 1000°C .
- (4) The size of the particles within the range $0.5\mu\text{m}$ to $6\mu\text{m}$ do not affect the properties of the fired deposit, but the shape of the particles is important. Only spherical particles give well sintered deposits.
- (5) Gold powders will not sinter when fired under vacuum, and do not sinter well under a nitrogen 10% hydrogen atmosphere. This is thought to be due to the inhibition of vapour phase transportation of gold at the start of the sintering mechanism.
- (6) Alloys of gold and other metals are possible, and preliminary work indicates that alloys of gold with iron or copper will make the best deposits. Pure gold deposits, which are in fact dilute alloys of iron and nickel, also perform well.
- (7) These deposits may have a use as the contact materials on reed switch blades.

10. FUTURE WORK.

(1) Life testing.

As this deposit was specifically designed for reeds, the next stage in the development would be to test the fired deposits on reed blades under accelerated life testing. To obtain reliable results it is important to have identical samples, so it would be necessary to obtain deposits of equal thickness, and the easiest way of doing this, would be to print via a silk screen printer. The results could then be compared to those obtained from electroplated pure gold deposits and comparable alloys.

(2) Development of new alloys.

One of the original aims of this work was to permit the development of alloys not easily obtainable by electrodeposition, and the work reported here has only scratched the surface of this field. Much work requires to be done, both on the alloys examined in this work and others. Alloys could be formed either by the co-deposition of alloy particles or mixing elemental powders, and the whole field of composite deposits remains untouched.

(3) Investigation of the sintering anomalies of gold 1% base metal alloys.

Work on this area would help to illuminate the main sintering mechanisms, as well as trying to find the cause of the lack of sintering in the low alloy content deposits. This is important, as low alloy gold deposits can be hard without considerable damage to the electrical resistance of the alloy.

(4) Investigations into other possible uses.

Although developed specifically for use on reed switches, further work may indicate other fields of usage, such as other light duty electrical switches. Some work is already progressing

in this area, as IBM have patented an electrical connector made from gold powder.⁽¹⁵⁹⁾ Other possible uses include filling the pores with a lubricant, for example stearic acid,⁽¹⁶⁰⁾ and using the deposit to make sliding electrical contacts, for example, slip rings.

- (5) Further work might be tried on the use of decals or transfers, which would be applied to the reed contact areas before firing. These would have many advantages, such as improving the surface finish of the printed deposit, and improving the coverage of the edges of the reeds; but their main advantages would be economic. Large sheets of transfers could be printed at once, thus lowering the printing cost per transfer. Reed users could then buy the transfers and apply them to the reeds, saving the capital costs of mixing, testing and printing equipment for the pastes. This should improve the chances of commercial acceptance of this method.

11. ACKNOWLEDGEMENTS.

The author would like to acknowledge the financial support given to this work by the Science Research Council. He would also like to thank Henry Wiggin & Co. for the donation of the nickel/iron substrates material, and Engelhard Industries for the donation and printing of some of the gold paste used in this work. Thanks are also due to Dr. Terry Davis, formerly of Plessey Ltd.; Mr. Geoff. Cullen and Mr. John Houlson of F. R. Electronics, for their help and advice.

Practically all the academic and technical staff of the Metallurgy Department of the University of Aston have been asked for help at one time or another, but especial thanks are due to Mr. J. Fuggle and Mr. C. Stewart for their help on the scanning electron microscope; and of course to Dr. D. J. Arrowsmith for his excellent encouragement and advice throughout this work.

Finally, thanks are due to Miss S. Longbottom for her help in preparing the manuscript.

12. REFERENCES.

1. H. Wiggin & Co. Publication No. 3571. 'Wiggin nickel alloys for electronics and instrumentation'.
2. W. D. Bishop, J. Real, and D. L. Kirk. 'Producing reed contacts for telecommunications'. *Systems Technology* 1975 (Feb.), 20, 2-11.
3. S. D. Entwistle & J. A. Craig. 'Avoidance of adhesion in multilayer diffused sealed contacts'. *Proc. Holm Seminar on Elec. Contact. Phenomena*, Chicago 1968, 129-141.
4. 'Germany connects with computerised telephones', *New Scientist*, 29th March, 1973, p.727.
5. R. L. Peek, Jr. 'Magnetization and pull characteristics of mating magnetic reeds'. *Bell Systems Technical Journal*, 1961, 40, 523-546.
6. Sales Technical Data Sheets.
7. O. M. Hovgaard & G. E. Perreault. 'The development of reed switches and relays'. *Bell Systems Technical Journal*, 1955, 34, 309-332.
8. H. N. Wager. Chs. 8 & 9, Vol. 3. of 'Physical design of electronic systems'. Ed. D. Baker et al., publ. Prentice-Hall; Englewood Cliffs, N.J. 1971.
9. H. N. Wager. 'Predicting the erosion of switching contacts that break inductive loads'. *Proc. Holm Seminar on Elec. Cont. Phenom.* Chicago 1968, 95-105.
10. L. J. Allen, D. J. Williams, & T. A. Davis. 'Whither electrical contacts in telephony?' *Auto. Teleph. & Elec. Tech. Soc.*, 30th Oct. 1967.
11. E. L. Bubb & J. Martin. 'The TXE3 experimental exchange and field trial experience'. *Switching Technique for Telecommunications*, 43-46, IEE Conference Report No. 52 1969.
12. R. S. Gibbs. 'The reality of solid state relays', paper 19; 19th National Ass. Relay Manufacturers Conference. Stillwater, Oa., 1971.
13. P. Johnson. 'A user orientated guide to the design and applications of solid state relays'. Paper 1; 21st Nat. Ass. Relay Manu. Conf. Stillwater, Oa., 1973.
14. D. J. Williams & W. D. Bishop. 'The reed relay', *Plessey Telec. Tech. Pub. No. 101*, 2-10.
15. P. Lapping. 'Everything you need to know about reed contact units', *Control and Instrumentation* 1974, 6(2), 34-35, 37.
16. N. C. Shaw. 'Contact Bounce Control', 10th Nat. Ass. Relay Manu. Conf. Stillwater, Oa., 1962, 82-91.

17. F. P. Bowden & D. Tabor. 'The friction and lubrication of solids', Clarendon Press. Part 1, 1954; Part 2, 1964.
18. R. Holm. 'Electrical Contacts', 4th Ed. Springer Verlag 1967.
19. J. A. Greenwood. 'Construction resistance and the real area of contact', British J Applied Physics 1966, 17, 1621-1632.
20. T. Utsumi. 'Low work function metal coated reed contacts: New methods of increasing life of sealed reed contacts'. J. App. Phys. 1973, 44 (7), 3060-3062.
21. L. H. Germer & F. E. Haworth. 'A low voltage discharge between very close electrodes'. Phys. Rev., 1948, 73, 1121.
22. T. A. Davis. 'Transfer of metal between light-duty electrical contacts'. J. Mat. Sci., 1968, 3, 314-320.
23. F. Llewellyn Jones. 'The physics of electrical contacts' O.U.P. 1957.
24. T. A. Davis. 'The behaviour of reed contacts switching small currents', IEE Conf. Pub. 52, 1969, 24-7.
25. R. S. Gomez. 'Contact protection for miniature reed switches' 13th Nat. Ass. Relay Manu. Conf., Stillwater, Oa., 1965.
26. Y. Ohki & H. Marnyama. 'Multilayer diffused contacts', 13th Nat. Ass. Relay Manu. Conf., Stillwater, Oa., 1965. also U.S. Patent 3,249,728.
27. D. Campbell, R. Chamberland & J. A. Craig. 'The role of base metal additions in controlling the contact properties of miniature reed switches'. 19th Nat. Ass. Relay Manu. Conf., Stillwater, Oa., 1971.
28. U.S. Patent 3,711,383.
29. U.S. Patent 3,222,486.
30. T. F. Egan & A. Mendizza. 'Creeping silver sulphide'. J. Electrochem. Soc., 1960, 107, 353-4.
31. J. O. Linde. Ref. in A. S. Darling, 'Gold alloys for Precision Resistances', Gold Bulletin, 1972, 5, 74-81.
32. U.K. Patent 1,254,249.
33. N. D. Millar. 'Development of a high voltage reed switch'. 18th Nat. Ass. Relay Manu. Conf., Stillwater, Oa., 1970.
34. U.S. Patent 3,177,328.
35. R. L. Rosenberg & A. J. Koda. 'Reed switching devices', Machine Design, 13th March, 1969, 41, 38-45.
36. H. Rensch. 'Characteristics and applications of reed contacts'. Electrical Communications, 1965, 40, 385-397.

37. L. D. Dumbould. 'Dry reed switches and switch modules'. Control Eng. 10, July 1963, 75-105.
38. L. Holt. 'Gold plating from acid cyanide system: some aspects of the effect of plating parameters on co-deposition'. Trans. I.M.F. 1973, 51 (4), 134-140.
39. D. J. Radstake, K. J. Schell, M. C. M. Verhoeven. 'Influence of current density on the properties of electrodeposited contact layer for reed contacts'. Metalloberfläche, 1972, 26, 310.
40. W. Jacobs, R. Kobler, J. Marley & H.R. Pieffer. 'A new contact material for reed switches and specifically relay applications'. 17th Nat. Ass. Relay Manu. Conf., Stillwater, Oa., 1969.
41. T. Sasamoto. 'New multilayer contact for reed switches'. 18th Nat. Ass. Relay Manu. Conf., Stillwater, Oa., 1970. Also N.E.C. Research and development, 1970, 19.
42. K. Ono, H. Arati, H. Yanagawa. 'New multilayer electrode'. Elec. Comm. Lab. Tec. J. 1971, 20 (12), 2651-2663.
43. J. A. Augis, J. M. English, and T. Utsumi. 'Experimental investigation of low work function metal coated reed contacts for lateral erosion enhancement'. Holm Seminar on Elec. Contact Phenomena, Chicago, 1973, 170-179.
44. T. A. Davis & P. Watson. 'Potassium inclusion in gold electrodeposits; their influence on reed relay contact behaviour'. Plating, 1973, 60 (11), 1138-1145.
45. U.S. Patent 3,222,486.
46. U.S. Patent 2,600,175.
47. L. Greenspan. 'Electrodeposition of osmium'. Plating 1972, 59 (2), 137-139.
48. A. Tomikawa. 'The reed switch with a gold amalgam contact'. 17th Nat. Ass. Relay Manu. Conf., Stillwater, Oa., 1969; Paper 5.
49. H. Okamoto. 'Intermetallic compounds of gold/mercury system used for contact material in reed switch'. 17th Nat. Ass. Relay Manu. Conf., Stillwater, Oa., 1969. Paper 9.
50. T. Yokogawa & C. Kawagita. 'High reliability switches with rhodium plated contacts'. 21st Nat. Ass. Relay Manu. Conf., Stillwater, Oa., 1973. Paper 13.
51. B. P. Richards. 'Some uses of electron microscopy in the study of plating problems'. Met. Fin. J. 1971, 17 (200), 208-213.
52. M. C. Angus. 'Materials for light-duty electrical contacts'. Net. Rev. No. 141., 1970, 15, 13-26.
53. J. Fischer & D. E. Weimer. 'Precious metal plating'. R. Draper, Teddington, 1964.

54. for example U.S. Patent 3,684,569; 3,653,946; 3,268,568 and others.
55. for example German Offen. 2,252,813.
56. K. E. Saeger & E. Vinaricky. 'Some trends in the use of gold for electrical contacts'. Gold Bulletin 1975, 8 (1), 2-6.
57. J. S. Gellatly. 'High production precious metal contact welding on relay and switch springs'. 15th Nat. Ass. Relay Manu. Conf., Stillwater, Oa., 1967. Paper 2.
58. U.S. Patent 3,672,850.
59. R. F. Janninak, C. R. Heider, and A. E. Grettersohn. 'A rapid loading and unloading coluseum type fixture for ion plating reed blades contacts'. J. Vac. Sci. & Tech., 1974, 11 (2), 535-536.
60. E. Groshart. 'Metallising non-conductors - VIII Spluttering'. Met. Fin. 1973, 71, 44-48.
61. W. Reichelt. 'Vapour deposition of gold alloys: developments in radio frequency spluttering of electrical contact surfaces'. Gold Bulletin, 1972, 5 (3), 55-57.
62. Thermophysical Properties of High Temperature Solid Materials. Ed. Y. S. Touloukian, Macmillan N.Y. 1967.
63. for example U.S. Patent 3,553,109; 3,598,761; 3,536,508 etc.
64. see for example U.S. Patent 2,822,279; 3,207,706; 3,536,508.
65. R. E. Trease & R. L. Dietz. 'Rheology of pastes in thick film printing'. Solid State Tec. 1972, 15 39.
66. U.S. Patent 3,502,489.
67. T. T. Hitch. 'Adhesion, phase morphology, and bondability of reactively-bonded and frit-bonded gold and silver thick film conductor'. J. Elec. Mat. 1974, 3 (2), 553-577.
68. for example, U.S. Patent 3,799,890; 3,799,891.
69. for example, U.S. Patent 3,717,483; 3,347,799; 3,817,758.
70. for example: C. J. Pukaite & J. P. Schwartz. 'Aspects of conduction mechanism in thick film resistors'. Amer. Ceram. Soc. Bulletin, 1971, 50, 754.
71. D. A. Cash. 'A novel thick film resistor system'. Proc. Internepcon, 1971, 215-221.
72. D. G. Kelemer. 'Metallographic aspects of thick film technology'. Met. Trans. 1970, 1 (3), 667-677.
73. D. Blower. Engelhard Industries. Private communication.
74. G. Cullen. F. R. Electronics. Private communication.

75. C. G. Goetzel. 'Treatise on powder metallurgy'. Interscience, N.Y., 1949.
76. Ed. J. J. Burke & V. Weiss. 'Powder metallurgy for high performance applications'. Proc. 18th Sagamore Army Materials Research Conf., 1971.
77. A. G. Walton. 'The formation and properties of precipitates. Interscience N.Y. 1967.
78. A. E. Nielsen. 'Kinetics of precipitation'. 1964, Pergammon, Oxford.
79. J. M. West. 'Electrodeposition and corrosion processes'. 1965, Van Nostrand Co. Ltd., London.
80. The Encyclopedia of Electrochemistry, Ed. C. A. Hampil, Reinhold N.Y., 1964.
81. 'The manufacture and properties of metal powders produced by the gaseous reduction of aqueous solutions'. Powder Met., 1958, 1, 40-52.
82. A. R. Burkin. 'Production of metal powders, and coating by precipitation techniques, and their fabrication'. Met. Rev. No. 111. 1967, 12, 1-14.
83. J. Turkevich, P. C. Stevenson, and J. Hillier. 'A study of the nucleation and growth processes in the synthesis of colloidal gold'. Disc. Faraday Soc. 1951, 11, 55-75.
84. R. Weiss. Ref. 27, chapter 1 of (77) above.
85. Kossel-Stranski, as in H. E. Buckley's 'Crystal growth', Wiley & Son, N.Y. 1951.
86. I. M. Kolthoff & B. van't Riet. 'Studies on formation and ageing of precipitates, XLVI Precipitation of lead sulphate at room temperature'. J. Physical Chemistry, 1959, 63, 817-823.
87. D. J. Robinson & D. Gabe. 'High speed electrodeposition of copper from conventional sulphate electrolytes'. Trans. I.M.F., 1970, 48, 35-42.
88. G. Frens. 'Controlled nucleation for the regulation of the particle size in monodispersed gold suspensions'. Nature, Physical Sciences, 1st Jan. 1973, No. 105, 241, 20-22.
89. F. J. W. Roughton & G. A. Millikan. 'Photoelectric methods of measuring the velocity of rapid reactions'. Proc. Roy. Soc. 1936, A155, 258-292.
90. H. E. Buckley, 'Crystal growth'. Wiley & Son, N.Y. 1951. Appendix.
91. R. H. Morriss & W. O. Milligan. 'Electron microscopic studies of the size and shape of colloidal gold particles'. J. Electron Mic. (Japan). 1960, 8, 17-23.

92. J. K. Dennis & J. J. Fuggle. 'The effect of metallic contamination on electrodeposited nickel, Part II, appearance and surface topography'. *Trans. I.M.F.* 1970, 48, 75-82.
93. M. Van Ardenne. *Z. Physic. Chem.*, 1940, A.187, 1, from Ref. (91) above.
94. N. Uyeda, M. Nishimo, and E. Suito. 'Nucleus intereactions and fine structures of colloidal gold particles'. *J. Colloid & Interface Sci.* 1973, 48, 75-82.
95. Rinde. 'The distribution of sizes of colloidal gold solutions prepared according to the nuclear method'. Uppsala 1928, ref. from (83) above.
96. C. A. Jacobson. 'Encyclopedia of chemical reactions'. Reinhold, N.Y. 1949.
97. S. Rashkov & A. M. Koulkes-Pujo. 'Morphology studies of the precipitation of metallic gold by irradiation of gold chloride solutions'. *J. de Chimie Physique* 1968, 65, 911-919.
98. Y. S. Chiang & J. Turkevich. 'Formation of platelike colloidal gold'. *J. Colloid Sci.* 1963, 18, 772-783.
99. S. Amelinckx. 'Growth spirals originating from screw dislocations on gold crystals'. *Phil. Mag.* 1952, 43, 562-567.
100. P. Kratochvil, B. Sprusil, and M. Heyrovsky. 'Growth of gold single crystals in gels'. *J. Crystal Growth* 1968, 3, 4, 360-362.
101. E. Suito & N. Uyeda. 'Spiral growth of lamellar single crystals of colloidal growth'. *J. Electromicroscopy.* (Japan). 1960, 8, 25-30.
102. N. Uyeda. 'The indented perimeter as the growth front of lamellar single microcrystal of colloidal growth'. *J. Electromicroscopy* (Japan) 1961, 10 (3), 170-174.
103. U.K. Patent 1,313,826. U.S. Patent 3,717,481.
104. U.K. Patent 1,355,444. U.S. Patent 3,725,035.
105. U.S. Patent 3,708,313. U.S. Patent 3,817,758.
106. L. C. Gratton & H. J. Fraser. 'Systematic packing of spheres with particular relations to porosity and permeability'. *J. Geology* 1935, 43, 785-909.
107. R. K. McGeary. 'Mechanical packing of spherical particles'. *J. Amer. Ceram. Soc.* 1961, 44 (10) 513-522.
108. B. S. Newman. Chapter 10 in 'Flow properties of dispersed systems'. Ed. J. J. Hermans, Amsterdam, 1953, North Holland Publ Co. 382-422.
109. V. A. Tracey & N. J. Williams. 'The production and properties of porous nickel for alkaline battery and fuel cell electrodes'. *Electrochemical Tech.* 1965, 3, 17-25.
110. N. J. Williams, D. J. Burr, and P. J. Bridges. 'The structure and properties of porous nickel plaques'. *Powder Met.* 1972, 15, (29) 42-54.

111. R. H. Zeien. 'Characterisation of thick film fritless metalisation'. Proc. for Int. Soc. for Hyb. Microelec. Symp., Boston U.S.A. 1974. pp. 7-15.
112. Z. F. Thümmeler & W. Thomma. 'The sintering process'. Met. Rev. No. 115. 1967, 12, 69-108.
113. G. C. Kuczynski. 'Fundamentals of sintering theory'. Paper 6 in 'Powder Met. for high performance applications' 1972. pp. 101-117.
114. G. C. Kuczynski. 'Self diffusion in sintering of metallic particles'. Met. Trans. (Trans. AIMME) 1949, 185 (2), 169-177.
115. V. V. Skorokhod & S. M. Solonin. 'The kinetics of interparticle contact growth in the sintering of impressed powders'. Sov. Pow. Met. & Metal Ceramics, 1972, 9, 141-145.
116. D. Duhl, K-I. Hirano and M. Cohen. 'Diffusion of iron, cobalt and nickel into gold'. Acta Met. 1963, 11, 1-7.
117. S. M. Kaufman, T. J. Whalen and L. R. Sefton. 'The utilisation of electron microscopy in the study of powder metallurgy phenomena: II the deduction of neck growth mechanism from the rate data for submicron copper and silver spheres'. Paper 3 in 'Advance Experimental Techniques in Powder Metallurgy', Ed. Hirschhorn & Roll, Plenum Press, N.Y. 1970, 41-60.
118. D. W. Pashley, M. J. Stowell, M. H. Jacobs and T. J. Law. 'The growth and structure of gold and silver deposits formed by evaporation inside an electron microscope'. Phil. Mag. 1969, 10, 127-158.
119. P. F. Stablein & G. C. Kuczynski. 'Sintering in multicomponent metallic systems'. Acta Met. 1963, 11, 1327-1337.
120. Ed. E. M. Wise. 'Gold; recovery, properties and applications'. Van Nostrand, Princeton N.J. 1964.
121. T. A. Allen. 'Particle size measurement'. Chapman & Hall Ltd. London, 1968.
122. G. C. Johnson Jr. & E. W. White. 'X-ray emission wavelengths and KeV tables for non-diffractive analysis'. A.S.T.M. Data Series DS. 46, 1970.
123. J. W. Mellor. 'A comprehensive treatise on inorganic and theoretical chemistry'. Longman, London. 1922-1937.
124. U.S. Patent 3,505,134.
125. F. Feigl. 'Spot tests in inorganic analysis'. Elsevier, Amsterdam 5th ed. 1958.
126. T. Rosenqvist. 'Principles of extractive metallurgy'. McGraw-Hill, N.Y. 1974.
127. Dr. J. L. Aston. Private communication.

128. J. Halpern, E. R. MacGregor and E. Peters. 'The nature of the activated intermediate in the homogeneous catalytic activation of hydrogen by cupric salts'. J. Phys. Chem. 1956, 60, 1455-1456.
129. J. Pelletie. Ann. Chin. Phys. 1820. 15 (2), 5, 113; reported in Mellor, ref. 123 above.
130. U.S. Patent 3,390,981.
131. Lange's 'Handbook of Chemistry' McGraw-Hill, 10th ed. 1967.
132. J. Turkevich & G. Kim. 'Palladium preparation and catalytic properties of particles of uniform size'. Science 1970, 169, 873-879.
133. A. Canas-Rodriguez. 'Hydrogenations with palladium precipitates in the presence of the substrate'. J. Chem. Soc. Perkins I 1972, 554-555.
134. U.K. Patent 1,371,834.
135. U.K. Patent 1,152,502.
136. Sales Literature, Engelhard Ltd.
137. A.S.T.M. standard E112-63.
138. Inspection certificate No. W.140846. 19th Feb. 1973. Henry Wiggin & Co., Ltd.
139. R. M. Williams. 'Automatic life testing of reed relay insets'. Plessey Communications Journal, 1966, 1 46-57.
140. D. B. Fox. 'A realistic and dynamic life test for reed switches'. Paper 8, 16th Nat. Ass. Relay Manu. Conf., Stillwater, Ca., 1968.
141. O. Michikomi. 'On the constriction resistance of diffused contacts'. J. App. Phys. (Japan) 1971, 10, 112-113.
142. D. Davies & J. A. Whittaker. 'Methods of testing the adhesion of metal coatings to metal'. Met. Rev. No. 112. 1967, 12, 15-26.
143. E. B. Saubestre, L. J. Durney, J. Hajdu and E. Bastenbeck. 'The adhesion of electrodeposits to plastics'. Plating 1965, 52, 982-1000.
144. H. Okomoto. 'Alteration of the lattice due to diffusion between gold and iron/nickel alloy'. J. App. Phys. (Japan), 1968, 7, 685-686.
145. V. R. Howes. 'Metal-oxide interface morphology for a range of iron-chromium alloys'. Corrosion Science 1970, 10, 99-103.
146. Illustrations, 'The Metallurgist and Materials Technologist', 1975, 7 (2), p. 105.
147. An. N. Nesmeyanov. 'Vapour pressure of the elements'. Infosearch Ltd., London, 1963.

148. N. Gane. 'Measurement of the strength of metals on a sub-micron scale'. Proc. Roy. Soc. A., 1970, 317, 367-391.
149. W. Köster & W. Ulrich. 'The ternary system, iron, nickel, gold'. Z. F. Metallkunde, 1961, 52, 383-391.
150. D. R. Mason, A. Blair and P. Wilkinson. 'Alloy gold deposits: have they any industrial use'. Trans. I.M.F., 1974, 52, 143-148.
151. U. Mayer. 'Über das Korrosionsverhalten galvanischer Edelmetallüberzüge'. Metalloberfläche, 1974, 28, 59-63.
152. M. Dettke & W. Riedel. 'Über Struktur und Eigenschaften von Gold und Goldlegierungsüberzügen'. Oberfläche-Surface 1973, 14, 130-134.
153. T. K. Rose & W. A. Newman. 'The metallurgy of gold'. Griffin & Co. 7th Ed., London, 1937.
154. B. Ya. Pines. Zhur. Teknu. Fizik. 1956, 26, p. 2086.
B. Ya. Pines & N. I. Sukhinin. Ibid. p. 2100. Both from ref. 112 (above).
155. M. Hansen. 'Constitution of binary alloys'. McGraw-Hill, N.Y., 1958.
156. R. P. Elliot. 'First supplement to constitution of binary alloys'. McGraw-Hill, N.Y. 1965.
157. C. Smithells. 'Metals reference book'. Butterworth, London, 4th Ed. 1967.
158. R. G. Baker. 'The evaluation of gold electrodeposits for use in dry circuit applications'. Trans. I.E.E.E., 1973, PHP-9, 36-39.
159. U.K. Patent 1,374,889.
160. J. Aronstein & W. E. Campbell. 'Contact resistance and material transfer in soft metal microcontacts'. Holm Seminar on Elec. Cont. Phenom. 1969, 7-27.